PREDETERMINATION OF THE SOUND PRESSURE LEVELS OF MAGNETIC NOISE IN MEDIUM INDUCTION MOTORS

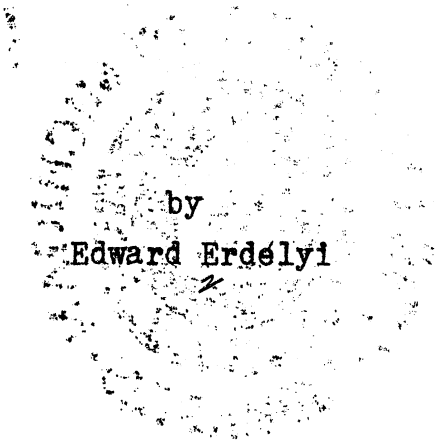

by
Edward Erdélyi

A dissertation submitted in partial fulfillment
of the requirements for the degree of
Doctor of Philosophy in the
University of Michigan
1955

Doctoral Committee:

Professor Edwin R. Martin, Chairman
Professor Stephen S. Attwood
Professor William G. Dow
Associate Professor Wilfred Kaplan
Associate Professor Norman R. Scott

Consultant to the Committee:

Mr. Philip L. Alger, Consulting Engineer
General Electric Company, Schenectady

To the Memory
of

Anna and Alexander Erdélyi

PREDETERMINATION OF THE SOUND PRESSURE LEVELS OF MAGNETIC NOISE IN MEDIUM INDUCTION MOTORS

by

Edward Erdélyi

Abstract

Chapter I: Introduction

A historical review of earlier work in the field of magnetic noise is given. It is noted that in most writings of the past the recommendations for low magnetic noise levels are intimately related with the question of slot combinations. The more complete single-ring theory of P. L. Alger is reviewed, and the inadequacies of this pioneering theory are discussed. The nature of the different types of noise in induction motors is described, and the origin of harmonic noise is explained. The difference between the single-ring theory and the more complete solution of the problem given in this thesis is illustrated by curves which show dynamic deflection versus frequency.

Chapter II: The Electromagnetic Force Waves in the Airgap

Expressions are developed for the magnetomotive force distribution in the airgap of induction machines. A simple method is given for treating the influence of the variable airgap permeance. The influence of the number of slots per pole per phase on the combination of slot and permeance harmonics is pointed out. Equations for the amplitude, frequency, and mode of the force waves are derived. The influence of factors which are not in agreement with the simplified assumptions is qualitatively discussed. The theory is applied to calculate the force waves of an experimental motor.

Chapter III: The Dynamic Response to the Electromagnetic Force Waves

Now the vibrating system of the stator is represented by two coupled concentric rings on a support. A brief review of the theory of Lagrange's equations and the theory of small oscillations is given. Expressions for the elastic and kinetic energies of the physical components of induction motors

are developed. Following certain simplifying assumptions the natural behavior of the experimental motor is carefully analyzed and numerical results obtained for the resonant frequencies of the stator. The forced response to the electromagnetic force waves is computed.

Chapter IV: Sound Radiated by the Vibrating Stator

The boundary value problem of the sound radiating motor which is represented as an infinite cylinder vibrating in a belt is solved by a Fourier transform method. The method of solution of the resulting integral is explained, and evaluated in detail for different operating conditions of the experimental motor.

Chapter V: Experimental Investigation of the Special Motor

The experimental arrangements and equipment for finding the natural frequencies and associated mode shapes are explained. The anechoic room and the test conditions for the recording of the motor noise on magnetic tape and the subsequent recording of sound spectra are described. The method for the determination of mode shapes under dynamic conditions is explained, and test results are recorded.

Chapter VI: Conclusions

A comparison between theoretical and experimental results is carried out, and it is concluded that the method of the thesis is applicable for the calculation of natural frequencies and the predetermination of the sound pressure levels of the magnetic noise in medium induction motors. A note of caution is made of the danger in transferring results of one design to that of another design. It is stressed that the analysis must be carried out individually for each type and design of machine, if significant results are desired.

ACKNOWLEDGEMENTS

The author wishes to thank his Committee, especially Professor E. R. Martin, for the permission to carry out the work connected with this thesis at the General Electric Company in Schenectady, and for their assistance in discussing with him the various aspects of this problem.

An expression of deep indebtedness and sincere gratitude is made to Mr. P. L. Alger, Consulting Engineer, Medium Induction Motor Department of the General Electric Company, for his suggestion of this investigation. It was he who offered both guidance and assistance during every phase of this complex assignment, and the author realizes that this work could not have been accomplished without Mr. Alger's generous help. Acknowledgement is also due to Dr. G. Horvay of the General Electric Company for introducing the author to the theories employed in Chapter 3, and to Dr. R. Plunkett of the General Electric Company for the critical review of the analysis in this chapter and for his very valuable suggestions.

Mr. J. W. Ward of Carrier Corporation, Inc., Syracuse, New York, was very helpful in carrying out the preliminary computations on the IBM 605 equipment.

Also the help of Dr. F.S. Beckman, and of Mr. J.F. Terlato of the Scientific Computing Service of the International Business Machine Corporation, Inc., New York, who programmed the final calculations for the IBM 701 Electronic Data Processing Machine is acknowledged. Thanks are due also to many associates at both the General Electric Company at Schenectady, and at Syracuse University.

Finally the author gratefully acknowledges the assistance and forbearance of his wife, Nelly; the services of Mrs. M. Wolman in typing this dissertation; and the assistance of Miss R. Shaver of the General Electric Company, in making many time- consuming arrangements.

This work was sponsored by the General Electric Company, Medium Induction Motor Department, Schenectady, New York.

TABLE OF CONTENTS

TABLE OF CONTENTS (Cont'd)

APPENDICES (Cont'd.)

LIST OF TABLES

LIST OF TABLES (Cont'd.)

LIST OF TABLES (Cont'd.)

LIST OF ILLUSTRATIONS

LIST OF ILLUSTRATIONS (Cont'd.)

LIST OF ILLUSTRATIONS (Cont'd.)

INDEX OF SYMBOLS FOR

CHAPTER II

Symbol		Page
A	differential area in airgap	72
A_σ	amplitude of the σ^{th} harmonic current layer	31
$a(x_1)$	ordinate of fictitious current distribution at x_1	89
B_{max}	max. flux density at tooth center	58
$\bar{B}_b$	max. reduction of flux density at slot center	58
B_1	amplitude of fundamental flux distribution	63
B_σ, B_ρ	amplitude of σ^{th} or ρ^{th} flux harmonic	64
$b(x_1,t)$	ordinate of flux distribution at x_1, at time t	63
$b^{(+)}$	flux distribution of positively rotating field	94
$b^{(-)}$	flux distribution of negatively rotating field	94
b_{ss}	flux distribution of stator slot harmonic	87
b_{sr}	flux distribution of rotor slot harmonic	87
C_3	an integer divisible by 3	82
c_2	any integer	40
c_{1s}	an integer except zero	37

Symbol		Page
dA	differential area	89
f	frequency	38
f^I	ordinate of mmf distribution of one phase	33
$f(x_1,t)$	ordinate of mmf distribution of a polyphase winding at point x_1 at time t	35
f_k	ordinate of mmf at k^{th} tooth	51
g	airgap	58
g'	airgap - corrected for variable permeance	63
g"	airgap - corrected for saturation	46
$g(x_1)$	variable airgap at (x_1)	104
$H(x_1)$	magnetic field intensity at (x_1)	105
h	magnetic field intensity	50
h	denotes a particular rotor bar in squirrel cage	40
I	R.M.S. value of phase current	39
$I'_{1\sigma}$	fundamental stator current referred to σ^{th} cage	55
i	instantaneous value of phase current	31
k_σ	σ^{th} winding factor	33

Symbol		Page
k'_σ	σ^{th} skew factor	97
k_1	correction coefficient	47
k_C	Carter correction coefficient	46
k_d	distribution factor	33
k_p	pitch factor	33
L	inductance of one phase including the effect of mutual inductance between phases	50
l_i	net iron length of stator	46
M_σ^I	amplitude of σ^{th} harmonic of mmf of one phase	33
M_σ	amplitude of σ^{th} mmf harmonic of a polyphase winding	35
m	number of phases	31
m_v	mode of radial force wave	75
n_s	synchronous speed	38
n	rotor mechanical speed	38
φ	permeance function	61
p	number of pole pairs	
Q_1	total number of stator slots	66

Symbol		Page
Q_2	total number of squirrel cage bars	66
R	radius of stator bore	91
R_1	primary resistance	44
$R_{2\sigma}$	resistance in the equivalent circuit of the σ^{th} cage	44
s	slip	38
s_{1o}	width of slot opening	58
t	time	33
u	a subscript denoting a phase	31
v_s	velocity of fundamental mmf	36
v_σ	velocity of σ^{th} harmonic mmf	36
W	magnetic energy density	71
w_1	number of turns in series per stator phase	33
X_1	leakage reactance of primary	44
X_{1s}	slot leakage reactance	49
X_{1e}	end connection leakage reactance	49
X_{1d}	differential leakage of stator	49

Symbol		Page
$X_{1m\sigma}$	magnetizing reactance of the stator σ^{th} harmonic	44
$X'_{2\sigma}$	leakage reactance of σ^{th} cage referred to the stator	49
$X_{2m\sigma}$	magnetizing reactance of the σ^{th} harmonic with resp. to the rotor	47
x_1	denotes the position of a point on rotor ($x_1 = 0$ at the center of the reference phase)	33
x_2	position of a point on the rotor	38
z	distance measured along the rotor axis	100
β	a simplifying function	60
Γ	ordinate of force wave	71
Γ_t	tangential component of force wave	91
Γ_z	axial component of force wave	103
ε	eccentricity of airgap	104
η	a coefficient in the permeance function	61
η_2	a factor of differential leakage	54
λ_{1d}	primary differential leakage factor	50
$\lambda_{2d\sigma}$	σ^{th} differential leakage reactance factor of the rotor	55
μ_o	permeability of free space	51
ξ	order of slot harmonic	84
ξ	distance measured from tooth center	59

Symbols		Page
Π	force wave amplitude in lb/radian	114
ρ	order of rotor harmonic	39
ρ'	$p\rho$	42
σ	order of stator harmonic	33
σ'	$p\sigma$	42
τ	pole pitch	33
τ_v	volume of airgap	51
τ_t	tooth pitch	58
τ_s	skew	100
Ψ	angle between two consecutive bars in a squirrel cage (measured in electrical radians)	40
ω	circular frequency	32
$\omega_{1\sigma}$	angular velocity of stator harmonic	36
ω_r	angular velocity of rotor	69

INDEX OF SYMBOLS FOR

CHAPTER III

Symbol		Page
A	area of cross section	140
A_1	amplitude of sinusoidally varying quantity	130
A_m	Fourier expansion coefficients	158
a_m	Fourier expansion coefficients	158
B_m	Fourier expansion coefficieht	158
b	subscript denoting bending	142
b_m	Fourier expansion coefficient	158
c	subscript	196
c_r	normalizing constant	
D	rigidity factor	142
d	subscript	195
E	Young's modulus	140
E'	$E/(1-\sigma^2)$	140
F	force	123

Symbol		Page
$F^{(e)}$	external force	123
F_m	elastic constant	160
f	frequency	131
f_m	elastic constant	160
G_m	inertia constant	159
g_m	inertia constant	159
I	subscript denoting inner ring	149
I	moment of inertia	141
i	subscript, summation index	123
j	subscript, summation index	123
K_r	constant to replace summation	195
k_{ij}	coefficient, potential energy	128
l	length	143
M	Bending moment	140
m	mass	123
m	order of mode, m = 2, ...	158
m_{ij}	coefficient in kinetic energy	129
N	normal force	140

Symbol		Page
n	number of particles	124
0	subscript, referring to outer ring	149
P	shear force	145
Q	generalized force	125
q	generalized coordinates	124
R	radius of outer ring	148
$\bar{r}$	radius vector	123
r	radius of inner ring	148
r	subscript referring to ribs	144
r	superscript denotes principal mode	131
r_o	mean radius of arc	138
s	subscript referring to supports	147
s	length of arc	138
T	kinetic energy	127
t	time	
t	subscript denoting extensional deformation	141
U	radial displacement of outer ring	155
u	radial displacement of inner ring	155
V	potential energy	127
V	elastic energy	141

Symbol		Page
W	tangential displacement of outer ring	155
W^e	work of external force	194
w	tangential displacement of inner ring	155
y	normalized eigenvector component	132
z	eigenvector of transformed system	184
θ	angle of position	138
ε	unit elongation	139
$\varkappa$	a constant	146
λ	eigenvalue	171
μ	mass per radian	159
Ψ	phase angle	130
Ψ	rotation of cross section	139
ω	circular frequency	
ζ	a coordinate	138
ξ	a coordinate	138

INDEX OF SYMBOLS FOR

CHAPTER IV

Symbol		Page
a	radius of cylinder	212
b	half width of vibrating belt	212
c	sound velocity	211
$d\sigma$	differential element of surface	209
F(h)	a coefficient function	217
G(h)	coefficient function	218
g(u)	Fourier transform of f(x)	217
$H_m^{(1)}$	Hankel function of order m	216
h	separation constant	213
I	sound pressure integral	219
k	a constant	212
m	order of mode	215
$\vec{n}$	normal	209
n	separation constant	213
P	pressure	210
P_o	static pressure	210

Symbol		Page
p	instantaneous pressure	209
$Q(\theta)$	a separation function	213
$\vec{q}$	velocity	207
$R(r)$	a separation function	213
r	a coordinate	212
s	condensation	208
t	time	212
V	volume	210
w	a variable	233
x	a variable	223
y	a variable	220
$Z(z)$	a separation function	213
Z_n	circular cylinder function	214
z	a coordinate	212
α	a constant	221
β	a constant	221
ΔV	elementary volume	206
ρ	density	207
θ	a coordinate	212
ω	circular frequency	212
η	a constant	221

THE PREDETERMINATION OF MAGNETIC NOISE OF POLYPHASE INDUCTION MOTORS

I. INTRODUCTION

Noise - unwanted sound - has become a serious threat to the well-being of everyone of us. It is with us everywhere and all the time. Although the harmful effects of noise on the well-being and efficiency of office and industrial workers are difficult to assess and there is a conspicuous disagreement among investigators on the psychological and physiological effects of noise, there seems to be, nevertheless, substantial evidence that noise reduction has an overall beneficial effect.

The general opinion seems to be that it should be possible to overcome the noise nuisance of our modern society. Many things of a practical nature have been undertaken to control injurious noises. These endeavors have lately been substantially accelerated by coordinating the efforts of workers in the sound abatement field. The training course on noise control at the University of Michigan in 1952[1], and the special summer program on noise reduction at M.I.T.

---

[1] 46

in 1953, are examples of such concerted endeavors.

Polyphase induction motors of all sizes are frequently producers and radiators of unpleasant noises. It is the aim of this thesis to contribute to the general effort to reduce noise in induction motors by evolving an analytical method for the calculation of the sound pressures in the vicinity of polyphase induction motors because of forced vibration of the motor frame caused by the radial and tangential forces. These result from interfering higher flux harmonics and produce the so-called magnetic noise.

1.1 Historical Review

Early research in the magnetic noise of induction motors has been closely linked with the investigation of other effects of higher harmonic flux waves. W. Stiel[1] systematically investigated the effects of higher harmonic fluxes on the torque-speed characteristic of polyphase induction motors and he was probably the first to recognize the relationship between slot numbers and magnetic noise. He rightly suspected magnetic radial forces were the cause of noise. Stiel also reported the effect of odd

---

[1] 65

rotor slot numbers on magnetic noise but did not give a theoretical explanation of the cause.

Fritze[1] analyzed Stiel's results in 1921 in a theoretical treatment, starting with an analysis of the airgap flux. He discovered that considerable vibration and magnetic noise occur in machines whose airgap flux contain two harmonic fluxes, the pole pairs of which differ by one. He attributed this fact to a resultant one-sided pull and proved that it could only occur in machines with odd numbers of rotor slots. Consequently, he concluded that only machines with odd numbers of rotor slots tend to be noisy.

For a long time Fritze's work formed the foundation for the investigation of the induction-motor noise problem. His opinion regarding odd numbers of rotor slots is still held valid though considered an overstatement, as machines with even slot numbers are also known to be quite noisy and strongly vibrating.

Simultaneously and independently, F. T. Chapman[2] dealt with the same subject, although his paper was not published before 1923. His study is still very valuable as it contains a lucid picture of the physical phenomena

---

1 27

2 18

of the one-sided pull. He used a squirrel-cage motor with five bars in the rotor to demonstrate the resultant dissymmetry, and gave an expression for the frequencies of the noises produced. Furthermore, he calculated the one-sided pull and provided a rule for rotor-slot numbers to be avoided. He clearly pointed out the danger of resonance of the disturbing forces occurring at the motor's critical speed, and in addition provided test results.

The series of papers published by Doherty and Nickle[1] in 1924, and the fundamental work on the performance of squirrel-cage induction motors by L. Dreyfus[2], together with the paper on higher harmonic leakage of induction motors by M. Krondl[3], greatly influenced the subsequent thinking of many designers. The attack on induction-motor problems became more general.L.E. Hildebrand[4] was the first to stop concentrating on the one-sided pull caused by an eccentric force wave and prescribed a more general treatment. His study was based on the noise test of some 1500 motors of 200 different designs and ratings, ranging from 1/4 to 15 horsepower.

Hildebrand clearly recognized the fact that a

---

1 22
2 23
3 42
4 34

motor is a source of sound because some parts of it are moved by periodically varying forces. He concluded that the detailed study of induction motor noise should include an exact investigation of the parts prone to vibrate and the forces moving them. It is unfortunate that he did not carry out such an analysis.

According to Hildebrand the noise producing components of induction motors can vibrate in many ways. A torsional vibration of the stator and rotor as a whole results from periodic torque variations. The noise may also result from a circular vibration, similar to a dynamically unbalanced rotor; this is caused by the previously mentioned one-sided pull. The stator, Hildebrand found, may also be distorted into a rotating elliptical shape. Or, if the forces are balanced in more than two radii, the stator may be deflected in the shape of a rotating polygon.

Hildebrand's study was of great importance for the fact that he put more emphasis on the effects of different factors on the field than on considerations of the field itself. He concluded that the field in the airgap and the noise of an induction motor depend on the stator and rotor winding arrangements, on eccentricities, and on saturation. He therefore strongly recommended even and concentric gaps and windings which would eliminate fields differing by one

or two pole pairs. He claimed that a motor would be quieter if the number of poles, stator slots, rotor slots, and winding repetitions bore simple relationships, and the larger the common divisor of these factors the quieter the motor would be. We cannot nowadays accept all of Hildebrand's conclusions without reservations. However, the fact that he only considered the first slot harmonics as dangerous, together with his belief that most common noise frequencies were exactly or nearly twice the applied frequency, proved his reasoning erroneous.

M. Krondl[1] in a general treatise gave a very thorough discussion on the different causes of parasitic forces in the airgap of induction motors, grouping them into radial and tangential components. He describes the effects of the radial and tangential components of these forces as: synchronous and asynchronous torques, periodic deformations of the stator core, and vibrations of constructional parts. According to Krondl the last two produce the magnetic noise. It was the aim of his paper to give useful and guiding principles for the design of induction motors and fundamental data for further experimental investigation. This paper was of great importance in the analysis of the noise problem since it was the first to discuss the mechanical vibrations and the acoustical aspect of the problem. His conclusions

---

[1] 43

about some sound-producing vibrations and the individual subjective sensitivity of the ear have thrown a new light on the problem of slot-number combinations. Krondl seems also to have been the first actually to have measured sound pressures rather than to have confined himself to a mere description of subjective impressions. It was he who also warned against the application of experimental data obtained from small motors to the problems of the noise in large machines.

One of the several difficulties in the development of noise theory during these early years was the lack of agreement on acoustical definitions and on sound measuring techniques and standards. The American Institute of Electrical Engineers took the initiative in starting discussions as early as 1930[1]. Stimulated by these discussions, the American Standards Association set up a technical committee to establish standards for the description of noise, and to suggest fundamental measuring methods to determine the loudness of any noise. The preliminary standards of 1935 have greatly influenced the further development of the noise theory.

At a meeting of the C.I.G.R.E. in 1933, it was again Krondl[2] who contributed to the progress of the theory,

---

[1] 76

[2] 44

when reporting on the noise problem of electrical machinery, reviewing his previous findings, and discussing the sound propagation of electrical machines.

At the same time G. Kron[1] tried again to derive certain rules for the number of slots. He ascribed the noise mainly to the deviations of the airgap from its average value caused by the slots. The importance of his paper lies, in addition to the explanation of hooks in the speed-torque curves, in the clever method of calculation which served as model for the further development of the theory. Morril's[2] paper was noted for its clear presentation of the problem, and for providing a well organized method for the calculation of the frequency of the force waves. The subject of subharmonic waves for the rare case where the number of squirrel-cage bars is small has also been treated in this paper. J.S. Gault[2] also published a detailed study of the current wave-shapes in rotor bars resulting from voltages induced by higher harmonic fluxes. The lucid presentation helped designers to visualize the composition of the airgap field.

The numerous contradictory individual experiences, and particularly test results proving that different machines with the same slot numbers produced different

---

1 41

2 52

3 28

magnetic noise, firmly convinced various designers that the statement of the noise problem in the light of slot numbers alone was incomplete. They found that the problem became entirely different when machines of different ratings were considered; e.g., a slot number combination yielding excellent results in small machines showed poor results in medium-sized motors. Consequently, they realized that the concept of most opportune slot numbers makes sense only for a definite type of motor.

These observations are proof that there are no magic prescriptions for the choice of slot numbers, and that the noise problem is not just an electro-magnetic one but also one of engineering mechanics and acoustics.

The first to visualize the problem in its entirety was P. L. Alger, whose pioneering efforts in the conquest of the noise frontier are still leading the way for many designers. According to his theories the induction motor, as regards its mechanical vibrations, can be represented as a simple inextensional ring, and the motor's natural behavior can therefore be approximately described by the behavior of this equivalent ring. Alger provides formulae for the calculation of the resonant frequencies of induction-motor frames, based on simple beam theory.

---

[1] 2;3

In addition to the calculation of natural frequencies, methods for calculating static deflections are given, but no extensive treatment to determine dynamic deflections at forced vibrations is provided. Alger arrived at these simple results by further assuming that the stator teeth and windings add only to the inertia forces and not to the rigidity of the structure. These last assumptions are justifiable, while the simple ring concept could be disputed. However, the first step is always the most difficult.

For the acoustic behavior of the motor, Alger chose to represent the motor by an infinitely long vibrating cylinder. He provided very valuable formulae for the designer, and in addition, curves of sound intensities on the cylindrical surface caused by different modes of vibration and correction curves for sound intensities at a distance from the induction motor.

The importance and influence of Alger's theories can hardly be overstated. The simplified theory demonstrates clearly how the different parameters affect the noise behavior of the induction motor. From his work it becomes obvious that the most effective remedy against noise is to prevent large radial deflections of the stator by stiffening it in medium-sized machines, and preventing certain modes of vibrations near resonance in larger machines.

H. Jordan[1] in Germany simultaneously investigated the noise problem of induction motors. His simplifying concepts resemble those of Alger. Jordan develops his formulae from a partial differential equation. The acoustic behavior of the motor is approximated by a radiating sphere, and he uses Gauss' theorem to determine the sound power level at a distance from the motor.

1.2 The Nature of Induction Motor Noise.

The sound of machinery noise may be that of unpitched or of pitched noise. The unpitched noise has a more or less uniform amplitude in a broad band of nearly continuous frequency distribution. It can be traced to recurring transient disturbances. Pitched noise, on the other hand, is of a distinct frequency generally related to the operation of the machine, and the frequency of the pitched noise changes with operating conditions. As nearly all noise produced by induction motors results from forces of definite frequencies, most of the noise is pitched noise of either mechanical, aerodynamical or electromagnetic origin.

Ball bearing noise is the most prominent among those attributable to mechanical causes. Continually occurring disturbances, resulting from the play of clearances in ball bearings, excite oscillations that tend to vibrate the motor. These vibrations may become more pronounced by mechanical

---

[1] 36;37

unbalance of the rotor, by an eccentric airgap, or by resonance of either the motor endshield or by any parts of the bearing supports. The same causes, to a smaller extent, may also be responsible for noise in sleeve bearings. Bearing noises can be controlled by appropriately designed bearing supports, good alignment, properly chosen shaft designs, and by bearings carefully manufactured to exact specifications.

Aerodynamic noise can be classified into two major groups: windage noises and the siren noises. The first are caused by fans, used to move the cooling air over rotor and stator surfaces. The frequency and amplitude of these noises depend on the number and shape of ventilator blades and on motor speed. Siren effects occur in motors when radial airducts are being used in both rotor and stator, and the number of rotor and stator slots differ by a small amount. The periodic, high-frequency interruptions of the radial airstream by the stator coils crossing the ducts occur nearly in time phase, thus causing a high-pitched noise. A pounding and cutting noise can be observed in induction motors when the high-velocity cooling air flows past a sharp edge, or when a sudden change occurs in the airflow cross-sections.

Noises of electromagnetic origin appear at different frequency ranges, depending on the origin of the

driving forces. The double-frequency noise is excited by the main airgap field. The magnetic field in the airgap rotates synchronously, and as a consequence the flux density at a fixed point in the airgap varies as a sinusoidal function of time. Owing to the change in the stored electromagnetic energy at that point, a radial force of double frequency, with a tendency to mutually attract stator and rotor, is created. The distribution of this force in the airgap has a constant component, and a sinusoidal component having twice as many pairs of poles as the original field. This latter force periodically deforms the stator into the shape of a rotating polygon, and therefore excites the vibration of the stator core. The forced vibrations of the stator core are transmitted to the outer frame by structural parts, connecting the stator to the frame, which in turn vibrate and radiate sound waves from its surface to the surrounding air: the so-called airborne noise.

This double-frequency noise is unavoidable, as the machine could not function without the main flux. It appears as the characteristic humming sound of induction motors. It is harmless in small or medium-sized machines with more than one pole pair. The deflections are not too large, as the resonant frequencies of the stator are generally much higher than the double supply frequency.

For large two-pole motors, where the double supply-frequency force wave has only two pole pairs, the vibrations may become very vigorous and the noise bothersome. In this case the problem is very similar to that of the vibration of turbine generators[1]. The only remedy to be applied is a stiffening of the outer structure of the motor. This double supply-frequency vibration may also become a problem in small 400 c.p.s aircraft equipment.

A component of the torque of polyphase induction machines working with unbalanced voltages pulsates with double supply-frequency and small changes of rotor speed occur. These pulsating torques may cause structural vibrations, directly transmitted to the foundations through the motor supports, and may excite noise-making resonances elsewhere. This noise, called the torque noise, is very pronounced in single-phase induction motors. Furthermore, the higher harmonics in the airgap, as described below, may cause oscillating higher-harmonic torques at frequencies well in the audio-range more awkward than the double supply-frequency torque noise.

The most troublesome noise of electromagnetic origin, the so-called magnetic noise, can be traced to radial and - in a much smaller measure - to tangential forces which

---

[1] 10

occur when the airgap flux contains two harmonic fluxes with pole pairs differing by a small integer. This noise generally contains several, almost pure, whistling tones of high amplitudes.

The higher harmonic fluxes in the airgap are practically unavoidable and inherent in the design of induction motors. The winding distribution introduces the so-called space harmonics, to be classified as slot- and as belt- harmonics. While the former result from the fact that each phase belt contains a limited number of slots, belt harmonics are caused by the limited number of phases. To wit, if a motor with an infinite number of phases and an infinite number of slots per phase could be designed, no such harmonics would occur. The amplitude of these space harmonics depends on the load current, and the noise caused by them increases with the load current.

The non-uniform permeance of the airgap caused by the open or semi-open slots of the stator creates a whole sequence of harmonics, the so-called permeance harmonics. The order of these and their frequency distribution are the same as those of the above-mentioned slot harmonics. The magnitude of the permeance harmonics depends on the supply voltage and is independent of the load current. These

permeance harmonics are mainly responsible for the so-called no-load noise.

There are two other major causes of such higher harmonic fluxes; i.e., an eccentric airgap, and the saturation of teeth.

The radial and tangential forces set the core into vibration, similar to the vibration previously described at the double supply frequency. Though the polepitch of the higher harmonic fluxes is small and the radial and tangential force distribution may consist of two complete sine waves only, marked deflections may yet occur in response to small radial forces. The frequency of these forces is considerably higher than the double supply frequency. The noise caused by these force waves is generally in the frequency range of 500 to 3,000 c.p.s., i.e., in a range where the human ear is most sensitive, which makes this noise all the more irritating. This thesis is actually intended to deal with the noise created by these radial forces.

For the sake of completeness, mention should be made of the magnetostriction noise. Steel, when magnetized, expands along the axis of magnetization. The expansion depends not only on the magnetic properties of the steel, but also on flux density, and is linearly proportional to

the length of the flux path. This flux path in the core is mostly circular, so that periodic variations of the length are taking place along concentric circles. While some parts of the core tend to expand, adjacent parts would contract, so that the average total circumference of the stator ring remains unchanged. The tangential deflections are extremely small, and magnetostriction is therefore not considered a noise producing factor in induction motors.

1.3 The Single-Ring Theory

It becomes clear from the historical review that continuous attention has been given in the last decades to the reduction of the magnetic vibrations and to noise of electrical machines. Before proceeding further it seems appropriate to discuss first the methods employed to date in the endeavor to build quiet machines, together with the shortcomings of each method.

The determining factor in the approach to the solution of the noise problem was generally the rating and size of the machine in question.

In the case of small induction motors, usually manufactured in large numbers, it is costumary to construct, test, and improve prototype machines before undertaking quantity production. In this case the selection of an

appropriate slot number is considered the crux of the problem.

Until recent years, purchasers of very large machines paid little or no attention to the noise problem, but at present they insist upon quiet operation. The structure of these machines is more or less regular, and the experience with large generators is being used by the designers of motors of several thousand horsepower ratings because the problem of large motors resembles the problem of synchronous generators. Pilot models in such sizes are prohibitive.

It has been suggested that full-size replicas of a representative stator section with only a fraction of the length of the machine[1] be constructed. Such a frame section would then be tested by means of mechanical shakers and the natural behavior of the frame studied. Such models, relatively expensive, require undue use of production facilities, and are of practical use only for two- to four-pole machines.

Models of large rotating machines scaled down to approximately 1/10 size have been used under laboratory conditions for quite some time. Using dimensional analysis, the dynamic behavior of the full-size machines could be predicted by these models. To construct such models from

---

[1] 10

steel has the disadvantage of the resulting frequencies being too high for reliable measurement and correlation. Plastic models have been suggested and tried, and replicas constructed that were scaled down to 1/4 - 1/8 of the original machine. These models performed well and their stability with temperature, humidity, time, and frequency proved satisfactory.

However, the above methods used for small and large machines become impracticable for medium induction motors. As mentioned before, the approach to these has been developed by P. L. Alger[1]. The slot combination still remains the nucleus of the problem. The mechanical behavior of the built-up core is assumed to be the decisive factor. The design is based on the performance of this stator core and proper corrections made for the inertia forces of the teeth and windings. The method of noise calculation based on Alger's theories will in this thesis be referred to as the "single-ring theory". This method assumes that the stiffening effect of the frame could be neglected, an assumption which could, with reservations, be accepted for very small motors, but is not justified for medium size induction motors. Thus it can be regarded as the Achilles heel of the single-ring theory. It is hoped that the following discussion will not be construed as

---

[1] 2;3

destructively critical, as the author fully recognizes the great importance and value of the single-ring theory in the present stage of noise prediction.

The mechanical structure of an induction motor stator is schematically shown in fig. 3.3.1. The frame, which in the following discussion will be referred to as outer ring, is strongly coupled to the stator core - which in turn will be referred to as inner ring. The natural frequencies of such a structure will differ considerably from the frequencies of the inner ring vibrating alone. Furthermore, the inner ring - when considered inextensional - has but one natural frequency in each mode[1], while a structure as shown in fig. 3.3.1 will have several important resonant frequencies for each mode of vibration. All these resonant frequencies must be considered if the best slot combination is to be selected to arrange mismatch between the natural frequencies of the frame and the frequencies of the driving electromagnetic forces.

The main aim of the vibration analysis of the induction motor structure is to find its natural behavior and the dynamic response to impressed force waves. According to the single-ring theory - assuming a constant amplitude force wave - the deflections would gradually increase

---

[1] The term mode denotes the number of complete periods of a sinusoidally distributed quantity along the periphery of the stator bore.

with frequency until resonance is reached and beyond this dangerous point they would strongly attenuate as illustrated in fig. 1.1. Fig. 1.2 shows the behavior of the structure consisting of two rings and connected by radial ribs mounted on a support. The amplitude becomes very large at several points of the frequency range, a fact that cannot be explained by the single-ring theory.

Unfortunately this is not the only objection to the single-ring theory. It can be verified that the sound waves radiated by the stator core are strongly attenuated by the outer ring. If the frame totally encloses the stator core, the attenuation may be of the order of 40 decibels. It therefore becomes obvious that the major part of the magnetic noise is caused by the vibration of the outer ring, a fact not accounted for by the single-ring theory.

The following argument may illustrate the reasoning still more distinctly. Let us assume that identical stator cores and rotors are fitted into frames of different designs. According to the single-ring theory, the noise of all these induction motors would be the same. Simple tests would, however, demonstrate that this is not the case, and that the acoustic behavior of the motors in different frames will vary considerably.

If the natural frequencies of small induction

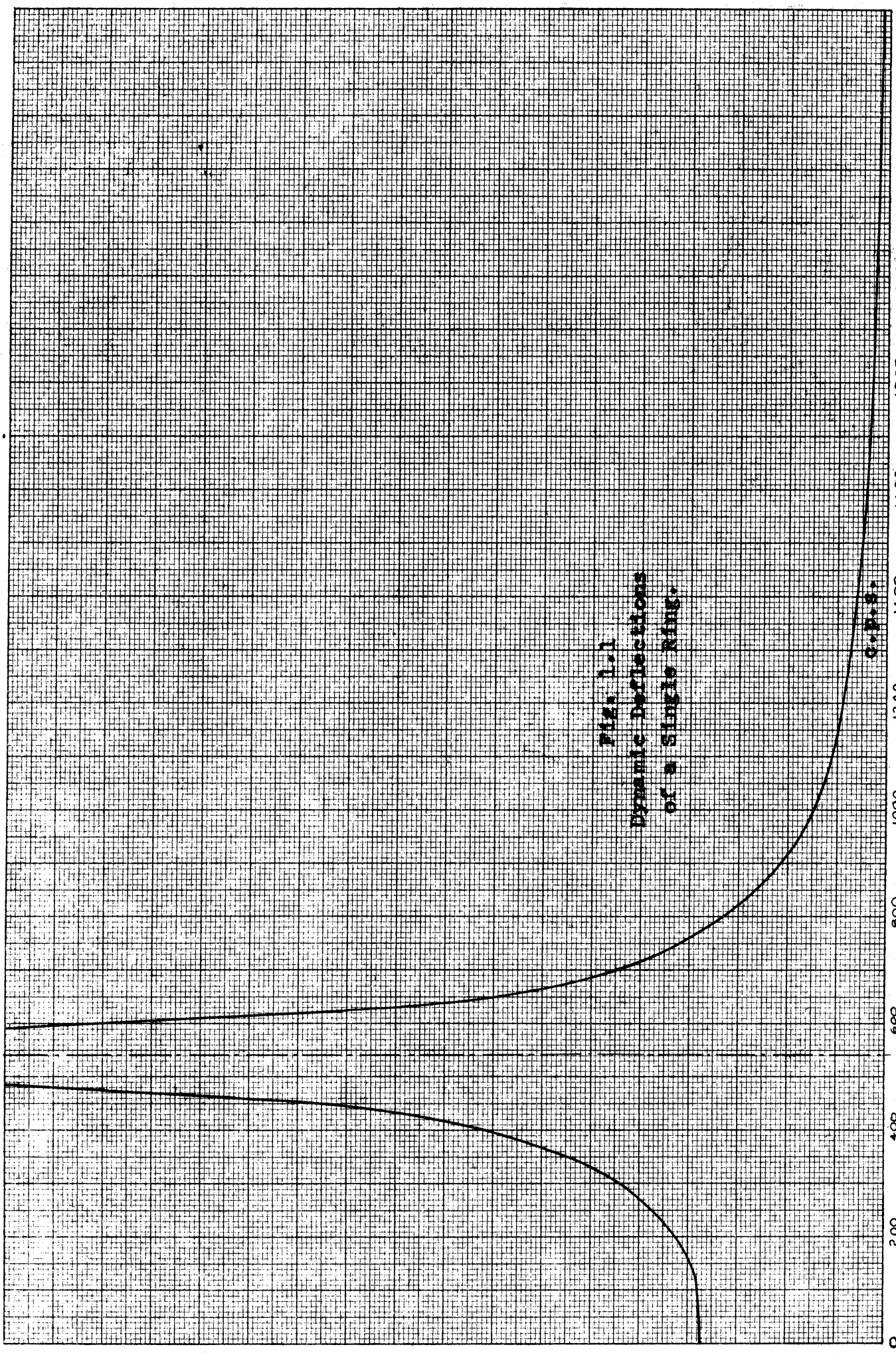

Fig. 1.1
Dynamic Deflections
of a single Ring.

motors with a small number of pole pairs are computed in accordance with the single-ring theory one cannot help feeling surprised on finding that the low mode frequencies agree quite well with test results. This may be explained by the fact that the flexural rigidity and the mass of the inner ring are large compared to those of the outer ring.

In medium induction motors the flexural rigidities and masses of the outer and the inner ring are of the same order of magnitude, and the influence of the outer ring on the complete structure vibrating as a system can not be ignored. In large multipole induction motors the flexural rigidity and the mass of the frame become larger than those of the core and will thus greatly influence the natural behavior of the induction motor structure.

1.4 The Statement of the Problem.

The purpose of this thesis is to extend the work started by P. L. Alger, and to put the predetermination of magnetic noise of polyphase induction motors on a sound theoretical basis. As the task is arduous and the complexity of the problem considerable, it often seemed presumptuous to the author to have undertaken this analysis.

As mentioned on page 20 and outlined in chapter 3,

there are several resonances for each motor vibration and the designer is therefore faced with the problem of selecting slot combinations so as to avoid all these resonances. The difficulty of his task is still further increased by other considerations to be taken into account in the design of induction motors. The designer is called upon not only to design quiet motors but also to avoid higher harmonic torques which reduce starting torque; or higher harmonic flux losses which decrease the efficiency of the machines. He may have to choose a slot combination which will create force waves of a small number of pole pairs. In such cases it is of great advantage to calculate the magnetic noise of the induction motor in advance.

The analysis as presented here involves three disciplines of physical science and is consequently treated in three different sections.

First an analysis of the electromagnetic conditions in the airgap is developed to enable the designer to calculate the frequency, mode, and amplitude of the force waves acting on the components of the motor. The influence of saturation, eccentricity of airgap, skewing, and of uninsulated squirrel-cage bars is also described.

In the following section, the vibrational aspect of the problem is given in treating the induction motor as

a continuous system, represented by two coupled concentric rings on a support. A method to find the natural frequencies in different modes of vibration, based on the Lagrangian equation of motion is evolved. Finally it is described how to calculate the response of the system previously determined.

In the chapter on the acoustic problem, the wave equation for the sound pressures near the frame has been solved. Here the motor is replaced by an infinitely long cylinder vibrating in a belt only. The theory is illustrated in each instance by an analysis of a medium-sized, polyphase induction motor. Design and electrical data of the motor are recorded in Appendix I. The experimental evidence at the end of this thesis is presented to verify the detailed theory.

The question of why this problem had not been attacked before may arise in the reader's mind, and the following comments may serve as a reply:

Fig. 1.3 shows a few representative samples of induction motor frames of modern design. The acoustic behavior of each of these frames with identical electrical designs must be computed individually. Considering the large number of frame sizes in each design and the different core and rotor combinations in each frame, the task of

treating all of this seems tremendous. Designers in need of quickly obtainable approximate answers were reluctant to attack this extremely complex problem, particularly at a time when noise suppression was not the critical problem it has since become.

Another answer may be found in the fact that the computational difficulties connected with the solution of the problem had been beyond the range of facilities available until recently. To solve the matrices of chapter 3 for eigenvalues with the aid of a desk computer might have taken many months, while eigenvalues and eigenvectors of the same matrices can nowadays be calculated with advanced electronic computers in a fraction of an hour. The present analysis could never have been performed without highly advanced computing facilities.

It has been the author's conviction that a solution to the present problem could be found. It likewise seemed apparent that the solution of the problem could be general in principle, but that each system must be individually analyzed, owing to the many factors that play a part in the overall production of noise. While the task is somewhat simplified in the case of induction motors belonging to a particular series, because of the numerous similarities in their design, it does not

always follow that fundamental differences within the series do not exist. In many cases, however, it might be possible to establish a single solution that is applicable to a complete line of induction motors.

II. THE ELECTROMAGNETIC FORCE WAVES IN THE AIRGAP

In this chapter a mathematical expression is developed for the distribution of the radial magnetic induction in the airgap of polyphase induction motors, as a function of position and time. This is pre-requisite to the calculation of mode, magnitude and frequency of the radial and tangential force waves in the airgap.

The radial magnetic induction in the airgap will be assumed as proportional to the magnetomotive potential difference radially across the airgap. The influence of the variable permeance that results from open slots of the stator is also considered. To simplify the writing of the text, the distribution of the magnetomotive force plotted along the airgap will be referred to as the "MMF" distribution.

In accordance with current practices the following assumptions will be made: (1) the stator contains a symmetrical, 3-phase, double-layer winding with 60° phase belts and a whole number of slots per pole per phase; (2) the stator coils may have widths shorter than a pole-pitch; (3) the rotor is fitted with a squirrel cage winding; (4) the airgap is concentric; (5) the stator has semi-closed slots and the rotor, fully-closed slots; and

(6) the supply voltages are sinusoidal and balanced.

The principle of superposition is very freely applied to combine field quantities; i.e., unsaturated machines and simplified permeance conditions are assumed in order to bring the mathematical formulation of the theory into a reasonably manageable form. It is not unusual to resort to this artifice in the solution of complicated induction motor problems.

The effects of saturation, eccentric airgap, skewing and bar cross-currents will be discussed at the end of the chapter.

2.1 The MMF Distribution in the Airgap due to Stator Currents

If the polyphase induction motor is connected to a balanced polyphase supply, the fundamental component of the phase currents in the stator may be expressed as,

(2.1.1) $$i_u = \sqrt{2}\, I_1 \sin[\, \omega t - (u\, 2\pi/m)\,] \text{ amp},$$

where

i_u is the instantaneous value of the fundamental component of the current at time t in the u^{th} phase; u = 0 for the reference phase.

I_1 is the r.m.s. value of the phase current

ω is the circular frequency

m is number of phases

Fig. 2.1.1 shows a schematic diagram of the phasebelt location in a polyphase induction motor.

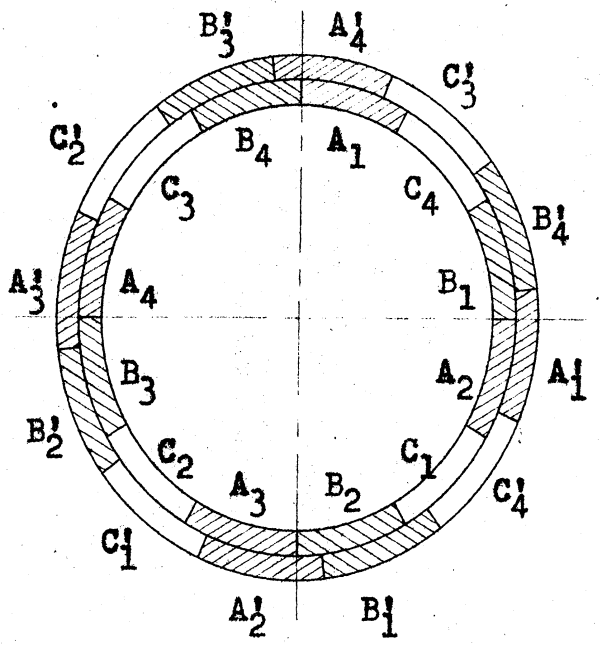

Fig. 2.1.1

Phasebelts of an Induction Motor

The MMF distribution of a single phase of a polyphase winding is a pulsating stepwave. This wave is a periodic function and may be represented by a Fourier series,

$$(2.1.2) \quad f^I(x_1,t)=\sum M^I_\sigma \sin \omega t \cos (\sigma \pi x_1/\tau) \text{ amp},$$

(2.1.3) $M_\sigma^I = (2\sqrt{2}/\pi) \cdot (w_1 k_\sigma / p)\ I_1$ amp.

The symbols in the above equation denote

$f^I(x_1,t)$ the value of the MMF distribution at point x_1 at time t; $x_1 = 0$ at the axis of the reference phase.

σ is the harmonic order of a component of the stator MMF distribution.

M_σ^I is the amplitude of the σ^{th} harmonic of the MMF distribution wave of one phase at time $t = \pi/2\omega$

w_1 is the number of turns in series per phase in the stator

k_σ is the winding factor of the σ^{th} harmonic, $k_\sigma = k_{d\sigma} \cdot k_{p\sigma}$, where

$k_{d\sigma}$ is distribution factor of the σ^{th} harmonic

$k_{p\sigma}$ is pitch factor of the σ^{th} harmonic

p is number of pole pairs

τ is pole pitch in meters

Although the stator windings of polyphase motors have three phases, the analysis is carried out for an m-phase winding, to have more general results also valid for squirrel cage windings.

The angle between two consecutive phase axes of the

symmetrical m-phase winding illustrated in fig. 2.1.1, will be $2\pi/pm$ mechanical radians or $2\pi/m$ electrical radians. The currents in consecutive phases have a time lag of $2\pi/m$ radians. The σ^{th} harmonic of the MMF wave of the u^{th} phase is therefore displaced in the direction of the phase sequence from the σ^{th} harmonic of the reference phase by $2\sigma\pi u/m$ electrical radians. The current i_u of the u^{th} phase lags the current of the reference phase by $2\pi u/m$ radians, so that the expression for the σ^{th} MMF wave harmonic of the u^{th} phase can be written,

$$(2.1.4) \quad f^I_{\sigma u}(x_1,t) = M^I_\sigma \sin(\omega t - 2\pi u/m).\cos[(\sigma\pi x_1/\tau) - (2\pi\sigma u/m)]$$

Applying the relation

$$2 \sin x. \cos y = \sin(x+y) + \sin(x-y),$$

equation 2.1.4 can be expressed as

$$f^I_{\sigma u}(x_1,t) = (1/2)M^I_\sigma \left(\sin\left[[\omega t - (\sigma\pi x_1/\tau)] + (\sigma-1)(2\pi u/m)\right]\right) +$$

$$(2.1.5) \qquad + (1/2)M^I_\sigma \left(\sin\left[[\omega t + (\sigma\pi x_1/\tau)] - (\sigma+1)(2\pi u/m)\right]\right)$$

For negative values of σ the first term in the bracket of 2.1.5 has the same value as the second term for positive values of σ, and equations can be rewritten simply as

$$(2.1.6) \quad f^I_{\sigma u}(x_1,t) = (1/2)M^I_\sigma \sin[\omega t - (\sigma\pi x_1/\tau) + (\sigma-1)(2\pi u/m)]$$

The MMF distribution of the σ^{th} harmonic resulting from all m phases will be,

$$f_\sigma(x_1,t) = (1/2)M_\sigma^I \sum_{u=0}^{u=m-1} \sin\left[\omega t-(\sigma\pi x_1/\tau)\right]+(\sigma-1)(2\pi u/m)\Big)$$

$$= (1/2)M_\sigma^I \sin[\omega t-(\sigma\pi x_1/\tau)] \sum_{u=0}^{u=m-1} \cos[(\sigma-1)(2\pi u/m)]+$$

(2.1.7)

$$+ (1/2)M_\sigma^I \cos[\omega t-(\sigma\pi x_1/\tau)] \sum_{u=0}^{u=m-1} \sin[(\sigma-1)(2\pi u/m)]$$

The expressions behind the summation signs of equation 2.1.7 mostly equal zero, as they represent the sum of m-vectors in which consecutive vectors are displaced by $(\sigma-1)(2\pi/m)$ radians. However, the sums will not become zero when all m-vectors are in phase; i.e., when

$$(\sigma-1)(2\pi/m) = c_1 \cdot 2\pi$$

or only for the values of σ which satisfy the condition

(2.1.8) $$\sigma = c_1 m + 1$$

where c_1 is a constant, which may be any positive or negative integer or zero. Balanced 60 degree, 3-phase windings do not generate any even harmonics, or harmonics whose order number is divisible by three. The constant c_1 for these windings must therefore be an even whole number, positive or negative, including zero. With this restriction, the sum of the sines in equation 2.1.7 will become zero, while the sum of the cosines will become m. Hence,

(2.1.9) $f_\sigma(x_1,t) = M_\sigma \sin[\omega t-(\sigma\pi x_1/\tau)]$ amp.,,

where

(2.1.10) $M_\sigma = (1/2)\ m\ M_\sigma^I = (\sqrt{2}mw_1k_\sigma I_1/\pi p\sigma)$ amp.

The direction of rotation and the velocity of the higher harmonics of the MMF distribution may be calculated by assuming that

$$\omega t - (\sigma\pi x_1/\tau) = \text{constant},$$

and then differentiating this expression with respect to the variable t. The mechanical velocity $v_{1\sigma}$ of the σ^{th} harmonic of the stator is,

(2.1.11) $v_{1\sigma} = (dx_1/dt) = (\omega t/\sigma\pi)$ meter per second

measured on the stator bore. The velocity of the fundamental stator MMF distribution v_s is

$$v_s = (2\pi f\tau/\pi) = 2f\tau \quad \text{meter per second}$$

so that the velocity of a harmonic of the MMF distribution can be simply expressed as,

$$v_{1\sigma} = v_s/\sigma \quad \text{meter per second.}$$

The angular velocity of any stator harmonic will be,

(2.1.12) $\omega_{1o} = \omega_1/\sigma$ radians per second.

For negative values of the constant c_1, σ will be negative and so will be the velocity of the wave. This is explained by the fact that the direction of rotation of the harmonic is opposite to the phase sequence; i.e.,

opposite to the direction of rotation of the fundamental MMF distribution.

In future considerations the greatest noise producing harmonics will be found to be the so-called slot-harmonics which satisfy the equation,

(2.1.13) $\sigma_s = c_1 q_1 m + 1,$

where q_1 is the number of slots per pole per phase. Denoting with Q_1 the total number of slots in the stator, the relation 2.1.13 can be rewritten as,

(2.1.14) $\sigma_s = (c_{1s} Q_1/p) + 1,$

where c_{1s} is a constant: any positive or negative integer except zero.

The amplitude of the fundamental component of the MMF wave of a distributed winding is reduced by a few per cent only as compared with a concentrated winding. This is because the winding factor is a number only slightly below unity. The winding factor of the belt harmonics is, by contrast, a small fraction, and the amplitude of these is therefore considerably reduced. A simple evaluation would verify that the winding factor of the slot harmonics equals that of the fundamental MMF wave and their amplitudes will consequently be reduced by the same small percentage as that of the fundamental.

2.2 MMF Distribution of the Squirrel Cage Rotor[1]

Before considering this topic it seems appropriate to calculate the frequency of the currents induced in the rotor by the airgap fluxes that result from higher harmonic components of the stator MMF distribution. For this purpose the stator MMF distribution is first related to the rotor periphery.

Let at instant $t = 0$, point $x_1 = 0$ of the stator coincide with a point $x_2 = 0$ on the rotor. Let the slip of the rotor be,

(2.2.1) $s = (n_s - n)/n_s$,

where,

n_s is synchronous speed of the stator fundamental MMF distribution in r.p.s., and

n is speed of the rotor in r.p.s.

The mechanical speed of the rotor will be

(2.2.2) $2f\tau(1-s)$,

and the position x of the rotor point x_2 at time t will be,

(2.2.3) $x_2(t) = x_1 - 2f\tau(1-s)t$

$$x_2(t) = x_1 - [\omega\tau(1-s)\,t/\pi]$$

or

$$x_1 = x_2(t) + [\omega\tau(1-s)t/\pi]$$

---

1 23;2

In the following discussion $x_2(t)$ will be simply written as x_2.

Introducing equation 2.2.3 into equation 2.1.9 the expression for the MMF distribution will become

(2.2.4) $$f_\sigma(x_2,t) = M_\sigma \sin\left([1-\sigma(1-s)]\omega t - (\sigma\pi x_2/\tau)\right)$$

On introducing

(2.2.5) $$s_\sigma = 1 - \sigma(1-s)$$

equation 2.2.4 can be written as,

(2.2.6) $$f_\sigma(x_2,t) = M_\sigma \sin[s_\sigma\omega t - (\sigma\pi x_2/\tau)]$$

The velocity of the stator harmonic in respect to the rotor will therefore be,

(2.2.7) $$v_{2\sigma} = (dx_2/dt) = s_\sigma v_s/\sigma$$

After this short explanation, expressions for the rotor MMF can be developed.

Consider next the most general case, i.e., that of the ρ harmonic of the rotor wave, induced by the σ^{th} harmonic of the stator. The instantaneous value of the rotor current for this case can be written as,

(2.2.8) $$i_{2\sigma} = \sqrt{2}\, I_{2\sigma} \sin(s_\sigma\omega t)$$

If Q_2 represents the total number of bars in the squirrel cage the angle between two consecutive bars

measured in electrical radians will be $\Psi = (2\pi p/Q_2)$. The ρ^{th} harmonic of the h^{th} bar will be displaced from the ρ^{th} harmonic of the reference bar by $(2\pi ph/Q_2)\rho$ radians. The phase angle of the currents of two consecutive bars will differ by $(2\pi p\sigma/Q_2)$ radians, hence the current in the h^{th} bar will lag the current in the reference bar by $(2\pi\sigma h/Q_2)$ radians.

In a manner analogous to equation 2.1.4 it may be written that,

$$(2.2.9)\quad f_\rho^I(x_2,t)_h = M_\rho^I \sin\left[s_\sigma\omega t - (2\pi p\sigma h/Q_2)\right] \cdot \cos\left[(\rho\pi x_2/\tau) - (2pp\pi/Q_2)h\right]$$

where,

$$(2.2.9a)\qquad M_\rho^I = (\sqrt{2}I_{2\sigma}Q_2/p\pi\rho)$$

Using the same transformation as before, equation 2.2.9 can be expressed as,

$$(2.2.10)\quad f_\rho^I(x_2,t)_h = M_\rho^I \sin\left(\left[s_\sigma\omega t-(\rho\pi x_2/\tau)+p(\rho-\sigma)(2\pi h/Q_2)\right]\right)$$

Once again the MMF distribution of all Q_2 bars may be added and an expression similar to 2.1.7 can be obtained. The sum of the terms containing the sines will again become zero, while the terms containing the cosines will not become zero if the following condition is fulfilled:

$$(2.2.11)\quad 2\pi p(\rho-\sigma)/Q_2 = 2\pi c_2$$

The constant c_2 may be any positive or negative integer

including zero. The harmonic order of the rotor MMF distribution components will satisfy the condition,

(2.2.12) $\rho = (c_2 Q_2/p) + \sigma$

The ρ^{th} harmonic of the MMF distribution resulting from the current in all Q_2 bars will be

(2.2.13) $f_\rho (x_2,t) = M_\rho \sin [s_\sigma \omega t - (\rho \pi x_2/\tau)]$

where,

(2.2.14) $M_\rho = (\sqrt{2}\, Q_2 I_{2\rho} / 2\pi p \rho)$

These equations are based on the hypothesis that a squirrel cage winding can be represented as polyphase winding with Q_2 phases, each phase consisting of half a turn. The distribution and pitch factors - that is, the winding factors of all rotor MMF harmonics - will be one.

An inspection of 2.2.12 suggests that the harmonic order ρ of the rotor MMF distribution component may have fractional values. To avoid these unconventional fractional harmonic order numbers in the Fourier series of the MMF distribution, it became customary to regard the whole circumference of the airgap as the fundamental period of the MMF distribution wave in lieu of the usual double pole pitch. The fundamental of the MMF wave based on the double pole pitch period will now become the p^{th} harmonic of the MMF distribution based on the total circumference

as a period. To avoid misunderstandings, the fundamental of the double pole pitch period will in future be referred to as the main wave. Based on the new convention, all previous harmonics have to be multiplied by p and will be denoted with a prime. Equation 2.2.12 can be expressed as

(2.2.12a) $\rho' = c_2 Q_2 + \sigma'$

where,

$$\sigma' = p\sigma \quad \text{and} \quad \rho' = p\rho$$

Equations 2.2.5, 2.2.13, and 2.2.14 can now be rewritten as,

(2.2.5a) $s_{\sigma'} = 1-(\sigma'/p)(1-s)$

(2.2.13a) $f_{\rho'}(x_2,t) = M_{\rho'} \sin [\, s_{\sigma'}\omega t - (\rho' \pi x_2/p\tau) \,]$

(2.2.14a) $M_{\rho'} = \sqrt{2}\, Q_2\, I_{2\sigma'}/2\pi\rho'$

The velocity of a harmonic of the rotor MMF distribution in respect to the rotor can be calculated by the same method as in 2.1.11, and results in

(2.2.15) $v_{2\rho} = (dx_2/dt = [\, s_\sigma \tau\omega/\rho\pi \,] =$

$= (1/\rho)\, [\, 1-\sigma(1-s) \,]\, v_s$

(2.2.15a) $v_{2\rho'} = (p/\rho')\, [\, 1 - (\sigma'/p)(1-s) \,]\, v_s$

Introducing into 2.2.13 the value of x_2 as given in 2.2.2, an expression of the σ^{th} harmonic of the rotor MMF distribution as a function of x_1 can be

obtained:

$$(2.2.16)\quad f_\rho(x_1,t) = M_\rho \sin\left(\left[1+ (\rho-\sigma)(1-s)\right] \omega t-(\rho\pi x_1/\tau) \right) \text{ or}$$

$$(2.2.16a)\quad f_{\rho'}(x_1,t)=M_{\rho'} \sin\left(\left[1+ \left[(\rho'-\sigma') (1-s) /p \right] \omega t - (\rho'\pi x_1/p\tau) \right] \right)$$

and the velocity of the ρ^{th} rotor MMF harmonic follows as,

$$(2.2.17)\quad v_{1\rho} =(dx_1/dt) = (1/\rho) \left[1 + (\rho-\sigma)(1-s) \right] v_s \text{ or}$$

$$(2.2.17a)\quad v_{1\rho'} = (p/\rho')\left(1 + \left[(\rho' - \sigma')(1-s) /p \right] \right) v_s$$

2.3. Rotor Current and the Reaction of the Rotor Harmonics

For future consideration an expression for the current in the rotor bars is needed because of the higher harmonic flux waves. Simultaneously, the question of the reaction of the rotor current will be discussed.

Introducing into equation 2.2.12 zero for c_2, one can readily see that every stator MMF distribution harmonic σ creates a rotor MMF harmonic $\sigma = \rho$. To be more exact, the σ^{th} harmonic of the stator MMF distribution will induce a current $I_{2\sigma}$ in the rotor of frequency $s_\sigma f_1$. This current in turn excites rotor MMF harmonics according to equation 2.2.11, from which $\rho^{th} = \sigma^{th}$ harmonic combines to give a resultant σ^{th} harmonic in the airgap. According to Alger[1] and Arnold[2]

---

1 2

2 6.

the influence of the higher harmonic fluxes on the performance of induction motors is best analyzed by adding an additional branch for each harmonic in to the equivalent circuit, as though all the higher harmonic rotor circuits were connected in series, as shown in fig. 2.3.1.

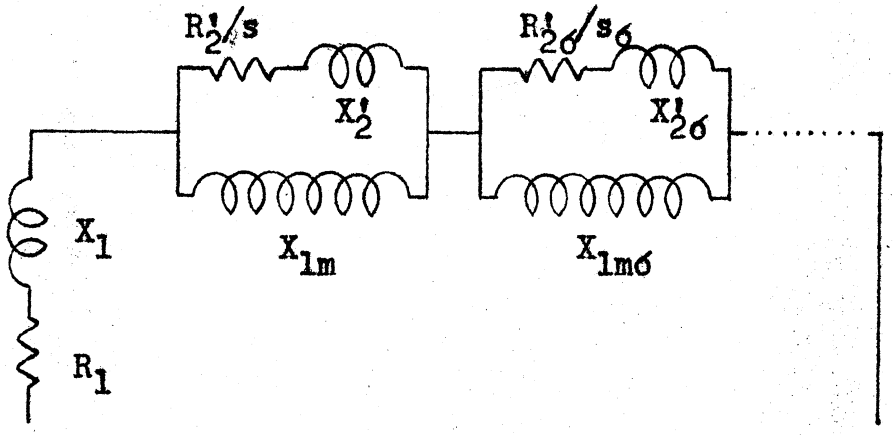

Fig.23.1

Equivalent Circuit of an Induction Motor

The symbols in this diagram denote the following:

$X_{1m\sigma}$ is the magnetizing reactance of the stator in regard to the σ^{th} stator harmonic

$R'_{2\sigma}/s_\sigma$ is the resistance and the load resistance of the secondary of the σ^{th} cage referred to the primary

$X'_{2\sigma}$ is the leakage reactance of the σ^{th} cage referred to the primary

R_1 is primary resistance

X_1 is leakage reactance of the primary

$I'_{2\sigma}$ is the current in the σ^{th} rotor referred to the primary

In this calculation it seems opportune to refer the primary current to the σ^{th} cage and to work with secondary quantities. The σ^{th} rotor branch represented in secondary quantities is shown in fig. 2.3.2.

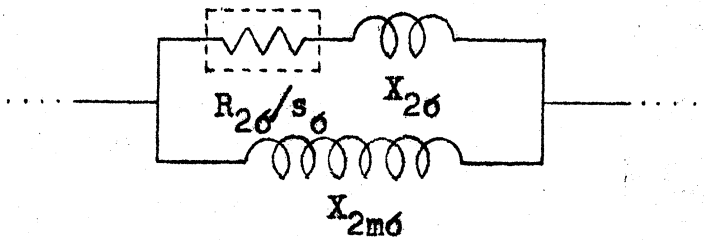

Fig. 2.3.2

Equivalent Circuit of the σ^{th} Rotor Cage

Before proceeding a review of the concept of the magnetizing and leakage reactance of an induction motor is in order.

The magnetizing reactance X_{1m} can be defined as the impedance of each phase of the induction motor with the squirrel cage rotor rotating synchronously under the condition that no higher harmonic fluxes exist, and neglecting leakage reactance, winding resistance, and iron losses. An expression for the magnetizing reactance for the main wave or any harmonic wave can be found by the following method:

Let the stator winding carry a balanced sinu-

soidal current of one amp. r.m.s. value, and express the MMF distribution in the airgap as a Fourier series. The ensuing distribution of the magnetic induction can then be determined and again expressed as a Fourier series. The numerical value of the r.m.s. voltage induced by any of the harmonic fluxes will be equal to the numerical value of the magnetizing reactance of the same harmonic flux in ohms.

Using such an approach the magnetizing reactance of the main wave of the stator can be shown to be,

$$(2.3.1) \quad X_{1m} = 1.6\ m\ f_1\ (w_1 \cdot k_1)^2 (\tau l_i / g'' p) \times 10^{-6} \text{ ohms}$$

and the magnetizing reactance of the 6^{th} harmonic,

$$(2.3.2) \quad X_{1m6} = 1.6\ m\ f_1\ (w_1 k_6)^2 (l_i / g'' p) \times 10^{-6} \text{ ohms}$$

In this expression, the symbol l_i is the net iron length of the stator measured in meters, and g'' is the corrected airgap in meters

$$(2.3.3) \quad g'' = k_C \cdot k_i \cdot g \text{ meters}$$

In this expression g is the airgap measured between two radially opposite tooth centers; k_C is a correction factor, a so-called Carter[1] coefficient which corrects the value of the airgap for stator slotting; and

---

[1] 17

k_1 takes care of the fact that only a part of the magneto-motive force is used up in driving the flux through the airgap while a smaller yet substantial part is consumed to establish the flux in the iron portion of the magnetic circuit.

Similar considerations will lead to the magnetizing reactance of the rotor. The magnetizing reactance of the main wave of the rotor may be calculated as,

(2.3.4) $X_{2m} = (0.4Q_2 f_1 \tau l_1 / g'' p) \times 10^{-6}$ ohms

and the magnetizing reactance of the σ^{th} harmonic

(2.3.5) $X_{2m\sigma} = (0.4Q_2 f_1 \tau l_1 / g'' p\sigma^2) \times 10^{-6}$ ohms

The magnitude of the leakage reactance is a very important prerequisite for the further analysis. The leakage reactance of induction motors consists of two components, each of an entirely different nature. One component - the so-called induction leakage - results from the simple fact that not all the flux lines of the current-carrying stator winding link the rotor winding, or the converse. The slot leakage and end-connection leakage are parts of the inductive leakage. The numerical value of the inductive leakage reactance is approximately the same for each higher harmonic branch of the equivalent circuit.

The origin of the other component of the leak-

age reactance, the so-called differential leakage reactance, can be traced to an entirely different cause and will be clarified by the following reasoning:

The instantaneous sum of all the fundamental frequency voltages in the stator must be equal to the instantaneous value of the supply voltage. The fundamental and higher harmonic fields that result from the primary current will induce just such voltages of fundamental frequencies in the stator, and therefore appear in the voltage equation of the primary. If the motor rotates, the individual higher harmonic fields of the stator will induce voltages of different frequencies in the rotor.

The fundamental current of slip frequency (sf) is induced by the main field of the primary and the magnitude of the current can be determined from the slip-frequency-voltage equation of the rotor. The voltages induced in the rotor by the higher harmonic flux fields of the stator do not appear in this main rotor equation but have to be found in separate voltage equations. Consequently it appears that the higher harmonic stator fluxes induce a voltage of fundamental frequency in the stator but not in the rotor. The voltages induced in the stator by the harmonic fluxes must therefore be considered as leakage-reactance drops. A similar observation leads also to the concept of the differential leakage of the rotor.

The total primary leakage reactance may be expressed as

(2.3.6) $X_1 = X_{1s} + X_{1e} + X_{1d}$,

in which expression,

X_{1s} is the slot leakage reactance of the primary,

X_{1e} is the end connection leakage of the primary,

X_{1d} is the differential leakage of the primary.

Replacing subscript 1 by subscript 2, a similar equation can be written for the main branch of the rotor circuit.

Expressions for calculations of the slot leakage reactance are well known and empirical values for the end connection leakage are readily available. It now remains to develop an expression for the differential leakage.

Neglecting the effect of saturation, stator slot opening, and rotor reaction, one can assume the differential leakage of stator and rotor to be mutually independent, making it possible to evaluate each leakage reactance separately by applying the same consideration that led to equation 2.3.1.

First, the voltage induced by all stator harmonics will be calculated for the stator winding carrying one ampere of current. In this way the numerical value of the

induced voltage will determine the total airgap reactance in ohms X_{lg} in the same manner as the main magnetizing reactance has been determined before. The differential leakage reactance can then be calculated as the total airgap reactance X_{lg} reduced by the main magnetizing reactance of the fundamental. Thus

$$X_{ld} = X_{lg} - X_{lm} \tag{2.3.7}$$

or we may write

$$X_{ld} = \lambda_{ld} X_m \tag{2.3.7a}$$

where λ_{ld} is the primary leakage factor defined as

$$\lambda_{ld} = (X_{lg}/X_{lm}) - 1 \tag{2.3.8}$$

The magnitude of X_{lg} can easily be calculated from energy consideration in the airgap[1]. The magnetic energy stored in the airgap of an induction motor with an m-phase winding is given by,

$$W = (m/2)L\ I^2 = (1/2)\int_{\tau_v} h\ b(d\tau_v) = (1/2)\mu_o \int_{\tau_v} h^2(d\tau_v)$$

where

L is the inductance of one phase including the effect of the mutual inductances of the other phases, measured in henries

h is the magnetic field intensity at a point of the airgap in amp. per meter

b is the magnetic induction in weber per meter^2

---

1 2;4

τ_v is the volume of the airgap in meter^3

μ_o is the permeability of free space $(4\pi/10^7)$ henries/meter.

The airgap reactance X_g can now be written,

$$X_g = 2\pi fL = (4\pi f/m)(W/I^2)$$

$$(2.3.9)\quad X_g = (2\pi f/m)(g''l_i\mu_o/I^2)\int_{x=0}^{x=2\pi} h^2 d(\pi x/\tau)$$

The value of h can be found by dividing the magnetomotive force at x by the corrected length of the airgap, that is,

$$(2.3.10)\quad h(x_1,t) = f(x_1,t)/g''$$

where $f(x_1,t)$ is given by equation 2.1.4. In the discussion following $f(x_1)$ will be used in lieu of $f(x_1,t)$.

The MMF distribution with our previous assumption can be taken to be a step wave. The integration in equation 2.3.9 can be replaced by a summation over all Q_1 slots of the stator as,

$$(2.3.11)\quad X_{lg} = (4\pi f l_i p\tau\mu_o/m\ g''I^2)\sum_{k=1}^{k=Q_1}(f_k^2/Q_1)$$

where f_k denotes the ordinate of the MMF distribution step wave over the k^{th} tooth.

Introducing the value of the amplitude of the main MMF wave, as given in equation 2.1.4, into 2.3.1, the main magnetizing reactance can be expressed as,

$$X_{1,m} = (2\pi f p \tau l_i)(\mu_o M_1^2)/(mg''I^2)$$

and the differential leakage factor of the fundamental calculated to be,

$$(2.3.12)\quad \lambda_{1d} = \left(2 \sum_{k=o}^{k=Q_1} f_k^2 / Q_1 M_1^2\right) - 1$$

Substituting the value of M_1 from equation 2.1.10 into 2.3.11, a more convenient form of the differential leakage coefficient can be obtained:

$$(2.3.12a)\quad \lambda_{1d} = \left(\left[(\pi p)/mk_1 w_1 I_1\right]^2 \sum_{k=o}^{k=Q_1} (f_k^2/Q_1)\right) - 1$$

From 2.3.12 it is obvious that λ_{1d} depends on the winding configuration of the stator. Consequently, it is necessary to establish the MMF distribution for each winding to get the value of f_k. As this would seem a rather cumbersome task the values of λ_{1d} have been tabulated for different windings in the reference quoted below[1].

The differential leakage coefficient of a squirrel cage rotor has still to be considered.

Equation 2.3.12a may be set as the starting point, and simplified to get an explicit formula for the differential leakage of the squirrel cage. The expression behind the summation sign can be calculated with ease from a sinor diagram of the bar currents illus-

---

[1] [2]

trated in fig. 2.3.3 below.

The sinor $\overline{01}$ represents the fundamental component $I_2\sqrt{2}$ of the rotor current in bar 1, and $\overline{12}$, the fundamental component in bar 2,

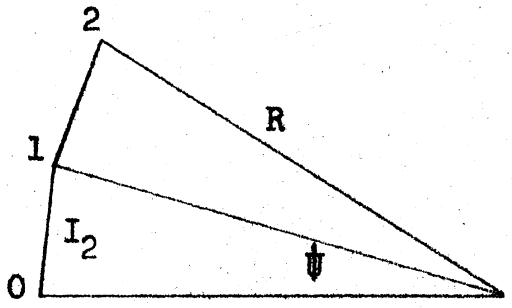

Fig. 2.3.3

Sinor Diagram of Bar Currents

and so on. The phase angle between two consecutive sinors is given by,

$$\psi = (2\pi p/Q_2)$$

The sinors constitute a polygon and the radius of the circumscribed circle can be expressed as

$$R = \sqrt{2}.I_{2,1}/\ [2(\sin \psi/2)\ ]$$

The magnitude of the MMF potential difference f_k at any rotor tooth is given by the ordinate from the polygon vertex to a so-called time axis. Choosing zero radius to vertex zero for the time axis, the vertical distance $\overline{2\ 2'}$ will be a measure of the MMF along the

flux line through rotor tooth 2

$$f_2 = \overline{2\,2'} = R \sin k\psi \quad \text{and}$$

$$\sum f_k^{\,2} = (1/2)\,[\,I_{2,1}/\sin(\psi/2)\,]^2 \cdot \sum_{k=1}^{k=Q_2} \sin^2(k\psi)$$

$$= (1/4)\;Q_2\,[\,I_{2,1}/\sin(\psi/2)\,]^2$$

The amplitude of the main wave of the rotor MMF distribution is given by 2.2.9a as

$$M_{2,1} = (\sqrt{2}\,Q_2\,I_{2,1}/2\pi p), \text{ so that}$$

$$\lambda_{2d,1} = \eta_{2,1}^2 - 1 \qquad (2.3.13)$$

where

$$\eta_{2,1} = (p\pi/Q_2)/\,[\,\sin(p\pi)/Q_2\,] \qquad (2.3.14)$$

or approximately

$$\eta_{2,1} \approx (1/3)\cdot(p\pi/Q_2)^2 \qquad (2.3.14a)$$

The differential leakage of the rotor resulting from the rotor current induced by the main wave of the stator MMF can now be written as,

$$X_{2d,1} = \lambda_{2d,1} \cdot X_{2m} \qquad (2.3.15)$$

For the calculation of the rotor current caused by the σ^{th} harmonic of the stator MMF distribution, the leakage reactance referred to the σ^{th} cage is needed. This leakage reactance consists of the slot, end connection, and differential leakage. The first two compo-

nents are nearly equal for all harmonics but the differential leakage varies and has to be computed. The same method is used as in the case of the main wave with the difference that the σ^{th} harmonic is now considered the main wave as though the motor had $p\sigma$ pole pairs. If the MMF distribution resulting from the current $I_{2\sigma}$ does not contain a component of main period, or if it is negligibly small, the differential leakage of the rotor in respect to the σ^{th} harmonic can be evaluated as,

$$(2.3.16) \qquad X_{2d\sigma} = \lambda_{2d\sigma} \cdot X_{2m\sigma}$$

where $X_{2m\sigma}$ is the magnetizing reactance of the rotor with respect to the σ^{th} harmonic as defined in equation 2.3.5., $\lambda_{2d\sigma}$ is the σ^{th} differential leakage coefficient of the rotor, and is defined as,

$$(2.3.17) \qquad \lambda_{2d\sigma} = \eta_{2\sigma}^2 - 1,$$

where

$$(2.3.18) \qquad \eta_{2\sigma} = (\sigma\pi p/Q_2) / [\sin (\sigma\pi p/Q_2)]$$

In order to solve the circuit, an expression for $I'_{1\sigma}$, (the fundamental stator current referred to the σ^{th} cage) has to be found, a task readily performed by the following reasoning:

The σ^{th} component of the stator MMF distribution resulting from current I_1 has σp pole pairs. This

harmonic can be separately considered and will induce a current in the rotor bars of the value $I'_{1\sigma}$ of such magnitude that the rotor MMF due to this current will have the same magnitude as the σ^{th} harmonic of the stator MMF. (The current in the magnetizing branch is neglected). This is easily accomplished by equating 2.1.10 and 2.2.14:

$$(2.3.19) \qquad I'_{1\sigma} = 2\,(m\, w_1 k_\sigma I_1/Q_2)$$

The current $I_{2\sigma}$ and its influence on the σ^{th} harmonic stator wave can be derived from the voltage equation of the σ^{th} cage

$$(2.3.21) \qquad \bar{I}_{2\sigma} = (-js_\sigma X_{2m\sigma} I'_{1,\sigma})/[R_{2\sigma} + js_\sigma(X_{2m\sigma}+X_{2\sigma})]$$

For small values of s - that is, the induction motor operating at rated condition - the value of

$$s_\sigma \gtrsim 5,$$

and the magnitude of $R_{2\sigma}$ becomes negligible as compared to

$$s_\sigma(X_{2m\sigma} + X_{2\sigma})$$

and 2.3.21 can be simply written as

$$(2.3.22) \qquad I_{2\sigma} = -\,|\, X_{2m\sigma}\, I_{1\sigma}/(X_{2m\sigma} + X_{2\sigma})|$$

2.4 Permeance Variation of the Airgap Resulting from Open Stator Slots

The semi-open slots of the stator of an induction motor cause a non-uniform distribution of the flux lines

in the airgap. It is not difficult to understand that the ensuing permeance of the airgap will vary as a periodic function with a tooth pitch as a period. This permeance variation will become the cause of a whole sequence of new harmonics, the so-called permeance harmonics. The amplitude of these harmonics depends on the permeance function, which in turn depends on the machine design and has to be evaluated in each case.

The permeance distribution in the airgap has in the past often been investigated, mainly for the purpose of finding the increase in the MMF required for the establishment of the flux in the magnetic circuit. F. W. Carter[1] was the first to arrive at a mathematical solution by the method of conformal transformations. He assumed an infinitely deep slot, and an infinitely long slot pitch. Since then many others have tried to improve on Carter's work, but only Frey's[2] paper is outstanding in this field. He published data for slots of finite depth. While these data are of great importance to designers, they can not be applied in an analytical manner for which another approach has to be made.

E. Weber[3] published in 1928 an approximate method of

---

1 17

2 26

3 73

expressing the airgap permeance function in an explicit form, also applicable to this analysis.

In the following, the variation of the airgap permeance is assumed to result entirely from the stator slot opening and to be unaffected by the saturation of the rotor teeth. Fig. 2.4.1 illustrates the flux pulsation caused by stator slot openings.

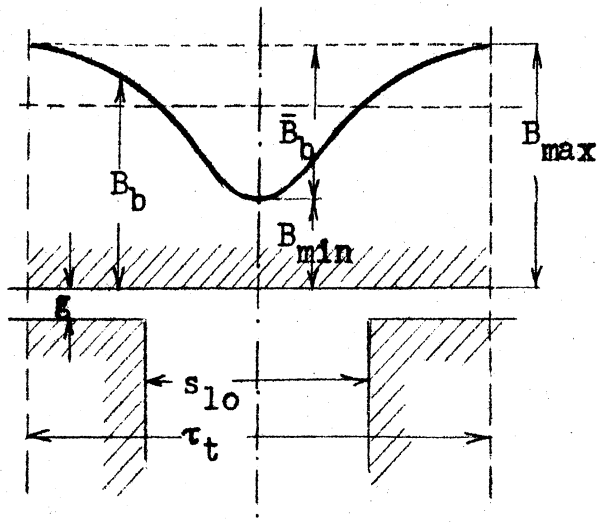

Fig. 2.4.1

The Pulsation due to Slot Openings.

In the above figure,

s_{lo} is the width of the slot opening

τ_t is the tooth pitch

g is the airgap

B_{max} denotes the maximum flux density at the tooth center

$\bar{B}_b$ denotes the maximum reduction of the flux density at the slot center

$B_b(\xi)$ is the flux density reduction at ξ ; ξ is measured from the tooth center.

Analyzing a number of tooth pulsation curves, Weber found that the flux distribution between the limits $0 \leq \xi \leq \tau_{can}$ be conveniently expressed by the trignometric function,

(2.4.1) $$B_b(\xi) = \bar{B}_b \sin^{2b}(\xi\pi/\tau_t),$$

where

(2.4.2) $$b = (\tau_t/s_{lo})-1$$

For integer values of b the above function can be expressed by a series of finite numbers of terms:

(2.4.3) $$\sin^{2b}(a\xi) = \Big(\cos(2ba\xi) - \binom{2b}{1} \cos[2(b-1)a\xi] + \binom{2b}{2} \cos[2(b-2)a\xi] + (-1)^{b-1}\binom{2b}{b-1} \cos(2a\xi) + (1/2(-1)^b\binom{2b}{b}\Big) \cdot (-1^b/2^{2b-1})$$

a is defined as,

(2.4.4) $$a = \pi/\tau_t$$

For non-integer values of b, the series 2.4.3 will have an infinite number of terms. Weber suggests that the coefficient of the series first be found for integer values of b and then interpolated.

The actual field distribution between two tooth-

centers, slotting considered, can,in accordance with fig. 2.4.1 and with equation 2.4.3 be expressed as,

$$(2.4.5) \quad B(\xi) = B_{max} - B_b = [\,1-2\beta\sin^{2b}(a\,\xi)\,]\,B_{max}$$

where

$$(2.4.6) \quad 2\beta = \bar{B}_b/B_{max}$$

The values of β are a function of (s_{1o}/g) and have been calculated by Carter. His results are shown in the graph of fig. 2.4.2

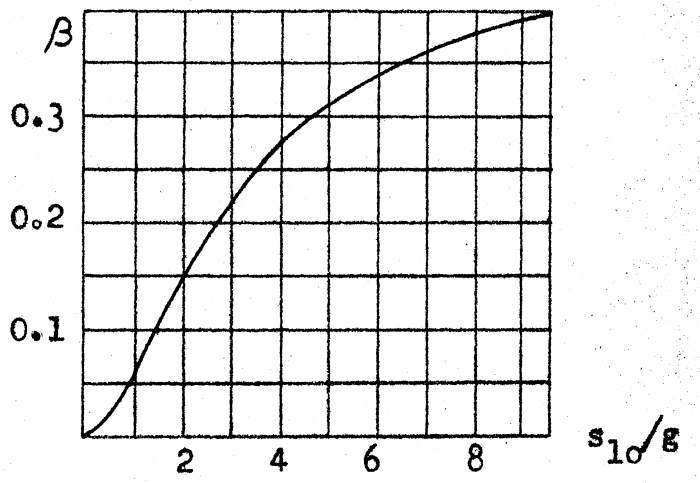

Fig. 2.4.2

The Function β

The expression in the square bracket of 2.4.5 can be considered the ratio of the permeance of the slotted airgap as compared to the permeance of a uniform airgap of the length g, or,

$$(2.4.7) \quad \mathcal{P}(\xi) = [\,1-2\beta\sin^{2b}(a\xi)\,]$$

where

(μ_o/g) the permeance of the unslotted airgap

$\mathcal{P}(\xi)$ the permeance function of the slotted airgap

Only a few terms of this permeance function are of practical value. Introducing into 2.4.7 the coefficient of the series 2.4.3, the expression for the airgap permeance will become

$$(2.4.8)\quad \mathcal{P}(\xi) = (\mu_o/g)\left([1-\beta(^{2b}_{b})] + 2\beta(^{2b}_{b-1}) \cos 2a\xi - 2\beta(^{2b}_{b-2}) \cos 4a\xi \right)\cdot(1/2^{2b-1})$$

The term in the square bracket $|1-\beta(^{2b}_{b})|$ indicates the reduction of the average value of the flux density in the airgap and is actually the reciprocal of the Carter coefficient k_c. Keeping in mind that $2p\tau = Q_1\tau_t$, and $a = (\pi Q_1/2p\tau)$, equation 2.4.8 can be expressed as

$$(2.4.9)\quad \mathcal{P}(\xi) = (\mu_o/gk_c)\left[1+2\eta_1 \cos\xi(\pi Q_1/p\tau) - 2\eta_2(2\pi Q_1/p\tau)\xi\right]$$

where

$$\eta_1 = \beta(^{2b}_{b-1}) \,/\, [2^{2b-1} - \beta(^{2b}_{b})]$$

$$(2.4.10)\qquad \eta_2 = \beta(^{2b}_{b-2}) \,/\, [2^{2b-1} - \beta(^{2b}_{b})]$$

In illustration of these equations, the coefficient for the experimental induction motor will be determined from design data as given in Appendix I

$\tau_t = 0.471"$; $s_{1o} = 0.125"$; $g = 0.023"$, hence

$(s_{1o}/g) = 5.44$, and from fig. 2.4.2, $\beta = 0.33$. The value of b calculated from equation 2.4.2 is 2.8. As expected, b is no integer, and therefore the coefficient η_1 will be determined for b = 2 and 3, and then a linear interpolation applied to find the value of η_1 for b = 2.8.

For b = 3; $\eta_1 = (0.33)\binom{6}{2}.2^5-(0.33)\binom{6}{3} = 0.195$;

for b = 2; $\eta_1 = (0.33)\binom{4}{1}.2^3-(0.33)\binom{6}{3} = 0.22$,

and by linear interpolation for b = 2.8; $\eta = 0.2$.

2.5 Flux Distribution in the Airgap

(neglecting Variations of Airgap Permeance)

The flux distribution in the airgap can be determined by multiplying the magnetomotive potential drop across the airgap at each point by the permeability μ_o, and by dividing these values by the corrected airgap g'. For convenience of treatment it may be advisable to determine fictitious flux distributions caused by the stator and rotor MMF separately and to apply the principle of superposition. It is worth notice that the ordinates of the MMF distribution are larger than the magnetomotive potential drop in the airgap. A not inconsiderable part of the total available MMF along a flux line is used to establish the magnetic induction in the iron. To account for this in a simple manner the corrected airgap

g' is multiplied by yet another correction factor k_i. This correction factor varies considerably with the harmonic order of the flux wave. For the main wave k_i will vary between 1.3 and 1,9. For the harmonics of higher order it will decrease to 1, as the flux distribution of these have many poles and the flux lines close through the tooth heads of the rotor and stator.

The main field is due to the resultant MMF distribution of the primary and secondary currents of fundamental frequency or simply the field established by the magnetizing current. This field is largest at no load and only slightly reduced at full load. This main flux distribution may be expressed as,

(2.5.1) $b_1(x_1,t) = B_1 \sin [\omega t-(\pi x_1/\tau) - \theta_1]$

where B_1 is the amplitude of the fundamental flux distribution and can be expressed as,

(2.5.2) $B_1 = (\mu_o/g'')(m \sqrt{2}\, w_1\, k_1\, I_1 m/\pi p)$ weber/meter^2

θ_1 is the angle by which the magnetizing current lags the primary current - that is, the reference current, and I_{1m} is the fundamental component of the magnetizing current.

The angular velocity and the mechanical velocity of this field can be evaluated as in section 2.2 and obviously be the same as that of the main MMF distribution.

The flux distribution of the higher stator har-

monic MMFs can be computed in a similar fashion. It will be necessary to consider the damping effect of the rotor wave of the order $\rho = \sigma$ for the lower belt harmonics as described in section 2.3. For these the value of k_1 will be slightly less than that of the main wave.

For the slot harmonics the reaction of the rotor can be neglected, and with sufficient approximation they can be written as,

(2.5.3) $b_\sigma(x_1,t) = B_\sigma \sin(\omega t - \sigma\pi x_1/\tau)$ weber/meter^2 or

(2.5.3a) $b'_\sigma(x_1,t) = B_\sigma \sin(\omega t - \sigma'\pi x_1/p\tau)$ weber/meter^2

where

(2.5.4) $B_\sigma = (\mu_o/g')(m\sqrt{2}\, w_1\, k_\sigma\, I_1/p\sigma)$ weber/meter^2, or

(2.5.4a) $B_\sigma = (\mu_o/g')(m\sqrt{2}\, w_1\, k_{\sigma'} I_1/\sigma')$ weber/meter^2

The angular velocity and the mechanical speed of these higher harmonic flux fields will be identical with the MMF distributions causing them.

The equation of the fictitious flux distributions of the rotor current is again obtained by multiplying the appropriate rotor MMF distribution by μ_o/g'' or by μ_o/g'.

(2.5.5) $b_\rho(x_2,t) = B_\rho \sin[s_\sigma\omega t - (\rho\pi x_2/\tau)]$ or

(2.5.5a) $b_{\rho'}(x_2,t) = B_{\sigma'}\sin[s_{\sigma'}\omega t - (\rho'\pi x_2/p\tau)]$

where

(2.5.6) $B_\rho = (\mu_o/g').\ (Q_2 \sqrt{2}\ I_2\sigma/2\pi p\rho)$

or

(2.5.6a) $B_{\rho'} = (\mu_o/g').\ (Q_2 \sqrt{2}\ I_2\sigma'/2\pi\rho')$

Referring this wave to the stator in the manner described in section 2, the flux distribution resulting from any rotor harmonic can be expressed as,

(2.5.7) $b_\rho(x_1,t) = B_\rho \sin\left([1+(\rho-\sigma)(1-s)]\omega t-(\rho\pi x_1/\tau)\right)$

or

(2.5.7a) $b_{\rho'}(x_1,t) = B_{\rho'}\sin\left([1+(\rho'-\sigma')(1-s)/p]\omega t-(\rho'\pi x_1/p\tau)\right)$

The speed of these harmonics can again be calculated as in section 2.3.

2.6 Airgap Flux Distribution considering Slot Openings[1]

The variable permeance of the airgap considerably changes the flux distribution described in section 2.5. It creates another series of flux harmonics, the so-called permeance harmonics. These harmonics of the flux wave are of the same order as the slot harmonics. The two series of harmonics will combine in a manner largely dependent on the quantity q. As the combination rule will be different for even and for odd values of q, it will be necessary to investigate both cases.

q is even: The expression for the permeance function has

---

[1] 73

been developed assuming $x = 0$ at a tooth center. With an even number of slots per pole per phase, the amplitude of the main wave will also be at a tooth center, according to equation 2.1.4.

For the sake of convenience the equation of the MMF distribution will be transformed to a new system of coordinate axes with the origin at the zero ordinate of the MMF wave at a time when the current in the reference phase is a maximum. Equation 2.1.4 can now be written as,

$$M_1(x_1,t)=M_p\cos[(x_1\pi/\tau)-\omega t]-M_{5p}\cos[(5x_1\pi/\tau)+\omega t]+$$

$$+M_{7p}\cos[(7x_1\pi/\tau)-\omega t]-M_{(Q_1-p)}\cos[(Q_1-p)(x_1\pi/p\tau)+\omega t]+$$

$$+M_{(Q_1+p)}\cos[(Q_1+p)(x_1\pi/p\tau)-\omega t] - \ldots \qquad (2.6.1)$$

Now that the main wave and the permeance function are related to the same origin - that is, a tooth center - the equation of the first order permeance harmonics can be established by multiplying the first term of 2.6.1 by the permeance function 2.4.9

$$b_p(x_1,t) = M_p\cos[(x_1\pi/\tau)-\omega t](\mu_o/gk_c)\ x$$

$$x\ [1+2\eta_1\cos(x_1\pi Q_1/p\tau)-2\eta_2\cos(2x_1\pi Q_1/p\tau)] \qquad (2.6.2)$$

The product to the right of the equation sign will have three terms.

The first term will represent the fundamental flux distri-

bution reduced by the factor k_C.

The second term, which is our main concern, can be rewritten after a simple trigonometric transformation:

$$(2.6.3)\quad b_p^{(1)}(x_1,t) = \eta_1 M_p \cos\left([(Q_1+p)x_1\pi/p\tau] - \omega t \right).(\mu_o/gk_C)$$
$$+ \eta_1 M_p \cos\left([(Q_1-p)x_1\pi/p\tau] + \omega t \right).(\mu_o/gk_C)$$

By comparing 2.6.3 with 2.6.1, the following striking observations can be made: The first term of 2.6.3 - that is, the positively rotating first permeance harmonic - has the same number of poles, direction of rotation, and angular velocity as the positively rotating first slot harmonic. Furthermore, the coefficient of the permeance harmonic has the same sign as the corresponding slot harmonic, and they will therefore add.

The second term of 2.6.3 - the negatively rotating first permeance harmonic - has again the same number of poles, direction of rotation, and angular velocity as the first negatively rotating slot harmonic of the order $(-Q_1 + p)$. However, this time the sign of its coefficient is opposite to the sign of the corresponding slot harmonic. Consequently the two waves will subtract.

The third term of 2.6.2 represents the second order slot harmonics which can be evaluated in the same fashion as those of the first order.

When combining slot and permeance waves of har-

monic order ($\pm Q_1 + p$), it is important to remember that the slot harmonics are produced by the MMF of the primary current, while the magnetizing current is responsible for the main field and the permeance harmonic. These two harmonics are out of phase by an angle of $(\theta_1 - \theta_m)$ and must therefore be combined vectorially.

q is odd: The origin of the MMF distribution is in this case in the middle of a slot. The expression for the permeance function has to be related to this origin by the simple transformation, $\xi' = \xi + \pi$, and we may express it as,

$$(2.6.4) \quad \mathcal{P}(x) = \Big(1 + 2\eta_1 \cos \left[(Q_1 \pi x_1 / p\tau) - \pi \right] - 2\eta_2 \cos \left(2Q_1 \pi x_1 / p\tau \right) \Big) (\mu_o / g k_c)$$

or

$$(2.6.4a) \quad \mathcal{P}(x) = \Big(1 - 2\eta_1 \cos (Q_1 \pi x_1 / p\tau) - 2\eta_2 \cos (2Q_1 \pi x_1 / p\tau) \Big) (\mu_o / g k_c)$$

The permeance harmonic of the fundamental may again be calculated by multiplying 2.6.4a with the first term of 2.6.1. As before, three terms will result, with the first and third term unchanged, while the second may be evaluated as,

$$(2.6.5) \quad b_p^{(1)}(x_1, t) = \Big(-\eta_1 \cos \left[(Q_1 + p)(x\pi/\tau) - \omega t \right] - \eta_1 \cos \left[(Q_1 - p)(x\pi/\tau) + \omega t \right] \Big) (\mu_o / g k_c)$$

A comparison of this expression with 2.6.1 demonstrates that in the case where q is odd, the sign of the positively

rotating first permeance harmonic is opposite to that of the slot harmonic of the same order. By contrast, the negatively rotating slot harmonic is of the same sign as its slot harmonic counterpart in the MMF wave, and they will therefore add. The addition must again be carried out by the parallelogram law.

At the start of this chapter we assumed closed rotor slots. The saturation of the slot bridges creates the same effect as slot openings, and permeance harmonics caused by rotor slots may also occur. These are difficult to evaluate and will therefore be described qualitatively. Suppose that at time $t = 0$, a rotor slot center of a smooth stator induction motor is at an angle ψ_o from the origin of the main MMF wave in the airgap. The permeance of the airgap resulting from rotor slotting can be then expressed as,

$$(2.6.6)\quad \mathcal{P}_r = \left[1-2\eta_1 \left[\cos Q_2(x_1\pi/p) - \psi_o - \omega_r t\right]\right](\mu_o/gk_c)$$

where the angular velocity of the rotor is expressed as

$$\omega_r = \omega_s(1-s)$$

The negative sign before η_1 takes care of the fact that the origin of the MMF wave coincides with a slot center.

The theoretical expression for the rotor permeance harmonics can be evaluated as before and is given for the first order harmonics as,

$$(2.6.7)\quad b_2^{(1)}(x_1,t) = \cos\left[(px\pi/\tau) - \omega t\right].(\mu_o/gk_c) \cdot \cdot\left(-\cos\left[Q_2\left[(x\pi/\tau)-\Psi_o-\omega_r\right]\right]\right)$$

which may again be expanded as previously into terms of the following form

$$(2.6.7a)\quad -\eta_1 \cos\left(\left[(Q_2+p)x\pi/\tau\right] - \omega t - Q_2\Psi_o - Q_2\omega_r t\right)$$
$$-\eta_1 \cos\left(\left[(Q_2-p)x\pi/\tau\right] + \omega t - Q_2\Psi_o - Q_2\omega_r t\right)$$

It follows from these terms that the positively rotating first permeance field adds to the rotor slot harmonic of the same order while the negatively rotating permeance field subtracts from it. It is rather difficult to get a numerical value for the field changes. A conservative estimate would indicate a change between 10 and 20 per cent.

2.7 The Radial Magnetic Force Waves

The main torque in an induction motor is the one created by the main flux distribution in the airgap and the main current distribution on the rotor. Besides its useful tangential forces, there are also parasitic forces in the airgap which do not contribute to the motor's useful operation. The radial components of these forces will be investigated as being the main cause of magnetic noise. The share of the tangential forces in noise production is negligible, as explained in section 2.8.

The radial forces can be readily determined from energy considerations because simplifying assumptions that the lines of force in the airgap are radial were already made. The differential area in the airgap can be expressed as $A = dx.l_1$. Now suppose that this differential area of the stator had moved towards the rotor by an amount dr. The change in magnetic energy in the elementary volume of

$$- dW = (1/2)\ h.b.A.dr = (1/2\mu_o)b^2A\ dr$$

The force on the differential area resulting from the change of the magnetic energy will be

$$P = dW/dr = (1/2\mu_o)b^2A, \text{ or}$$

$$P/A = - (1/2\ \mu_o)\ .\ b^2 \text{ newtons/meter}^2$$

Denoting the electromagnetic pressure with Γ, the following equation may be written:

(2.7.1) $\Gamma(x_1,t) = (1/2\ \mu_o)\ b^2(x_1,t)$

where $b_1(x_1,t)$ is the resultant magnetic induction in the airgap.

To further simplify the equations the quantity $\Gamma(x_1,t)$ will be disregarded for the time being and the quantity $b^2(x_1,t)$ investigated. With the previous assumption that all magnetic lines cross the airgap radially,

(2.7.2) $b(x_1,t) = b_1(x_1,t) + b_2(x_1,t)$

The expression for $b_1(x_1,t)$ and $b_2(x_1,t)$ has been developed

in equations 2.5.3 and 2.5.7 and is repeated below:

$$b_1'(x_1,t) = \sum_{\sigma'} B_{\sigma'} \sin\left[\omega t - (\sigma'\pi x_1/p\tau)\right]$$

$$b_2'(x_1,t) = \sum_{\rho'} B_{\rho'} \sin\left[\omega t\left[1 + (\rho'-\sigma')(1-s)/p\right] - (\rho'\pi x_1/p\tau)\right]$$

For the sake of simplification the frequency term in the second equation will be written,

$$(2.7.3) \quad \omega_{\rho'} = \left(1 + \left[(\rho' - \sigma')(1-s)\right]/p\right)\omega,$$

so that the expression for the square of the flux density can be written as

$$(2.7.4) \quad \left[b'(x_1 t)\right]^2 = \left(\sum_{\sigma'} B_{\sigma'} \sin\left[\omega t - (\sigma'\pi x_1/p\tau\right] + \sum_{\rho'} B_{\rho'} \sin\left[\omega_{\rho'} t - (\rho'\pi x_1/p\tau)\right]\right)^2$$

where the primes denote the previously mentioned convention that the whole armature circumference is considered to be the fundamental period of the Fourier series. The order of σ' and ρ' for which the summation has to be carried out is given in equations 2.18 and 2.1.12a.

The trigonometric rules

$$2\sin^2 x = 1 - \cos 2x \quad \text{and}$$

$$2\sin x.\sin y = \cos(x-y) - \cos(x+y)$$

will be used to represent the results of the square of 2.7.4 in an organized manner, but it seems advisable to

discuss first the nature of the different terms in the results. As for the phase angles and fractions, they will be disregarded in the following description.

Upon squaring the first summation sign, the following terms will result:

First term: $\sum_{\sigma'} B^2_{\sigma'}$ represents a constant force uniformly distributed over the whole armature circumference. This distribution does not cause vibrations.

Second term: $\sum_{\sigma'} B^2_{\sigma'} \cos \left[2\omega t - (2\sigma' x_1/p\tau) \right]$ are the so-called double frequency force waves. They pulsate with double supply frequency and are responsible for the hum characteristic of induction motors. Only the case of $\sigma' = \rho'$ may acquire importance in 2 or 4 pole motors where the double frequency force waves have two or four pole pairs. The next smallest order of $\sigma' = 5p$ (the fifth harmonic) would cause a 10-pole-pair force wave in a 4-pole motor of double supply frequency. The flexural rigidity of the stator structure at such a high mode is so large that the deflection caused by these force waves is negligibly small. Furthermore, 120 c.p.s. sound pressures must be fairly large to fall into the range of audibility.

Third term:

$$(2.7.5) \qquad \sum_{\sigma_1'=\sigma'} \sum_{\sigma_2'=\sigma'} B_{\sigma 1'} \cdot B_{\sigma 2'} \quad \cos 2\omega t - \left[(\sigma_1' + \sigma_2')(\pi x_1/p\tau) \right]$$

where $\sigma_1' \neq \sigma_2'$. These are again double frequency force waves.

They will be discussed later.

Fourth term: $\sum_{\sigma_1'=\sigma} \sum_{\sigma_2'=\sigma} B_{\sigma 1'} \cdot B_{\sigma 2'} \cos\left[(\sigma_1-\sigma_2)(\pi x_1/p\tau)\right]$

where $\sigma_1'=\sigma_2'$, represents non-pulsating constant force waves sinusoidally distributed and not causing vibrations.

Fifth term: $\sum B_{\rho'}^2$ is again a constant pressure uniformly distributed as in the first term.

Sixth term: $\sum B_{\rho'}^2 \cos\left[2\omega_\rho t-(2_{\rho'}\pi x_1/p\tau)\right]$; ρ' is generally a large number and the force distribution in $2_{\rho'}$ pole pairs will cause only negligible deflections. Should ρ' be a small integer, $B_{\rho'}$ will become so small as to appear negligible.

Seventh term:

$$(2.7.5a)\qquad \sum_{\rho 1=\rho'} \sum_{\rho_2=\rho'} B_{\rho' 1} \cdot B_{\rho' 2} \cos\left((\omega_{\rho'1} \mp \omega_{\rho'2})t - \right.$$
$$\left. -\left[(\rho'_1-\rho_2)(\pi x_1/p\tau)\right] \right)$$

where $\rho_1' \neq \rho_2'$. These force waves result from interaction of two rotor flux waves and will be investigated later.

The most important term is the cross product of the expressions behind the summation sign which yield the

Eighth term:

$$(2.7.6)\qquad \sum_{\sigma'} \sum_{\rho'} B_{\sigma'} B_{\rho'} \cos\left((\omega \mp \omega_{\rho'})t - \left[(\sigma' \pm \rho')(\pi x_1/p\tau)\right] \right),$$

where $(\rho' \pm \sigma')$ may have a low integer value in some of the terms which represent force waves of a small number of pole

pairs distributed over the airgap periphery. The bending moments caused by these force waves may become significant by causing considerable vibration and noise.

To simplify the writing of the force wave equations, the quantities $(\sigma'_1 \pm \sigma'_2)$ in 2.7.4, $(\rho'_1 \pm \rho'_2)$ in 2.7.5, and $(\sigma' \pm \rho')$ in 2.7.6, will be denoted m_v, the mode of the force wave. This quantity represents the number of complete periods of the force distribution along the airgap; for example, $m_v = 2$ will represent a second mode force wave.

The mode of the forced vibration of the stator largely depends on the mode of the force wave and differs for $m_v = 0$, $m_v = 1$, $m_v = 2$ or larger than 2.

The equation of the force wave for $m_v = 0$ can be written as,

$$(2.7.7) \quad \Gamma(x_1,t) = \Gamma_{max} \cos [(\omega-\omega_{\rho'})t]$$

This equation illustrates a uniform force distribution pulsating with a frequency $\omega - \omega_{\rho'}$. The forced vibration of the stator structure will under this condition be similar to that of a steam pipe under periodical pressure variations. The stator rings will be subjected to extensional deformations resulting in extremely small amplitude vibrations, because of the very large extensional rigidity of the stator. The sound pressures resulting from such vibrations will be below the threshold of audibility.

The case where $m_v = 1$ will only occur if the interacting flux waves differ by 1 pole pair counted around the whole armature periphery. It is obviously the case of the one-sided pull. The airgap flux density will be a maximum at one point, and a minimum at a diametrically opposite point. The expression for the force wave may be written as,

$$(2.7.8) \quad \Gamma(x_1,t) = \Gamma_{max} \left[(\omega_1 \pm \omega_\rho)t \pm (\pi x_1/p\tau) \right]$$

Fig. 2.7.1 shows the resultant flux density for the case of $\sigma' = 4$, and $\rho' = 3$. The force wave caused by the interaction of these two fields is illustrated by dotted lines.

The magnitude of the one-sided pull can be found by resolving the force at every point in the airgap into a component parallel to the maximum force at that instant, and another perpendicular to this direction.

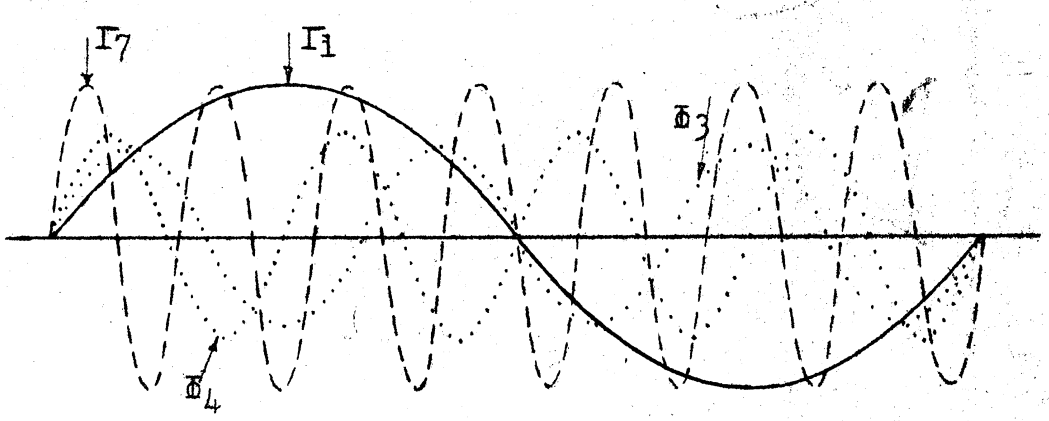

Fig. 2.7.1

Interacting Flux Waves differing by 1 Pole Pair

The integral of the first component along the whole periphery represents the magnetic pull. The integral of the

second component is zero.

The one-sided pull constituting a bending load on the shaft causes deformations as illustrated in fig. 2.7.2 on page 78. The resultant one-sided force revolves around the airgap with an angular velocity $(\omega_1 \pm \omega_{\rho'})$. If this frequency is near the critical frequency of the rotor, the vibrations caused by this one-sided pull build up to a dangerous shaking. The amplitudes under such resonant conditions may become so large as to make the rotor grind on the stator. An excessively loud, howling noise ensues, a phenomenon familiar to designers who will have no difficulty in finding a slot combination to avoid such an occurrence.

The case $m_v = 2$ will arise if there are two fields with pole pairs differing by two in the airgap. In this instance the equation is,

$$(2.7.9) \quad \Gamma(x_1,t) = \Gamma_{max} \cos\left((\omega-\omega_{\rho'})t - (2\pi x_1/p\tau)\right)$$

The sinusoidally distributed force wave will have two complete cycles along the airgap. There is no eccentric force on the stator or rotor and the force waves represent a bending load. Rigidity of the rotor is very large so that its deformation can be neglected. The stator will be deformed into the shape of an ellipse as shown in fig. 2.7.3 on page 78. The vibration amplitudes in this mode will become

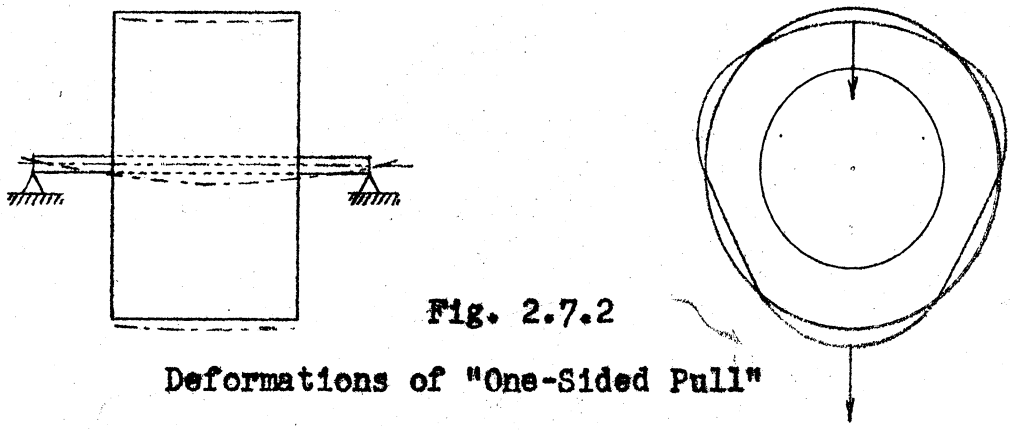

Fig. 2.7.2

Deformations of "One-Sided Pull"

Fig. 2.7.3

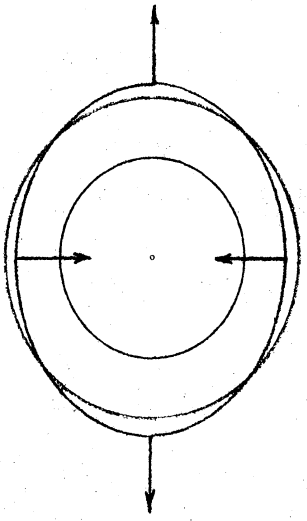

Elliptical Deformations

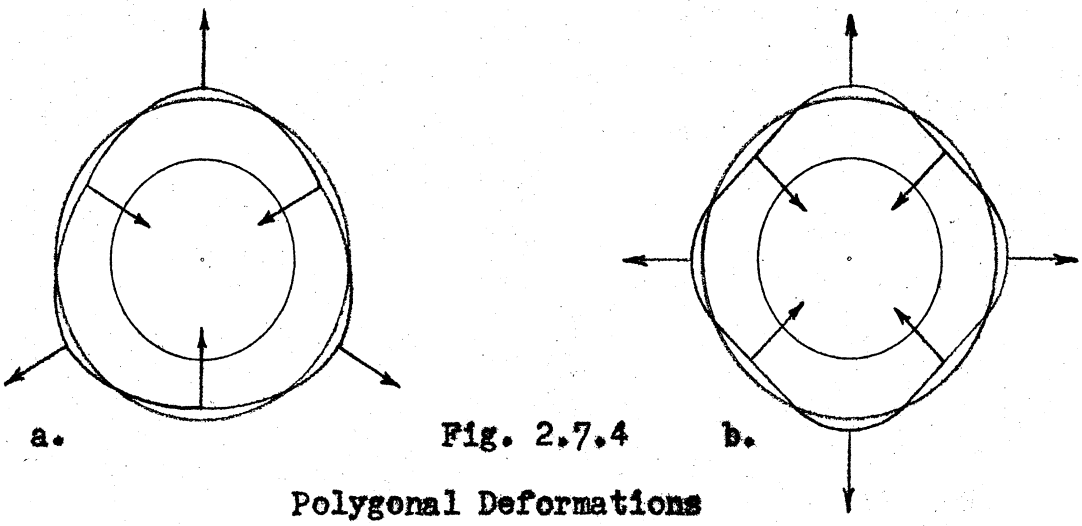

a.

Fig. 2.7.4

b.

Polygonal Deformations

quite large as verified in the analysis of chapter 3.

The conditions where m_v is larger than two but still a small number are very similar to case $m_v = 2$. The sinusoidal force wave distributions will have a few periods around the circumference, with a tendency to deform the stator into the shape of a polygon, as shown in figures 2.7.4a, and 2.7.4b, for $m_v = 3,4$, respectively.

The flexural rigidity of the stator structure increases rapidly with the order of the mode m_v. Consequently, the deflections will decrease rapidly with increased mode orders. In most medium induction motors it will therefore suffice to consider force waves to the third mode only, with the exception of the case where the frequency of the m_v force wave coincides with the resonant frequency of the stator structure in the same mode. For large induction motors it will be necessary to consider also values of m_v larger than 3.

From force equation 2.7.6 it would appear that the force itself could become negative, denoting a repulsion force between stator and rotor. As this is physically impossible it requires clarification. In the discussion of terms it could be noted that the first term represents a uniformly attracting force over the whole armature. Because $B_1^2 + B_2^2$ is always larger than $2 B_1 B_2$, the total at-

tracting force always remains positive; i.e., the negative terms only reduce the magnitude of the attracting forces.

The preceding discussion indicates that there is a vast number of interfering flux waves and force waves. It is possible however to exclude a large number of the force waves by analyzing the conditions for their occurrence, though the analysis is valid only for machines with concentric airgaps.

For force waves that result from the interaction of two stator fields the condition,

(2.7.10) $m_v = \sigma_1' \pm \sigma_2'$,

has to be satisfied. Recalling that

$$\sigma_1' = p\,(c_1\, m + 1)\ ;\quad \sigma_2' = p\,(c_2\, m + 1)$$

the mode of the force wave can be expressed as,

(2.7.10a) $m_v = p\,\left[(c_1 + c_2)\, m + 2\right]$

For $m_v = 1$, this reduces to $p\left[(c_1 + c_2)m + 2\right] = \pm 1$;

as c_1 and c_2 are whole numbers it would seem as though this condition could be satisfied only in a machine where $p = 1$; that is, in a two pole machine. However this will apply only to 120° phase belt machines. For the latter case, c_1 and c_2 have to be even numbers, and a one-side pull could not

occur in a modern induction motor because of interference of two stator force waves.

To differ by m_v, the general condition for the harmonic order of two stator waves of 60° phase belt machines is given by

(2.7.11) $(c_{11} + c_{12}) = \pm (m_v/p)-2,$

and this sum must be an even multiple of 3 or 0.

For $m_v = 2$, it is only satisfied in two-pole machines where $\sigma_1 = -5$, and $\sigma_2 = +7$, may create a two-pole pair force wave. The frequency of these waves is the double supply frequency which will add to the vibrations caused by the fundamental field. Equation 2.7.11 cannot be satisfied for odd modes which means that no odd modes will occur that result from interference between two stator waves in a 60° winding.

The conditions for the rotor field to interact and thus create an m_v force wave are,

(2.7.12) $(\rho'_1 \pm \rho'_2) = \pm m_v$

Introducing into these equations the values of

$$\rho'_1 = c_{21} Q_2 + \sigma'_1, \quad \rho'_2 = c_{22} Q_2 + \sigma'_2;$$

and for 3-phase motors,

$$\sigma'_1 = p(3c_{11} + 1) \text{ and } \sigma'_2 = p(3c_{22} + 1),$$

the condition for the interaction of the rotor waves can be written as two equations,

$$Q_2(c_{21} + c_{22}) + 3p\,(c_{11} + c_{12}) + 2p = m_v$$

or

$$Q_2(c_{21} - c_{22}) - 3p\,(c_{11} - c_{12}) = m_v$$

To simplify these equations the following constants are introduced: C_2 for $(c_{21} + c_{22})$ or $(c_{21} - c_{22})$; and C_3 for $(c_{11} - c_{12})$ or $(c_{11} - c_{12})$, where C_2 can be any integer except zero, while C_3 can be any even integer divisible by 3, except zero.

Condition 2.7.12 can be restated as

(2.7.13a) $Q_2\,C_2 + p\,C_3 = \pm\, m_v$,

and

(2.7.13b) $Q_2\,C_2 + p(C_3+2) = \pm\, m_v$

For $m_v = 1$, Q_2C_2 must be an odd number; i.e., the number of rotor bars must be odd. Introducing other values for m_v, similar conditions can be developed for low mode force waves caused by the interference of two rotor fields.

The low mode force waves resulting from the interference of one stator and one rotor harmonic are the most frequent and dangerous ones from the viewpoint of noise production, and will have to be investigated. The

condition for their occurrence is bound to the equation

(2.7.14) $m_v = \rho' \pm \sigma'$

or for 3-phase machines,

(2.7.15) $p(3\ c_{11} + 1) \pm p(3\ c_{12} + 1) \pm c_{22}Q_2 = m_v$

Introducing the same constants which led to equation 2.7.13, 2.7.15 can be split into two conditions

(2.7.15a) $p(C_3 + 2) \pm C_{22}Q_2 = \pm m_v$

or

(2.7.15b) $p\ C_3 \pm C_{22}Q_2 = \pm m_v$

For force waves of mode $m_v = 1$ to occur the following equations have to be satisfied:

$$p(C_3 + 2) \pm C_{22}Q_2 = \pm 1$$

$$p\ C_3 \pm C_{22}Q_2 = \pm 1,$$

wherein the first terms on the left are even numbers. Force waves of the first mode can therefore only appear in machines with odd numbers of rotor bars.

The conditions for $m_v = 2$ are

$$p(C_3 + 2) \pm c_{22}Q_2 = \pm 2 \text{ or } p\ C_3 \pm c_{22}Q_2 = \pm 2$$

Similar conditions can also be established for other low mode terms.

The interaction of flux waves of slot harmonic order creates force waves belonging to this class and deserve careful consideration.

The order of the stator slot harmonic is given in equation 2.1.14

$$\sigma_s = (C_{1s}\, Q_1/p) + 1$$

or with the condition introduced on p. 36,

(2.7.16) $\sigma_s' = C_{1s}\, Q_1 + p$

and the rotor slot harmonics by,

(2.7.17) $\rho_s' = C_{2s}\, Q_2 + C_{1s}\, Q_1 + p$

It is worth while to recall that C_{1s} and C_{2s} may be any integer except zero. C_{1s} and C_{2s}, though both constants of the primary winding, are by no means equal.

The first order stator slot harmonic has

$Q_1 + p$ and $-Q_1 + p$ pole pairs

counted on the whole armature periphery. The ξ th order stator slot harmonic has

$\xi Q_1 + p$ and $-\xi Q_1 + p$ pole pairs,

where ξ is any positive integer excluding zero.

The slot harmonics of the rotor resulting from the fundamental rotor current can be calculated by assuming $C_{1s} = 0$, in equation 2.7.17. The first order slot harmonic will have

$Q_2 + p$ and $-Q_2 + p$ pole pairs

counted on the whole armature, and those of the ξ th order

will have

$$\xi Q_2 + p \quad \text{and} \quad -\xi Q_2 + p \text{ pole pairs}$$

also counted on the whole armature periphery.

The first order slot harmonics produce the following force waves of low modes;

a) Positively rotating first order stator slot harmonic with positively rotating first order rotor slot harmonic,

$$m_v = (Q_1 + p) - (Q_2 + p) = Q_1 - Q_2$$

b) Negatively rotating first order stator slot harmonic with positively rotating first order rotor slot harmonic,

$$m_v = (-Q_1 + p) + (Q_2 + p) = -Q_1 + Q_2 + 2p$$

c) Positively rotating first order stator slot harmonic with negatively rotating first order rotor slot harmonic,

$$m_v = (Q_1 + p) + (-Q_2 + p) = Q_1 - Q_2 + 2p$$

d) Negatively rotating first order stator slot harmonic with negatively rotating first order rotor slot harmonic,

$$m_v = (-Q_1 + p) - (-Q_2 + p) = -Q_1 + Q_2$$

The higher order slot harmonics also combine to create force waves whose modes are however higher than those of the first order slot harmonics. They can be calculated as:

$$m_v = \xi Q_1 + p - (\xi Q_2 + p) = \xi (Q_1 - Q_2)$$

$$m_v = -\xi Q_1 + p + \xi Q_2 + p = \xi(-Q_1 + Q_2) + 2p$$

$$m_v = \xi Q_1 + p - \xi Q_2 + p = \xi(Q_1 - Q_2) + 2p$$

Table 2.7.1 shows the inequalities for $|Q_1 - Q_2|$ to be observed for the purpose of avoiding low modes of force waves in normal induction motors.

Table 2.7.1

Inequalities for Low Modes

m_v mode to be avoided	$Q_1 - Q_2$ must be unequal to
0	$0 \; ; \; (2p/\xi)$
1	$1 \; ; \; (2p \pm 1/\xi)$
2	$2/\xi; \; (2p \pm 2/\xi)$
3	$3/\xi; \; (2p \pm 3/\xi)$

The frequency of the force waves is of utmost interest and can be calculated from equation 2.7.8. The frequency equation differs slightly for force waves created by fluxes rotating in the same direction from those created by fluxes rotating in opposite directions. The resultant frequencies of the former subtract, while frequencies of the latter add.

(2.7.19) $\omega_f = \omega_1 \pm \omega_2$

One of the frequencies resulting from the interaction of two stator waves represents constant sinusoidally distributed pressures, while the other is the 120 c.p.s. noise.

The frequencies of the force waves originating from the interaction of two rotor harmonics can again be determined by using equation 2.7.8. Assuming both waves to be caused by the fundamental stator MMF, the resultant frequency will be either $[2+(\rho_a+\rho_b)(1-s)]\omega$ or $[(\rho_a-\rho_b)(1-s)]\omega$.

The frequencies of the force waves caused by the interference of one stator and one rotor harmonic are most important. In the following the harmonics are assumed to be the result of the respective fundamental currents. The frequency of the stator harmonic will be ω, and that of the rotor harmonic $\omega_\rho = \omega[1+(\rho-1)(1-s)]\omega$. The resultant frequencies will therefore be

$$\omega_f = [2+(\rho-1)(1-s)]\omega \text{ , and}$$
$$\omega_f = [(\rho-1)(1-s)]\omega \qquad (2.7.20)$$

The frequencies of the force waves caused by the first slot harmonics deserve closer investigation. It is best to write down the equations of these harmonics and then calculate the frequency for each interaction. In the following, b_{ss} stands for stator slot harmonic, and b_{sr} for rotor slot harmonic. The + or - sign marks the direction of rotation.

$$b_{ss(+)}(x_1,t) \approx \sin[\omega t-(Q_1+1)(x_1\pi/p\tau)]$$

$$b_{ss(-)}(x_1,t) \approx \sin[\omega t+(Q_1-1)(x_1\pi/p\tau)]$$

$$b_{sr(+)}(x_1,t) \approx \sin\left([1+(Q_2/p)(1-s)]\omega t-(Q_2+1)(x_1\pi/p\tau)\right)$$

$$b_{sr(-)}(x_1,t) \approx \sin\left(\left[\,1-(Q_2/p)(1-s)\,\right]\omega t-(Q_2-1)(x_1\pi/p\tau)\right)$$

The positively rotating first stator and rotor slot harmonic will create a force wave of frequency,

(2.7.21) $\omega_{(+,+)} = (Q_2/p)(1-s)$

The negatively rotating first stator and positively rotating first rotor slot harmonic will create a force wave of frequency,

(2.7.22) $\omega_{(-,+)} = \left[\,2 + (Q_2/p)(1-s)\,\right]\omega$

The positively rotating first stator and negatively rotating first rotor slot harmonic will create a force wave of frequency,

(2.7.23) $\omega_{(+,-)} = \left[\,2-(Q_2/p)(1-s)\,\right]\omega$

The negatively rotating first stator and negatively rotating first rotor slot harmonic will have a force wave frequency of,

(2.7.24) $\omega_{(-,-)} = (Q_2/p)(1-s)$

Similar formulae may be established for any harmonic combination. It is advisable to record the equation of the flux waves and determine the resultant frequency by carrying out the trigonometric operations .

2.8 The Tangential Forces in the Airgap

Just as the fundamental flux distributions create tangential forces, so do the higher harmonics. They are responsible for parasitic torques and also contribute in a small measure to the noise of induction motors.

The tangential force on an elementary area can be calculated by Biot-Savart's law as

$d\tau_t = i.b \cdot dA$, or, for the case of tangential forces in the airgap of an induction motor, as,

(2.8.1) $d\tau_t = a(x_1) \cdot b(x_1) \cdot dA$,

In this expression $a(x_1)$ is the ordinate of the fictitious continuous current distribution of the rotor at point x_1.

As the concept of a continuous current distribution is not frequently applied, the following definition may help to clarify it.

Neglecting the magnetomotive potential drop in the iron, the total MMF along the flux line can, according to Ampere's law of circuitation, be expressed as

(2.8.2) $\oint H.ds = f(x_1,t) + f(x_1',t) = \sum I$,

where $f(x_1 t)$ and $f(x_1,t)$ are the magnetomotive potential drops at the points of the airgap where the flux line crosses the airgap. $\sum I$ denotes the sum of the discrete currents enclosed by the flux line. Using further the theorem of the continuity of flux; that is,

$$\int_0^{2\pi} B \, d(x\pi/\tau) = 0,$$

the familiar step-shaped MMF distribution along the airgap can be constructed.

In section 2.1, the Fourier series expansion of such MMF distributions has been given, as it appeared inconvenient to work with a discontinuous step wave. It is just as unfavorable to work with discrete currents. To overcome this difficulty, the harmonic components of the MMF distribution can be assumed to result from fictitious, continuous, sinusoidal current distributions on the armature, instead of discrete currents in slots. As the MMF distribution is the result of a summation of the discrete currents, the current distribution is necessarily the first derivative of the MMF distribution, or,

(2.8.3) $\quad a(x_1,t) = df(x_1,t)/dx$

Introducing for $f(x_1,t)$ equation 2.1.9, the current distribution can be written,

(2.8.4) $\quad a_\sigma(x_1,t) = -\sqrt{2}m\, w_1\, k_\sigma\, I_1 \cos\left[\omega t-(\sigma\pi x_1/\tau).(1/p\tau)\right],$

and in a similar way the current distribution of a rotor harmonic is,

(2.8.5) $\quad a_\rho(x_1,t) = -\sqrt{2}\, Q_2 I_{2\sigma} .\cos\Big(\left[1+(\rho-\sigma)(1-s)\omega t\right] - (\sigma\pi x_1/\tau)\Big).\,(1/2p\tau)$

Introducing into the above expression,

(2.8.6) $A\rho = -\sqrt{2}\, Q_2 I_2 \sigma_1 / 2p\tau,$

equation 2.8.5 can be rewritten as,

(2.8.5a) $a_\rho(x_1,t) = A\rho \cos\left([1+(\rho-\sigma)(1-s)\omega t] - (\rho\pi x_1/\tau)\right)$

The expression for the force wave can now become,

(2.8.7) $\Gamma_t(x_1,t) = B\sigma A\rho \sin[\omega t-(\sigma\pi x_1/\rho)] \cdot \cos\left([1+(\rho-\sigma)(1-s)]\omega t-(\rho\pi x_1/\tau)\right)$

The above equation may be resolved in the same fashion as equation 2.1.6. Two tangential force waves of mode $(\sigma \pm \rho)$ and of frequency $(\omega_\sigma \pm \omega_\rho)$ will be created.

Comparing the resultant expression with 2.7.6, a striking similarity appears: For each radial force wave there is a tangential force wave of the same mode and frequency. The amplitude of this tangential force wave is simply related to the amplitude of the radial wave. By comparing 2.8.6 with 2.5.6a, a new equation may be formulated:

$$A_{\rho'} = B\rho' g' \rho' / \mu_o R$$

Introducing this value into 2.8.7, the tangential force can now be expressed as,

(2.8.8) $\Gamma_t(x_1,t) = (1/2)(B\sigma B\rho'/\mu o)g/R)\rho'$

or

$$\Gamma_t(x_1,t) = \Gamma(x_1,t)(g'/R)\rho' \text{ newton/meter}^2$$

These forces cause additional bending moments producing vibrations of the same mode as the radial forces and they will add vectorially to the deflections of the latter. The numerical value of $(g'\rho/R)$ is of the order of $1/10^{th}$ so that the tangential force becomes inconsequential and can be ignored. Eventual extensional deformations are also negligible because the extensional rigidity of the frames is large. There is very little probability of the occurrence of tangential vibrations in the stator. The frame may, however, transmit these vibratory forces to the substructure, and if any part of the foundations have resonant frequencies coinciding with the frequencies of the tangential forces, considerable vibrations could be created.

2.9 Influence of Magnetic Saturation, Skew and Airgap Eccentricity

At the start of our investigations, simplifying assumptions were made to bring the mathematical treatment of the conditions in the airgap within reasonable bounds. While it is very difficult to give an exact answer to the effect of non-ideal conditions encountered in practice, they still have to be dealt with. Amplitude changes may occur in some of the force waves if ideal conditions are realized, and in addition, new force waves may be created.

Magnetic saturation in the iron will have two different effects depending on the stator winding connection.

The magnetizing current in a wye-connected machine is sinusoidal because no triple harmonic currents can flow. Even at low saturation of the iron the flux distribution will cease to be sinusoidal as illustrated in fig. 2.9.1.

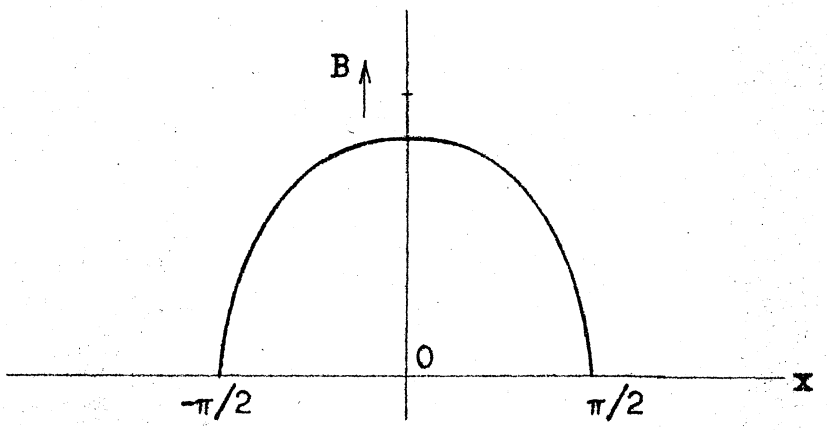

Fig. 2.9.1

Field Shape in a Wye-Connected Stator

The field shape is flat-topped and can be resolved into a Fourier series. The whole flux distribution rotates synchronously and all components therefore have the same speed and direction. Thus, new rotating flux waves occur and the equation of the flux distribution may be written as,

$$(2.9.1)\quad b(x_1,t) = B_1 \sin[\omega t-(x_1\pi/\tau)] - B_3 \sin 3[\omega t-(x_1\pi/\tau)] - B_5 \sin 5[\omega t-(x_1\pi/\tau)]-..$$

In a highly saturated machine the amplitude of B_3 may be 20 to 30 per cent of the amplitude of B_1, and the value of B_5

may reach 15 per cent of B_1.

The conditions are somewhat different in a delta-connected motor. The field distribution is here more or less sinusoidal, but the magnetizing currents now contain higher harmonic components with a third and fifth harmonic predominating as shown in fig. 2.9.2

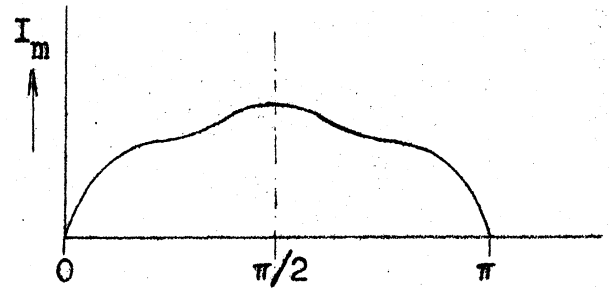

Fig. 2.9.2

The Magnetizing Current in a Phase of a Delta-Connected Machine

The third harmonic components of the magnetizing currents in the three phases are in time phase, and as a consequence the resultant flux in the airgap will pulsate. In a 60° machine, the pole pitch of this alternating field will be $(\tau/3)$. It can be conveniently resolved into two oppositely rotating fields:

$$(2.9.2) \quad b_3^{(+)}(x_1,t) = (1/2)\, B_3 \sin 3[\omega t-(\pi x_1/\tau)]$$

$$b_3^{(-)}(x_1,t) = (1/2)\, B_3 \sin 3[\omega t+(\pi x_1/\tau)]$$

The fifth harmonic component of the magnetizing current will create a field distribution of fundamental period, but its frequency will be 5f. The fifth harmonic current is a negative sequence component of the magnetizing current and the flux field resulting from it will therefore rotate in the negative direction.

$$(2.9.3) \quad b_5^{(s)}(x_1,t) = B_{s(5)}\left[5\omega t - (\pi x_1/\tau)\right]$$

These saturation harmonics in the airgap will be considerably reduced by the damping effect of the rotor as described in section 2.3. The flux waves that result from saturation may interact with the other flux waves in the airgap, and the method for the calculation of the force waves will be the same as for other harmonics.

There may also be a secondary effect which will change the amplitude of the force waves in the airgap. The saturation of the tooth tips of the stator slot openings will effectively increase the slot openings and therefore increase the amplitude of the permeance waves. The rotor slot bridges may also become saturated, as described in section 2.6. The increase of the effective slot opening will also reduce the slot leakage and slightly increase the magnetizing reactance, which means an increased damping effect on the rotor currents.

The Influence of Skewing. For the suppression of

higher harmonic parasitic torques the rotor bars of small induction motors are often skewed. Skewing has two different effects on the flux distribution in the airgap. In the following discussion insulated rotor bars will be assumed.

As shown in the next section by the calculation of the main noise-producing force waves, there is a large number of flux combinations which create force waves of the same mode and frequency that have to be vectorially combined. Only a few of them have sufficiently large amplitudes to produce any effect. The force waves created by the interaction of the two first slot harmonic force waves will have the largest amplitude. Others are caused by higher harmonic currents in the rotor. The component of the force waves resulting from the interaction of slot harmonic fluxes is not reduced by skewing. The force wave itself seems twisted to the left and to the right along the rotor axis. The magnitude of the force waves caused by a flux that results from a higher harmonic current is frequently reduced so that these components of the resultant force wave can be considered negligible. Before discussing these effects, the theory of skewing will be described.

Fig. 2.9.3 shows the developed plan of a squirrel-cage skewed winding. The voltage induced in the skewed bars

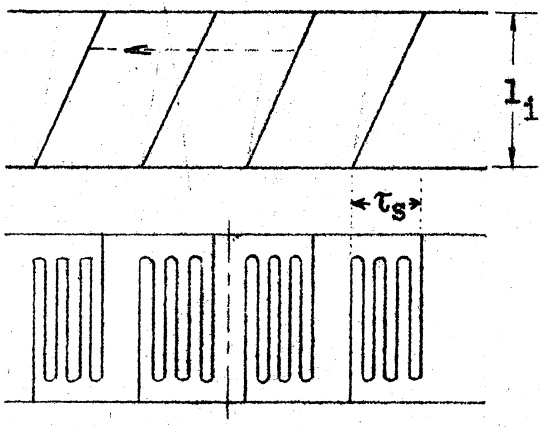

Fig. 2.9.3

A developed skewed Squirrel Cage Rotor

will be reduced compared with the voltages induced in straight bars, and the reaction of the secondary currents on the primary will also be different. Both effects are best analyzed with the aid of a skew factor k'_σ by using the product of the winding factor $k_\sigma \cdot k'_\sigma$, instead of the winding factor of the secondary alone, which is usually unity.

With the rotor bars skewed by τ_s, the fundamental and higher harmonic voltages induced in the bar will be reduced because the voltages of adjacent bar elements will be out of phase. The bar behaves as though it were a uniformly distributed winding as shown in fig. 2.9.3. The skew factor k'_σ will therefore be of the same form as the distribution factor of a continuous winding and can be expressed as,

$$(2.9.4) \quad k'_\sigma = \sin\left[(\sigma\tau_s\pi/2\tau)\right]/(\sigma\tau_s\pi/2\tau)$$

or

(2.9.4a) $k_{\sigma}' = \sin(\sigma' \tau_s \pi / 2p\tau) / (\sigma' \tau_s \pi / 2p\tau)$

The main and harmonic magnetizing reactance of the rotor are considerably reduced and by using the same method as for the straight bar it can be proved that equation 2.3.5 will be transformed to,

(2.9.5) $X_{2m\sigma} = (0.4\, Q_2 f_1 \tau l_1 / g' p)(k'_{\sigma}/6)^2 \cdot 10^{-6}$ ohms

By contrast, the differential leakage will be considerably increased and equation 2.3.13, with skewing taken into account, will become

(2.9.6) $\lambda_{2d,\sigma} = (\eta_2, 6/k'_{\sigma})^2 - 1$

The slot leakage and resistance of the bar are also increased in the ratio of the skewed bar length to the straight bar length.

On calculating the rotor currents of a skewed squirrel cage, the values given in 2.9.5 and 2.9.6, have to be inserted into the equivalent circuit of fig. 2.3 for $X_{2m\sigma}$ and $X_{2\sigma}$. With these new impedances the higher harmonic currents in the rotor bars will be considerably reduced, so that the flux waves created by them will become negligibly small.

The second factor that reduces the overall effect of slot harmonic force waves is caused by the spatial phase shift of the rotor slot harmonic flux resulting from the

fundamental current. This will be illustrated in fig. 2.9.4.

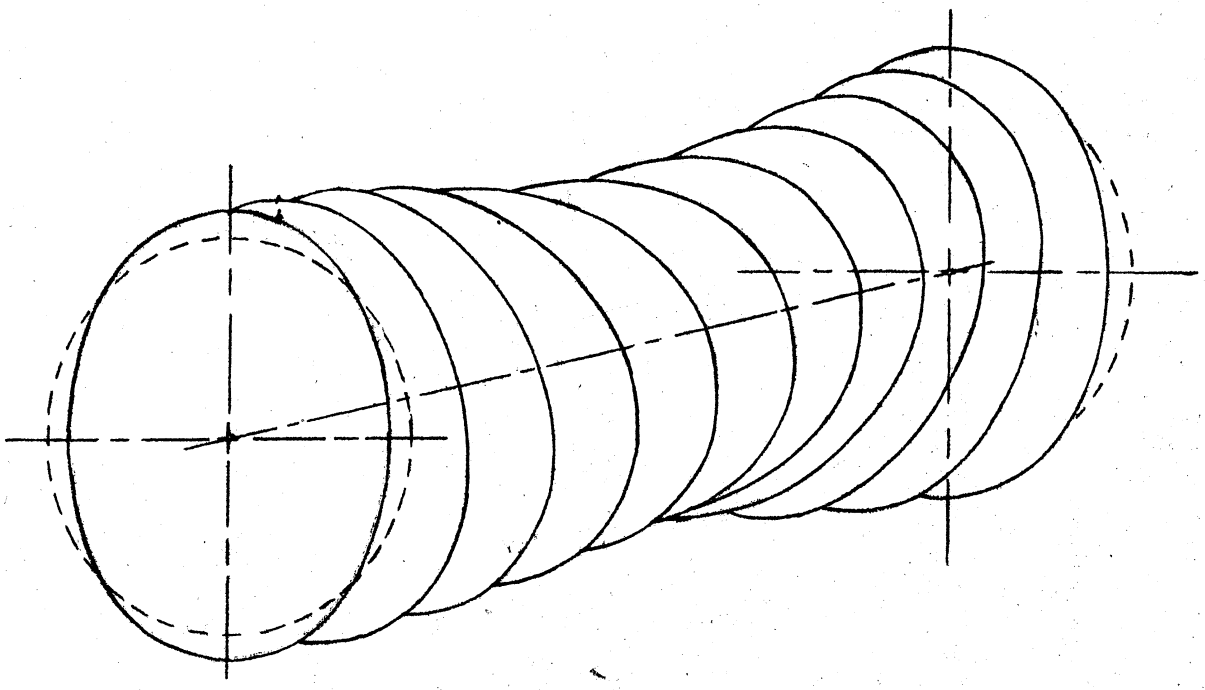

Fig. 2.9.4

Shift of the Force Waves created by Slot Harmonics

In section 2.2, rotor MMF distribution has been related to the stator under the assumption that at $t = 0$, a point on the stator $x_1 = 0$, coincides with point $x_2 = 0$ on the rotor. On choosing x_2 in the middle of the bar, traveling in one direction from the middle up, x_2 will be to the left of x_1, and traveling in the opposite direction along the bar, x_2 will be on the right. Assuming insulated bars, there is no change in the phase and magnitude of the rotor current along the skewed bar, so that the MMF wave of the rotor will be shifted accordingly. This phenomenon can be taken care of by introducing in lieu of x_2 in equa-

tion 2.5.7, $x_2-(\tau_s z/l_i)$, where z is a distance along the rotor axis with $z=0$ at the middle of the bar, and τ_s is the skew measured in meters.

The equation of the flux density distribution can now be expressed as,

$$(2.9.7)\quad b_\rho(x_1,t,z) = B_\rho \sin\left([1+(\rho-\sigma)(1-s)\omega t]-(x_1\rho\pi/\tau) + +(\rho\pi/\tau)(\tau_s z/l_i)\right)$$

To offer a practical example, the force wave as a function of z is given for the negatively rotating first stator slot harmonic, and the positively rotating first rotor slot harmonic

$$(2.9.8)\quad f(x_1,t,z)=f_{max}\cos\left([2+(Q_2/p)(1-s)]\omega t-(Q_1-Q_2-2)(x_1\pi/p\tau)+ -(Q_2+1)(\tau_s z/l_i p)\right)$$

Introducing into this equation

$$\omega_r = [2+(Q_2/p)(1-s)]\omega,$$

$$m_v = (Q_1-Q_2)p \quad \text{and} \quad \tau_s = 2p\tau/Q_1$$

and applying the trigonometric relation,

$$\cos(x+y) = \cos x \cos y - \sin x \sin y ,$$

the equation can be written as,

$$f(x_1,t,z) = f_{max}\cos[\omega_r t-(m_v/p)(x_1\pi/\tau)].\cos[2\pi(Q_2+1)z/(Q_1 l_i)] -$$

$$(2.9.8a)\quad -f_{max}\sin[\omega_r t+(m_v/p)(x_1\pi/\tau)].\sin[2\pi(Q_2+1)z/(Q_1 l_i)]$$

In the above equation it is assumed that the squirrel cage bar is skewed exactly by one primary slot pitch.

This equation demonstrates that the force distribution which had been uniform along a generatrix of the rotor becomes split into two parts:
The first part represents a cosine-shaped force distribution along the length of the stator core with the period $(l_i\ Q_1)/(Q_2+1)$, and an amplitude at mid-point of the stator as illustrated in fig. 2.9.5a. This wave is in time phase with the skewed force wave.

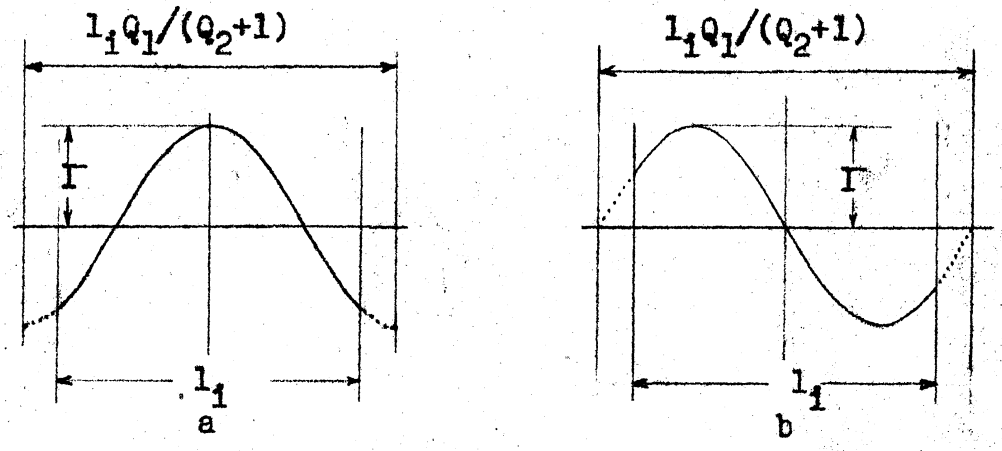

Fig. 2.9.5

Force Distribution along a Generatrix in Skewed Bar Rotors

The second part represents a sine-shaped force distribution along the length of the stator core with the period $l_i\ Q_1/(Q_2+1)$. The origin of the sine wave is in the middle of the core as shown in fig. 2.9.5b. This wave is displaced

by 90° along the armature periphery.

As previously mentioned, insulated squirrel cage bars have been assumed. However, production machines do not have insulated bars and are known to have higher than calculated losses caused by currents flowing from bar to bar across the laminations. After investigating this effect, Rossmaier and Schuisky[1] attributed the increased losses to the higher harmonic current components flowing in the iron from bar to bar (shown by the dotted line in fig. 2.9.3). At the end of his investigation, Schuisky regrets that he is unable to calculate the magnitude of the cross currents because no data were available for the impedance of the current path across the iron between two bars.

Judging by the curves presented in Schuisky's paper, it would seem as though there were little change in the fundamental rotor current resulting from non-insulated bars, and that only the higher harmonic components of the rotor currents have changed current densities across the bars. Because most of the noise is caused by slot harmonics that result from the fundamental current, it appears that non-insulated bars would have little effect on the motor's acoustic behavior.

The question of whether any vibrational axial

---

[1] 62; 63

forces are created by skewing still remains open. Bradford and Rhudy[1] have shown that a constant non-vibrational force exists because of skewing, whose magnitude is given in,

(2.9.9) $\Gamma_z = (-6\Gamma_t/R).\tan(\tau_s\pi/\tau)$

where

Γ_z is the axial force

Γ_t is the tangential force, and

R is the radius of the stator bore.

An expression for the tangential force resulting from the higher harmonic fluxes and higher harmonic current layers was derived in section 8. This expression can be easily transformed to include the effect of skew. The tangential force distribution will again be split into a cosine and sine term in the fashion demonstrated for the radial forces in equation 2.9.8a. The resultant axial forces should contain the average value of Γ_t; that is, of the tangential force. The average value of the sine term will be zero, while the average value of the cosine term may yield a small remainder term depending on the ratio of $(Q_2 \pm 1)/Q_1$.

The resultant axial thrust on the rotor is obtained by integrating this remainder term over the whole bore. As there are integral numbers of tangential force-

---

[1] 16

wave periods, this integral will be zero so that no vibratory axial forces will occur under the assumptions made.

Influence of Airgap Eccentricity[1]

The airgap of medium induction motors may be a mere fraction of one per cent of the stator bore. Bearing clearances may amount to 10 per cent of the airgap, and the clearances of bearing mountings, to an equal amount. Airgap eccentricity is therefore likely to occur in induction motors and must be investigated.

In the following analysis, a cylindrical stator and a balanced cylindrical rotor are assumed, but the rotor axis is displaced from the stator center by a small distance ε, as shown in fig. 2.9.6 below.

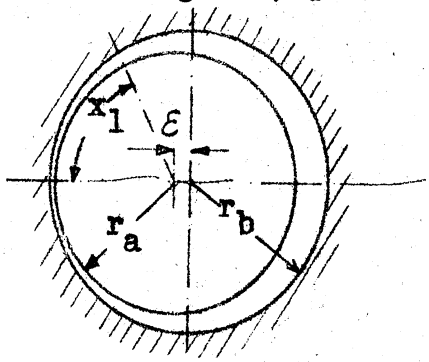

Fig. 2.9.6

Airgap Eccentricity

The flux lines are again assumed to be radial, and the magnetomotive difference in the iron, negligible. In the following analysis, the symbol

$g(x_1)$ is the airgap at point x_1, and

[1] 1

$H(x_1)$ is the magnetic field intensity in the airgap at point x_1.

Using Ampere's law of circuitation, the magnetic field intensity at point x_1 can be expressed as,

$$(2.9.10)\quad H(x_1) = \left[H(0)\, g_o - \int_o^x a(x_1,t)dx\right] \cdot \left[1/g(x_1)\right]$$

where H(0) is determined by the condition,

$$\int_o^{2\pi} b(x_1)\, dx = \mu_o \int_o^{2\pi} H(x_1)dx = 0$$

Introducing this condition into 2.9.10, H(0) can be expressed,

$$(2.9.11)\quad H(0)=\left(\int_o^{2\pi} [1/g(x_1)]dx \int_o^x [a(x_1,t)dx]\left[1/\int_o^{2\pi} [1/g(x_1)dx]\right]\right) \cdot [1/g(0)]$$

Introducing equations 2.9.11 and 2.8.4 into 2.9.10, and carrying out the integration, the field intensity at any point of the airgap is found by

$$(2.9.12)\quad H(x_1,t)=[M\sigma'/g(x_1)]\ -\sin(\omega t)+\sin[\omega t-(\sigma'\pi x_1/p\tau)]+\sin(\omega t)-\left[\int_o^{2\pi} [1/g(x_1)]\right]\sin[\omega t-(\sigma'\pi x_1/p\tau)]dx \cdot \left[1/\int_o^{2\pi} [1/g(x_1)]dx\right]$$

and the magnetic induction in the airgap as,

$$(2.9.13)\quad b(x_1,t) = [\,\mu_o M\sigma'/g(x_1)\,]\,.\sin\,[\omega t-(\sigma'\pi x_1/p\tau)\,] - [\,\mu_o M\sigma'/g(x_1)\,]\Big(\int_o^{2\pi}\sin\,[\omega t-(\sigma'\pi x_1/p\tau)\,]dx.\Big) \cdot\Big[1/\int_o^{2\pi}[1/g(x_1)\,]\,.dx\Big]$$

Using the notation in fig. 2.9.6, the function $g(x_1)$ can be expressed,

$$(2.9.14)\quad g(x_1) = r_a+\varepsilon\cos\,(x_1\pi/p\tau)-\sqrt{\varepsilon^2\cos^{\,2}(x_1\pi/p\tau)-r_b^2-\varepsilon^2}$$

Because ε is much smaller than r_b, the expression for the airgap may be simplified into,

$$(2.9.15)\quad g(x_1) = g + \varepsilon\cos\,(x_1\pi/p\tau)$$

This value can be introduced in equation 2.9.13, and the result will contain two terms of different character. The first term is,

$$(2.9.16)\quad b_o(x_1,t) =\Big(\mu_o M\sigma'/\,[g+\varepsilon\cos\,(x_1\pi\,/p\tau)\,]\Big)\,.\,\sin\,[\omega t\,-(\sigma'\pi x_1/p\tau)]\,.$$

while the second term representing pulsating fields which for $\sigma'>1$ will become negligibly small and therefore ignored in the following.

Since it is inconvenient to have the expression 2.9.15 in a denominator of a fraction, this difficulty can be overcome by developing the reciprocal of the variable airgap into the power series by simple division :

$$(2.9.17)\quad 1/[g+\varepsilon\cos(\pi x_1/p\tau)]=(1/g).\Big(1-[(\varepsilon/g)\cos\,(\pi x_1/p\tau)] - -[(\varepsilon/g)^2\cos^2\,(\pi x_1/p\tau)]-\ldots\Big)$$

This can be still further simplified as,

$$(2.9.18)\quad (1/g(x_1)=(1/g)\Big(a_0+a_1(\cos(\pi x_1/p\tau)+a_2\cos(2\pi x_1/p\tau)+ +a_v\cos(v\pi x_1/p\tau)+\cdots \Big)$$

Introducing this series into 2.9.16, the resultant airgap induction of the σ^{th} harmonic becomes

$$(2.9.19)\quad b_\sigma'(x_1,t)=(\mu_o M\sigma'/g)\sum_{v=o}^{v}\sin[\omega t-(\sigma' x\pi/p\tau)]\cdot \cdot a_v\cos(v\pi x_1/p\tau)$$

Again, this can be resolved into two fields:

$$(2.9.20)\quad b_\sigma'(x_1,t)=[\mu_o M\sigma'/g]\sum_{v\neq o}^{v}a_v\sin[\omega t-(\sigma'+v)(x\pi/p\tau)]+ +[\mu_o M\sigma'/g]\sum_{v=0}a_v\sin[\omega t+(\sigma'-v)(x\pi/p\tau)]$$

An inspection of 2.9.20 illustrates that an eccentric airgap will become responsible for harmonic fluxes of the order of $(\sigma' + v)$ and $(\sigma' - v)$ pole pairs, counted along the circumference of the stator. Because v may have the value of one, (1) there may be fields in the airgap that differ only by one pole pair, counted along the circumference of the armature. Such an occurrence will originate the eccentric forces already discussed under the heading of "One-sided Pull".

If the rotor shaft is not in the same line with the axis of the rotor cylinder, the variable airgap will also become a function of the rotor speed. The treatment

of such a problem is parallel to that of the variable airgap just mentioned, and it is merely necessary to replace $(\pi x_1/p\tau)$ in equation 2.9.18, by $(\pi x_1/p\tau)-\omega_r t$, where ω_r is the angular velocity of the rotor.

2.10 The Force Waves in the Experimental Motor

It is well to visualize first the large number of higher harmonic flux waves in the airgap with the aim of finding those flux combinations which create the greatest noise effect. All calculations will be based on data given in Appendix I. For the first part of the discussion it will suffice to know that the 4-pole motor has 60 slots and 54 rotor bars.

Table 2.10.1 lists the harmonic order of the airgap flux waves to the first slot harmonic based on equations 2.1.8 and 2.2.12. There are 44 airgap harmonics within the range of the first slot harmonics, creating a vast number of force waves. As a first step it is best to investigate the first slot harmonics. Using equations 2.7.14 and 2.7.21 to 2.7.24, table 2.10.2 can be assembled. From this table it can be observed that the frequencies of the force waves caused by slot harmonics are well in the audible range, and it can also be easily established that their amplitudes are of the same order of magnitude. But only the force wave resulting from the interference of the negatively rotating 29^{th} stator harmonic, and the positively rotating 28^{th} rotor

Table 2.10.1

Airgap Harmonics of the Experimental Motor

Stator Harmonics	Associated Rotor Harmonics		
σ	$\rho = \sigma$	$\rho = 27+\sigma$	$\rho = -27+\sigma$
1	1	28	-26
-5	-5	22	-32
7	7	34	-20
-11	-11	16	-38
13	13	40	-14
-17	-17	10	-44
19	19	46	-8
-23	-23	4	-50
25	25	52	-2
-29	-29	-2	-56
31	31	58	4

Table 2.10.2

Force Waves resulting from First Order Slot Harmonics

Rotor Harmonics	Stator Harmonics -29	Stator Harmonics +31
-26	$m_v = 6$ $f_f = 27(1-s)f$	$m_v = 10$ $f_f = 2-27(1-s)f$
+28	$m_v = 2$ $f_f = 2+27(1-s)f$	$m_v = 6$ $f_f = 27(1-s)f$

harmonic will acquire significance. In fact the force wave will be responsible for most of the pure tone noise, just because it is of a low order number.

An inspection of the calculations and results in sections 3.5 and 3.6 would prove that the second mode deflection amplitudes as a response to the second mode 100 lb force wave is of the order of 10 microinches for frequencies between 1,500 and 1,900 c.p.s. A 6th mode force wave of the same amplitude would cause deflections of the order of 1/10 of a microinch in the same frequency range. As the sensitivity of the ear is logarithmic, the sound pressures caused by the vibrations of the motor in the 6th mode would be well below the threshold of hearing. There is, however, an exception to this statement. If the m^{th} mode force wave frequency approaches the resonant frequency of the stator structure in the m^{th} mode, the deflection amplitudes may become considerable, and the noise output troublesome. As can be seen from table 3.5.11, part 2, the lowest resonant frequency in the 6th mode is at 4,240 c.p.s., while the 6th mode force wave frequency is 1,475 c.p.s. The same reasoning, to a still larger extent, applies to the 10th mode force wave.

At a slip of 0.015, the frequency of the second mode force wave, produced by the negative 29th harmonic of stator flux and the positive 28th harmonic of the rotor flux, will in accordance with equation 2.7.24, be given by

$$f_f = 2 + 27(1-0.015)60 = 1,716 \text{ c.p.s.}$$

The motor operated at lower frequencies with the same magnetic and electric loading will slightly increase its slip. Operating from a 50 c.p.s. supply, the main noise frequency will be at 1,419 c.p.s. Operating from a 40 c.p.s. supply, the main noise frequency occurs at 1,121 c.p.s. At no-load, operating from a 60 c.p.s. supply, the motor's main noise frequency will be at 1,735 c.p.s.

A closer inspection of table 2.10.1 reveals the interesting fact that other harmonic flux combinations, as listed in table 2.10.3, will result in second mode force waves of the same frequency as the second mode force wave of the slot harmonics.

Table 2.10.3

Second Mode Force Waves in the Experimental Motor of Frequency 2 + 27(1-s)f

Interfering Flux Waves		Rotor Harmonic induced by Stator Harmonic	Remarks
Stator σ	Rotor p		
-29	28	1	significant
-23	22	-5	
-17	16	-11	
-11	10	-17	
-5	4	-23	
1	-2	-29	significant

A detailed calculation will show that only the first and the last force waves have large enough amplitudes to be

considered. The force waves involving flux combinations of two belt harmonics will generally be negligibly small, as the winding distribution and coil shortening reduce their amplitudes, a fact easily observed from the winding factors.

In table 2.10.4,flux combinations creating second mode force waves of the same frequency as the two other slot harmonic combinations, i.e. 1,475 c.p.s., are given.

Table 2.10.4

Second Mode Force Waves in the Experimental Motor of Frequency 27(1-s) f

Stator Harmonic	Rotor Harmonic	Rotor Harmonic Induced by Stator Harmonic	Remarks
31	-32	-5th	significant
7	- 8	19	
19	-20	7	
13	-14	13	
1	- 2	25	significant

Here again only two flux combinations acquire significance. On closer investigation one can find that in many medium induction motors slot harmonic combinations yielding a second mode force wave, and the flux combination consisting of the main flux and a second rotor harmonic, are the important ones. However there may be many exceptions to this statement.

In the following the amplitudes of the second mode

force wave at 1,716 c.p.s. and 1,475 c.p.s. will be calculated. The former will be referred to as the main noise force wave, the latter as the side noise force wave. In all calculations 40 amp. load current or no-load condition are assumed. The terminal voltage is assumed to be the zero time axis.

Calculation of the Main Noise Producing Force Wave. The 29^{th} stator harmonic flux is the resultant of the slot and permeance harmonics. As explained in section 2.6, these will add vectorially, as q is odd and the harmonics rotate in the negative direction.

The amplitude of the 29^{th} slot harmonic calculated by equation 2.5.4a,

$$B_{29,s} = (4\pi.10^{-7}/6.7x10^{-4})\ 3\sqrt{2}\ (160)(0.874)(23.2)/(58\pi)$$
$$= 0.1415 \text{ weber/meter}^2$$

The amplitude of the main airgap flux is

$B_1 = 0.725$ weber/meter^2. The value of η_1 has been calculated in section 3.4, as $\eta_1 = 0.2$. Hence, by equation 2.6.7 the permeance harmonic flux wave will be

$$B_{29,p} = B_1 \cdot \eta_1 = (0.725)(0.2) = 0.1450 \text{ weber/meter}^2$$

The phase angle between slot and permeance harmonic is 68.2^o, so that

$B_{29} = 0.1415 + (0.1450 \angle -68.2^o)$, and the equation of the 29^{th} flux wave with the terminal voltage as time axis,

$$B_{29}(x_1,t) = 0.235 \sin [\ \omega t-(61.5\pi/180)+29(\pi x_1/\tau)]$$

The fundamental rotor current can be calculated by elementary methods and is found to be 322 amp. The amplitude of the 28^{th} flux of the rotor will, by 2.5.6, be

$$B_{28,s} = (4\pi.10^{-7}/6.7x10^{-4})(54)\ 2(322/4\pi)(1/28)$$
$$= 0.1315 \text{ weber/meter}^2$$

Applying a 20 per cent correction as discussed in section 6,

$$B_{28} = (1.2)(0.1315) = 0.1580 \text{ weber/meter}^2$$

and the equation of the flux wave

$$B_{28}(x_1,t) = 0.1580 \sin 28\ [\omega t-(11.2\pi/180)-(28\pi x_1/\tau)]$$

The formula for the amplitude of the resulting force wave can be established from equations 2.7.1 and 2.7.6, as

$$(2.10.1) \quad = (1/2)(10^7/4\pi)B_1.B_2 \text{ newton/meter}^2$$

In the numerical computations of the forced response of the experimental motor, the amplitude of the force waves will have to be inserted in pound/radian. Recalling that 1 newton/meter^2 equals 1.45×10^{-4} lb/square inch, the desired force wave amplitude will be

$$(2.10.2) \quad \Pi = (1/2)(10^7/4\pi)(1.45x10^{-4})l_s R\ B_1B_2 \text{ lb/rad.}$$

Here l_s is the stator length, and R the stator bore radius, both in inches. B_1 and B_2 are still in weber/meter^2. With the dimensions of the motor, the amplitude of the force wave will be

$$(2.10.3) \quad \Pi = (1/2)(10^7/4\pi)(1.45x10^{-4})(5.75)(4.5)B_1B_2$$
$$= 1{,}495\ B_1B_2 \text{ lb/radian}$$

The amplitude of the force wave caused by the interference of the 29^{th} stator and 28^{th} rotor harmonic flux waves will be

$$\Pi_1 = 1{,}495(0.235)(0.158) = 55.4 \text{ lb/ radian}$$

and the equation of the force wave

$$\Pi_1 = 55.4 \cos \left[29\omega t - (14\pi/180) - (\pi x_1/\tau) \right]$$

To calculate the second significant component of the force wave, the equivalent circuit of the 29^{th} rotor cage, as shown in figure 2.3.2, has to be established. The magnetizing reactance branch of the equivalent circuit is calculated by equation 2.3.5

$$X_{2m,29} = (0.4)54(60)\ (0.13)(0.18)x10^{-6} / \left[6.7x10^{-4}(2)(29^2)\right]$$

$$= 1.98 \times 10^{-5} \text{ Ohm.}$$

The differential leakage reactance of the circuit is evaluated by equations 2.3.16, 2.3.17 and 2.3.18, will be

$$X_{2d,29} = \left(\left[(58\pi/54)/\sin (58\pi/54) \right]^2 - 1 \right) 1.98 \times 10^{-5}$$

$$= 4.34 \times 10^{-3} \text{ Ohm.}$$

The slot leakage of a bar at high frequencies is 1.01×10^{-4} ohm, so that the total leakage reactance is 4.45×10^{-3} ohm. The armature current, according to equation 3.2.22 is

$$I_{2,29} = 322(1.98 \times 10^{-5})/(4.45 \times 10^{-3} + 1.98 \times 10^{-5})$$

$$= 1.43 \text{ amp.}$$

The influence of the 29^{th} permeance harmonic flux wave can be taken into account by increasing the current by the

ratio of the resultant 29^{th} harmonic flux to the 29^{th} slot harmonic flux

$$I_{2,29} = 1.43\ (0.2350/0.1415) = 2.36 \text{ amp.}$$

The amplitude of the second harmonic flux due to this current will be,

$$B_2 = (4\pi.10^{-7}/6.7 \times 10^{-4})(54/2)(0.9)(1/2) \times 2.36$$

$$= 0.027 \text{ weber/meter}^2, \text{ and the equation of this flux wave is}$$

$$B_2(x_1,t) = 0.027 \sin\left(28\ [\omega t-(61.6\pi/180)+(2x_1\pi/\tau)] \right)$$

The equation of the fundamental flux wave can be given as

$$B_1 = (0.725)[\omega t - (94.7\pi/180)-(\pi x_1/\tau)] \text{ weber/meter}^2$$

The magnitude of the force wave can be calculated to be

$$\Pi_2 = (0.027)(0.725) \times (1495) = 29.2 \text{ lb/radian,}$$

and its equation is

$$\Pi_2(x_1,t) = 29.2 \cos\ [29\ \omega t-(16.7\pi/180)+(\pi x_1/\tau)] \text{ lb/rad.}$$

The two force waves of 1,716 c.p.s. are 2.7^{o} apart, and the resultant wave will be

$$\Pi_m = |55.4 + 29.2\angle -2.70| = 84.5 \text{ lb/radian}$$

<u>The No-Load Noise</u>. At no-load, the fundamental armature current will become negligible and with it the 28^{th} slot harmonic flux wave. Consequently the first component of the previously calculated force wave can be entirely ignored. The second component of the force wave caused by

the main flux, and the second harmonic rotor flux will, although slightly reduced, be still existent. The 29^{th} slot harmonic's flux density has to be reduced in the ratio of the no-load current to the full-load current, and will be

$$B_{29,5} = (0.1415)(6.8/23.2) = 0.0415 \text{ weber/meter}^2$$

The 29^{th} permeance harmonic flux is unchanged, but the two flux components are now in phase and add directly so that the total 29^{th} flux will be

$$B_{29} = (0.1450 + 0.0415) = 0.1865 \text{ weber/meter}^2$$

The amplitude of the second harmonic flux wave will be reduced, and is

$$B_2 = 0.027(0.1865/0.2350) = 0.0214 \text{ weber/meter}^2$$

Finally the amplitude of the force wave responsible for the no-load noise will be

$$\Pi_m = (0.0214)(0.725)(1495) = 23.1 \text{ lb/radian}$$

<u>Calculation of the Force Wave creating 1,475 c.p.s. Side Noise</u>

This second mode force wave has the same frequency as the 6^{th} mode force wave of the slot harmonics. From a practical point of view it is unimportant, as it will increase the total noise of the motor only by 1/20 of a decibel. Its calculation is being carried out partly as a further check of the theory, and partly to demonstrate the combination of a flux and slot harmonic which subtract

vectorially.

There is again a string of harmonic flux combinations to create this noise. As mentioned before, only those involving flux waves of slot harmonic order, or the main flux wave will become significant. The first component of the force wave is the one due to the 31^{st} stator flux and the 32^{nd} rotor flux, associated with the 5^{th} stator harmonic. The second component of the force wave is created by the main wave and the second rotor harmonic induced by the 25^{th} stator harmonic.

The 31^{st} harmonic airgap flux is again the resultant of the respective slot and permeance harmonic fluxes. The amplitude of the 31^{st} slot harmonic flux will be given by 2.5.4a

$$B_{31,s} = 0.1325 \text{ weber/meter}^2$$

and the permeance harmonic

$$B_{31,p} = 0.1450 \text{ weber/meter}^2$$

The resultant will be

$$B_{31} = |0.1325 - (0.1450)\angle -68.2^{\circ}| = 0.1570 \text{ weber/meter}^2$$

To calculate the 32^{nd} rotor harmonic flux wave it is again necessary to establish the equivalent circuit of the 5^{th} harmonic rotor cage. By equation 2.3.5

$$X_{2m,5} = 6.68 \times 10^{-4} \text{ ohm}$$

The differential leakage reactance calculated by using equations 2.3.16, 2.3.17, and 2.3.18, can be written

$$X_{2d,5} = 1.1 \times 10^{-4} \text{ ohm.}$$

Adding the slot leakage of 1.01×10^{-4} ohm, the total leakage reactance will be 2.11×10^{-4} ohm.

The armature current caused by the 5^{th} harmonic flux, referred to the primary, will be calculated by equation 2.3.19

$$I_{1,5} = [(2)(3)\ 160\ (0.1)/54](23.2) = 41.2 \text{ amp.,}$$

and referred to the secondary, according to 2.3.22

$$I_{2,5} = (41.2)(6.68/8.79) = 31.6 \text{ amp.}$$

Finally the flux density of the 31^{st} harmonic, calculated by equation 2.5.6 is

$$B_{32} = 0.022 \text{ weber/meter}^2$$

The amplitude of the force wave caused by the 31^{st} stator and the 32^{nd} rotor slot harmonic flux waves will be, according to equation 2.10.3

(2.10.3) $\Pi_1 = (1495)(0.1570)(0.022) = 5.15$ lb/radian

For the calculation of the second significant component of the force wave, the equivalent circuit of the 25^{th} rotor cage has to be established. Using again equation 2.3.5, it can be calculated to be

$$X_{2m,25} = 2.67 \times 10^{-5} \text{ ohm}$$

The differential leakage reactance calculated by 2.3.16, 2.3.17, and 2.3.18, is

$$X_{2d,25} = 3.77 \times 10^{-3} \text{ ohm}$$

Adding the slot leakage of 1.01×10^{-4} ohms, the total leakage reactance of the 25^{th} cage will be 3.871×10^{-3} ohm.

Using equation 2.3.19, the primary current referred to the secondary 25^{th} cage, will be

$$I_{1,25} = 62.9 \text{ amp.},$$

and the secondary current by equation 2.3.22 is

$$I_{2,25} = 0.42 \text{ amp.}$$

Using equation 2.5.6, the flux density of the second harmonic rotor flux can be now calculated as

$$B_2 = 0.005 \text{ weber/meter}^2$$

and the magnitude of the force wave caused by the fundamental and the second harmonic rotor flux wave will be

$$\Pi_2 = 1495\ (0.005)\ (0.725) = 5.42 \text{ lb/radian}$$

The two components of the force wave creating the side noise are 128.4° apart, and the resultant force wave will therefore be

$$\dot{\Pi}_s = 4.6 \text{ lb/radian}$$

Table 2.10.5

Summary of Calculated Force Waves

Motor Operation	Descript. of Noise	Frequency c.p.s.	Mode m_v	Amplitude lb/radian
40 amp.,440 volt	main	1,716	2	84.5
no load,440 volt	main	1,735	2	23.1
40 amp.,440 volt	side	1,475	2	4.6

III. THE DYNAMIC RESPONSE TO ELECTROMAGNETIC FORCE WAVES

The force waves - whose modes, frequencies and amplitudes have been calculated in the previous chapter - set the motor into continuous vibration. As the next step in the solution of the noise problem, the natural behavior and the forced response of the stator will be investigated.

The study of the natural behavior of the stator is of threefold importance. Designers are in need of information on the resonant frequencies of the stator so that they can choose a winding combination for the mismatch of electromagnetic driving-force frequencies with the natural frequencies of the stator. Secondly, the problem of steady state vibrations can be easily solved once the eigenvalues and eigenvectors of the system are determined. And finally, the resonant frequencies can without difficulty be experimentally established and thus constitute a convenient check for the elastic equations of the system.

The topic of this chapter pertains to the field of engineering mechanics, and methods used in that area of science will have to be applied extensively. Furthermore, the system under consideration is a continuous one, the solution of which leads to systems of partial differential equations. Setting up equations for a system as complex as

the stator of an induction motor is not without its difficulty. Recourse will therefore be taken to determine them from Lagrange's equations of motion. The energy expressions will be established with the aid of the principles formulated by Rayleigh and Ritz. Because few electrical engineers are familiar with these methods, it seems advisable to review the theorems which form the foundation of the method.

The stator structures of induction motors may differ greatly in design, but they all consist of cylindrical shells, rings, radial and tangential ribs, and supports. General expressions for the elastic energy of these structural parts will be developed first. To make the problem susceptible to numerical solution it is essential to define the structural relation of the elements which determine the dynamic behavior of the system as a whole. Moreover, it is necessary to make assumptions based upon empirical observations, such as the effect of damping and related matters. The method itself is strictly applicable to small vibrations about an equilibrium position, and assumptions will have to be made pertinent to all calculations based on Lagrange's equation of motion. Finally the methods will be applied in general to a series of induction motors and the numerical calculations will be carried out for the experimental motor described in Appendix I.

3.1 Lagrange's Equation of Motion[1] and the Energy Method of Rayleigh - Ritz

As an introduction to the basic concepts of engineering mechanics it is desirable to start with a system of particles. In the following discussion mass will be assumed constant.

According to Newton's second law, the force $\bar{F}$ applied to a single particle can be expressed as

$$\bar{F} = m(d\bar{v}/dt) \tag{3.1.1}$$

In generalizing this equation to a system of particles, one must distinguish between external and internal forces, the latter being known as constraints. Both have to be considered, and the equation of motion can be written,

$$\bar{F}_{ji} + \bar{F}_i^{(e)} = m_i(d\bar{v}_i/dt) = m_i(d^2\bar{r}_i/dt^2) \tag{3.1.2}$$

where

$\bar{F}_i^{(e)}$ stands for external force,

$\bar{F}_{ji}$ is the constraint between the j^{th} and i^{th} particles, and

$\bar{r}$ is the radius vector to the path of the particle.

This restriction takes care of the fact that the individual particles are not free to move in all directions.

---

[1] 7;29;39169

A system consisting of n particles not connected can be defined by 3n quantities and denoted as a system of 3n degrees of freedom. If there are k constraints between these particles the degrees of freedom of the system will be reduced to 3n-k. The motion of the system can be fully described by using 3n-k equations of motion and k conditions of constraint. This approach leads to lengthy calculations and it is for that reason of great advantage to follow Lagrange in choosing 3n-k independent variables, so that the 3n orthogonal coordinates become functions of these new 3n-k variables called "generalized coordinates". The relation between the original and generalized coordinates can be expressed by a system of equations:

$$(3.1.3) \qquad \vec{r}_i = \vec{r}_i(q_1, q_2, \ldots\ldots, q_{3n-k}, t) \qquad i=1,2,\ldots.n$$

The principle of virtual displacement will be most helpful when considering equilibrium conditions of a complicated system. According to this principle, the work done by all the forces on a small displacement consistent with the constraint of the system must equal zero for systems in equilibrium.

$$(3.1.4.) \qquad \sum_i \vec{F}_i \cdot \delta\vec{r}_i = 0 \qquad\qquad i=1,2,\ldots.n$$

In the above equation, F_i represents the sum of all external and constraining forces. Restricting all further considerations to systems for which the virtual

work of constraints is zero, the same equation can simply be written as,

$$(3.1.5) \qquad \sum_i \vec{F}_i^{(e)} \cdot \delta\vec{r}_i = 0 \qquad i=1,2,.....n$$

where $F_j^{(e)}$ denotes external forces only. In the following discussion the superscript will be omitted.

Equation 3.1.5 may be extended readily to dynamic conditions, using d'Alembert's principle. Equation 3.1.1 can be written as

$$(3.1.6) \qquad \vec{F} - m(d\vec{v}/dt) = 0$$

and the principle of virtual work stated thus :

$$(3.1.7) \qquad \sum_i [\vec{F}_i - m_i(d\vec{v}/dt)] \cdot \delta\vec{r}_i = 0 \quad i=1,2,.....n$$

To express the above principle in generalized coordinates it is only necessary to indroduce for $\vec{v}_i$,

$$(3.1.8) \qquad \vec{v}_i = \sum_j (\delta\vec{r}_i/\delta q_j)\dot{q}_j + (\delta\vec{r}_i/\delta t), \quad i=1,2,....n$$

and for the virtual displacement,

$$(3.1.9) \qquad \delta\vec{r}_i = \sum_j (\delta\vec{r}_i/\delta q_j)\, \delta q_j$$

The first term of 3.1.7 can now be expressed as,

$$(3.1.10) \qquad \sum_i \vec{F}_i \cdot \delta\vec{r}_i = \sum_{i,j} \vec{F}_i \cdot (\delta\vec{r}_i/\delta q_j)\, \delta q_j = \sum_j Q_j \delta q_j$$

where Q_j is the j^{th} component of the so-called generalized

force corresponding to coordinate q_j, that is,

$$(3.1.11)\quad Q_j = \sum_i \vec{F}_i \cdot (\partial \vec{r}_i / \partial q_j) \qquad i = 1,2...n$$

It must, however, be remembered that generalized forces by no means need to have the dimensions of force. It is solely necessary that the product of the generalized force and the corresponding generalized coordinate represent work.

The second term of 3.1.7 may be transformed by the use of the complete differential that follows:

$$\frac{d}{dt}\left[\frac{d\vec{r}_i}{dt} \cdot \frac{\partial \vec{r}_i}{\partial q_j}\right] = \frac{d^2\vec{r}_i}{dt^2} \cdot \frac{\partial \vec{r}_i}{\partial q_j} + \frac{d\vec{r}_i}{dt} \cdot \frac{d}{dt}\left(\frac{\partial \vec{r}_i}{\partial q_j}\right)$$

but

$$\frac{d}{dt}\left(\frac{\partial \vec{r}_i}{\partial q_j}\right) = \frac{\partial \vec{v}_i}{\partial q_j} \text{ and from 3.1.8 } \frac{\partial \vec{v}_i}{\partial \dot{q}_j} = \frac{\partial \vec{r}_i}{\partial q_j}$$

Using these relations, the second member of 3.1.7 can be expressed as

$$(3.1.12)\quad \sum_j \left((d/dt)\,(\partial/\partial \dot{q}_j)\left[\sum_i (1/2) m_i v_i^2\right] - \partial/\partial q_j \sum_i (1/2)(m_i v_i^2)\right) \delta q_j$$

The expression behind the summation sign denotes the kinetic energy. Recalling that the virtual displacements are independent of each other, it can be written that,

$$(3.1.13)\quad (d/dt)(\partial T/\partial \dot{q}_j) - (\partial T/\partial q_j) = Q_j$$

Such an equation may be established for each generalized coordinate of the system; and the number of equations will equal the number of degrees of freedom.

The generalized forces in 3.1.13 may be constant or variable forces, or functions of time or position, or they may even fulfill other conditions. If the external forces are conservative - that is, the work done by these forces equals the change of the potential energy of the system - then, $Q_j = -\partial V/\partial q_j$, where $V = V(q_1, q_2 \cdots q_n)$ and equation 3.1.13 may be restated as,

$$(3.1.14) \quad (d/dt)(\partial T/\partial \dot{q}_j) - (\partial T/\partial q_j) + (\partial V/\partial q_j) = 0$$

If forces $\bar{Q}_j$ other than those represented by a potential act on the system, equation 3.1.13 can be completely written as,

$$(3.1.15) \quad (d/dt)(\partial T/\partial \dot{q}_j) - (\partial T/\partial q_j) + (\partial V/\partial q_j) = \bar{\bar{Q}}_j$$

These equations are called "Lagrange's equations of motion."

Theory of Small Oscillations. Lagrange's equations of motion supply the most convenient tool for treating the problem of small oscillations about an equilibrium position needed for the development of this thesis.

The potential energy of a conservative system of particles depends on the instantaneous configuration of the system, so that the potential energy can be expressed

as a function of the generalized coordinates only:

$$V = V(q_i) \qquad i = 1,2,.....n$$

Under such a condition the potential energy can be expanded by Taylor's theorem about the equilibrium position

$$(3.1.16)\quad V(q_i) = V_i(q_i)_o + \sum_i (\partial V_i/\partial q_i)_o q_i + \sum_i \sum_j (\partial^2 V_i/\partial q_i \partial q_j)_o\, q_i q_j + \cdots$$

$$i,j = 1,2.....n$$

The term linear in q_i will vanish in consequence of the condition that $(\partial V_i/\partial q_i)_o$ must be equal to zero for the system to be in equilibrium. Neglecting terms of higher than quadratic order as negligibly small, and neglecting the constant term as inconsequential, the potential energy can be expressed as a function of the quadratic term only. Thus,

$$(3.1.17)\quad V = \sum_i \sum_j (1/2)(k_{ij})\, q_i\, q_j$$

In this equation, k_{ij} stands for the second derivative of the expression behind the double summation sign in equation 3.1.16. This can be considered a constant because it depends only on the equilibrium values of the q_i's. For a system to be stable the potential energy must be a minimum in equilibrium position. Since V is zero at equilibrium, it follows that V is of a positive, definite quad-

ratic form. The partial differentiation behind the double summation sign can be interchanged. Consequently,

$$k_{ij} = k_{ji}, \quad \text{i.e., V is symmetric.}$$

The kinetic energy is a function of the generalized velocities,

$$\dot{q}_i = dq_i/dt$$

and by the same reasoning as was used in the case of the potential energy it can be proved that the kinetic energy may also be expressed as a definite quadratic form:

$$(3.1.18) \quad T = \sum_i \sum_j (1/2)(m_{ij})\dot{q}_i \dot{q}_j$$

The kinetic energy is by definition always positive and the order of indices of m can be interchanged. Consequently, the kinetic energy is a positive, symmetric, quadratic form.

Because no dynamic coupling exists in the system treated in this thesis, equation 3.1.18 can be simplified to

$$(3.1.18a) \quad T = (1/2) \sum_i m_i(\dot{q}_i)^2$$

Introducing equation 3.1.18a and 3.1.17 into the generalized equation of motion, and keeping in mind that the kinetic energy is independent of the generalized coordinates, the equation of motion can be written

$$(3.1.19) \quad \sum_j m_{ij} \ddot{q}_j + \sum_j k_{ij} q_j = 0$$

Substituting this value for T, Lagrange's equation gives

$$(3.1.20)\quad m_i \ddot{q}_i + \sum_j k_{ij} q_j = 0$$

The last equation represents a system of n differential equations of the same type as the one encountered in the theory of electric circuits. A solution will therefore be attempted by setting,

$$(3.1.21)\quad \begin{aligned} q_i &= A_i \sin(\omega t + \psi) \\ \ddot{q}_i &= -\omega^2 A_i \sin(\omega t + \psi) \end{aligned}$$

On substituting the values of q_i and $\ddot{q}_i$ into the system of equations represented by 3.1.20, n simultaneous equations will result. Lest the system have only a trivial solution, the determinant of the coefficients of the system must vanish:

$$(3.1.22)\quad \begin{vmatrix} k_{11}-m_1^2, & k_{12} \cdots & k_{1n} \\ \vdots & & \vdots \\ k_{1n} & k_{2n} \cdots & k_{nn}-m_n^2 \end{vmatrix} = 0$$

The determinant will have n roots in ω^2 which are denoted as characteristic values or eigenvalues. The developed determinant is referred to as characteristic equation. The roots of these equations stand for the square of the natural frequency f_r multiplied by 2π, and the frequency can easily be calculated, as

(3.1.23) $f_r = (\omega_r/2\pi)$

For that reason the characteristic equation is referred to as the frequency equation, and the natural frequencies of the systems are functions of eigenvalues.

On introducing the eigenvalues into equation 3.1.22, solutions for the value of A_i can be obtained. Because there are n eigenvalues, n sets of such solutions, each representing a principal mode of vibration, will result. The A_i quantities are usually referred to as eigenvectors of the system. There will be altogether n eigenvectors, each having n components.

The solution of q_i can be obtained by superposing all complementary solutions as follows:

$$(3.1.24) \quad q_i = \sum_{r=1}^{n} A_i^{(r)} \sin(\omega_r t + \Psi_r)$$

The set of eigenvectors of $A_i^{(r)}$ determine the principal r^{th} mode of oscillation which is purely harmonic, i.e., all particles move with the same frequency and phase. Generally, there are n such modes of oscillation for a system of n particles. These modes are orthogonal, which means that

$$\sum_{i=1}^{n} A_i^{(r)} A_i^{(s)} = 0$$

The magnitudes of $A_1^{(r)}, A_2^{(r)}, \ldots A_i^{(r)} \ldots$ are not

independent and are determined only so far as their ratio is concerned. It is of advantage to choose the value so that,

$$\sum (A_i^{(r)})^2 = 1$$

which condition is called the "normalizing" condition, and to express the eigenvectors as,

$$(3.1.25) \quad y_i^{(r)} = A_i^{(r)} \Big/ \sum (A_i^{(r)})^2,$$

called the "normalized" eigenvectors. The relation between the normalized eigenvectors and the eigenvectors is given by,

$$(3.1.26) \quad A_i^{(r)} = c_r \, y_i^{(r)},$$

where c_r is a constant equal to $\left[1 \Big/ \sum (A_i^{(r)})^2 \right]$

The forced response of the system - that is, the dynamic deflections caused by vibratory forces - is of utmost interest to the problem discussed in this thesis. The equation of motion can in this case be expressed by,

$$(3.1.27) \quad (d/dt(\partial T/\partial \dot{q}_i) + (\partial V/\partial q_i) = Q_i \sin(\omega t + \Psi)$$

where Q_i is the amplitude of the i^{th} component of the generalized force as defined by equation 3.1.11. Introducing again the values for the kinetic and potential energy given in 3.1.17 and 3.1.18, the equation of motion can be expressed,

$$(3.1.28) \quad m_i \ddot{q}_i + \sum_j q_j k_{ij} = Q_i \sin(\omega t + \Psi), \quad i = 1 \ldots n$$

There are n equations of the type 3.1.28 that can be estab-

lished, and together they constitute a system of n non-homogeneous equations. The solution can be found by classic methods which, however, become very lengthy for a large number of equations. The eigenvalues and eigenvectors represent the solutions to the homogeneous equations and may be used with ease to find the roots of the system of equation 3.1.28, by applying the principle of superposition and the following reasoning:

Suppose the forced vibration deflections in the r^{th} mode can be expressed as

$$(3.1.29) \quad q_i = \sum_{i=1}^{n} y_i^{(r)} c_r \cos(\omega t + \Psi)$$

Note that this equation is similar to 3.1.24, with the difference that the former contains the forcing frequency ω, instead of ω_r as in the latter.

Substituting 3.1.29 into 3.1.28, there results,

$$(3.1.30) \quad -m_i y_i^{(r)} c_r \omega^2 + c_r \sum_{j=1}^{n} k_{ij} y_j^{(r)} = Q_i$$

The second term to the left of the equation sign in 3.1.30 represents the potential energy of the system, a quantity independent of time. It can be proved that the maximum potential energy is of the same magnitude as the maximum kinetic energy. Consequently, equation 3.1.30 can be simply expressed,

$$(3.1.31)\quad m_i\, y_i^{(r)} c_r\, (\omega_r^2 - \omega^2) = Q_i$$

In the following it will be convenient to represent the generalized force in the form of a series. Thus,

$$(3.1.32)\quad Q_i = \sum_{r=1}^{n} b_r\, m_i\, y_i^{(r)}$$

Taking into account the orthogonality properties of the eigenvectors it can be shown that,

$$(3.1.33)\quad \sum_{j=1}^{n} Q_j\, y_j^{(r)} = b_r \sum_{j=1}^{n} m_j\, [y_j^{(r)}]^2$$

and on solving equation 3.1.33 for b_r

$$(3.1.34)\quad b_r = \sum_{j=1}^{n} Q_j\, y_j^{(r)} \Big/ \sum_{j=1}^{n} m_j\, [y_j^{(r)}]^2$$

Next, inserting this value of b_r into 3.1.32, an expression for Q_i is obtained. On substituting this expansion into 3.1.31, the deflection of 3.1.29 can be given as,

$$(3.1.35)\quad q_i = \sum_{r=1}^{n} \left(\sum_{j=1}^{n} Q_j y_j^{(r)} y_i^{(r)} \Big/ \sum_{j=1}^{n} m_j [y_j^{(r)}]^2 (\omega_r^2 - \omega^2) \right)$$

On setting $\omega=0$ in the above equation, the term in the large round brackets can be written as,

$$(3.1.36)\quad q_{is}^{(r)} = \sum_{j=1}^{n} Q_j y_j^{(r)} y_i^{(r)} / \omega_r^2 \sum_{j=1}^{n} m_j [y_j^{(r)}]^2,$$

this is referred to as the static deflection in the r^{th}

normal mode, and the dynamic deflection can thus be written

$$(3.1.37)\quad q_i = \sum_{r=1}^{n} q_{is}^{(r)} \left(\omega_r^2 / (\omega_r^2 - \omega^2) \right)$$

The term behind the square bracket in 3.1.37 is referred to as the resonance factor.

For the sake of simplicity, the Lagrangian equations of motion, used to find the natural frequencies and forced vibrations, have been developed here for a system of discrete, finite number of particles. The problem treated in this thesis involves a continuous system such as can be handled as a limiting case of an infinite number of discrete particles, as suggested by H. Goldstein[1] and W. Kaplan[2]. It will, as a rule, be difficult to express the elastic constraints between particles which in most cases can be formulated with the aid of recursion formulae, as difference equations. On carrying out the transition from finite to infinite numbers of particles, equations of motion will result containing, in addition to the derivative with respect to time, derivatives in respect to the position coordinates of all points. As a matter of fact, the position coordinates will take on the role of the subscripts i and j in the previous equations. The equation of motion of a continuous

---

[1] 29

[2] 38

system will therefore become a partial differential equation. The summations of the discrete particle systems will be replaced in the limit by integrations.

The questions of convergence occurs at such a transitional limiting process. Courant[1] investigated this convergence with results that can be summarized as follows: If a partial difference equation converges to a partial differential equation, the solution of the difference equations converges to the solution of the differential equations in the case of equations of elliptical type. Partial differential equations of a vibrating solid body are of this type.

A further aid for the solution of the vibration problem is the method of Rayleigh[2], as extended by Ritz[3]. On applying this method, assumptions are made for the deflection curve of the vibrating body which satisfy given boundary conditions. The eigenvalues and eigenvectors are, in this case, established from the consideration of the energy in the system. Truly to represent a continuous system such a method should assume a deflection curve expressed in an expanded form as the sum of an infinite set of

---

[1] 20

[2] 67

[3] 68

functions having undetermined coefficients. In general, each term of the expansion must satisfy the geometrical boundary values of the problem.

As the next step the kinetic and elastic energies of the system are calculated, and introduced into Lagrange's equations of motion. The undetermined coefficients are used as generalized coordinates. This leads to a system of linear equations. As mentioned before, these equations have non-vanishing solutions only if the determinant of the coefficients vanishes. The vanishing of this determinant yields the eigenvalues and eigenvectors of the system.

Should the set of functions used be a complete set, capable of representing the deflections at every point, the solution is in principle exact. Since, however, the deflection expansion has an infinite number of terms, the exact determinant yielding the eigenvalues is infinite. In engineering problems it becomes a practical necessity to consider finite rather than infinite determinants by assuming as negligible the higher order of the members representing the deflection curve. The result will thus be approximate only.

3.2 Energies in Components of Induction Motors

Energy in Cylindrical Shells. The outer frame and the inner core can be considered to be cylindrical shells. The elastic

energy of bending and extensional deformation in the cylindrical shell[1] will be expressed as a function of the radial displacement u, and the tangential displacement w. The effect of rotary inertia and the additional deflections caused by shear will be neglected.

Consider an element of a circular arc of a mean radius r_o in a rectangular system of coordinates x and z as illustrated in fig. 3.2.1

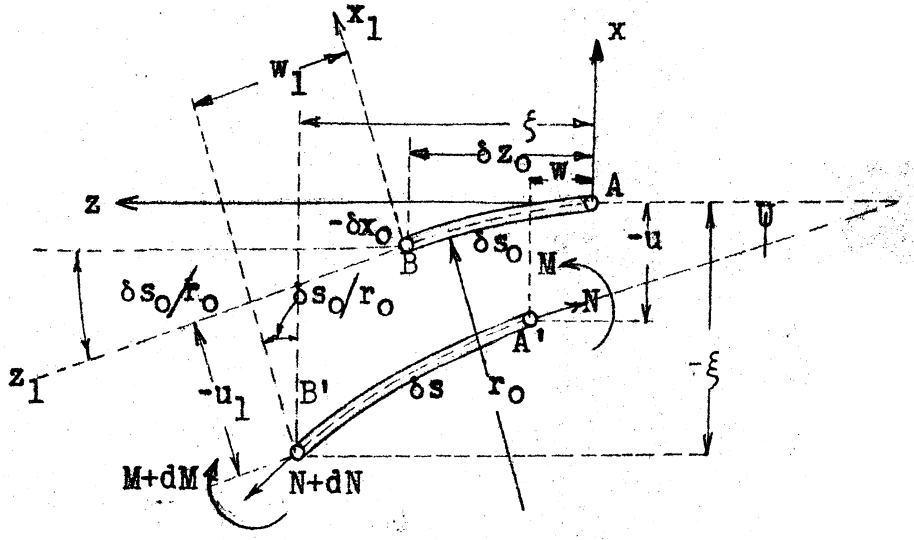

Fig. 3.2.1

Deformation of a Circular Arc

An element of a circular arc of length δs_o is shown before deformation between points A and B. After deformation, the element will have the position A' and B', and a length δs. Let A coincide with the origin of the x,z, system, and B have coordinates δx_o and δz_o. Suppose A' to have coordinates u and w, and B', ξ and ξ.

---

[1] 25;71

The position of B' with respect to the circular arc shall be fixed by the coordinates u_1, w_1. The displacement B to B' will be defined by u and w in reference to the x,z, system.

The rotation ψ of the cross section in A - that is, the angle between the tangents at A and A' - can be expressed by the sine or cosine of the angle. The limiting value of these for $\delta s_o \longrightarrow 0$ is given by,

$$\sin \psi = \lim [(-\xi + u)/\delta s] \text{ for } \delta s_o \longrightarrow 0$$

(3.2.1)

$$\cos \psi = \lim [(\zeta - w)/\delta s] \text{ for } \delta s_o \longrightarrow 0$$

Let ε denote the unit elongation of the middle fibre. Then,

$$\delta s = (1 + \varepsilon)\, \delta s_o$$

From the inspection of fig. 3.2.1, the following relations can be derived:

(3.2.2a) $\xi = u_1 \cos (\delta s_o/r_o) - w_1 \sin (\delta s_o/r_o) + \delta x_o$,

(3.2.2b) $\zeta = u_1 \sin (\delta s_o/r_o) + w_1 \cos (\delta s_o/r_o) + \delta z_o$

Because the angles in question are small they may be approximated by,

$$\sin (\delta s_o/r_o) = \delta s_o/r_o$$

where

$$\lim (\delta x_o/r_o) = 0; \quad \lim (\delta z_o/\delta s_o) = 1;$$

$$\lim \cos (\delta s_o/r_o) = 1$$

$$\lim [(-u_1+u)/\delta s_o] = 0; \quad \lim [(w_1-w_o)/\delta s_o] = dw/ds$$

It follows that,

(3.2.3a) $\sin \psi = [1/(1+\varepsilon)] . [-du/ds) + (w/r_o)]$

(3.2.3b) $\cos \psi = [1/(1+\varepsilon)] . [1+(dw/ds) + (u/r_o)]$

Setting $\sin \psi \approx \psi$ $\cos \psi = 1$, and assuming $\varepsilon \ll 1$, the following equations may be written:

(3.2.4) $\psi = (-du/ds)+(w/r_o)=(1/r_o). [(-du/d\theta)+w]$

(3.2.5) $\varepsilon = (u/r_o)+(dw/ds) = (1/r_o)\cdot [u+(dw/d\theta)]$

The bending strain is,

(3.2.6) $\varepsilon_b = [x/(r_o + x)] . [d\psi/d\theta] = (x/r_o)(d\psi/d\theta)$,

and the combined fibre strain is,

(3.2.7) $\varepsilon_x = \varepsilon + \varepsilon_b = (1/r_o) [u + (\partial w/\partial\theta) + (x d\psi/d\theta)]$

The normal force and the moment can now be expressed by displacement u and w. Recalling that $\varepsilon_x = \sigma_x (1-\sigma^2)/E$ and

$$\int_{(A)} x . dA = 0,$$

the normal force may be written

(3.2.8) $N = \int \sigma_x dA = E' \int \varepsilon_x dA = [E'\varepsilon A + (E'/r_o)(d\psi/d\theta) \int x dA] =$

$= (E'A/r_o) [(dw/d\theta)+u]$

where $E' = E/(1-\sigma^2)$, and the moment expressed as,

(3.2.9) $M = -\int \sigma_x x dA = -E'\varepsilon \int x dA - (E'/r_o)(d\psi/d\theta) \int x^2 dA =$

$= (-E'I/r_o)(d\psi/d\theta)$

$= [+E'I/r_o^2] [(d^2u/d\theta^2) - (dw/d\theta)]$

The symbols in these equations are:

$E' = E/(1-\sigma^2)$

A = area of cross section

I = moment of inertia in respect of the neutral axis at (r_o, θ)

$1-\sigma^2$ = Poisson's ratio

In medium induction motors the cylindrical shell may be assumed as inextensional, as suggested by Rayleigh[1]. This condition can be easily taken care of by setting $\varepsilon = 0$. As a consequence

(3.2.10) $\quad u = -dw/d\theta$

and

(3.2.4a) $\quad \psi = (1/r_o)[(d^2w/d\theta^2)+w]$

hence

(3.2.9a) $\quad M = (E'I/r_o^2)[(d^2u/d\theta^2)+u]$

The extensional strain energy caused by the normal force can be calculated by the formula

$$dV = (1/2)\, A\, \sigma_x \varepsilon\, dx,$$

where $dx = r_o d\theta$, and for a shell of constant cross section by

(3.2.11) $\quad V_t = (1/2E'a)\int N^2\, r_o d\theta$

On substituting N from equation 3.2.8, the expression for the extensional energy in the ring can be written as,

---

[1] 59

$$(3.2.12)\quad V_t = (E'A/2r_o) - \int_0^{2\pi} [(dw/d\theta)+u]^2 . d\theta$$

The elastic energy of bending caused by the moment can be calculated by using a formulae,

$$(3.2.13)\quad dV_b = [M^2/2E'I]\, dx$$

where dx is again $r_o\, d\theta$.

Substituting the value from equation 3.2.9, the elastic energy is,

$$(3.2.14)\quad V_b = [E'I/2r_o^3] \int_0^{2\pi} [(d^2u/d\theta^2)+(dw/d\theta)]^2\, d\theta$$

For inextensional deformation the extensional energy will obviously be zero, and the strain energy caused by bending deformation can be simplified to,

$$(3.2.15)\quad V_b = (E'I/2r_o^3) \int_0^{2\pi} [(d^2u/d\theta^2)+u]^2\, d\theta$$

Introducing, in agreement with Timoshenko[1], the flexural rigidity of the vibrating shell,

$$D = E'I$$

the potential energy of bending of an inextensional shell can be written,

$$(3.2.15a)\quad V_b = (D/2r_o^3) \int_0^{2\pi} [(d^2u/d\theta^2) + u]^2\, d\theta$$

---

[1] 71

The kinetic Energy of Vibrating Shells. Suppose a uniform vibrating mass distribution of μ slugs per radian. The kinetic energy for an elementary volume can then be expressed

(3.2.16) $dT = (1/2)\,\mu\,(\dot{v})^2\,d\theta$

and the kinetic energy of the whole ring

$$T = (\mu/2)\int_0^{2\pi} (\dot{v})^2\,d\theta$$

Substituting $\dot{v}^2 = \dot{u}^2 + \dot{w}^2$, the kinetic energy can be expressed

(3.2.17) $$T = (\mu/2)\int_0^{2\pi} (\dot{u}^2 + \dot{w}^2)\,d\theta$$

The Elastic Energy of the Radial Ribs. The radial ribs interconnecting the two cylindrical shells are, during vibrations, subjected to extensional and bending deformations. The tangential ribs add but little to the elastic energy of the system which will be numerically demonstrated in Appendix IV.

At standstill, the rib is at A and B, as illustrated in fig. 3.2.2. Let the rib move radially during vibration, so that its new position will be given by A_1 and B_1. Denoting the distances $\overline{AA_1}$ by u_a, and $\overline{BB_1}$ by u_b, the unit elongation can be expressed by,

(3.2.18) $\varepsilon = (u_a - u_b)/l_r$,

where l_r is the length of the rib. The extensional energy during deformation can be calculated according to equation 3.2.11 as,

$$(3.2.19)\quad V_t = (1/2\ E_r\ A_r) \int_0^{l_r} N^2\ dx,$$

where $N = E_r\ A_r(u_a - u_b)l_r$

Assuming this normal force is uniform over the whole length of the rib, the extensional energy is,

$$(3.2.19a)\quad V_t = (1/2\ l_r)\ E_r\ A_r\ (u_a - u_b)^2$$

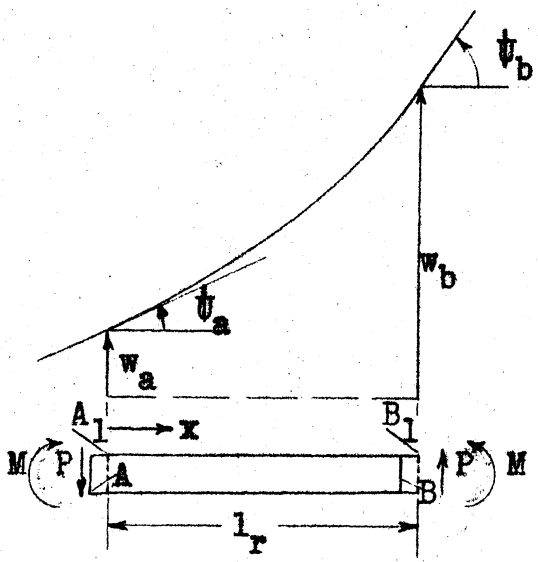

Fig. 3.2.2

Deformation of a radial Rib

For the calculation of the potential energy of bending, the rib is assumed in a condition of equilibrium, and under the action of the bending moments and shears acting at the points where the rib is built into the two cylindrical shells. The end points A and B have moved in tangential directions, by the distances w_a and w_b respectively from the unrestrained position, and received rotations ψ_a and ψ_b respectively.

The conditions of equilibrium require that the shear at any point x be,

(3.2.20) $P_x = P_a = P_b$

and that the bending moment M at any point x be,

(3.2.21) $M_x = M_b + (l_r - x)\, P_b$

The positive direction of x is from A to B. For sake of brevity, M will be written for M_b, and P for P_b.

The bending energy of the rib can be expressed as in equation 3.2.13, and for the whole rib as,

(3.2.22) $V_b = (1/2D_r) \int_0^{l_r} M_x^2\, dx$, where $D_r = E_r I_r/(1-\sigma^2)$

Introducing M from 3.2.21, the expression for the bending energy can be written,

$$V = (1/2D_r) \int_0^{l_r} (M^2+2PMl_r-2PMx+P^2l_r^2-2P^2l_rx+P^2x^2)dx$$

Carrying out the integration, this can be evaluated to,

(3.2.23) $V_b = (1/2D_r)\, [M^2 + PMl_r + (P^2l_r^2/3)].l_r$

To express the strain energy as a function of the deflections and rotations, Castigliano's[1] theorem can be conveniently applied:

(3.2.24) $\partial V_b/\partial P = w_b - w_a - l_r U_a = (l_r/2D_r)\,[Ml_r + (2/3)Pl_r^2]$

---

1 70

and

$$(3.2.25) \qquad \partial V_b/\partial M = \psi_b - \psi_a = (l_r/2D_r)(2M + Pl_r)$$

The values of M and P can now be calculated byssolving 3.2.24 and 3.2.25 as simultaneous equations. To facilitate the solution equation 3.2.21 is written as,

$$(3.2.26) \qquad V_b = \alpha\left([M + (Pl_r/2)]^2 + (Pl_r)^2/12\right); \alpha = l_r/2D_r$$

From equations 3.2.24 and 3.2.25, it follows that,

$$(3.2.24a) \qquad M + (2/3)Pl_r = (1/\alpha)\left(-[(w_a - w_b)/l_r] - \psi_a\right)$$

and

$$(3.2.25a) \qquad M + (1/2)Pl_r = (1/2\alpha)(\psi_b - \psi_a)$$

Subtracting equation 3.2.25a from 3.2.24a gives,

$$(3.2.27) \qquad (1/6)Pl_r = (1/2\alpha)\left([2(w_b - w_a)/l_r] - (\psi_a + \psi_b)\right)$$

Next,substituting 3.2.25a and 3.2.27 into 3.2.26, the elastic energy can be expressed as,

$$(3.2.28) \qquad V_b = (1/4\alpha)\left((\psi_b - \psi_a)^2 - 12[(w_b - w_a)/l_r](\psi_a + \psi_b) + \right.$$
$$\left. + 12[(w_b - w_a)/l_r]^2 + 3(\psi_a + \psi_b)^2\right)$$

Finally reverting to the original meaning of α, equation 3.2.28 can be expanded to,

$$(3.2.29) \qquad V_b = 6(D_r/l_r^3)(w_b - w_a)^2 - 6(D_r/l_r^2)(w_b - w_a)(\psi_a + \psi_b) +$$
$$+ 2(D_r/l_r)(\psi_a^2 + \psi_b^2 + \psi_a\psi_b)$$

Elastic Energy of the Supports can be derived in the same way as that of the rib. Because there is generally sufficient play in the bolts which fasten the motor to the base plate, extensional energies will be disregarded. The notation is similar to those of the previous section and is clarified in fig. 3.2.3:

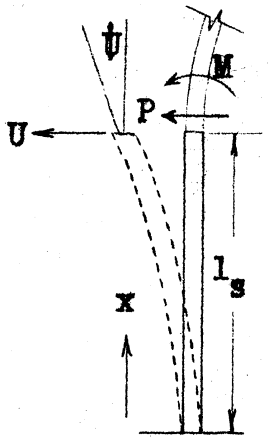

Fig. 3.2.3

Deformation of the Support

The strain energy of bending is given by 3.2.22 as,

$$V_b = (1/2\ D_s) \int_0^{l_s} Mx^2\ dx$$

where

(3.2.30) $M_x x = M + P\ (l_s - x)$

and

(3.2.31) $V_b = [l_s/2D_s]\ [M^2 + MP\ l_s + (1/3)P^2\ l_s^2]$

Again applying Castigliano's theorem, the deflection can once more be evaluated as,

(3.2.32) $u = (\partial V_b/\partial P) = (l_s/2D_s)\ [M\ l_s + (2/3)P\ l_s^2]$,

and the rotation,

(3.2.33) $\psi = (\partial V_b/\partial M) = (l_s/D_s)(M+(1/2)P\ l_s)$

Solving 3.2.32 and 3.2.33 as simultaneous equations, the values of P and M can be expressed by terms of u and ψ. Substituting the results of the simultaneous equations and bending energy of the supports into equation 3.2.31 gives,

(3.2.34) $V_b = [D_s/l_s].[(6\ u^2/l_s^2) - (6u\psi/l_s) + 2\psi^2]$

3.3 Assumptions and Notations

The theoretical elements and energy expressions developed in section 2 will be applied in section 4 in a general manner to a line of induction motors so that Lagrange's equations for the dynamic behavior of the motors may be written. The motor in Appendix I does in fact belong to this line of motors. Because the number of parameters is large and new concepts are being introduced, it seems advisable to elaborate on the notations and assumptions here prior to a detailed treatment in section 4.

A typical cross section of the line of motors under discussion is drawn in fig. 3.3.1 on page 150. The cast iron frame constituting the outer shell of the motor will be named the outer ring, an expression customarily used by designers. The following symbols will be employed in connection with the outer ring:

R is the radius to the centroid of a radial cross-section of the ring;

l_0 is the length of the outer ring;

I_0 is an area moment of inertia of the cross-sectional area about an axis through its centroid parallel to the axis of the cylinder;

A_0 is the area of a radial cross section;

The subscript 0 will generally be used in connection with the outer ring.

The stator core will be referred to as the inner ring and the following notation applied:

r is the mean diameter of the inner shell. The surface described by the circle of radius r will, in accordance with Rayleigh, be named the median surface;

l_I is the length of the inner ring;

I_I is an area moment of inertia of the cross-sectional area about an axis through its centroid parallel to the axis of the cylinder;

A_I is the radial cross section of the inner ring;

I is used as subscript for parameters belonging to the inner ring.

The short plates connecting the outer and the inner ring will be called ribs, and the following notation applied to the radial ribs:

l_r is the effective radial length of the rib;

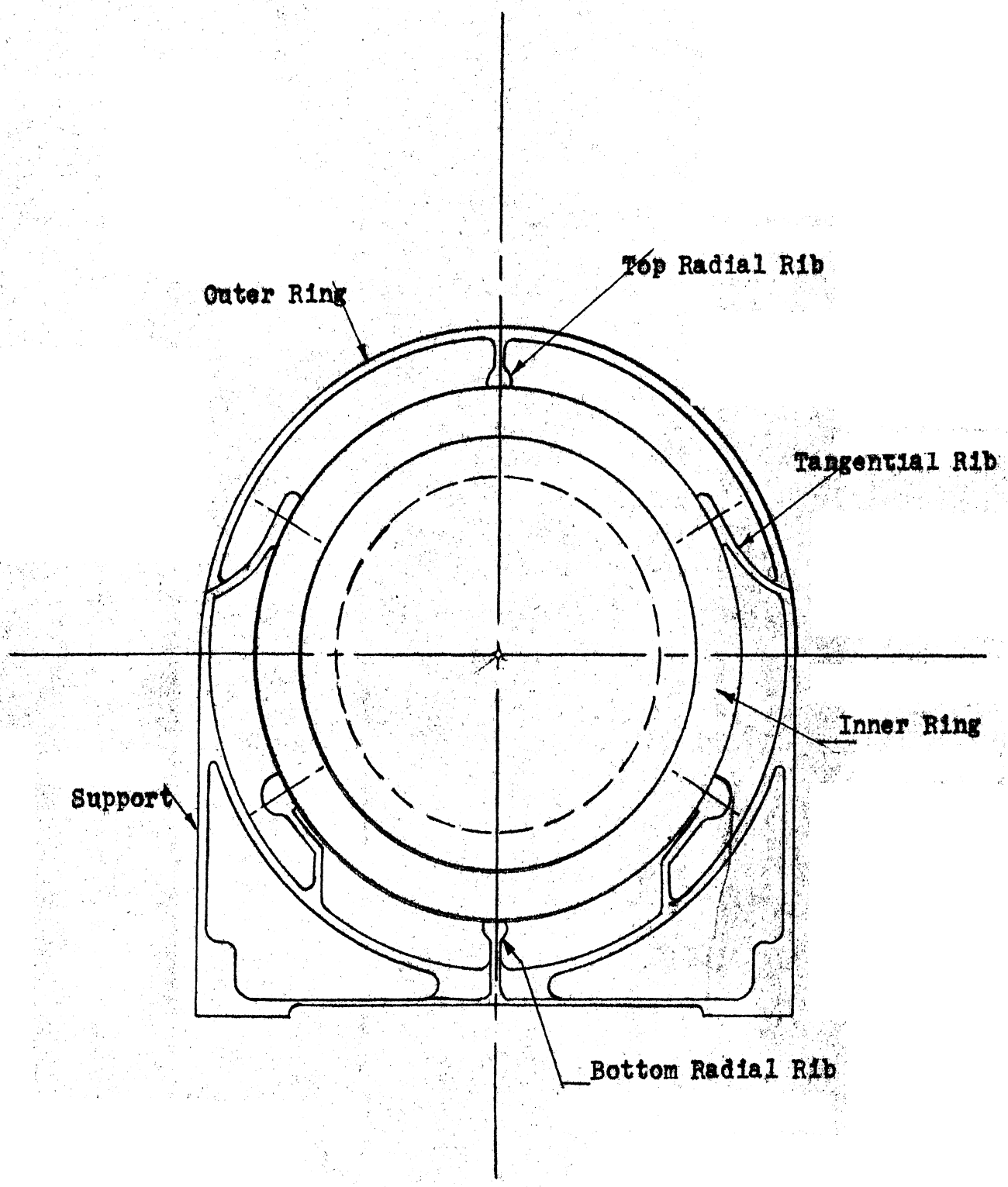

Fig. 3.3.1

Simplified Cross Section of Experimental Motor

A_r is the area of the rib in a plane cut by a concentric cylinder;

I_r is an area moment of inertia of the sectional area about an axis through its centroid parallel to the axis of the cylinder.

The subscript r will be used in connection with the ribs.

In Appendix IV, it will be shown numerically that the tangential ribs have little effect on the behavior of the system, and for the sake of clarity the necessary notation will be provided there.

The plates on both sides of the outer cylindrical shell will be denoted as supports, and the following symbols applied:

l_s is the length of the supports;

I_s is the effective moment of inertia of the supports.

In order to bring the treatment into reasonable bounds, the following assumptions based on empirical evidence will be made:

1) all displacements are extremely small compared with the dimensions of the system;
2) all vibrations take place in planes perpendicular to the axis of the shell;
3) the stator core made up of steel laminations will be considered a homogeneous body;

4) the cross-section determining the rigidities of the stator extends radially from the bottom of a stator slot to the outside diameter of the stator punchings. This is equivalent to the statement that the stator teeth and windings do not add to the rigidity of the stator core, but add to the mass.

5) the outer ring will be considered a complete cylinder. The local effects of plates and free edges of ventilating openings will be ignored in this treatment since they can be treated as secondary effects.

6) the mass of the ribs, supports, and other integral components of the outer frame's casting will be supposed to be uniformly distributed when calculating the kinetic energy of the outer ring;

7) the end shields will be ignored. It has been experimentally determined that the effect of the end shield on the mode shapes and frequencies of the main system is negligible. This is because the frequencies are so high and the amplitudes so small that the coupling is small in comparison to the effective masses of the two systems;

8) the motor will be analyzed as if it were a free body in space. Measurements show that the natural frequencies and modes are almost the same whether the motor is bolted to the base or supported on rubber blocks. The experiments of R. Plunkett[1] have proved that a normal

---

1 56

base has negligible effective mass compared to that of the motor at frequencies above 500 c.p.s.

The important question of damping causes difficulties in the dynamic treatment of mechanical systems. In its nature, damping may be inherent elastic damping or the result of friction between constructional parts. It will be necessary to make different assumptions for the two cases.

A study of information and experimental evidence indicates that elastic damping can be considered entirely negligible if the system be not at, or very near to, resonance. Fig. 3.3.2, shows the logarithmic decrement curve for the experimental motor at 1,140 c.p.s. resonance. From this it may be seen that the energy dissipated by damping in a cycle is about 3.7 per cent of the maximum kinetic energy. Using the analogy of an electric circuit, it can be stated that the Q of the system is large and that the damping forces may be considered negligible compared with inertia forces outside a narrow band around a resonant frequency. The decrement curve would indicate that elastic damping becomes important in a band width of approximately 2 per cent around resonance.

The system of the stator is composite. The stator core is pressed into the frame and it therefore appears that non-elastic displacements between the rings may occur.

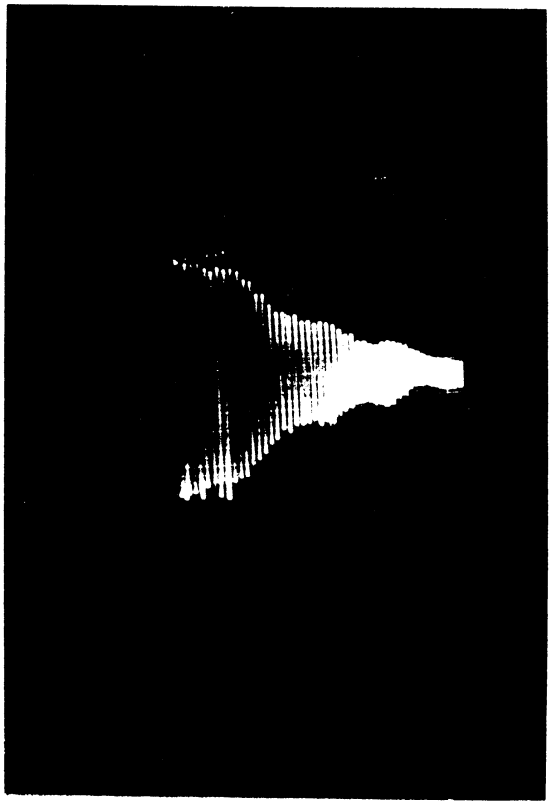

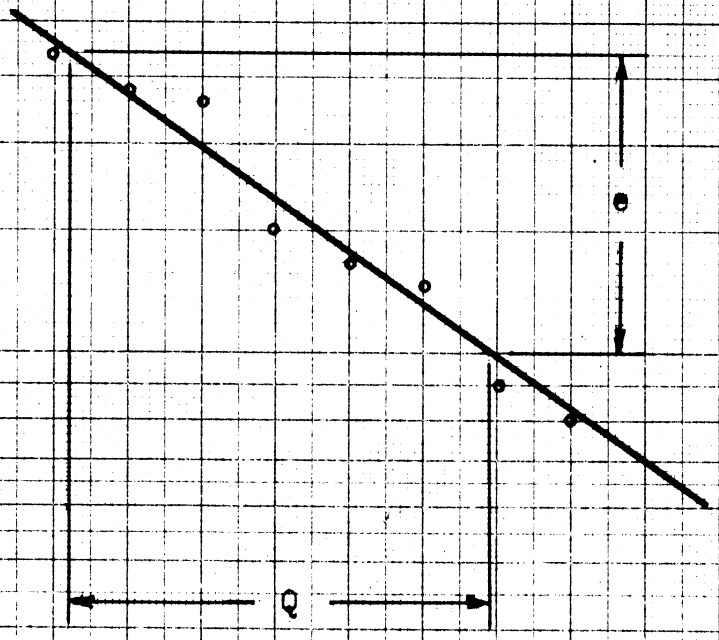

Fig. 3.3.2

Logarithmic Decrement Curve .

0 10 20 30 40 CYCLES

It has been impossible to excite the predicted modes involving opposite radial motion of the rings at the ribs. It would appear that the damping involved in such motion is so large that the modes are heavily overdamped and thus suppressed. These modes can then be ignored in practical analysis.

The system of coordinates and the notation for the displacement of the inner and outer ring are demonstrated in fig. 3.3.3.

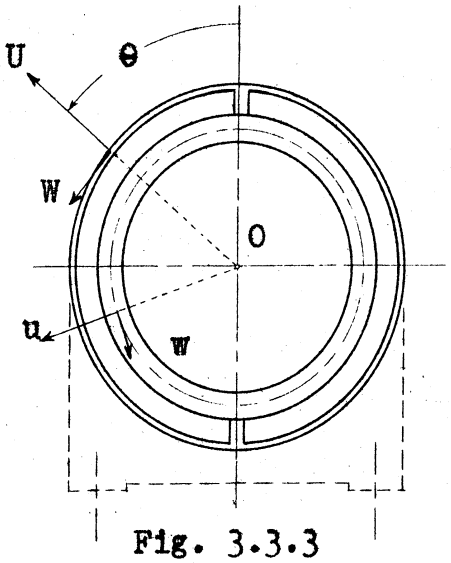

Fig. 3.3.3

System of Coordinates for the Vibrating Stator

The origin O of a polar system of coordinates is chosen at the center of the concentric rings. The argument of the radius vector will be supposed to be positive, counter-clockwise, with $\theta = 0$, at the center line of the top radial rib, and $\theta = \pi$, at the center line of the bottom rib.

The radial displacement U of the outer ring and

the radial displacement u of the inner ring will be assumed positive, directed away from the origin. The positive direction of the tangential displacement of the outer ring W, and of the inner ring w, will be supposed to coincide with the positive direction of the argument. Displacements will be measured from the unstrained position.

Several concepts which need definition will be used in the following analysis. The term mode or order of a mode will imply the number of complete periods of a sinusoidally distributed quantity along the periphery of the ring. The quantity may be displacement, velocity, acceleration, or force.

The single uniform ring is symmetrical about any diameter. For this reason there will be two vibrations of the same frequency associated with each mode as defined above. The designation of one is arbitrary and the origin of coordinates of the other will be displaced from it by a quarter wave length. In an actual manufactured ring there are certain assymetries which fix the origin of the modes and also separate the frequencies. In the motor frame a vertical diameter is an axis of symmetry which fixes these modes.

Since the motor is made up of two such rings, there will be four frequencies associated with each such mode, two each connected with each ring, modified by the coupling

between them. If the sinusoidal distribution of the displacement has its amplitude at the top radial rib, as shown in fig. 3.5.1a, the mode will be defined as a direct or a cosine mode. Should the zero amplitude of the sine wave displacement of the mode coincide with the center of the top rib as illustrated in fig. 3.5.1b, the mode will be defined to vibrate in a quadrature or sine mode. If two points on the same radial line, each belonging to one ring, move both outward at the same instant, the mode of vibration will be referred to as an in-tact mode. Should, however, the point of the outer ring move outward, while the point on the same radial line of the inner ring moves inward, the vibration mode will be referred to as a counter-tact mode.

3.4 The Equations of Motion of a Vibrating Motor Stator.

On the basis of the actual solution of the dynamic equations of the system it was found that the consideration of extensional energies of the outer and inner rings change the dynamic behavior of the lower modes of the medium induction motor by a negligible amount. However, the extensional energies cannot be ignored in either small or medium 2-pole motors or for the higher modes of medium sized motors. In the following, the solution will be established by supposing the ring to be inextensible. The corresponding solution for the extensional case will be provided in Appendix II.

The radial displacements of the outer ring can,

in the most general case, be represented by a Fourier series of the form

$$(3.4.1) \quad U = \sum_m (A_m \cos m\theta + B_m \sin m\theta)$$

Correspondingly, the radial displacement of the inner ring may be represented by the expression

$$(3.4.2) \quad u = \sum_m (a_m \cos m\theta + b_m \sin m\theta)$$

The values of m in expansions 3.4.1, and 3.4.2, must be chosen as 2,3,... This will also apply to all of the subsequent expansions of this section. But as already mentioned in section 1, it is impracticable to work with infinite determinants, and it is therefore supposed that six terms in the Fourier expansion will represent the functions with a sufficient approximation for practical purposes.

The condition of deformations without extension can be satisfied by requiring that the tangential and radial displacements be related by the equation

$$(3.2.10) \quad u = (-\partial w/\partial\theta)$$

The tangential displacement of the outer ring will therefore be expressed by the series

$$(3.4.3) \quad W = \sum (1/m) (B_m \cos m\theta - A_m \sin m\theta)$$

For the tangential displacement of the inner ring, the relationship is,

$$(3.4.4) \quad w = \sum (1/m) (b_m \cos m\theta - a_m \sin m\theta)$$

The coefficients A_m B_m, a_m,b_m are time dependent functions, and each is of the sinusoidal form. They can be expressed as $A_m(t) = A_m \cos \omega t$

The amplitudes A_m, B_m, a_m, b_m, will be the generalized co-ordinates of the system considered.

The Kinetic Energy of the Vibrating Rings can be calculated by combining expansion 3.4.1 to 3.4.4, with equation 3.2.17, and by using the solution of the following integrals

$$\int_0^{2\pi} \cos m\theta . \sin m\theta \, d\theta = 0; \quad \int_0^{2\pi} \cos m\theta . \cos n\theta \, d\theta = 0 \quad \text{for } m \neq n$$

$$\int_0^{2\pi} \sin m\theta \sin n\theta \, d\theta = 0; \quad \text{for } m \neq n$$

$$\int_0^{2\pi} \cos^2 m\theta \, d\theta = \int_0^{2\pi} \sin^2 m\theta \, d\theta = \pi$$

The kinetic energy of the outer ring is found to be

$$(3.4.5) \quad T_O = (\pi \mu_O/2) \sum [(m^2+1)/m^2] \cdot (\dot{A}_m^2 + \dot{B}_m^2)$$

The kinetic energy of the inner ring is

$$(3.4.6) \quad T_I = (\pi \mu_I/2) \sum [(m^2+1)/m^2] \cdot (\dot{a}_m^2 + \dot{b}_m^2)$$

Defining for convenience,

$$(\pi \mu_O/2) \; [(m^2+1)/m^2] = G_m$$

$$(\pi \mu_I/2) \; [(m^2+1)/m^2] = g_m$$

the kinetic energies can concisely be written as

(3.4.5a) $T_O = G_m (\dot{A}_m^2 + \dot{B}_m^2)$

(3.4.6a) $T_I = g_m (\dot{a}_m^2 + \dot{b}_m^2)$

The Potential Energy of Bending of the Vibrating Rings may be calculated by using equation 3.2.15 which is rewritten for convenience,

(3.2.15) $V_b = (D/2\, r^3) \cdot \int_0^{2\pi} [(d^2u/d\theta^2) - u]^2 \, d\theta$

Using the expansion 3.4.1 and the integral relation as in the case of the kinetic energy, the potential energy of bending of the outer ring can be evaluated as

(3.4.7) $V_{bO} = (\pi D_O/2R^3) \sum (1-m^2)^2 \cdot (A_m^2 + B_m^2)$

For the inner ring, the potential energy is

(3.4.8) $V_{bI} = (\pi D_I/2r^3) \sum (1-m^2)^2 \cdot (a_m^2 + b_m^2)$

For convenience, the following constants are introduced:

for $(\pi D_O/2R^3)(1-m^2)^2 = F_m$

for $(\pi D_I/2r^3)(1-m^2)^2 = f_m$

Substituting these constants in equations 3.4.7 and 3.4.8, the bending energy of the outer ring can be expressed as

(3.4.7a) $V_{bO} = \sum F_m (A_m^2 + B_m^2)$

and the bending energy of the inner ring is

(3.4.8a) $V_{bI} = \sum f_m (a_m^2 + b_m^2)$

The Bending Energy of the Supports will be evaluated by sub-

stituting the Fourier expansions 3.4.1 into equations 3.2.33. With the coordinate system as chosen in section 3, the rotation ψ can be evaluated from the relation

$$\psi = -(1/R)(\partial U/\partial\theta) \tag{3.4.9}$$

The supports are at $\theta = (\pi/2)$ and $\theta = (-\pi/2)$. The appropriate values of U and ψ at these points have to be established and substituted in equation 3.2.33. It follows from equation 3.4.1, subject to the proper conditions on θ, that,

$$\begin{aligned}
U_{\theta=(\pi/2)} &= -A_2 - B_3 + A_4 + B_5 + A_6 + B_7 - \ldots \\
U_{\theta=(-\pi/2)} &= A_2 + B_3 + A_4 - B_5 - A_6 - B_7 - \ldots \\
R\psi_{\theta=(\pi/2)} &= 2B_2 + 3A_3 + 4B_4 - 5A_5 - 6B_6 + 7A_7 - \ldots \\
R\psi_{\theta=(-\pi/2)} &= 2B_2 - 3A_3 + 4B_4 + 5A_5 - 6B_6 - 7A_7 - \ldots
\end{aligned} \tag{3.4.10}$$

On evaluating the bending energy of both supports one finds no product-term containing a generalized coordinate of odd subscript multiplied by a generalized coordinate of even subscript. This same fact, it will be found later, will be repeated in the energy expression of the radial rib, and also holds true for both the kinetic and elastic energies of the rings. This is a very fortunate situation indeed, as it indicates that no coupling exists between the vibration modes of odd and of even order. This will make it possible to write the determinants leading to the frequency equations for even and for odd modes separately, which means that the order of these determinants will be

reduced by one half, without impairing the approximation attempted. In the following therefore, all energy expressions will be written separately for even and for odd modes.

The potential energy of bending of both supports is given by equation 3.4.11, for even modes, and by equation 3.4.12 for odd modes. These equations follow: For the even modes,

$$V_s = [12D_s/l_s^3]\,[A_2^2 + A_4^2 + A_6^2 - 2A_2A_4 + 2A_2A_6 - 2A_4A_6] +$$
$$+ [12D_s/l_s^2R]\,[2A_2B_2 - 4A_2B_4 + 6A_2B_6 - 2A_4B_2 + 4A_4B_4 - 6A_4B_6 +$$
$$+ 2A_6B_2 - 4A_6B_4 + 6A_6B_6] +$$
$$+ [4D_s/l_sR^2]\,[4B_2^2 + 16b_4^2 + 36B_6^2 - 16B_2B_4 + 24B_2B_6 - 48B_4B_6] \qquad (3.4.11)$$

and for odd modes,

$$V_s = [12D_s/l_s^3]\,[B_3^2 + B_5^2 + B_7^2 - 2B_3B_5 + 2B_3B_7 - 2B_5B_7] +$$
$$+ [12D_s/l_s^2R]\,[3A_3B_3 + 5A_5B_3 - 7A_7B_3 + 3A_3B_5 - 5A_5B_5 +$$
$$+ 7A_7B_5 - 3A_3B_7 + 5A_5B_7 - 7A_7B_7] +$$
$$+ [4D_s/l_sR^2]\,[9A_3^2 + 25A_5^2 + 49A_7^2 - 30A_3A_5 + 42A_3A_7 - 70A_5A_7] \qquad (3.4.12)$$

The extensional energy of the radial rib will be calculated by adapting equation 3.2.19a for the stator, by writing $u_a = U$, and $u_b = u$. The energy of the top rib is then

$$V_t = (1/2\, l_r)\, E_r A_r\, [U_{\theta=0} - u_{\theta=0}]^2 \qquad (3.4.13)$$

and the energy of the bottom rib is

$$V_t = (1/2\ l_r)\ E_r A_r\ [U_{\theta=\pi} - u_{\theta=\pi}]^2$$

Now there is introduced into this equation the expansions for U and u. Also the energies for both ribs are added. Since all terms containing products of coefficients of one even and one odd subscript vanish, the extensional energy of the rib can be written separately for the even modes and for the odd modes. For the even modes:

$$\begin{aligned} V_t &= [E_r A_r/l_r]\ [(A_2-a_2)+(A_4-a_4)+(A_6-a_6)]^2 = \\ &= [E_r A_r/l_r]\ [A_2^2 + a_2^2 + A_4^2 + a_4^2 + A_6^2 + a_6^2 - 2A_2a_2 - \\ &\qquad -2A_4a_4 - 2A_6a_6 + 2A_2A_4 + 2A_2A_6 + 2A_4A_6 + \\ &\qquad +2a_2a_4 + 2a_2a_6 - 2a_4a_6 - 2a_2A_4 - 2A_2a_4 - \\ &\qquad - 2A_2a_6 - 2A_4a_6\ ] \end{aligned} \tag{3.4.14}$$

and for the odd modes

$$\begin{aligned} V_t &= [E_r A_r/l_r]\ [(A_3-a_3)+(A_5-a_5)+(A_7a_7)]^2 = \\ &= [E_r A_r/l_r]\ [A_3^2 + a_3^2 + A_5^2 + a_5^2 + A_7^2 + a_7^2 - 2A_3a_3 - 2A_5a_5 - \\ &\qquad -2A_7a_7 + 2A_3A_5 - 2A_3A_7 + 2A_5A_7 + 2a_3a_5 + 2a_3a_7 + \\ &\qquad +2a_5a_7 - 2a_3A_5 - 2a_3A_7 - 2a_5A_7 - 2A_3a_5 - 2A_3a_7 - \\ &\qquad -2A_5a_7] \end{aligned} \tag{3.4.15}$$

The bending energy of the ribs consists of three terms, each containing different constants. As the expressions are very long it seems reasonable to treat each term separately.

Introduce the expansion for W and w into the first term of equation 3.2.29. It can be evaluated for even modes to yield

$$V_{brl} = (6D_r/l_r^3)\left[(W-w)^2_{\theta=0} + (W-w)^2_{\theta=\pi}\right]$$

$$= (12D_r/l_r^3)(1/2)\left[(B_2-b_2)-(1/4)(B_4-b_4)-(1/6)(B_6-b_6)\right]^2 \quad (3.4.16)$$

This expression is expanded, and yields for the even modes, the form:

$$\begin{aligned} V_{brl} = (12D_r/l_r^3)\,[&(1/4)B_2^2 -(1/2)B_2b_2+(1/4)b_2^2+(1/16)B_4^2 \\ &-(1/8)B_4b_4+(1/16)b_4^2+(1/36)B_6^2-(1/18)B_6b_6+ \\ &+(1/36)b_6^2+(1/4)B_2B_4+(1/6)B_2B_6+(1/12)B_4B_6+ \\ &+(1/4)b_2b_4+(1/6)b_2b_6+(1/12)b_4b_6-(1/4)b_2B_4- \\ &-(1/6)b_2B_6-(1/12)b_4B_6-(1/4)B_2b_4-(1/6)B_2b_6- \\ &-(1/12)B_4b_6\,] \end{aligned} \quad (3.4.16a)$$

The corresponding expressions for the odd modes is

$$V_{brl} = (12D_r/l_r^3)\left[(1/3)(B_3-b_3)+(1/5)(B_5-b_5)+(1/7)(B_7-b_7)\right]^2 \quad (3.4.17)$$

which may be expanded to the form

$$\begin{aligned} V_{brl} = (12D_r/l_r^3)\,[&(1/9)B_3^2-(2/9)b_3B_3+(1/9)b_3^2+(1/25)B_5^2 - \\ &-(2/25)b_5B_5+(1/25)b_5^2+(1/49)B_7^2-(2/49)b_7B_7+ \\ &+(1/49)b_7^2+(2/15)B_3B_5+(2/21)B_3B_7]+ \end{aligned} \quad (3.4.17a)$$

(continued on next page)

(Equation 3.4.17a continued from previous page)

$$+(12D_r/l_r^3)\cdot[+(2/35)B_5B_7+(2/15)b_3b_5+(2/21)b_3b_7 +$$
$$+(2/35)b_5b_7-(2/15)b_3B_5-(2/21)b_3B_7 -$$
$$-(2/35)b_5B_7-(2/15)b_5B_3-(2/21)b_7B_3 -$$
$$-(2/35)b_7B_5\,]$$

The second term of 3.2.29 for both ribs can be calculated as

$$V_{br2}=[12D_r/l_r^2]\cdot[(1/2)(B_2-b_2)+(1/4)(B_4-b_4)+(1/6)(B_6-b_6)]\cdot$$
$$\cdot\Big(2\,[(B_2/R)+(b_2/r)]+4\,[(B_4/R)+(b_4/r)\,]$$
$$+6\,[(B_6/R)+(b_6/r)\,]\Big) \qquad (3.4.18)$$

This expression can be expanded to yield for the even modes:

$$V_{br2}=[12D_r/l_r^2R]\cdot[B_2^2+B_4+B_6^2-B_2b_2+(1/2)B_2B_4-(1/2)B_2B_4$$
$$+(1/3)B_2B_6-(1/3)B_2b_6+2B_2B_4-2b_2B_4-B_4b_4+$$
$$+(2/3)B_4B_6-(2/3)B_4b_6+3B_6B_2-3B_6b_2 +$$
$$+(3/2)B_6B_4-(3/2)B_6b_4-B_6b_6-\,] + \qquad (3.4.18a)$$
$$+\,[12D_r/l_r^2r]\cdot[-b_2^2-b_4^2-b_6^2+B_2b_2+(1/2)b_2B_4-(1/2)b_2b_4+$$
$$+(1/3)b_2B_6-(1/3)b_2b_6+2B_2b_4-2b_2-b_4+B_4b_4+$$
$$+(2/3)B_6b_4-(2/3)b_4b_6+3B_2B_6-3b_2b_6$$
$$+(3/2)B_4b_6-(3/2)B_6b_4-B_6b_6\,]$$

For odd modes, the second term of 3.2.29 will be

$$V_{br2} = [12D_r/l_r^2]\ [(1/3)(B_3-b_3)+(1/5)(B_5-b_5)+(1/7)B_7-b_7\ ]\cdot$$

$$3\Big([(B_3/R)+(b_3/r)]+5\ [(B_5/R)+(b_5/r)\ ]+$$

(3.4.19)

$$+7\ [(B_7/R)-(b_7/r)\ ]\Big)$$

which can be expanded to

$$V_{br2} = [12D_r/l_r^2R]\cdot[B_3^2+B_5^2+B_7^2-B_3b_3+(3/5)B_3B_5-(3/5)B_3b_5$$

$$+(3/7)B_3B_7-(3/7)B_3b_7+(5/3)B_3B_5-(5/3)b_3b_5-$$

$$-B_5b_5+(5/7)B_5B_7-(5/7)B_5b_7+(7/3)B_3B_7$$

(3.4.19a)

$$-(7/3)b_3B_7+(7/5)(B_5B_7-(7/5)b_5B_7-B_7b_7]+$$

$$+\ [12D_r/l_r^2r]\cdot[-b_3^2-b_5^2-b_7^2+b_3B_3+(3/5)b_3B_5-(3/5)b_3b_5\ +$$

$$+(3/7)b_3B_7-(3/7)b_3b_7+(5/3)B_3b_5-(5/3)b_3b_5+$$

$$+B_5b_5+(5/7)b_5B_7-(5/7)b_5b_7+(7/3)B_3b_7-$$

$$-(7/3)b_3b_7-\ (7/5)B_5b_7-(7/5)b_5b_7+B_7b_7\ ]$$

The third term of 3.2.29 for even modes can be expressed as

$$V_{br3}= [4D_r/l_r]\ [(1/R^2)(2B_2+4B_4+6B_6)^2\ -\ (1/Rr)(2B_2+4B_4+$$

(3.4.20)

$$+6B_6)(2b_2+4b_4-6b_6)\ +\ (1/r^2)(2b_2+4b_4+6b_6)^2]$$

which is expanded to

$$V_{br3} = [4D_r/l_rR^2]\ [4B_2^2+16B_4^2+36B_6^2+16B_2B_4+24B_2B_6+48B_4B_6\ ]+$$

$$+[4D_r/l_rRr]\ [4B_2b_2+8B_4b_2+12B_6b_2+8B_2b_4+16b_4B_4+24B_6b_4+$$

(3.4.20a)

$$+12B_2b_6+24B_4b_6+36B_6b_6\ ]+$$

$$+[4D_r/l_rr^2]\ [4b_2^2+16b_4^2+36b_6^2+16b_2b_4+24b_2b_6+48b_4b_6\ ]$$

The third term for the odd modes will be

$$V_{br3} = [4D_r/l_r].[(1/R^2)(3B_3+5B_5+7B_7)^2$$

(3.4.21) $$+(1/Rr)(3B_3+5B_5+7B_7)(3b_3+5b_5+7b_7)+$$

$$+(1/r^2)(3b_3+5b_5+7b_7)^2]$$

which can be expanded to

$$V_{br3} = [4D_r/l_rR^2]\ [9B_3^2+25B_5^2+49B_7^2+30B_3B_5+42B_3B_7+70B_5B_7]\ +$$

$$+\ [4D_r/l_rRr]\ [9B_3b_3+15B_5b_5+21B_7b_3+15B_3b_5+25B_5b_5\ +$$

(3.4.21a) $$+35B_7b_5+21B_3b_7+35B_5b_7+49B_7b_7]+$$

$$+\ [4D_r/l_rr^2]\ [9b_3^2+25b_5^2+49b_7^2+30b_3b_5+42b_3b_7+70b_5b_7]$$

The above expressions for the kinetic and elastic energies should now be introduced into the equation of motion 3.1.20. Twelve equations of motions result for the even modes, and another twelve equations result for the odd modes. The coefficients of these equations will constitute the determinants, similar to 3.1.22, from which the frequency equations are obtained. To write out all 144 members of each determinant in general terms would require a great effort, many unnecessary pages and would serve no immediate purpose. Instead numerical values of the terms are used. As a representative example, Lagrange's equation of motion with respect to the generalized coordinate A_2 is given below

$$(d/dt)(\partial T/\partial \dot{A}_2)+(\partial V/\partial A_2)= [-2G_2\omega^2+2F_2-(24D_s/l_s^3)+(2E_rA_r/l_r)]A_2+$$
$$+(24D_s/l_s^2R_2)B_2+[-(2E_rA_r/l_r)]a_2+$$
$$+[(-24D_s/l_s^3)+(2E_rA_r/l_r)]\ A_4+$$
$$+[-48D_s/l_s{}^2R]B_4+(-2E_rA_r/l_r)a_4+ \qquad (3.4.22)$$
$$+\ [24D_s/l_s^3)+(2E_rA_r/l_r)]A_6$$
$$+\ (72D_s/l_s^2R)B_6+(-2E_rA_r/l_r)A_6 = 0$$

The numerical values of the constants may be easily obtained and used for the coefficients for the undetermined equations. This work is carried out in section 5, by using the kinetic and potential energy expressions derived in detail in this section.

3.5 Calculation of the Natural Behavior of the Experimental Motor

Both the theory and the assumptions in sections 1, 2 and 4, will be applied to the experimental motor, in order to find the eigenvalues (resonant frequencies), and eigenvectors of the system. The data of this stator are given in Appendix I, where the respective areas, moments of inertia, and mass per radian are also calculated. The following tables list the needed coefficients in accordance with these assumptions.

Table 3.5.1

Inertia Constants of the Outer and Inner Ring

$$G_m = (m^2+1)\pi\mu_O/2m^2 \quad ; \quad g_m = (m^2+1)\pi\mu_I/2m^2$$

m	2	4	6	3	5	7
$G_m x10^2$	7.690	6.537	6.324	6.830	6.399	6.278
$g_m x10^2$	9.713	8.256	7.986	8.633	8.081	7.929

Table 3.5.2

Elastic Constants of the Outer and Inner Ring

$$F_m = \pi D_O(1-m^2)^2/2R^3 \quad ; \quad f_m = \pi D_I(1-m^2)^2/2r^3$$

m	2	4	6	3	5	7
$F_m x10^{-6}$	0.302	7.548	41.095	2.147	19.323	154.585
$f_m x10^{-6}$	1.122	28.061	152.777	7.982	71.836	287.346

Table 3.5.3

Elastic Constants of the Radial Rib

$(E_r A_r/l_r)$	$12D_r/l_r^3$	$12D_r/l_r^2R$	$12D_r/l_r^2r$
$46.000x10^6$	$10.465x10^6$	$0.989x10^6$	$1.092x10^6$

$4D_r/l_rR^2$	$4D_r/l_rRr$	$4D_r/l_rr^2$
$4.200x10^4$	$4.600x10^4$	$5.000x10^4$

Table 3.5.4

Elastic Constants of the Supports

$(12D_s/l_s^3)$	$(12D_s/l_s^2R)$	$4D_s/l_sR^2$
5.110×10^4	5.580×10^4	2.027×10^4

In tables 3.5.5 and 3.5.6, the determinants yielding the characteristic equations have been assembled. All terms except the coefficients of ω^2 should be multiplied by 10^6, though these multiplications are not recorded on the above tables for the sake of brevity. Furthermore it has been necessary to write the determinants in two sections. Part I contains columns 1-6, and Part II those of 7-12.

The task of finding the eigenvalues and eigenvectors was carried out on the Electronic Data Processing Machine. The programing on the computer required:

1) the coefficient in front of the frequency term to be unity,
2) the sum of the squares of all elements of the determinants to be less than one, and
3) the determinants to be symmetric to the main diagonal.

All elements of the r^{th} row and r^{th} column were divided by the square root of the coefficient of the r^{th} frequency term. This procedure assures the retention of the symmetry of the original determinants, and compliance with condition 1. The second condition was satisfied by dividing all elements by 10^{10}.

In the following it will be necessary to distinguish between the determinants as given in tables 3.5.5 and 3.5.6, and the determinants resulting from the transformations. The former will be referred to as the original determinant, while the latter will be denoted as the transformed determinant.

The transformed determinants are recorded in tables 3.5.7 (even modes) and 3.5.8 (odd modes). In these λ has been written for $\omega^2.10^{-10}$.

The data in determinants 3.5.7 and 3.5.8 have been programmed for the Electronic Data Processing Machine. The resultant eigenvalues and eigenvectors are recorded in table 3.5.9 for the even, and in table 3.5.10 for the odd modes. The method used for these calculations is explained in Appendix III.

For the solution of the vibration problem it is essential to evaluate the eigenvalues and eigenvectors of the original system. The procedure for this evaluation is explained below.

To find the eigenvalues of the original system it is only required to keep in mind that λ has been substituted for $\omega^2.10^{-10}$. The eigenvalues of the transformed system multiplied by 10^{+10} will yield the eigenvalues of the original system.

The required transformation of the eigenvectors can be obtained by the following reasoning (on page 184)

Table 3.5.5, Part I

Original Determinant of the Even Modes, Column 1-6

		1 A_2	2 B_2	3 a_2	4 b_2	5 A_4	6 B_4
1	A_2	$92.706-0.1538\omega^2$	0.112	-92.000		91.900	-0.223
2	B_2	0.112	$8.195-0.1538\omega^2$		-5.012	-0.112	5.21
3	a_2	-92.000		$94.245-0.1943\omega^2$		-92.000	
4	b_2		-5.012		$5.57-0.1943\omega^2$		-3.792
5	A_4	91.900	-0.112	-92.000		$107.19-0.1307\omega^2$	0.223
6	B_4	-0.223	5.205		-3.794	0.223	$19.917-0.1307\omega^2$
7	a_4	-92.000		92.000		-92.000	
8	b_4		-0.685		0.420		-0.715
9	A_6	92.102	0.112	-92.000		91.000	-0.223
10	B_6	0.335	5.92		-3.680	-0.335	3.393
11	a_6	-92.000		92.000		-92.000	
12	b_6		1.572		-1.090		0.846

Table 3.5.5, Part II

Original Determinant of the Even Modes, Columns 7-12

		7	8	9	10	11	12
		a_4	b_4	A_6	B_6	a_6	b_6
1	A_2	-92.000		92.102	0.335	-92.000	
2	B_2		-0.685	0.112	5.92		1.572
3	a_2	92.000		-92.000		92.000	
4	b_2		0.42		-3.68		-1.09
5	A_4	-92.000		91.900	-0.335	-92.00	
6	B_4		-0.715	-0.223	3.393		0.846
7	a_4	$148.122-0.1651\omega^2$		-92.00		92.00	
8	b_4		$56.32-0.1651\omega^2$		-0.896		0.101
9	A_6	-92.00		$174.29-0.1265\omega^2$	0.335	-92.00	
10	B_6		-0.896	0.335	$88.21-0.1265\omega^2$		0.624
11	a_6	92.00		-92.00		$397.52-0.1597\omega^2$	
12	b_6		0.101		0.624		$306.32-0.1597\omega^2$

Table 3.5.6, Part I

Original Determinant of the Odd Modes, Columns 1-6

		1 A_3	2 B_3	3 a_3	4 b_3	5 A_5	6 B_5
1	A_3	$96.691-0.1367\omega^2$	-0.167	-92.000		91.337	0.167
2	B_3	0.167	$9.1962-0.1367\omega^2$		-1.953	0.279	4.119
3	a_3	-92.00		$107.964-0.1727\omega^2$		-92.000	
4	b_3		-1.953		$16.706-0.1727\omega^2$		-1.673
5	A_5	91.337	0.279	-92.000		$131.750-0.128\omega^2$	-0.279
6	B_5	0.167	4.119		-1.673	-0.279	$42.959-0.128\omega^2$
7	a_5	-92.000		92.000		-92.000	
8	b_5		0.547		-0.335		-0.014
9	A_7	92.927	-0.391	-92.00		90.45	0.391
10	B_7	-0.167	5.004		-2.197	0.279	4.602
11	a_7	-92.00		92.00		-92.00	
12	b_7		1.768		-0.615		1.240

Table 3.5.6, Part II

Original Determinant of the Odd Modes, Columns 7-12

		7	8	9	10	11	12
		a_5	b_5	A_7	B_7	a_7	b_7
1	A_3	-92.000		92.927	-0.1674	-92.000	
2	B_3		0.547	-0.391	5.004		1.768
3	a_3	92.000		-92.000		92.000	
4	b_3		-0.335		-2.197		-0.615
5	A_5	-92.000		90.450	0.279	-92.000	
6	B_5		-0.014	0.391	4.602		1.24
7	a_5	$235.67-0.1616\omega^2$		-92.000		92.000	
8	b_5		$143.98-0.1616\omega^2$		-0.124		0.62
9	A_7	-92.000		$248.753-0.1256\omega^2$	-0.391	-92.000	
10	B_7		-0.124	-0.391	$159.82-0.1256\omega^2$		0.97
11	a_7	92.00		-92.00		$666.69-0.1586\omega^2$	
12	b_7		0.62		0.97		576.133

Table 3.5.7, Part I

Transformed Determinant of the Even Modes, Columns 1-6

		1	2	3	4	5	6
		A_2	B_2	a_2	b_2	A_4	B_4
1	A_2	.06027700-λ	.00007260	-.05323000	.00000000	.06480000	.00015740
2	B_2	.00007260	.00532800-λ	.00000000	-.00290000	-.00008180	.00367000
3	a_2	-.05323000	.00000000	.04851700-λ	.00000000	-.05773000	.00000000
4	b_2	.00000000	-.00290000	.00000000	.00286700-λ	.00000000	-.00238100
5	A_4	.06480000	-.00008180	-.05773000	.00000000	.08198700-λ	.00017000
6	B_4	-.00015740	.00367000	.00000000	-.00238100	.00017000	.01523000-λ
7	a_4	-.05774000	.00000000	.05137900	.00000000	-.06261900	.00000000
8	b_4	.00000000	-.00042990	.00000000	.00023460	.00000000	-.00048670
9	A_6	.06603700	.00008000	-.05893000	.00000000	.07147000	-.00017360
10	B_6	.00024000	.00424500	.00000000	-.00235700	-.00026000	.00263900
11	a_6	-.05870300	.00000000	.05224300	.00000000	-.06366800	.00000000
12	b_6	.00000000	.00100300	.00000000	-.00061900	.00000000	.00058550

Table 3.5.7, Part II

Transformed Determinant of the Even Modes, Columns 7-12

		7	8	9	10	11	12
		a_4	b_4	A_6	B_6	a_6	b_6
1	A_2	-.05774000	.00000000	.06603700	.00024000	-.05870300	.00000000
2	B_2	.00000000	-.00042990	.00008000	.00424500	.00000000	.00100300
3	a_2	.05137900	.00000000	-.05893000	.00000000	.05224300	.00000000
4	b_2	.00000000	.00023460	.00000000	-.00235700	.00000000	-.00061900
5	A_4	-.06261900	.00000000	.07147000	-.00026000	-.06366800	.00000000
6	B_4	.00000000	-.00048670	-.00017360	.00263900	.00000000	.00058550
7	a_4	$.08971000-\lambda$	.00000000	-.06367700	.00000000	.05666400	.00000000
8	b_4	.00000000	$.03411000-\lambda$	.00000000	-.00061880	.00000000	.00006220
9	A_6	-.06367700	.00000000	$.13778000-\lambda$	.00036400	-.06474000	.00000000
10	B_6	.00000000	-.00061880	.00026460	$.06973000-\lambda$	.00000000	.00043910
11	a_6	.05666400	.00000000	-.06474000	.00000000	$.24891600-\lambda$	.00000000
12	b_6	.00000000	.00006220	.00000000	.00043910	.00000000	$.19181000-\lambda$

Table 3.5.8, Part I

Transformed Determinant of Odd Modes, Columns 1-6

		1	2	3	4	5	6
		A_3	B_3	a_3	b_3	A_5	B_5
1	A_3	.07072200 $-\lambda$	-.00012200	-.05988000	.00000000	.06907000	.00012650
2	B_3	-.00012200	.00672600 $-\lambda$	.00000000	-.00127100	.00021080	.00311300
3	a_3	-.05988000	.00000000	.06252900 $-\lambda$	.00000000	-.06190000	.00000000
4	b_3	.00000000	-.00127100	.00000000	.00967600 $-\lambda$	.00000000	-.00112600
5	A_5	.06907000	.00210800	-.06190000	.00000000	.10292900 $-\lambda$	-.00021800
6	B_5	.00012650	.00311300	.00000000	-.00112600	-.00021800	.03356200 $-\lambda$
7	a_5	-.06189000	.00000000	.05508000	.00000000	-.06398000	.00000000
8	b_5	.00000000	.00036800	.00000000	-.00020000	.00000000	-.00000974
9	A_7	.07090000	-.00029800	-.06248000	.00000000	.07135000	.00030800
10	B_7	-.00012770	.00381800	.00000000	-.00149200	.00022000	.00363000
11	a_7	-.06248000	.00000000	.05561000	.00000000	-.06459000	.00000000
12	b_7	.00000000	.00120000	.00000000	-.00037200	.00000000	.00008705

Table 3.5.8, Part II

Transformed Determinant of Odd Modes, Columns 7-12

		7	8	9	10	11	12
		a_5	b_5	A_7	B_7	a_7	b_7
1	A_3	-.06189000	.00000000	.07090000	-.00012770	-.06248000	.00000000
2	B_3	.00000000	.00036800	-.00029800	.00381800	.00000000	.00120000
3	a_3	.05508000	.00000000	-.06248000	.00000000	.05561000	.00000000
4	b_3	.00000000	-.00020000	.00000000	-.00149200	.00000000	-.00037200
5	A_5	-.06398000	.00000000	.07135000	.00022000	-.06459000	.00000000
6	B_5	.00000000	-.00000974	.00030840	.00363000	.00000000	.00008705
7	a_5	.14584000-λ	.00000000	-.06457500	.00000000	.05747000	.00000000
8	b_5	.00000000	.08909600-λ	.00000000	-.00008705	.00000000	.00038730
9	A_7	-.06457500	.00000000	.09805000-λ	-.00031100	-.06519300	.00000000
10	B_7	.00000000	-.00008705	-.00031100	.12725000-λ	.00000000	.00068740
11	a_7	.05747000	.00000000	-.06519300	.00000000	.42034000-λ	.00000000
12	b_7	.00000000	.00038730	.00000000	.00068740	.00000000	.36320000-λ

Table 3.5.9, Part I

Eigenvalues and Eigenvectors of the Transformed Determinant for Even Modes, Col. 1-6

		1	2	3	4	5	6
		A_2	B_2	a_2	b_2	A_4	B_4
Eigenvalues		.429799	.005123	.000827	.000351	.006608	.016787
Eigenvectors 1	A_2	+.334485	-.030576	+.668162	+.155638	-.518493	-.015605
2	B_2	+.000068	+.760054	-.140689	+.540286	-.073077	+.316374
3	a_2	-.298358	+.053920	+.706090	+.173042	+.508764	+.006378
4	b_2	-.000001	-.514512	-.185667	+.808629	+.039123	-.209075
5	A_4	+.372309	+.057456	-.022430	+.001154	+.669767	+.005632
6	B_4	-.000154	-.384095	+.012780	-.001158	+.017318	+.920991
7	a_4	-.350197	-.008082	+.007513	+.001144	-.110657	-.006377
8	b_4	$-.000000_3$	+.007874	-.000333	+.001153	-.000943	+.033718
9	A_6	+.434341	+.002862	-.002440	-.000872	+.062768	+.005886
10	B_6	+.000273	-.052582	-.000579	-.006114	+.010106	-.080075
11	a_6	-.590930	-.001274	+.001302	+.000195	-.016672	-.000639
12	b_6	$+.000000_4$	-.004464	+.000099	-.000199	+.000448	-.005445

Table 3.5.9, Part II

Eigenvalues and Eigenvectors of the Transformed Determinant for Even Modes, Col. 7-12

			7	8	9	10	11	12
			a_4	b_4	A_6	B_6	a_6	b_2
	Eigenvalues		.025204	.034119	.051839	. 07028	.152906	.191822
Eigenvectors	1	A_2	+.268786	+.000250	-.180848	+.000652	+.206132	+.000004
	2	B_2	+.000329	-.016087	-.000034	+.069938	+.000203	+.005590
	3	a_2	-.246328	+.000000	+.160824	+.002428	-.184769	+.000000
	4	b_2	-.001230	+.009404	+.000827	-.039732	-.000015	-.003455
	5	A_4	+.535358	-.000395	-.253567	-.007897	+.240820	-.000005
	6	B_4	+.009083	-.027013	-.005053	+.054145	-.000409	+.003536
	7	a_4	+.737584	-.000531	+.505858	+.005079	-.254961	+.000000
	8	b_4	+.000695	+.999221	+.000569	-.018848	-.000005	+.000348
	9	A_6	-.186490	-.000302	+.785322	+.009304	+.394668	+.000007
	10	B_6	+.002161	+.021905	-.011993	+.995006	+.001095	+.003932
	11	a_6	+.039626	+.000000	-.065886	-.001549	+.802873	+.000000
	12	b_6	-.000044	-.000216	+.000062	-.004625	-.000011	+.000064

Table 3.5.10, Part I

Eigenvalues and Eigenvectors of the Transformed Determinant for Odd Modes, Col. 1-6

		1	2	3	4	5	6
		A_3	B_3	a_3	b_3	A_5	B_5
Eigenvalues		.266263	.005913	.005357	.009922	.019960	.033803
1	A_3	.257327	+.182372	.725983	.004959	-.448169	.009857
2	B_3	-.000459	+.926376	-.224485	-.279262	+.014597	.110089
3	a_3	-.233463	+.150412	+.640312	+.009296	.592931	-.006648
4	b_3	+.000005	+.276157	-.076870	+.956661	-.002524	-.049352
5	A_5	+.293202	-.028169	-.071769	+.003831	.656592	-.003995
6	B_5	+.000503	-.091069	+.017965	+.079473	.009965	+.991629
7	a_5	-.349722	+.006227	+.023089	-.000083	-.095287	+.003063
8	b_5	-.000000	-.003456	+.000818	+.003735	-.000086	-.000801
9	A_7	+.496062	-.003789	-.023853	-.000811	+.081742	-.005383
10	B_7	-.000882	-.022782	+.006434	+.018781	-.002534	-.043798
11	a_7	+.651863	+.001462	+.005396	-.000019	-.019381	+.000519
12	b_3	+.000011	-.002753	+.000657	+.001895	-.000051	-.000626

Table 3.5.10, Part II

Eigenvalues and Eigenvectors of the Transformed Determinant for Odd Modes, Col. 7-12

		7	8	9	10	11	12
		a_5	b_5	A_7	B_7	A_7	B_7
Eigenvalues		.06256	.089097	.107047	.127541	.538649	.363267
Eigenvectors 1	A_3	+.009857	+.295591	-.115421	+.001141	-.267950	-.000002
2	B_3	+.110089	+.002637	-.001825	+.032713	+.000149	+.003405
3	a_3	-.006648	-.300152	.114217	-.002083	+.240900	-.000000
4	b_3	-.049352	+.000149	-.000207	-.013359	-.000000	-.001078
5	A_5	-.003995	+.599491	-.181714	+.005333	-.290699	+.000004
6	B_5	+.991630	-.006430	+.003928	+.039768	-.000160	+.000333
7	a_5	+.003063	+.613679	+.636780	-.006594	+.293084	-.000000
8	b_5	-.000801	-.000046	-.000097	-.001920	+.000000	+.001417
9	A_7	-.005383	-.288856	+.729981	-.009048	-.360881	-.000008
10	B_7	-.043799	-.002619	+.012110	+.998497	+.000200	+.002979
11	a_7	+.000519	+.055227	-.045664	+.001095	+.754672	-.000007
12	b_7	-.000626	-.000002	-.000025	-.003111	+.000001	+.999988

The eigenvectors $y_1, y_2, \ldots y_n$ of the r^{th} principal mode of the original system must satisfy the set of equations.

$$
\begin{aligned}
&(a_{11}-b_1\lambda)y_1+a_{12}\,y_2+ \ldots\ldots\ldots\ldots a_{1n}\,y_n = 0\\
&a_{21}y_1 + (a_{22}-b_2\lambda)y_2-\ldots\ldots\ldots\ldots a_{2n}\,y_n = 0\\
&a_{n1}y_1 + a_{n2}\,y_2 - \ldots\ldots\ldots\ldots + (a_{nn}-b_n\,)y_n=0
\end{aligned}
\qquad (3.5.1)
$$

The superscripts and subscripts r were omitted.

The eigenvectors $z_1, z_2 \ldots . z_n$ of the transformed matrix in the r^{th} mode satisfy the system of

$$
\begin{aligned}
&[(a_{11}/b_1)-\lambda)]\,z_1-(a_{12}/\sqrt{b_1b_2})z_2- \ldots(a_{1n}/\sqrt{b_1b_n})z_n=0\\
&(a_{21}/\sqrt{b_1b_2})z_1-[(a_{22}/b_2)-\lambda]\,z_2- \ldots(a_{2n}/\sqrt{b_2b_n})z_n=0\\
&\vdots\\
&(a_{n1}/\sqrt{b_1b_n})z_1- (a_{22}/\sqrt{b_2b_n})z_2\ldots[(a_{nn}/b_n\,)-\lambda]\,z_n=0
\end{aligned}
\qquad (3.5.2)
$$

The superscripts and subscripts have again been omitted.

By dividing the first equation of 3.5.1 by $\sqrt{b_1}$, and in the general case, by dividing the j^{th} equation $\sqrt{b_j}$ where j = 1..n, the system of equations given below will follow.

$$
\begin{aligned}
&[(a_{11}/\sqrt{b_1})-\sqrt{b_1}\lambda]\,y_1+ (a_{12}/\sqrt{b_1})y_2-\ldots(a_{1n}/\sqrt{b_1})y_n=0\\
&(a_{21}/\sqrt{b_2})y_1 \quad +[(a_{22}/\sqrt{b_2})-\sqrt{b_2}\lambda]\,y_2-..(a_{2n}/\sqrt{b_2}).\\
&\qquad\qquad\qquad\qquad\qquad\qquad\qquad\qquad\qquad\qquad .y_n = 0\\
&\vdots\\
&(a_{n1}/\sqrt{b_n})y_1 \quad + (a_{n2}/\sqrt{b_n})y_2- ..+[(a_{nn}/\sqrt{b_n})-\sqrt{b_n}\lambda].\\
&\qquad\qquad\qquad\qquad\qquad\qquad\qquad\qquad\qquad\qquad .y_n = 0
\end{aligned}
\qquad (3.5.3)
$$

Now multiply and divide each term of the i^{th} column by $\sqrt{b_i}$, i = 1,2...n. Equation 3.5.3 can be rewritten as

$$[(a_{11}/b_1)-\lambda]\sqrt{b_1}y_1+(a_{12}/\sqrt{b_1b_2})\sqrt{b_2}y_2+..(a_{1n}/\sqrt{b_1b_n})\cdot\sqrt{b_n}y_n = 0$$

$$(a_{21}/\sqrt{b_1b_2})\sqrt{b_1}y_1+[(a_{22}/b_2)-\lambda]\sqrt{b_2}y_2+..(a_{2n}/\sqrt{b_2b_n})\cdot\sqrt{b_n}y_n=0$$

$$\vdots$$

$$(a_{n1}/\sqrt{b_1b_n})\sqrt{b_1}y_1+(a_{n2}/\sqrt{b_2b_n})\sqrt{b_2}y_2-..[(a_{nn}/b_n)-\lambda]\cdot\sqrt{b_n}y_n = 0$$

On comparing 3.5.4 and 3.5.2 it can be observed that

(3.5.5) $$\sqrt{b_j}y_j = z_j$$

hence

(3.5.6) $$y_j = z_j/\sqrt{b_j}$$

The eigenvectors of the original system can therefore be evaluated simply by dividing the j^{th} eigenvector component by the square root of the frequency term's coefficient in the j^{th} column of the original matrix.

Table 3.5.11 contains the natural frequencies, eigenvalues and eigenvectors of the experimental motor frame for the first three even modes. The resulting eigenvectors in this table were obtained by applying the transformation 3.5.6 to the eigenvectors, as calculated by the electronic data processing machine and recorded in 3.5.9.

Similarly, by applying the same transformation to

the data in table 3.5.10, the natural frequencies, eigenvalues and eigenvectors of the experimental motor frame in the first three odd modes are obtained. These are recorded in table 3.5.12. For better understanding, the fundamental displacement distribution of the first four principal modes of vibration have been sketched in fig. 3.5.1, for the even modes. A similar sketch is given for odd modes in fig. 3.5.2.

The Mode shapes in fig. 3.5.1 illustrate the following vibrations:

a) the counter-tact cosine resonating at 10,430 c.p.s.;
b) the counter-tact sine resonating at 1,140 c.p.s.;
c) the in-tact cosine resonating at 460 c.p.s.;
d) the in-tact sine resonating at 490 c.p.s.

The Mode shapes in fig. 3.5.2 demonstrate the following vibrations:

a) the counter-tact cosine resonating at 8,200 c.p.s.;
b) the in-tact sine resonating at 1,225 c.p.s.;
c) the in-tact cosine resonating at 1,170 c.p.s.;
d) the counter-tact sine resonating at 1,580 c.p.s.;

The real modes of vibration contain also harmonic components which complicate the shape of the displacement along the directrix of the vibrating cylinders. Similar diagrams could, without difficulty, be drawn for all other principal modes.

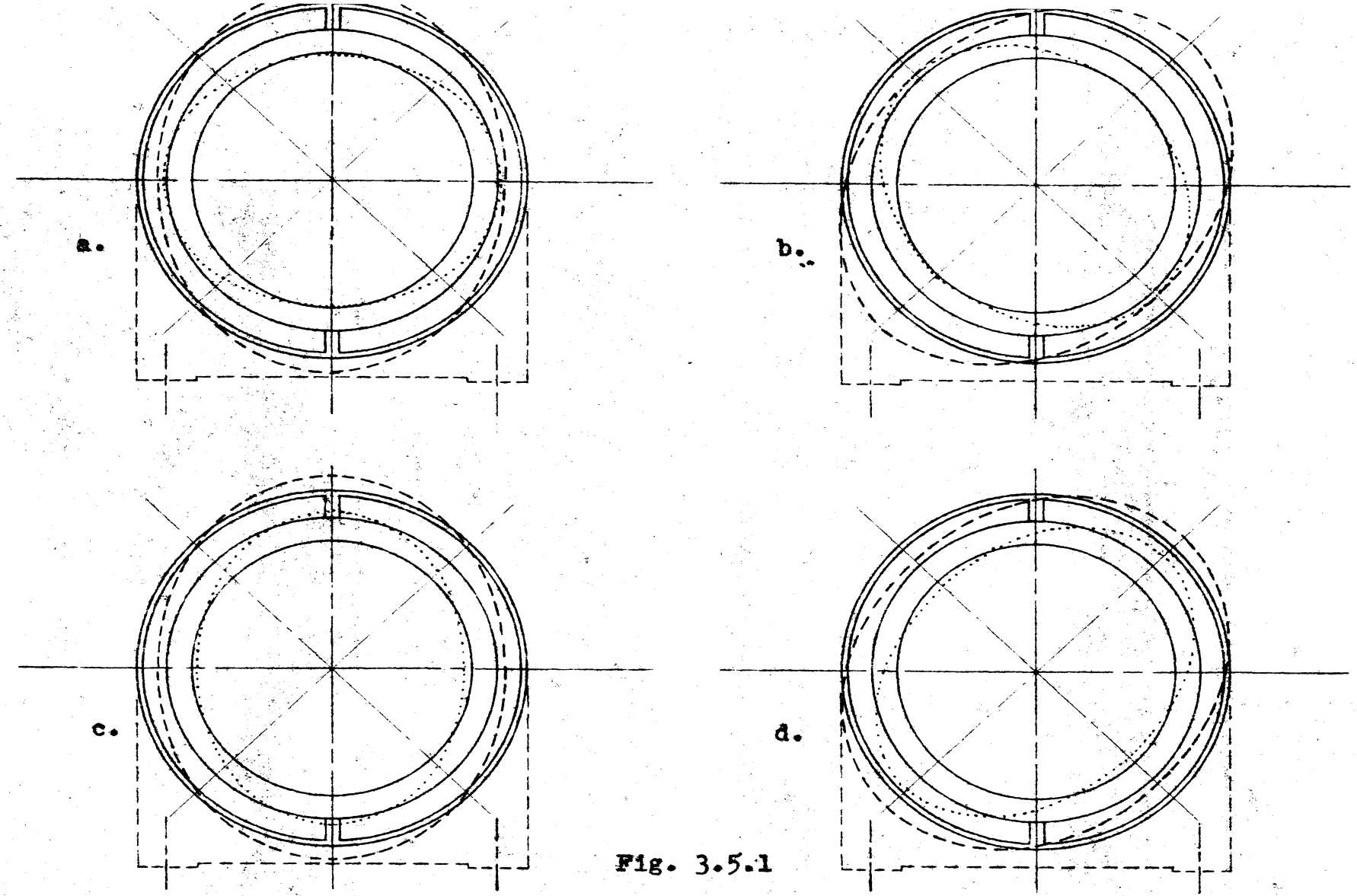

Fig. 3.5.1

Theoretical Second Mode Vibration of the Exp. Motor

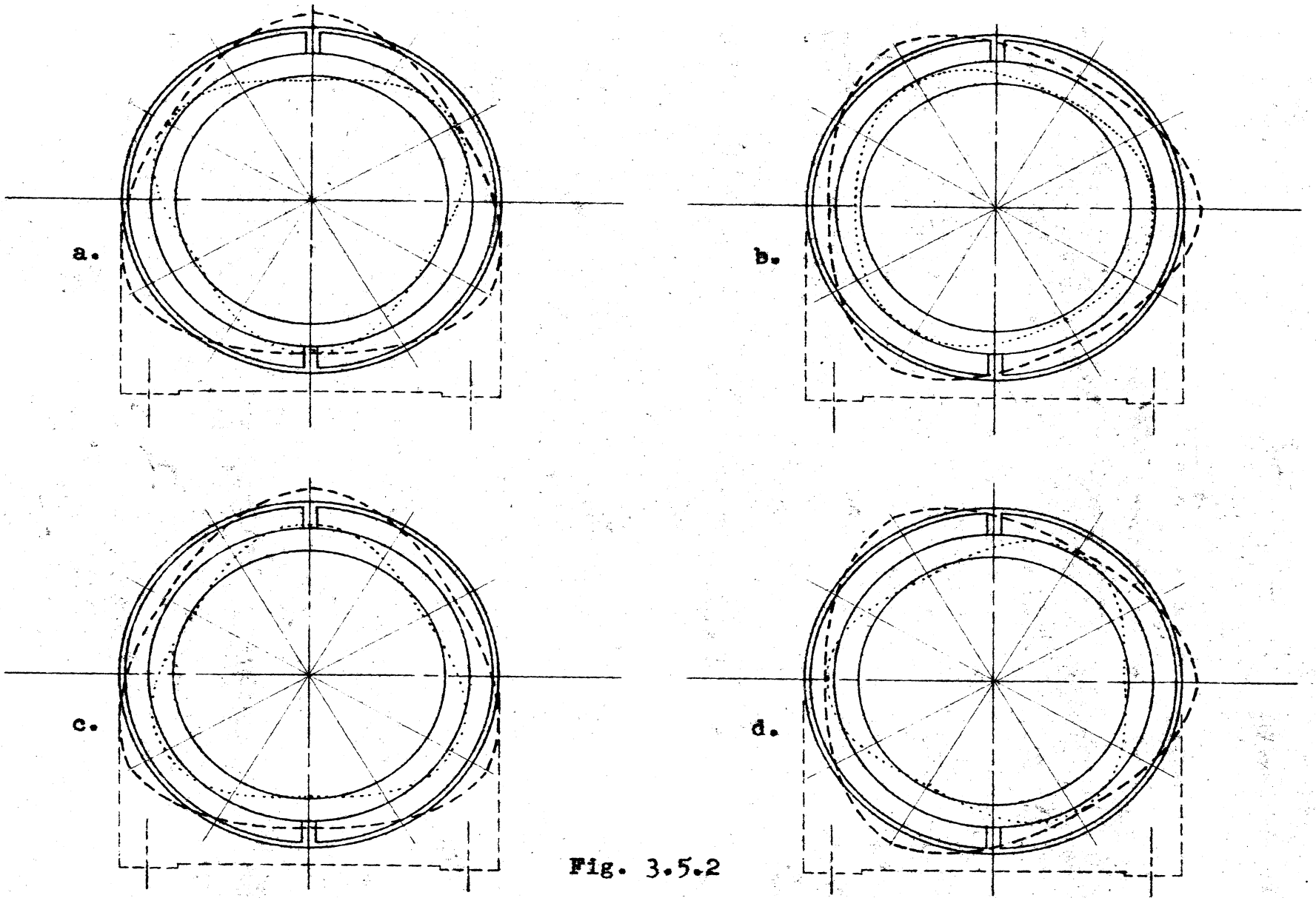

Fig. 3.5.2

Theoretical Third Mode Vibrations of the Exp. Motor

Table 3.5.11, Part I

Eigenvalues and Eigenvectors of the Original System for Even Modes, Columns 1-6

		1	2	3	4	5	6
		A_2	B_2	a_2	b_2	A_4	B_4
Frequency		f=10,430	f=1,140	f=460	f=490	f=1295	f=2060
Eigenvalues		4297.99×10^6	51.236×10^6	8.268×10^6	9.51×10^6	66.08×10^6	167.87×10^6
Eigenvectors	1 A_2	0.85284	-0.07796	1.70361	0.396830	-1.322000	0.039790
	2 B_2	0.000180	+1.93791	-0.358710	1.377560	-0.186320	0.80666
	3 a_2	-0.676970	0.122340	1.602120	0.392630	1.154380	0.014470
	4 b_2	-0.000003	-1.167430	-0.421280	1.834780	0.088770	-0.474390
	5 A_4	1.029430	0.158860	-0.062010	+0.003192	1.851910	0.015570
	6 B_4	-0.000430	-1.062000	0.035340	-0.003200	0.047880	2.546540
	7 a_4	-0.861830	-0.019890	0.018490	0.002814	-0.272330	-0.015690
	8 b_4	-0.000000	+0.019380	-0.000820	0.002840	-0.002320	0.082980
	9 A_6	1.221360	0.008050	-0.006860	-0.002450	0.176500	0.016550
	10 B_6	0.000770	-0.147860	-0.001630	-0.017190	0.028420	-0.225170
	11 a_6	-1.47910	-0.003190	0.003260	0.000490	-0.04173	-0.001600
	12 b_6	0.000000	-0.011170	0.000250	-0.000500	0.001120	-0.01368

Table 3.5.11, Part II

Eigenvalues and Eigenvectors of the Original System for Even Modes, Columns 7-12

		7	8	9	10	11	12
		a_4	b_4	A_6	B_6	a_6	b_6
Natural Frequency		2,560	2,940	3,660	4,240	6,240	6,980
Eigenvalues		252.03×10^6	341.18×10^6	518.39×10^6	702.80×10^6	1529×10^6	1918.21×10^6
1	A_2	0.685320	0.000640	-0.461110	0.001660	0.525580	0.000010
2	B_2	0.000840	-0.041020	-0.000090	0.178320	0.000520	0.014250
3	a_2	-0.55892	0.000000	0.364900	0.005510	-0.419240	0.000000
4	b_2	-0.002790	0.021340	0.001880	-0.090150	0.000033	-0.007840
5	A_4	1.480270	-0.001090	-0.701110	-0.021830	0.665870	-0.000013
6	B_4	0.025110	-0.074690	-0.013970	0.149710	-0.001130	0.009770
7	a_4	1.815190	-0.001310	1.244920	0.012490	-0.627460	0.000000
8	b_4	0.001710	2.459080	0.001400	-0.046380	-0.000012	0.000860
9	A_6	-0.524410	-0.000850	2.208320	0.026160	1.109810	0.000020
10	B_6	0.060760	0.061600	-0.033730	2.798000	0.003080	0.011060
11	a_6	0.099180	0.000000	-0.164910	-0.003880	2.009600	0.000020
12	b_6	-0.000110	-0.000540	0.000160	-0.011580	-0.000030	2.502910

Eigenvectors

Table 3.5.12, Part I

Eigenvalues and Eigenvectors of the Original System for Odd Modes, Columns 1-6

		1	2	3	4	5	6
		A_3	B_3	a_3	b_3	A_5	B_5
Natural Frequencies		8,200	1,225	1,170	1,580	2,240	2,940
Eigenvalues		$2662.\times10^6$	59.13×10^6	53.57×10^6	99.22×10^6	199.60×10^6	338.03×10^6
Eigenvectors 1	A_3	0.069590	0.049320	0.196320	0.001340	0.121190	0.002670
2	B_3	-0.000120	0.250510	-0.060710	-0.075520	0.003950	0.029770
3	a_3	-0.056190	+0.036200	0.154100	0.002240	0.142700	-0.001600
4	b_3	0.000000	0.066460	-0.018500	0.230240	-0.000610	-0.011880
5	A_5	0.081970	-0.007870	-0.020060	0.001070	0.183560	-0.001120
6	B_5	0.000140	-0.025460	0.005020	0.022220	0.002790	0.277220
7	a_5	-0.087000	0.001550	0.005740	-0.000020	-0.023700	+0.000760
8	b_5	-0.000000	-0.000860	+0.000200	+0.000930	-0.000020	-0.000200
9	A_7	0.139970	-0.001070	-0.006730	-0.000230	+0.02307	-0.00152
10	B_7	-0.00025	-0.006430	0.001820	0.005300	-0.000720	-0.012360
11	a_7	0.163700	-0.000370	0.001360	0.000000	-0.00487	0.000130
12	b_7	0.000000	-0.000690	0.000690	0.000480	-0.000010	-0.000160

Table 3.5.12, Part II

Eigenvalues and Eigenvectors of the Original System for Odd Modes, Columns 7-12

		7	8	9	10	11	12
		a_5	b_5	A_7	B_7	a_7	b_7
Natural Frequencies		3,950	4,750	5,200	5,580	11,650	9,780
Eigenvalues		621.56×10^6	890.97×10^6	1070.5×10^6	1275.41×10^6	5386.49×10^6	3632.67×10^6
1	A_3	0.079930	-0.000000	-0.031210	0.000310	-0.07246	-0.000000
2	B_3	0.000710	0.001240	-0.000490	0.008850	0.000040	0.000920
3	a_3	-0.072240	+0.000000	+0.02749	-0.000500	+0.057980	-0.000000
4	b_3	0.000040	-0.000630	-0.000050	-0.003220	-0.000000	-0.000260
5	A_5	0.16759	0.000010	-0.050800	0.001490	-0.081270	0.000000
6	B_5	-0.001800	0.000070	0.001100	0.011120	-0.000040	0.000090
7	a_5	0.152660	0.000020	0.158410	-0.001640	+0.072910	-0.000000
8	b_5	-0.000010	0.248760	-0.000020	-0.000480	+0.000000	0.000350
9	A_7	-0.08151	+0.000010	+0.205980	-0.002550	-0.101830	-0.000000
10	B_7	-0.00740	0.000490	0.003420	0.281750	0.000060	0.000840
11	a_7	0.013870	-0.000000	-0.011470	0.000280	0.189520	-0.000000
12	b_7	-0.000000	-0.000360	-0.000010	-0.00078	+0.000000	+0.251130

3.6 Calculation of the Forced Response of the Experimental Motor

There is a large number of force waves in the air-gap which tend to set the motor into vibration. While those of low order and high amplitude are the source of magnetic noise, others, of high order and low amplitude can generally be neglected. In the following discussion only the vibration amplitudes caused by single-mode, single-frequency force waves will be treated. Any picture of the complete vibration can be constructed by using the principle of superposition. The essentials of the theory for the calculation of the forced response is given in equations 3.1.27 to 3.1.37.

The rotating force wave can be represented by equation

(3.6.1) $P(\theta,t) = P_{m'} \cos(\omega t - m'\theta)$

In this equation m' is the mode of the specific force wave, and $P_{m'}$ is the amplitude of the force wave in pounds per radian.

On carrying out the trigonometric expansion in 3.6.1 one obtains

(3.6.2) $P(\theta,t) = P_{m'} \cos \omega t \cos m'\theta + P_{m'} \sin \omega t \sin m'\theta$

This last equation represents two pulsating force distributions displaced by one quarter wave length along the armature circumference, and lagging by one quarter of a cycle. The maximum amplitude of each wave is the same as the amplitude

of the rotating force wave. The first term stands for a direct or cosine mode force, and the second for a quadrature or sine mode force.

The work done by the cosine force wave during deflection is given by

$$(3.6.3) \quad W^{(e)} = (1/2) \int_0^{2\pi} P_{m'} \cos m'\theta \, (a_m \cos m\theta + b_m \sin m\theta) d\theta$$

But the integral of the products containing sin $m\theta$ and all the terms containing cos $m\theta$ for $m \neq m'$ will vanish. The value of integral 3.6.3 thus reduces to the expression

$$(3.6.4) \quad W^{(e)} = (\pi/2) \, P_{m'} a_{m'}$$

The strain energy of deformation in the r^{th} principal mode according to 3.1.30 , is equal to the kinetic energy, and therefore

$$(3.6.5) \quad P_{m'}(\pi/2)a_{m'} = \omega_r^2 \sum g_m \, (a_m^2 + b_m^2) + G_m \, (A_m^2 + B_m^2)$$

In both the last and the following equations the superscripts r of the generalized coordinates are being omitted.

To find the static deflection A_n of the outer ring in the r^{th} principal mode, both sides of equation 3.6.5 will be multiplied by A_n

$$(3.6.6) \quad P_{m'} (\pi/2) a_{m'} A_n = A_n \omega_r^2 \sum g_m (a_m^2 + b_m^2) + G_m \, (A_m^2 + B_m^2)$$

A_n can now be evaluated as

$$(3.6.7) \quad A_n = P_m (\pi/2) a_{m'} A_n / \omega_r^2 \sum g_m (a_m^2 + b_m^2) + G_m \, (A_m^2 + B_m^2)$$

All deflections in the r^{th} principal mode are, according to

equation 3.1.25, proportional to the components of the eigenvectors. These components may be used on the right side of the equation sign in 3.6.5, as the factor of proportionality c_r cancels out. The deflection A_n in the r^{th} principal mode can therefore be expressed as

$$(3.6.8)\quad A_n = P_{m'}(\pi/2)y_{am'}y_{An}/\omega_r^2 \sum g_m(y_{am}^2+y_{bm}^2) + G_m(y_{Am}^2+y_{Bm}^2)$$

For the sake of convenience in writing the constant K_r is defined as

$$(3.6.9)\quad K_r = \omega_r^2 \sum g_m(y_{am}^2 + y_{bm}^2) + G_m(y_{Am}^2+y_{Bm}^2)$$

Equation 3.6.8 may now be written as

$$(3.6.8a)\quad A_n = P_{m'}(\pi/2)\, y_{am'} \cdot y_{An}/K_r.$$

Proceeding from the static to the dynamic deflection in the r^{th} principal mode, equation 3.6.8 has now to be multiplied by the resonance factor, in accordance with the same argument used to deduce equation 3.1.37. The dynamic deflection in the r^{th} principal mode can thus be expressed as

$$(3.6.9)\quad A_n^{(r)} = P_{m'}(\pi/2)\, y_{am'}^{(r)} \cdot y_{An}^{(r)}\, \omega_r^2/K_r(\omega_r^2 - \omega^2)$$

In what follows, the discussion will be continued by using a second-mode force wave and by considering the second mode deflection of the outer ring. The corresponding subscripts of the eigenvectors in table 3.5.11 will be used.

The deflection at the top rib caused by the second mode cosine distribution can now be written

$$(3.6.10)\quad A_{2d}^{(r)}(t) = \left[P_2(\pi/2)y_3^{(r)}y_1^{(r)}\omega_r^2/K_r(\omega_r^2-\omega^2)\right]\cos\omega t$$

and the analogous expression for the deflection at the top rib as a result of the sine component of the force wave will be

$$(3.6.11)\quad A_{2c}^{(r)}(t) = [P_2(\pi/2)y_4^{(r)}y_1^{(r)}\ \omega_r^2/K_r(\omega_r^2-\omega^2)]\sin\omega t$$

In order to find the magnitude of the total displacement of the outer ring at the top rib, it is necessary first to add the deflections produced by the r^{th} principal modes caused by the cosine component of the force wave. Then the deflections produced by the r^{th} principal modes corresponding to the sine component of the force wave are summed separately. Finally the two resultant deflections are combined by the parallelogram law. The result is

$$(3.6.12)\quad A_2 = \left(\left[\sum_{r=1}^{r=n} A_{2d}^{(r)}\right]^2 + \left[\sum_{r=1}^{r=n} A_{2c}^{(r)}\right]^2\right)^{(1/2)}$$

To facilitate the numerical solution for the experimental motor, the constants K_r have first been computed and then assembled in table 3.6.2. The inertia constants given in table 3.5.1, and the eigenvalues and eigenvectors given in table 3.5.11 have been used. The overdamped modes, i.e. the counter-tact cosine modes as explained in section 4, have been omitted. The effect of modes 9 to 12 was found to be entirely negligible for the second mode amplitudes and is therefore not recorded here. Table 3.6.1 shows the detailed calculation of the constant K_3.

Table 3.6.3 illustrates the calculation for the

static deflections and resonance factors for the displacement of a point on the outer ring at $\theta = 0$, caused by a second mode force wave of 100 lb per radian amplitude. Table 3.6.4 illustrates the detailed calculations for the deflection A_2 at the main noise frequency of the motor at full load, that is at 1,716 c.p.s. The amplitude of the forcewave has again been assumed to be 100 lb per radian. Table 3.6.5 gives a summary of the calculated second mode deflections in the cosine mode caused again by a second mode rotating forcewave of 100 lb per radian amplitude for the whole frequency range between 100 and 2100 c.p.s. These calculated values have been plotted in Fig. 1.2. Finally table 3.6.6 lists the deflection amplitudes in the cosine modes for the response of the force waves listed in table 2.10.5.

Table 3.6.1

Calculation of Constant K_3

Eigenvector Component	y_m^2		G_m or g_m $\times 10^{-2}$	$\frac{y_m^2 \times G_m}{g_m} \times 10^{-2}$
1	2.9193			
2	0.1287	3.0480	7.69	23.49
3	2.5667			
4	0.1775	2.7442	9.71	26.654
5	0.0038			
6	0.0013	0.0051	6.54	0.033
7	0.0034			
8		0.0034	8.26	
9				
10				$\sum = 50.18 \times 10^{-2}$
11	negl.			
12				

$$\omega_3^2 = 8.268 \times 10^6$$

$$K_3 = 8.268 \times 10^6 \times 50.12 \times 10^{-2} = 4.144 \times 10^6$$

Table 3.6.2

Summary of Constants K_r

Princ. Mode	2	3	4	5	6	7	8
K_r	22.41	4.144	4.755	83.93	126.02	169.6	169.6 x 10^6

Table 3.6.3

Second Mode Deflection Amplitudes in the Cosine Axis caused by a Rotating Forcewave of 100 lb per Radian Amplitude

Princ. Mode	y_1	y_3	y_4	K/r_6 x10^6	Static defl. x10^{-6} cos.	sine	Resonance factor
2	-0.078	0.123	-1.167	22.41	5.47x10^{-3}	-0.617	$51.24/(51.24-\omega^2 x10^{-6})$
3	1.704	1.602	-0.421	4.144	100.50	-26.4	$8.26/(8.26-\omega^2 x10^{-6})$
4	0.397	0.393	1.835	4.755	5.00	23.4	$9.51/(9.51-\omega^2 x10^{-6})$
6	-0.04	0.0145	-0.474	83.93	-1.86x10^{-3}	3.4x10^{-2}	$167.87/(167.87-\omega^2 x10^{-6})$
7	0.685	-0.559	-0.0028	126.02	-0.505	2.3x10^{-3}	$252.3/(252.3-\omega^2 x10^{-6})$
8	0.0006	0.000	0.0213	169.6		negligible	

Table 3.6.4

Calculation of the Second Mode Deflection in the Cosine Axis caused by a 100 lb/Radian Amplitude Rotating Forcewave of 1,716 c.p.s.

Prine. Mode	Resonance Factor	Deflections by cosine component Static μ inches	dynamic μ inches	by sine component Static μ inches	dynamic μ inches
2	-.877	-4.8×10^{-3}	-0.0042	-0.54	0.475
3	-0.0744	100.5	-7.82	-26.4	1.96
4	-0.09	5	-0.45	+23.4	-2.09
6	3.25	-1.86×10^{-9}	-0.0063	3.4×10^{-2}	0.1
7	1.85	-0.505	-0.936	2.3×10^{-9}	0.004
			-9.22		0.48

Total Deflection 9.23 μ inches

Table 3.6.5

Calculated Second Mode Cosine Axis Deflections caused by a Second Mode 100 lb/ Radian Rotating Forcewave as Function of Frequency

Frequency c.p.s.	Ampl. μ inches	Frequency c.p.s.	Ampl. μ inches	Frequency c.p.s.	Ampl. μ inches
100	110.25	700	80.45	1700	9.25
350	251.80	900	36.6	1715	9.23
450	306.14	1000	25.4	1735	9.15
468		1100	23.4	2000	7.27
470	1774.	1110	26.0	2050	7.55
480	890.	1140		2070	
490		1160	21.2	2100	6.9.
492	829	1200	19.80		
500	651	1400	14.48		

Table 3.6.6

Summary of Calculated Deflections
for 2nd Mode Force Waves of the
Experimental Motor

Motor Operating			Noise fr.	100 lb/rad Defl.	Force Wave lb/rad	Defl.	Defl.
A.	V.	cps	cps	μ-inch		μ/inch	μ-cm
40	440	60	1,716	9.23	84.5	7.8	19.6
40	367	50	1,419	14.4	84.5	12.17	30.7
40	294	40	1,121	28.2	84.5	23.9	60.5
N.L.	440	60	1,735	9.15	23.1	2.12	5.34
40	440	60	1,475	12.98	4.6	0.6	1.51

3.7 Investigation of the Convergence of Eigenvalues

As mentioned at the start of this chapter, the exact solution of the dynamic behavior of continuous systems is given in terms of determinants of infinite order. Also, to keep the numerical work within manageable bounds, a determinant made up of only the first few rows and columns is considered to be a sufficient approximation of the infinite determinant. It was decided to use only 24 generalized coordinates. Consequently a 24th degree characteristic equation resulted which, fortunately, could be factored into two 12th degree equations. It remains to be demonstra-

ted that the use of a larger number of terms in the Fourier expansion of the radial and tangential displacements would not alter the numerical results materially.

With this aim in mind, the eigenvalues for even and for odd modes have been calculated, assuming that the radial and tangential displacements in both the even and the odd modes could be represented by the first four generalized coordinates. In other words, it is supposed that equation 3.4.1 which represents the radial displacement can be simplified to read

$$U = A_2 \cos 2\theta + B_2 \sin 2\theta$$

(3.7.1)

$$u = a_2 \cos 2\theta + b_2 \sin 2\theta$$

while 3.4.1 for the odd modes can be written as

$$U = A_3 \cos 3\theta + B_3 \sin 3\theta$$

(3.7.2)

$$u = a_3 \cos 3\theta + b_3 \sin 3\theta$$

As a further step, the next term in the Fourier expansions has been added to 3.7.1 and 3.7.2, and the eigenvalues of the 8^{th} order determinant found. To permit ready comparison of these results, the eigenvalues of the first four principal modes, as calculated from the 4^{th}, 8^{th}, and 12^{th} order determinants, have been assembled in table 3.7.1, for the even modes, and in 3.7.2 for the odd modes.

An inspection of tables 3.7.1 and 3.7.2 reveals an

excellent convergence of eigenvalues and natural frequencies in the 2nd, 3rd, and 4th principal modes. The selection of only 24 coordinates for these modes seems therefore fully justified. The regrettable unruly behavior of the first principal mode is of no importance as the frequency of this over-damped mode is very high. This mode has no influence on the steady-state behavior of the vibrating stator as explained in the assumptions, and pointed out again in chapter 5. In the numerical calculation of the steady-state deflections a similar result was obtained. The effects of the 9^{th} to 12^{th} principal modes on the second mode deflection were entirely negligible.

The above statements apply exactly only to the first even and odd modes of vibrations. For the calculation of higher mode deflections the number of terms selected for the Fourier series should be increased. The capabilities of the Electronic Data Processing Machine are by no means exhausted by a 12 x 12 determinant. The method as explained here can therefore be extended with sufficient accuracy for the deflections in higher modes.

Table 3.7.1

Comparison of Eigenvalues and of Natural Frequencies in the Even Modes

		Principal Mode			
		1	2	3	4
		Eigenvalues			
		$x10^6$	$x10^6$	$x10^6$	$x10^6$
Calculated from Determinant	4x4	1079.51	49.736	8.426	9.922
	8x8	2459.91	53.027	8.275	9.535
	12x12	4297.99	51.236	8.268	9.511
		Natural Frequencies c.p.s.			
	4x4	5,140	1,123	464	500
	8x8	6,870	1,164	461	492
	12x12	10,430	1,140	460	490

Table 3.7.2

Comparison of Eigenvalues and Natural Frequencies of the Odd Modes

		Principal Mode			
		1	2	3	4
		Eigenvalues			
		$x10^6$	$x10^6$	$x10^6$	$x10^6$
Calculated from Determinant	4x4	1266.45	62.373	66.218	101.482
	8x8	2861.43	59.800	64.401	99.602
	12x12	2662.63	59.130	63.576	99.226
		Natural Frequencies c.p.s.			
	4x4	5,670	1,247	1,290	1,605
	8x8	8,540	1,233	1,272	1,590
	12x12	7,020	1,226	1,266	1,585

IV. SOUND RADIATED BY THE VIBRATING STATOR

The small amplitude vibrations of the stator create periodic disturbances in the medium in contact with the surface of the stator. These disturbances are characterized by alternate compressions and rarifications of the contacting air layers. The air, being an extended medium with the properties of distributed mass and elasticity, propagates the disturbances of the contact surface when excited. This results in a periodic change of the air pressure everywhere around the motor about the static value, and in a periodic change of the velocity of the air particles above and below an average motion. This phenomenon specifies, and is referred to as the sound waves radiated by the stator.

It is the purpose of this chapter to calculate a characteristic quantity of the radiated sound waves. Since virtually all modern sound detectors respond directly to variations of the pressure in the wave disturbance, the sound pressure at a characteristic point near the induction motor will be determined.

The consideration of the elastic and inertial properties of the air leads to the partial differential equation of sound propagation, the acoustic wave equation. This will be established as the first step, assuming the air to be a continuous, isotropic medium, having the properties of

perfect elasticity and zero vicosity. In addition, field free conditions will be assumed.

The stator of an induction motor is by no means of a shape that lends itself easily to the radiation and boundary value problem. It becomes essential therefore to make approximations without losing sight of the physical significance of the problem. The stator, as illustrated in fig. 4.2.1, will be extended on both sides by semi-infinite cylinders, so that the vibrations of the stator will not be transmitted to the extensions. This artifice can be interpreted to represent an infinitely long cylinder vibrating in a belt only. The solution of the boundary value problem will be carried out by a Fourier transform method. The resulting integral for the sound pressure will be numerically evaluated.

The results of the sound pressure integral will appear in dynes per square centimeter. It has become customary to express the sound pressure as a sound pressure level with respect to a reference sound pressure. For airborne sound pressures, 0.0002 dyne per square centimeter has been generally accepted as a standard reference sound pressure. On account of the sensitivity of the ear, and the range of pressures it responds to, a decibel scale similar to the one in communication engineering has been universally adopted. This is consistent with the fact that the human ear

is capable of detecting a very small increase in sound pressures when the ambient sound pressure is low. At a higher ambient level the sound pressure increases have to become considerably larger to be perceived. It has been demonstrated, in fact, that the human ear responds logarithmically to the sound pressure. To take care of this faculty of the human ear the sound pressure level is specified in terms of a unit called decibel, which by definition is equal to twenty times the logarithm to base ten of the ratio between the sound pressure in dynes per square centimeter to the reference pressure 0.0002 dyne per square centimeter.

$$(SPL) = 20 \log_{10} (SP/0.0002)$$

where SP and 0.0002 are in dyne/cm^2

4.1 Derivation of the Wave Equation[1]

The physical theorems which form the basis of the mathematical manipulations leading to the acoustical wave equations comprise: (1) the principle of conservation of mass represented by the continuity equation; (2) the principle of conservation of momentum as given by Newton's second law; and (3) the principle of conservation of energy.

In the following discussion a small element of the medium, i.e. the air, of volume ΔV in the vicinity of the sound field will be considered, as shown in figure 4.1.1. This particular volume has a surface S and is supposed to

---

[1] 7;32

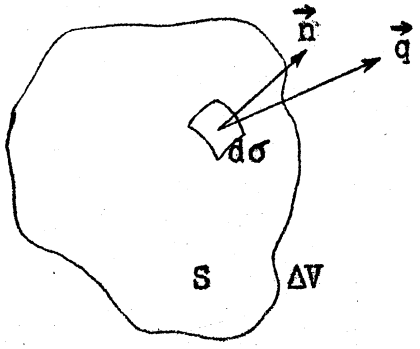

Fig. 4.1.1

Volume Element in Sound Field

be fully enclosed by an ideally deformable, massless, impermeable membrane, so that no mass may escape through this membrane. This is equivalent to the statement that the mass within the volume will remain constant. In the following discussion the expression "particle" will be used to denote the elementary volume.

It can be shown that the equation of continuity can be written,

(4.1.1) $\partial\rho/\partial t + \vec{q} \cdot \nabla\rho + \rho\nabla \cdot \vec{q} = 0$

In this equation ρ denotes the density, and $\vec{q}$ the velocity of the particle.

In order to describe mathematically the conservation of mass for a specific particle considered, it is of great help to transform the continuity equation in such a way as to have the coordinates of the system attached to the particle itself. This procedure makes it possible to represent

the time variation of the mass of a specific volume element. In hydrodynamics this operation is commonly represented by $D\rho/Dt$. It is not difficult to prove that

$$(4.1.2) \quad (D\rho/Dt) = (\partial\rho/\partial t) + \vec{q} \cdot \nabla\rho$$

The requirement of conservation of mass of a specific volume element is expressed by

$$(4.1.3) \quad \rho\,(\Delta V) = \text{const}$$

Taking the time derivative at a point moving with the particle, this may be written as

$$(4.1.4) \quad \rho\,[D(\Delta V)/Dt] + (\Delta V)(D\rho/Dt) = 0$$

Now combine equation 4.1.2 with 4.1.3. It follows that

$$(4.1.5) \quad (1/\Delta V)\,[D(\Delta V)/Dt] + (1/\rho)\,(\partial\rho/\partial t) + \vec{q} \cdot \nabla\rho = 0$$

It can also be shown that

$$(4.1.6) \quad \nabla \cdot \vec{q} = [1/(\Delta V)]\,[D(\Delta V)/Dt]$$

Introducing this last equation into 4.1.5, one obtains

$$(4.1.7) \quad \nabla \cdot \vec{q} + (1/\rho)[(\partial\rho/\partial t) + \vec{q} \cdot \nabla\rho] = 0$$

Before continuing the discussion, the condensation or fractional increment of density will be defined as

$$(4.1.8) \quad s = (d\rho/\rho_o) = (\rho-\rho_o)/\rho_o$$

hence

$$(4.1.9) \quad \rho = \rho_o(1+s)$$

where ρ_o is the density of the volume element with no sound wave present. Introducing equation 4.1.9 into 4.1.7, the latter can be expressed as

$$(4.1.10) \quad \nabla \cdot \vec{q} + [(1/(1+s))]\,[(\partial s/\partial t) + \vec{q} \cdot \nabla s] = 0$$

Consider next a differential area element $d\sigma_o$ on the ideal membrane with its normal unit vector $\vec{dn}$ directed outwardly. Let the instantaneous sound pressure be p and assume no varying body forces on the medium. In consequence of Newton's second law, the total incremental force normal to the surface

$$\int_S \vec{n}\, p\, d\, \sigma$$

may be equated to the acceleration force

$$\rho(\Delta V)(D\vec{q}/Dt)$$

In the last expression $D\vec{q}/Dt$ again represents the time variation of velocity of this specific particle which, for a vector quantity, is given by

$$(4.1.11)\quad D\vec{q}/Dt = \partial\vec{q}/\partial t + (\vec{q}\cdot\nabla)\,\vec{q}$$

hence

$$(4.1.12)\quad \int \vec{n}\, p\, d\sigma + [(\partial\vec{q}/\partial t) + (\vec{q}.\nabla)\vec{q}\,]\,\rho\,(\Delta V) = 0$$

Dividing this equation by ΔV, and taking the limit by letting the element become infinitely small, this equation is transformed to

$$(4.1.13)\quad \nabla p + [(\partial\vec{q}/\partial t) + (\vec{q}.\nabla)\vec{q}]\,\rho = 0$$

A relationship between the sound pressure p and the condensation s has to be established from the volume changes. It can be brought about by the use of the principle of conservation of energy. As the heat conductivity of gases is low, it is safe to conclude that the heat exchange in the wave at audible frequencies is negligible, that is, that the

deformations are adiabatic. This is expressed mathematically as

$$PV^{\gamma} = \text{const.}$$

where γ is a constant ratio of the specific heats at constant pressure and constant volume. One may state that as a direct consequence of the adiabatic expansions

$$p/P_o = \gamma s$$

where s is the condensation as defined before, and P_o is the static sound pressure. Hence

(4.1.14) $p = P_o \gamma s$

Restricting further discussions to small signals, and neglecting second and higher order terms in equation 4.1.10, this can be expressed as

(4.1.10a) $\nabla . \vec{q} + (\partial s/\partial t) = 0$

Introducing into this equation the relationship between s and p, it can be written as

(4.1.15) $\nabla . \vec{q} + (1/\gamma P_o)(\partial p/\partial t) = 0$

and similarily, equation 4.1.13 can, for small signals, be written as

(4.1.16) $\nabla p + \rho_o(\partial \vec{q}/\partial t) = 0$

If now 4.1.15 is differentiated with respect to the time, the divergence operation on 4.1.16 is carried out, and remembering the interchangeability of the operation divergence and differentiation, this equation may be rewritten as

(4.1.15a) $\nabla . (\partial \vec{q}/\partial t) + (1/\gamma P_o)(\partial^2 p/\partial t^2) = 0$

and

(4.1.16a) $\nabla.\nabla p + \rho_o \nabla.\ (\partial \vec{q}/\partial t) = 0$

The acoustic behavior equations resulting from the combination of these last two equations can be written as

(4.1.17) $\nabla^2 p = (1/c^2)(\partial^2 p/\partial t^2)$

where

$$c^2 = (P\gamma/\ \rho_o)$$

is the square of the sound velocity in the medium.

4.2 The Integral of the Sound Pressure[1]

To find the sound pressures in the field near the induction motor it is necessary to solve the partial differential equation represented by the wave equation for the special case of the vibrating stator. This will require two major steps: first, to find all possible solutions of the equation and secondly, to choose from these solutions the particular combination which satisfies the boundary condition of this special radiation problem.

To facilitate the solution, an appropriate system of coordinates will be chosen. The boundary conditions are given on a circular, cylindrical surface. It is only natural to select a system of circular cylindrical coordinates as illustrated in fig. 4.2.1.

---

[1] 66

The vibrations of the outer stator are harmonic in time and one may, therefore, conclude that the sound pressures caused by these disturbances are also harmonic in time, and set them as

(4.2.1) $p = p \exp(-j\omega t)$

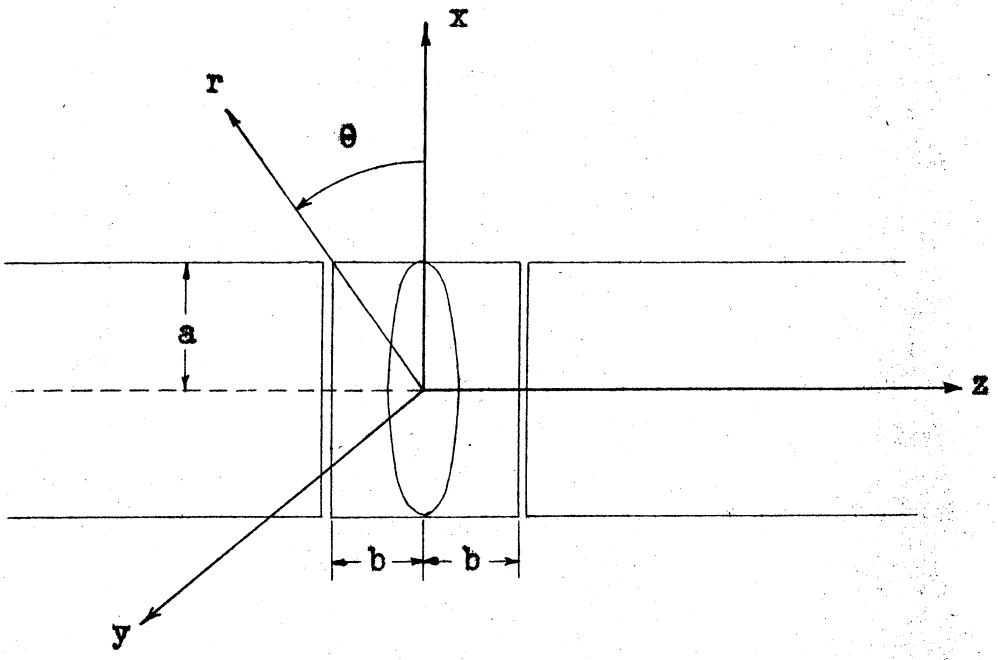

Fig. 4.2.1

System of Coordinates for the Vibrating Cylinder

Introducing 4.2.1 into equation 4.1.17, the wave equation in its well known form will result

(4.2.2) $(\nabla^2 + k^2)p = 0$; where $k^2 = \omega^2/c^2$

Substituting the Laplacian operator in cylindrical coordinates, the wave equation can be written as

(4.2.3) $(1/r)(\partial/\partial r)\,[\,r(\partial p/\partial r)] +$

$$+(1/r^2)(\partial^2 p/\partial\theta^2) + (\partial^2 p/\partial z^2)+k^2 p = 0$$

The usual method of solution consists of the separation of variables by seeking a product function

(4.2.4) $R(r)\,Q(\theta)\,Z(z)$

which will split the partial differential equation into three ordinary differential equations.

Proceeding in this manner, equation 4.2.4 is introduced into equation 4.2.3, and the whole equation divided by RQZ, which results in

(4.2.5) $(1/rR)(d/dr)\,[r(dR/dr)] + (1/r^2Q)(d^2Q/d\theta^2) + (1/Z)(d^2Z/dz^2) + k^2 = 0$

Since all terms except the third are independent of z, the third term must be a constant and may be set equal to $-h^2$. Thus

(4.2.6) $(1/Z)(d^2Z/dz^2) = -h^2$

Substituting 4.2.6 into 4.2.5, and multiplying the result by r^2, it follows that

(4.2.7) $(r/R)(d/dR)\,[r(dR/dr)] + (1/Q)(d^2Q/d\theta^2) + (k^2-h^2)r^2 = 0$

With the same reasoning as applied in 4.2.5, one can assume the second term to be a constant, and we now set it equal to

(4.2.8) $(1/Q)(d^2Q/d\theta^2) = -n^2$

Introducing 4.2.8 into 4.2.7, the latter reduces to

(4.2.9) $r(d/dr)\,[r(dR/dr)] + [(k^2-h^2)r^2-n^2]R = 0$

The first task to split the partial differential equation is now accomplished. The product of the solutions

of equations 4.2.6, 4.2.8, and 4.2.9, is the separated solution of the acoustic wave equation in cylindrical coordinates.

The solution of 4.2.6 is given by expressions of the form

(4.2.10) $Z = \exp(jhz)$

Analogously, the solution of 4.2.8 given by

(4.2.11) $Q = \exp(jn\theta)$

Equation 4.2.9 is Bessel's differential equation and its solution in series is given by

(4.2.12) $R = Z_n(r\sqrt{k^2-h^2})$

where Z_n is a circular cylinder function of the order n and argument $r\sqrt{k^2-h^2}$.

The solution of the wave equation for sound pressure is given by linear combinations of the product of 4.2.10, 4.2.11, and 4.2.12. These products are referred to as the elementary wave functions and written as

(4.2.13) $p = \exp(jn\theta).Z_n(r\sqrt{k^2-h^2}).\exp(jhz-j\omega t)$

This last equation represents a nondenumerable infinity of solutions that may be superposed in any arbitrary manner. The solution p, as given, is therefore not unique. In order to get a definite solution to equation 4.2.9 it will be necessary to express the constants in such a way as to satisfy the boundary condition, that is the prescribed behavior on the boundary. In other words, the boundary con-

dition will serve to extract from the infinity of solutions the particular solution appropriate to the specified boundary condition.

The boundary conditions are partly determined by the vibrations of the cylinder and by the behavior of function p at infinity.

The amplitude and frequency of the vibration of the cylindrical surface determine the velocity of the particles on the cylindrical surface when secondary reaction effects are neglected. The gradient of pressure and the time differential of velocity are correlated by Newton's second equation of motion; hence

$$(4.2.14) \qquad \rho(\partial q/\partial t) = -\partial p/\partial r$$

Considering each single mode and single frequency vibration individually, the sound pressure on the cylindrical surface ($r=a$) must, for all values of z, between $+b$ and $-b$, satisfy the condition

$$(4.2.15) \qquad (\partial p/\partial r)_{r=a} = jA_m\omega^2\rho \exp(jm\theta - j\omega t)$$

and be zero for any other value of z on the cylindrical surface. The distance $2b$ is the length of the stator.

According to Sommerfeld[1], wave propagation problems are not uniquely specified by their prescribed sources in the

---

[1] 64;9

finite domain. In addition to the above boundary values, Sommerfeld's "Endlichkeitsbedingung" and "Ausstrahlungsbedingung"[1] as given in 4.2.16 must also be satisfied.

(4.2.16) $|rp| < k$ as $r \to \infty$

$r(\partial p/\partial r - jkp) \to 0$ as $r \to \infty$

The sound pressure distribution on the cross sectional circle of the cylinder is periodic with the period $(2\pi/m)$. This condition requires the periodicity in equation 4.2.13 to be the same as in 4.2.15, that is $n = m$. Moreover, the propagated wave is a diverging one, and must be represented by outwardly traveling waves. Also it does not include the axis of the cylinder. Hankel functions must therefore be substituted for the circular cylinder function in 4.2.12. The time dependence is given by 4.2.1, and is a function of $-j\omega t$. Consequently it becomes necessary to select a function of the form

(4.2.16a) $$H_m^{(1)}(r\sqrt{k^2-h^2}) = J_m(r\sqrt{k^2-h^2}) + jY_m(r\sqrt{k^2-h^2})$$

as the solution 4.2.12 to satisfy equation 4.2.16. With this modification the elementary wave function for the boundary problem at hand is given by

(4.2.17) $$p = \exp(jm\theta)\cdot H_m^{(1)}(r\sqrt{k^2-h^2})\cdot\exp(jhz)\cdot\exp(-j\omega t)$$

If the boundary condition along the generatrix of the

---

1 The author is indebted to Dr. R. C. F. Bartels for calling his attention to this condition.

cylinder were periodic, the next step would require the solution for each harmonic component of the boundary condition. The final solution is obtained by the summation of all components. The boundary condition on the generatrix of the stator is here given by a step function, that is, an aperiodic function, with a continuous frequency spectrum in space from zero to infinity. Consequently the summation of discrete solutions will be replaced by an integration and the solution for the sound pressure is thus given by

$$(4.2.18)\quad p \mp \exp(jm\theta - j\omega t)\cdot \int_{-\infty}^{+\infty} F(h)\cdot H_m^{(1)}(r\sqrt{k^2-h^2})\cdot \exp(jhz)dh$$

F(h)dh replaces the coefficients of the discrete components of the periodic case. In what follows, the term $\exp(jm\theta - j\omega t)$ will, for the sake of brevity, be omitted, though it will be added again at the end of this derivation.

The incorporation of the remaining boundary condition, that is, the finding of function F(h) to satisfy the behavior on the boundary, will be carried out by a Fourier transform method as suggested by R.F. Harrington[1] and J.A. Stratton[2]. A Fourier transform pair is given by

$$(4.2.19)\quad g(u) = (1/\sqrt{2\pi}) \int_{-\infty}^{+\infty} f(x)\, \exp(-jux)dx$$

---

[1] 31

[2] 66

$$(4.2.19) \qquad f(x) = (1/\sqrt{2\pi}) \int_{-\infty}^{+\infty} g(u) \exp(jux)\, du$$

The existence of the transform g(u) implies certain restrictions of f(x) discussed by R.V. Churchill[1]. That the transform arising in the problem considered does exist can be shown from the known behavior of solutions to the wave equation.

It is assumed provisionally that the integral in equation 4.2.18 is uniformly convergent, hence it may be differentiated under the sign of integration with respect to the parameter r. This results in the expression

$$(4.2.20) \quad (\partial p/\partial r) = \int_{-\infty}^{+\infty} F(h)(1/\sqrt{k^2-h^2})[H_m^{(1)}]'(r\sqrt{k^2-h^2}) \cdot \exp(jhz)\, dh$$

Hence over the surface of the cylinder where r = a

$$(4.2.21) \quad (\partial p/\partial r)_{r=a} = \int_{-\infty}^{+\infty} F(h)(1/\sqrt{k^2-h^2})[H_m^{(1)}]'(a\sqrt{k^2-h^2}) \cdot \exp(jhz)\, dh$$

Now introduce the following notation

$$(4.2.22) \quad (\sqrt{2\pi})F(h)(1/\sqrt{k^2-h^2})[H_m^{(1)}]'(a\sqrt{k^2-r^2}) = G(h)$$

Equation 4.2.21 can be rewritten as

$$(4.2.21a) \quad (\partial p/\partial r)_{r=a} = (1/2\pi) \int_{-\infty}^{+\infty} G(h) \exp(jhz)\, dh$$

If we now compare 4.2.21a with 4.2.19, it becomes obvious that the coefficients of G(h) must be the Fourier transforms of $(\partial p/\partial r)$, that is

---

[1] 19

$$(4.2.23)\quad G(h) = (1/\sqrt{2\pi}) \int_{-\infty}^{+\infty} (\partial p/\partial r)_{r=a} \exp(-jhz)\, dz$$

Recalling the boundary conditions, namely

$$(\partial p/\partial r)_{r=a} = 0 \text{ for } |z|>b$$

$$(\partial p/\partial r)_{r=a} = \text{const. } A \text{ for } |z|<b$$

the integral can be expressed as

$$(4.2.24)\quad G(h) = (1/\sqrt{2\pi})\, A \int_{-b}^{+b} \exp(jhz)\, dz$$

$$= (A/\sqrt{2\pi}) \left[(\exp(-jhb)-\exp(jhb)\right]/(-jh)$$

$$(4.2.25)\quad G(h) = (2Ab/\sqrt{2\pi}) \left[\sin (hb)/hb\right]$$

On introducing this value into equation 4.2.22 one obtains for

$$(4.2.26)\quad F(h)=(Ab/\pi)\left[\sin (hb)/hb\right](1/\sqrt{k^2-h^2})\left[1/H_m^{(1)}\right]'(a\sqrt{k^2-h^2})$$

and the solution of 4.2.3 satisfying all boundary conditions can be expressed as

$$(4.2.27)\quad p(r,\theta,z,t) = (Ab/\pi) \exp(jm\theta - j\omega t)\, I(m,b,r,z)$$

where

$$(4.2.28)\quad I(m\ b\ r\ z) = \int_{-\infty}^{+\infty} \left[\sin (hb/hb)\right] \exp(jhz) \frac{H_m^{(1)}(r\sqrt{k^2-h^2})}{\left[H_m^{(1)}\right]'(a\sqrt{k^2-h^2})}\, dh$$

If the integral is evaluated at z=0, the middle of the vibrating belt,

$$(4.2.29)\quad I(m,b,r)_{z=0}=2 \int_{0}^{\infty} \left[\sin (hb)/hb\right] \frac{H_m^{(1)}(r\sqrt{k^2-h^2})}{\left[H_m^{(1)}\right]'(a\sqrt{k^2-h^2})}\, dh$$

By introducing the value of the constant A in 4.2.27 the expression for the sound pressure at time t=0, at a

point $\theta=0$, and $z=0$, will be

(4.2.30) $p(r) = (\omega^2 \rho_o A_m/\pi).I(m,b,r)_{z=0}$

(4.3 The Solution of the Sound Pressure Integral

It would seem at first as though the integral 4.2.28 might be evaluated by integration in the complex plane. Unfortunately a tabulation of the roots of derivatives of Hankel functions is not available, so that the method of residues cannot here be applied. It is therefore necessary to carry out the tedious work of numerical integration. But even this method involves some difficulties. At $k^2=h^2$, the integrand becomes indefinite. In order to overcome this obstacle the integral will be evaluated from zero to δ with $0 \gtrless \delta \gtrless k$.

The part of the integral from zero to δ will be denoted as integral I_1, and the remaining part from δ to ∞, as integral I_r. For the computation of I_r a new variable

(4.3.1) $$y = a\sqrt{k^2-h^2}$$

will be introduced. Hence,

(4.3.2) $$\sqrt{k^2-h^2} = (y/a); \quad h = (1/a)\sqrt{a^2k^2-y^2}$$

and

$$dh = (ydy/a\sqrt{a^2k^2-y^2})$$

Introducing 4.3.1 and 4.3.2 into I_r, it can be written as

(4.3.3) $$I_r = \int_{a\sqrt{k^2-\delta^2}}^{-j\infty} \frac{\sin(\alpha\sqrt{\eta^2-y^2})}{\alpha(\eta^2-y^2)} \cdot \frac{H_m^{(1)}(y)}{[H_m^{(1)}]'(y)}\,dy$$

The constants in this integral are defined as follows:

$$\alpha = (b/a); \qquad \beta = (r/a); \qquad \eta = ak$$

Before proceeding further the behaviour of the fraction containing the Hankel functions at zero will be investigated. Assuming $m > 0$ and $y \ll 1$, the Hankel functions can be approximated by

$$H_m^{(1)}(y) = (y^m/2^m \cdot m!) - j\,[2^m(m-1)!/\pi y^m]$$

Substituting these values for the Hankel functions, the fraction can be expressed as

$$(Ay^m - jBy^{-m})/(Cy^{m-1} - jD\,y^{-(m-1)} + Ey^{m-1} - jFy^{-(m+1)})$$

In this equation A....F are functions of m, but not of y. By multiplying the numerator and denominator by y^{m+1} it can be written as

$$(Ay^{2m+1} - jBy)/(Cy^{2m} - j\,Dy^2 + Ey^{2m+1} - jF)$$

The limit of this fraction as $y \to 0$ will be $(0/-jF)$, that is, the integrand at $y = 0$ will be zero.

The integral I_r itself will be split into two parts: the first part representing integration on the real axis, and the second on the imaginary axis. The integration along the real axis will be

$$(4.3.5) \qquad I_2 = \int_0^{a\sqrt{k^2-\delta^2}} \frac{\sin(\alpha\sqrt{\eta^2-y^2}}{\alpha\sqrt{\eta^2-y^2}} \cdot \frac{H_m^{(1)}(\beta y)}{[H_m^{(1)}]'(y)}\,dy$$

and on the imaginary axis

$$(4.3.6) \qquad I_3 = -2 \int_0^{j\infty} \frac{\sin(\alpha\sqrt{\eta^2-y^2})}{\alpha(\eta^2-y^2)} \cdot \frac{H_m^{(1)}(y)}{[H_m^{(1)}]'(y)} dy$$

To evaluate integral I_3 a new variable x is introduced, with

$$(4.3.7) \qquad y = jx \; ; \quad dy = jdx$$

Using the relation

$$K_m(x) = (\pi/2)\, j^{(m+1)}\, H_m^{(1)}\, jx$$

where $K_m(x)$ is the modified Bessel function of the second kind, integral I_3 can be expressed as,

$$(4.3.8) \qquad I_3 = -4 \int_0^{\infty} \frac{\sin(\alpha\sqrt{\eta^2-x^2})}{\alpha(\eta^2-x^2)} \cdot \frac{K_m(\beta x)}{K_{m-1}(x) + K_{m+1}(x)} dx$$

From a practical viewpoint it is not necessary to carry out the integration to infinity, but it is sufficient to evaluate it from zero to a finite upper limit, and then estimate the order of the unevaluated part of the integral. In section 4 it will be demonstrated that it can be entirely neglected, so that the sound pressure integral can be written as,

$$(4.3.8) \qquad I = I_1 + I_2 + I_3$$

4.4 Numerical Evaluation of Sound Pressure.

The numerical value of integral I has to be established first before calculating the sound pressure. In this section, the detailed computations for the experimental

motor are carried out for a point on a radial line through the geometric center of the top rib, at a distance of 1 foot from the stator surface. The integral is evaluated for a frequency range from 1,000 to 2,000 c.p.s. The results are assembled in table 4.4.4, and plotted in fig. 4.4.1. In the numerical work

$$c = 34{,}400 \text{ cm/second}; \qquad \rho_o = 0.00121 \text{ gram/cm}^3,$$

i.e., values at 20°C and 760 mm mercury pressure are used. The other constants, occurring in the integral, taken from fig. A 1.2, are

$$a = 21 \text{ cm}; \qquad b = 13.2 \text{ cm}; \qquad r = 51.5 \text{ cm}$$

As a representative example the detailed calculations for f = 1,700 c.p.s. are assembled in tables 4.4.1 to 4.4.3. The magnitude of the remainder term is estimated below.

The Remainder of the Integral can be obtained as follows: As the fraction of the Hankel functions in integral I_3 decreases monotonically, it may be assumed to be less than 5×10^{-5}. The unevaluated part of the integral I_3 may therefore be written

$$|I_{3,R}| < (0.629) \times 4(5) \times 10^{-5} \int_6^{\infty} \frac{\sin\left(0.629 \sqrt{6.51^2 + x^2}\right)}{0.629 \times (6.51^2 - x^2)^{1/2}} dx$$

Now introduce

$$w = 0.629 \sqrt{6.51^2 + x^2} \quad \text{and} \quad dx \simeq dw/0.629$$

The unevaluated part of the integral will be

$$|I_{3,R}| < 2\times10^{-4} \int_{5.6}^{\infty} (\sin w/w^2)\, dw <$$

$$< 2\times10^{-4} \int_{5.6}^{\infty} (1/w^2)\, dw < 2\times10^{-4} \left|1/x\right|_{5.6}^{\infty}$$

$|I_{3,R}| < 4\times10^{-5}$, this value is entirely negligible.

Using Simpson's rule the value of integral I for 1,700 c.p.s. can be calculated to be

$$I = (4/3)\,[(0.02)(12.598+j\ 14.802)+(0.829)(-0.024-j\ 0.1017)-$$
$$+(1)(0.00292)]$$

$$I = 0.316 + j\ 0.381 = (0.495)\ \underline{/50.3^{\circ}}$$

Finally the sound pressures of the main and the side noise of the experimental motor are calculated in table 4.4.5. The results in this table represent the theoretical solution.

Table 4.4.1 Part I

Calculation of Integral I, for 1700 cps; K = 0.310

1	2	3	4	5	6	7	8	9	10
	h	$\sqrt{k^2-h^2}$	13.2h	$\frac{\sin 13.2h}{13.2h}$	$\frac{\text{Col 5}}{\text{Col 3}}$	$\frac{H_2^{(1)}(r\sqrt{k^2-h^2})}{[H_2^{(1)}]'(a\sqrt{k^2-h^2})}$	Col 7 x Col 6		Col 8 x Col 9
						l j	l	j	l j
1	0	.3100	0	1	3.226	.068 + .315	.219	+ 1.016	1 .219 + 1.016
2	.02	.3094	.264	.988	3.194	0.079 + .314	.252	+ 1.003	4 1.008 + 4.012
3	.04	.3074	.528	.954	3.104	0.097 + .311	.301	+ .965	2 .602 + 1.930
4	.06	.3041	.792	.899	2.955	0.127 + .292	.375	+ .863	4 1.500 + 3.452
5	.08	.2995	1.056	.824	2.752	0.173 + .276	.476	+ .760	2 .952 + 1.520
6	.1	.2934	1.320	.734	2.501	0.221 + .239	.553	+ .598	4 2.212 + 2.392
7	.12	.2858	1.584	.631	2.209	.273 + .181	.603	+ .400	2 1.206 + 0.80
8	.14	.2766	1.848	.521	1.882	.319 + .087	.600	+ .164	4 2.40 + 0.656
9	.16	.2655	2.112	.406	1.528	.327 -0.022	.500	- .034	2 1.000 - 0.068
10	.18	.2524	2.376	.291	1.153	.294 - .151	.339	- .174	4 1.356 - 0.696
11	.20	.2369	2.640	.182	.769	.186 - .276	.143	- .212	1 0.143 - 0.212

$\sum$(Col 10) = 12.598+j 14802

Table 4.4.1 Part II

Ratio of Hankel Functions for I_1 of 1700 cps

1	2	3	4		5		6		7		8	
	$21\sqrt{k^2-n^2}$	$51.5\sqrt{k^2-h^2}$	$H_2^{(1)}$(Col 3)		$H_1^{(1)}$(Col 2)		$H_3^{(1)}$(Col 2)		Col 5 - Col 6		Col 4/Col 7	
			1	j	1	j	1	j	1	j	1	j
1	6.510	15.97	.184	-0.077	-.151	-.275	.038	-.328	-.113	- .603	.068	+.315
2	6.497	15.93	.180	-0.085	-.154	-.274	.035	-.329	-.119	- .603	.079	.314
3	6.455	15.83	.172	- .103	-.166	-.267	.022	-.331	-.144	- .598	.097	+.311
4	6.386	15.66	.152	- .132	-.185	-.257	.000	-.334	-.185	- .591	.127	.292
5	6.289	15.42	.118	- .165	-.210	-.240	-.027	-.336	-.237	- .576	.173	.276
6	6.161	15.11	.063	- .195	-.242	-.214	-.066	-.335	-.308	- .549	.221	.239
7	6.002	14.72	-.016	- .208	-.277	-.175	-.115	-.328	-.392	- .503	.273	.181
8	5.809	14.24	-.111	- .180	-.309	-.122	-.171	-.311	-.480	- .433	.319	.087
9	5.576	13.67	-.194	- .095	-.336	-.050	-.235	-.279	-.571	- .329	.327	-.022
10	5.300	13.00	-.218	.046	-.346	.045	-.305	-.223	-.651	- .178	.294	-.151
11	4.975	12.20	-.125	.193	-.325	.155	-.368	-.141	-.693	+ .014	.186	-.276

Table 4.4.2 Part I

Calculation of Integral I_2 for 1700 cps

$\eta = a.k = 6.51$ $\alpha = 0.629$ $\beta = 2.452$

1	2	3	4	5	6	7		8		9	10	
	y	$\sqrt{\eta^2-y^2}$	$\sqrt{\eta^2-y^2}$	$\frac{\sin(\text{Col } 4)}{\text{Col } 4}$	$\frac{\text{Col } 5}{\text{Col } 3}$	$\frac{H_2^{(1)}(\beta y)}{[H_2^{(1)}]'(y)}$		Col 7 x Col 6			Col 8 x Col 9	
						1	j	10^{-2}	$jx10^{-2}$		10^{-2}	$jx10^{-2}$
1	0.	6.510	4.095	-0.199	-.031							
2	0.829	6.457	4.061	- .196	-.030	-.0628	-.041	.190 +	.124	4	.76 +	.496
3	1.658	6.295	3.960	- .184	-.029	.238	-.171	-.697 +	.501	2	-1.4 +	1.00
4	2.487	6.016	3.784	- .158	-.026	.123	.326	-.323 -	.857	4	-1.29 -	3.43
5	3.316	5.602	3.524	- .106	-.019	-.323	.151	.610 -	.285	2	1.22 -	.57
6	4.145	5.019	3.157	- .005	-.010	-.216	-.258	-.207 +	.248	4	- .828+	.992
7	4.975	4.199	2.641	.182	+.043	.160	-.233	.692 -	.889	1	+ .692-	.889

$$\sum (\text{Col } 10) = -(2.2+j\ 1.5) \times 10^{-2}$$

Table 4.4.2 Part II

Ratio of Hankel Functions for I_2 of 1700 cps

1	2	3	4		5		6		7		8	
	y	βy	$H_2^{(1)}$	(βy)	$H_1^{(1)}$	y	$H_3^{(1)}$	y	Col 5 - Col 6		Col 4/Col 7	
			1	j	1	j	1	j	1	j	1	j
1												
2	.829	2.033	.359	- .602	.380	- .944	-.011	+10.29	.369	+ 9.352	-.0628	-.041
3	1.658	4.066	.347	+ .234	.575	- .310	-.080	+ 1.65	.495	+ 1.340	.238	-.171
4	2.487	6.099	-.261	+ .204	.499	+ .145	-.215	.763	.284	+ 0.908	.123	.326
5	3.316	8.132	-.077	- .273	.215	+ .389	-.362	+ .423	-.147	+ .812	-.323	.151
6	4.145	10.16	.250	+ .033	-.120	+ .376	-.434	+ .131	-.554	+ .507	-.216	-.258
7	4.975	12.198	-.124	+ .193	-.324	+ .156	-.370	+ .138	-.694	+ .018	.160	-.233

Table 4.4.3

Calculation of Integral I_3 for 1700 cps

$\eta = a.k = 6.51$ $\alpha = 0.629$ $\beta = 2.452$

1	2	3	4	5	6	7	8	9	10	11	12
x	$\sqrt{\eta^2+x^2}$	$\frac{dx}{\text{Col 2}}$	$\frac{\sin(\text{Col 3})}{\text{Col 3}}$	$\frac{\text{Col 4}}{\text{Col 2}}$	βx	$K_2(\beta x)$	$K_1(x)+K_3(x)$	$\frac{\text{Col 7}}{\text{Col 8}}$	Col 9 x Col 5		Col 9 x Col 10
				$\times 10^{-2}$		$\times 10^{-2}$		$\times 10^{-2}$	$\times 10^{-4}$		$\times 10^{-4}$
0											
1	6.587	4.143	-.203	-3.08	2.45	13.0	7.70	1.69	-5.20	4	-23.8
2	6.810	4.283	-.212	-3.11	4.90	.596	.787	.76	-2.40	2	- 4.8
3	7.168	4.509	-.217	-3.03	7.36	.037	.162	.23	- .70	4	- 2.80
4	7.640	4.806	-.207	-2.71	9.81	+ .003	.042	.071	- .40	2	- .80
5	8.209	5.163	-.175	-2.13	12.26	+ .000	.012	.016	- .00	4	- .00
6	8.853	5.569	-.118	-1.33	14.71	+ .000	.003	.000	- .00	1	- .00

$$\sum(\text{Col 12}) = -29.2 \times 10^{-4}$$

Table 4.4.4

Calculated Values of the Soundpressure

Integral for

$m = 2$; at $\theta = 0$; $z = 0$

		Integral I			
Frequency cps.	r cm.	Re	Im	Magn.	Arg. ^{o}
1000		-0.646	-0.163	0.67	-194.0
1100		-0.597	-0.286	0.663	-154.3
1250	51.5	-0.243	-.525	0.58	-105.4
1400		0.337	-0.455	0.566	- 53.4
1500		0.504	-0.2	0.542	- 21.5
1600		0.511	+0.139	.526	15.2
1700		0.316	0.381	.495	50.3
1800		0.029	0.469	0.470	86.8
1900		-0.27	0.417	0.48	122.0
2000		-0.398	0.23	0.46	150.0
1700	82.0	-0.242	-0.203	0.315	-140.2

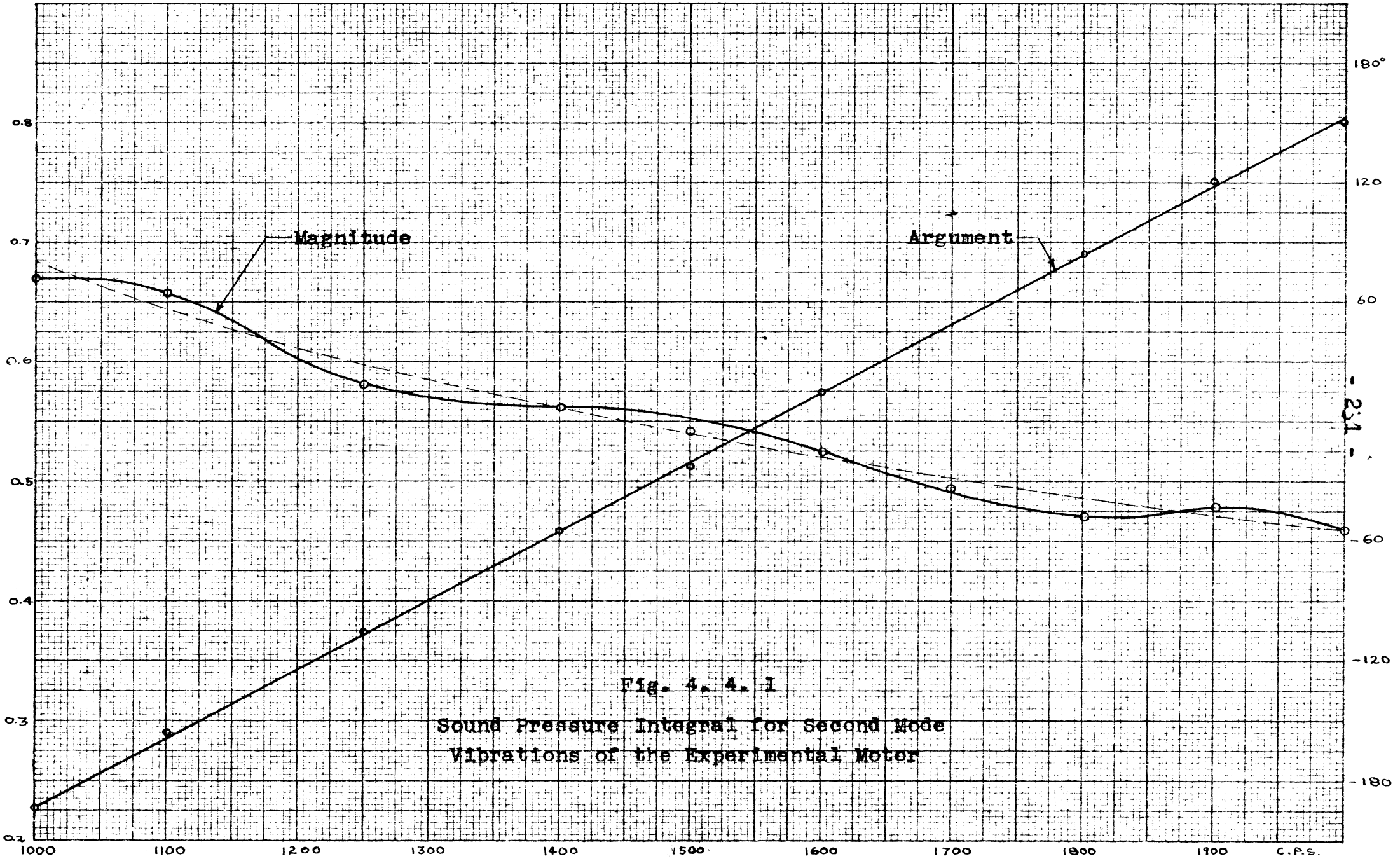

Fig. 4. 4. 1

Sound Pressure Integral for Second Mode
Vibrations of the Experimental Motor

Table 4.4.5

Calculated Sound Pressures of the Experimental Motor

1	2	3	4	5	6	7	8	9
Motor Operating A, V, cps	Noise f cps	defl. cm 10^{-6}	I		ω^2 10^{+6}	10^4	$\log_{10}$ Col 7	RMS. SPL. db.
40, 440, 60	1,716	19.6	0.492		116.0	1.98	4.296	85.9
40, 367, 50	1,419	30.7	0.560		79.0	2.43	4.385	87.7
40, 294, 40	1,121	60.5	0.650	17.8	49.6	3.47	4.540	90.8
N.L.,440,60	1,475	5.34	0.485		118.9	0.55	4.738	74.8
40, 440, 60	1,735	1.51	0.545		86.0	0.126	3.100	62.0
40, 440, 60	1,716	19.6	0.315		116.0	1.28	4.107	82.1

Col. 3 identical with last Col. of Table 3.6.6 on page 200.
Col. 4 values are taken from fig. 4.4.1 on page 231.
(Col. 5) = $|bp/\pi\ 2(0.0002)|$ = $(13.2x1.21x10^{-3}x5x10^{3}/\pi\ 2)$ = 17.8
Col. 7 is the product of Columns 3,4,5, and 6
The value of r is 51.5 cm in all rows, except the last row where r = 82.0 cm

V. EXPERIMENTAL INVESTIGATION OF THE SPECIAL MOTOR

The aim of the experimental investigation of the special motor was to obtain a check on the calculated results, and thereby to verify the theory as developed in chapters 2 to 4. While the tests are considered auxiliaries to the theoretical work, their importance should not be underestimated. In this very complex problem test results serve as invaluable signposts for assumptions to be made for any future analysis.

At an early stage in the author's special assignment which led to this analysis it became clear that the main purpose of his endeavors should be directed towards the theoretical predetermination of the sound levels of the magnetic noise, rather than towards the development of some special test equipment. Consequently only commercially produced or already existing apparatus had to be used. The lack of special instrumentation did not limit the scope of the investigation to any considerable extent.

The importance of the resonant frequencies for the analysis has been stressed at the start of chapter 2. Because of the predominant role of the eigenvalues the tests for natural frequencies and associated mode shapes were performed on an unloaded motor. Subsequent tests, however, were carried out with the motor under load. These

tests consisted of sound pressure level measurements and the search for mode shapes of vibrations.

5.1 Test for Natural Frequencies and Associated Mode Shapes.

Description of Equipment and Tests. In this test an external vibratory force was applied to the motor and the ensuing vibrations examined. The general arrangement for this test is shown in fig. 5.1.1

The vibratory force was supplied by an electromagnetic shaker, as illustrated on the top of the motor in fig. 5.1.1, and marked A. This shaker was a simple iron core coil whose magnetic circuit partly closed through the motor under test. A small airgap was maintained between shaker and motor in order to avoid saturation effects. The high impedance of the coil (approximately 500 ohms at 1,000 c.p.s. measured with its magnetic circuit open) limited the usefulness of the shaker to a frequency range from 20 to 2,000 c.p.s. The force exerted by the coil, an inverse function of the airgap, was of the order of 1-3 lb. In actual tests the position of the shaker was varied to drive the motor at the amplitude of the mode shape, in order to achieve clear results. Most of the time the shaker was applied inside the stator and it became necessary to remove the two end shields and the rotor.

A variable frequency supply as shown on the right of fig. 5.1.1 was used to energize the coil of the shaker.

A Hewlett Packard Oscillator Model 200D and a 200 watt power amplifier served this purpose. The frequency of the oscillator and of the flux pulsations in the coil were the same. The attractive force of the coil, proportional to the square of the flux density in the airgap between shaker and motor, has a uniform and a second harmonic component. The latter set the stator into vibration.

The vibration of the stator driven by the shaker was sensed by an inertia-operated piezo-electric pickup. The sensitive element of this device consisted of 96 per cent barium titanate, 4 per cent lead titanate crystal of 0.25 inch diameter, and was 0.025 inch thick. The maximum outer diameter of the pickup was 0.6 inch and the height 0.8 inch. The accelerometer was mounted on a small magnet. From the electrical point of view the accelerometer may be considered as a zero impedance charge generator in series with its capacitance. The voltage sensitivity was about 0.4 millivolt on the end of a 3-ft cable.

The output of the acceleration pickup was applied to an amplifier, in this case a General Radio Sound Level Meter, Type 1551-A. The amplifier in turn was connected to the Y terminals of a Cathode Ray Oscilloscope, and the X terminals of the C.R.O. to the output of the oscillator.

The oscillator was gradually varied by the opera-

tor who simultaneously followed the Lissajous figure on the screen of the C.R.O. The trace he saw was the characteristic figure eight of the superposition of two component oscillations, where the frequency of one oscillation was the double that of the other.

When resonance was reached, the Y deflection on the C.R.O. was a maximum and the Lissajous figure assumed the shape of a parabola. On slightly increasing and decreasing the frequency a phase change of the trace could be observed. Now the outer and the inner ring were sensed with the pickup and the shaker moved to the position of maximum amplitude. Keeping the shaker at a resonant frequency the pickup was moved along the outer and the inner ring and the phase of the Lissajous figure, which changed continuously, again observed. At a point of zero displacement on the stator, the amplitude of the Lissajous figure was a minimum, and the phase of the trace became indefinite. Such a point is generally referred to as a node of vibration. Moving the pickup still further a change of phase occurred. The amplitude of the Lissajous figure increased steadily until the position of another maximum amplitude was reached. The shape of the Lissajous figure at this second maximum amplitude was the mirror image of the first amplitude's trace. This procedure was continued till the whole stator had been sensed.

The positions of maximum deflections and nodes

give a more or less clear picture of the vibration mode. The nodes on the actual motor, as seen from the test records, were not as neatly and regularly spaced as the calculations of the simplified structure in fig. 3.3.1 would indicate. This was due to the fact that the mass distribution is not entirely symmetrical. As a consequence of irregularities in the casting and incomplete symmetry in some instances, two modes of vibration, though clearly of the same category, but differing by a few cycles were found.

The results of this investigation are recorded in fig. 5.1.2 for the second mode vibration, and in fig. 5.1.3 for the third mode case. The comparison of calculated and measured resonant frequencies and mode shapes is provided in the next chapter, while only the difference between tests and theoretical results is being pointed out here. The theoretical analysis yields counter-tact cosine modes at 10,000 and 1,290 c.p.s., that is in the first and the fifth principal modes. It was impossible to excite these resonances on test, which was not surprising in the case of the first principal mode as its frequency was well beyond the range of the shaker. A thorough search for the fifth principal mode was therefore made with a more powerful shaker[1], again without succeeding to excite this mode

---

1 The additional tests were carried out through the courtesy of Dr. R. Plunkett, at the General Engineering Laboratory of the General Electric Company.

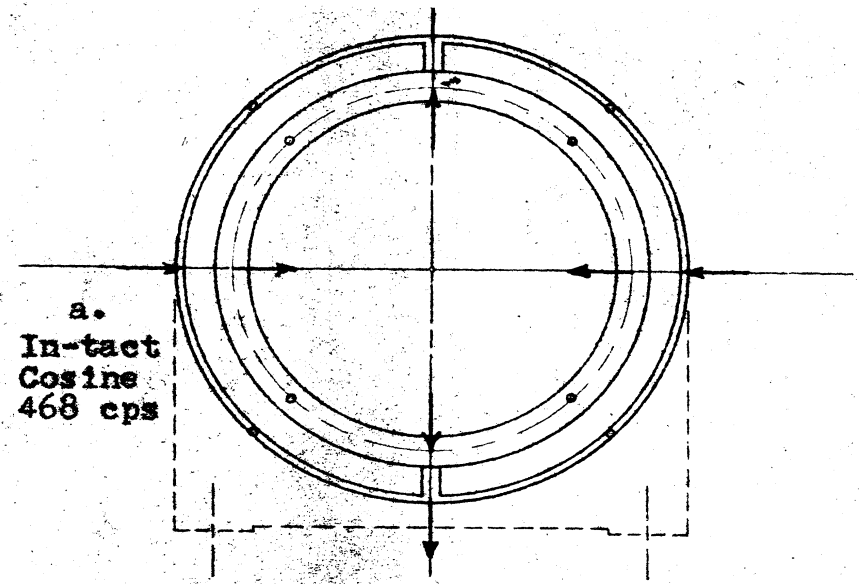

a.
In-tact
Cosine
468 cps

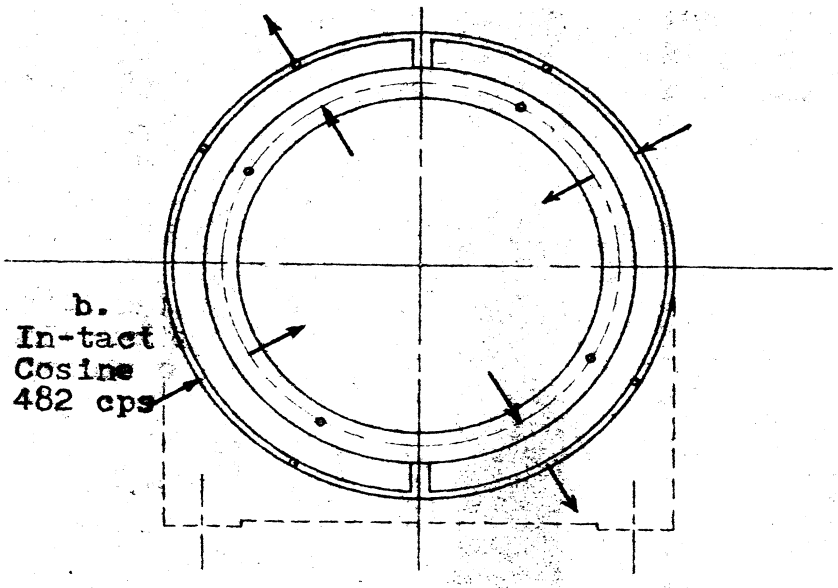

b.
In-tact
Cosine
482 cps

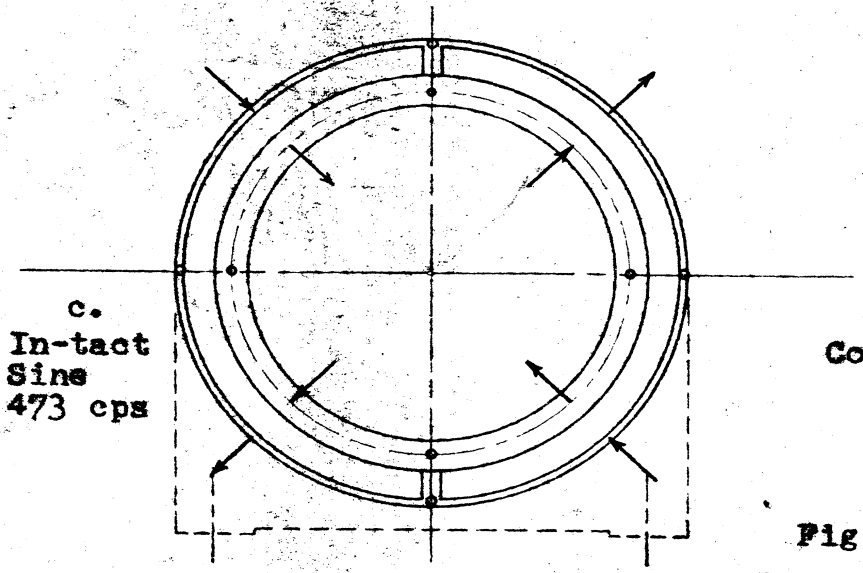

c.
In-tact
Sine
473 cps

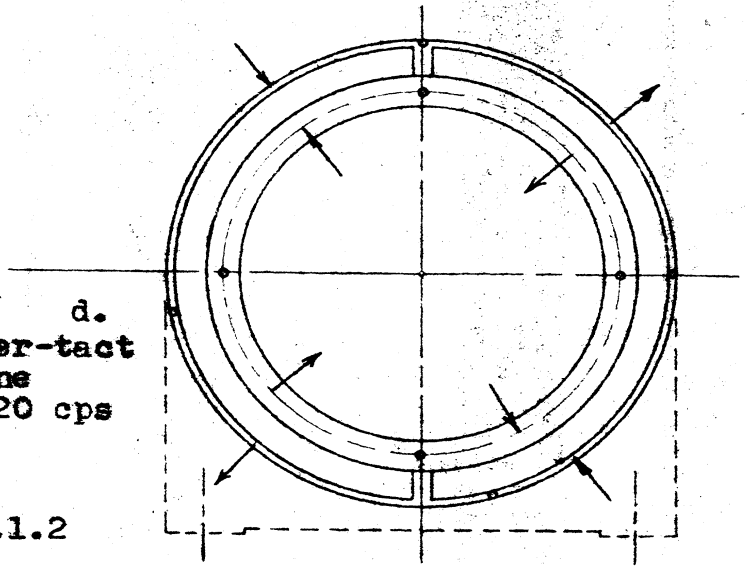

d.
Counter-tact
Sine
1220 cps

Fig. 5.1.2

Second Mode Resonances of the Experimental Motor (Measured)

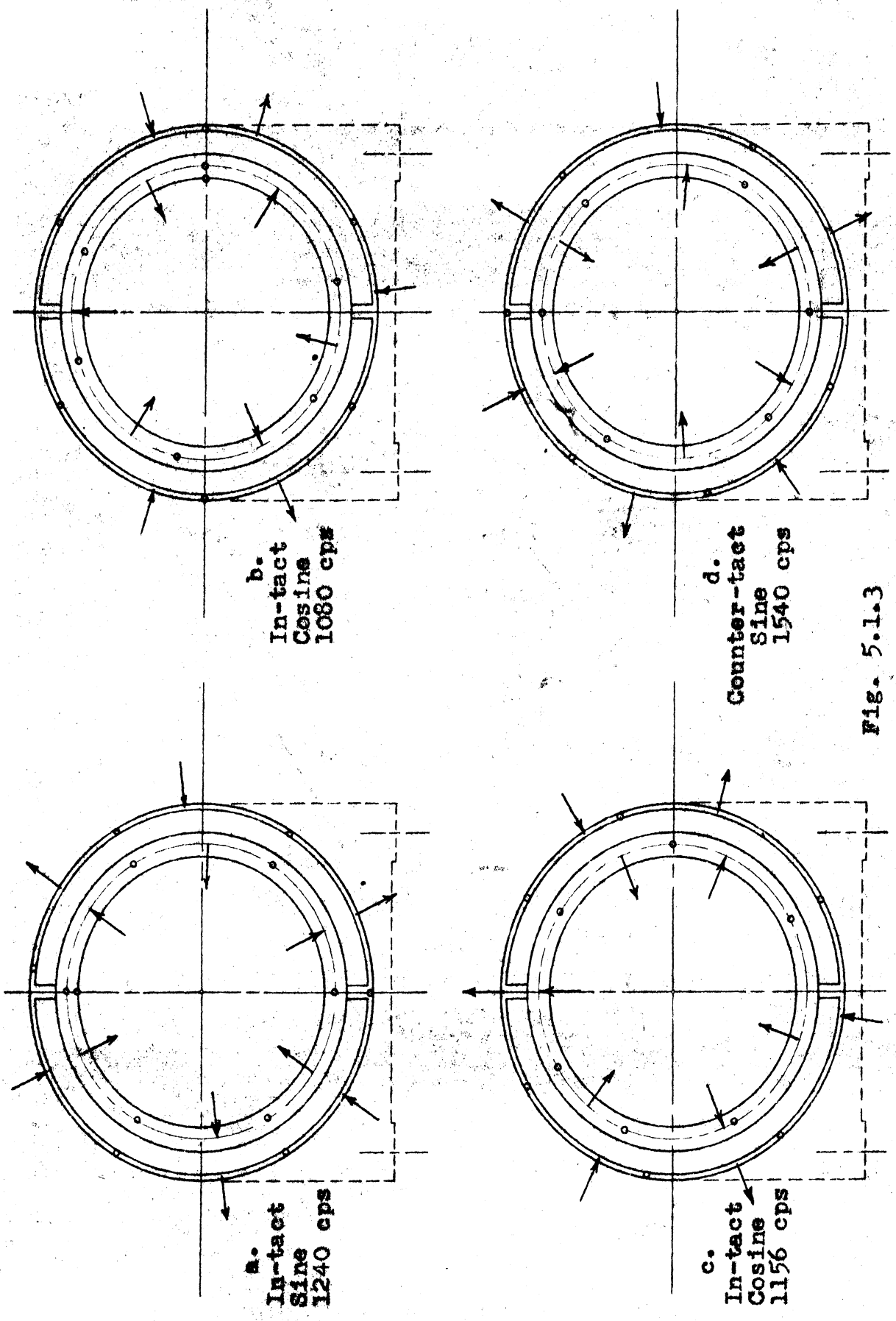

Fig. 5.1.3 Third Mode Resonances of the Experimental Motor (Measured)

of vibration. It was therefore concluded that the construction of the stator as illustrated in fig. 5.1.4 was responsible for the overdamped conditions in the counter-tact cosine modes, as discussed in section 3.2.

5.2 Measurement of Motor Noise Sound Pressure Levels.

This investigation consisted of two major steps. First the motor noise was recorded on a magnetic tape at different operating conditions. Later the magnetic tape was used to record the amplitude of the sound pressure levels as a function of frequency.

The Recording of the Motor's Noise Output[1] was carried out in an anechoic room. An outline of the room and the position of the motor in the room are illustrated in fig. 5.2.1. Fig. 5.2.2 shows the relative position of the motor and the microphone. The air deflectors have been removed for this test.

The difficulty of constructing a suitable anechoic room for as large an equipment as a medium induction motor should not be underestimated. It would be almost financially prohibitive to construct a chamber with perfect sound absorbing walls, as described by Beranek and Sleeper[2]. It also seems practically impossible to mount

---

1 11;55

2 13

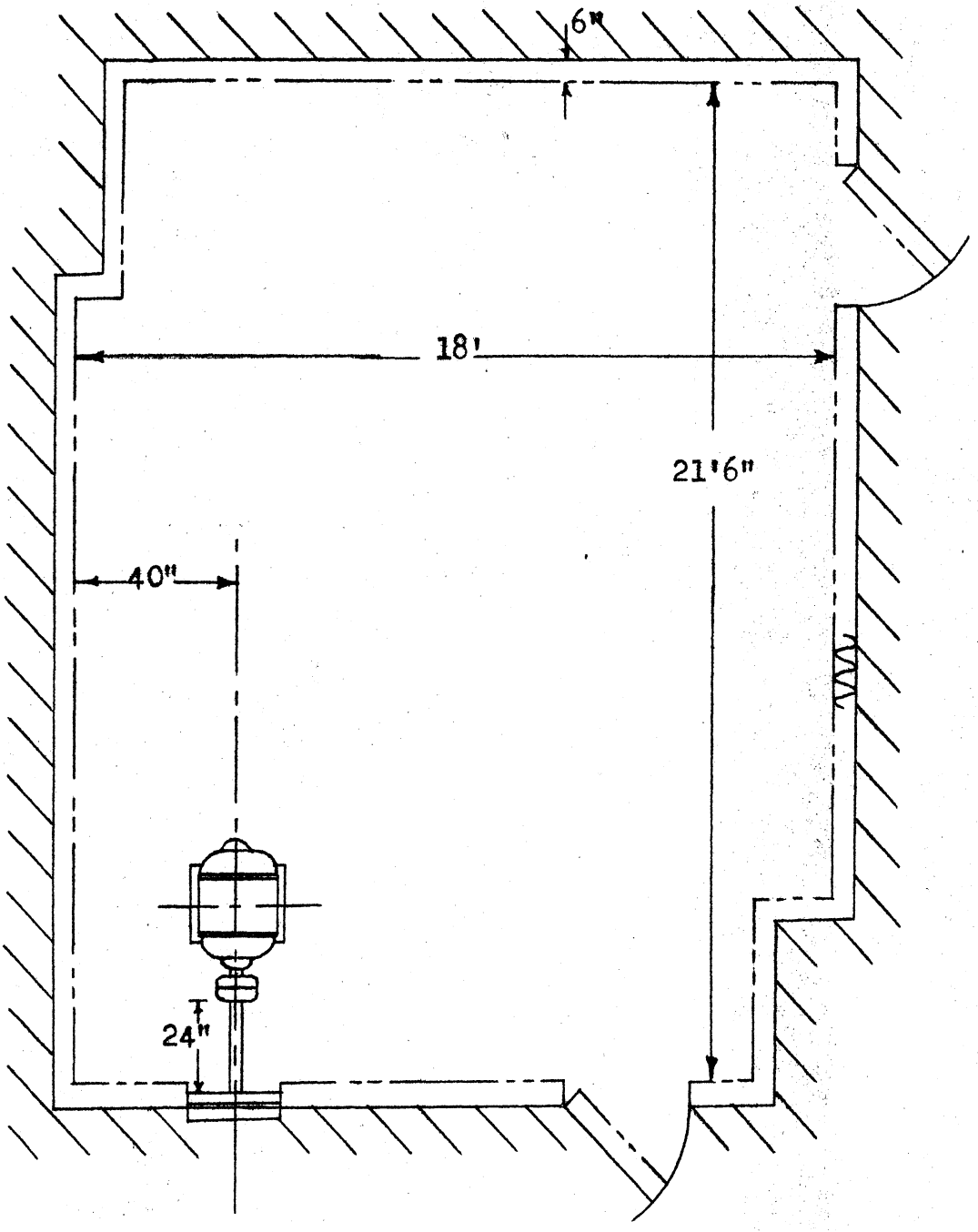

Fig. 5.2.1

Position of Motor in Noise-Measurement Laboratory

induction motors, weighing 200 - 2,000 lb, on a suspended, tightly stretched steel net, to conform with the design of anechoic chambers, which are usually divided into upper and lower halves.

The vertical walls of the anechoic room used for this test were lined with a 6" deep and 1" thick corrugation of Fiberglass pads, and protected by a chicke wire fence. The ceiling at a height of 18' was also covered with a layer of Fiberglass pads. Unfortunately the equipment of a traveling crane and a system of pipes cluttered up the area near the ceiling.

The floor of the sound room was constructed of concrete covered by Fiberglass quilts and protected by steel grids. One corner of the floor consisted of 48 steel blocks each 14 inch square, as seen in fig. 5.1.1. During tests these blocks were also covered by Fiberglass quilts. The anechoic room located in a production area had common foundations with the main building. As a consequence, all low frequency vibrations, such as are always present in factories, were directly transmitted to the sound room.

The best position for the motor would have been at the geometric center of the room, but the machine was actually mounted on a 30" high base in a corner of the room. This relatively unfavorable position was required by a hydraulic absorption dynamometer which

was mounted outside of the sound room. The dynamometer served as a load to the motor and had been originally designed as a loading device for motors of 500 - 1,500 HP. It proved difficult to operate the motor at a uniform output even for the short periods of sound recording. A 30" x 24" double-glass window (which served for communication with the switchboard operator, controlling the load of the motor) located above the protruding shaft most probably acted as a sound reflector. In short, the sound measurement room left much to be desired to meet the stringent requirements of field free conditions for precise and constant measurements. However, ideal conditions for tests of large equipment are ordinarily difficult, if not impossible, to establish.

A non-directional microphone of the Rochelle crystal-diaphragm type (as the first element of the sound recording circuit) was mounted on a tripod one foot above the center of the motor. A low capacitance line connected the microphone to a General Radio Sound Level Meter, Type 1551-A.

The Sound Level Meter is basically a calibrated attenuator amplifier, including an indicating meter and a weighing network to modify the amplifier response to simulate response conditions of the human ear to pure tones at specified levels. The amplifier is stabilized by means of inverse feedback and has a fairly flat fre-

quency characteristic over the range from 20 - 20,000 c.p.s.

The output of the amplifier was connected to a Magnecorder Type PT-6 decade amplifier. This amplifier with a flat frequency response from 20 - 20,000 c.p.s. has a low hum and noise level and low linear distortion. The output of the amplifier was fed into a Magnecorder Type PT-6 tape recorder, a high quality instrument with a wide dynamic range and of excellent constant speed. The speed of the tape during recording was approximately 18" per second.

Before, during, and after the test the whole sound recording circuit was calibrated with a General Radio Type 1552-A Sound Level Calibrator.[1] The calibrator consisted of a small stabilized loudspeaker mounted in an enclosure. The enclosure is so designed that the speaker is always connected at the correct distance from the microphone diaphragm, that is fitted tightly over the microphone. The loudspeaker was supplied by a tuning-fork operated, fixed frequency oscillator of 400 c.p.s. When the adjustable output voltage of the oscillator was set to two volts, the calibrator produced an 85 db SPL at the microphone diaphragm.

The Recording of the Sound Spectrum

---

[1] 30

The amplitude of the noise plotted against frequency, and referred to as a sound spectrum,was recorded with the aid of an arrangement as shown in fig. 5.2.3.

First a representative sample of the tape of each recording was selected, spliced into an endless loop, and fitted to the previously described Magnecorder Type PT-6 recorder. The output of the tape recorder was supplied through the Magnecorder Type PT-6 amplifier to a General Radio Type 736-A Wave Analyzer.

The wave analyzer is actually an a-c operated vacuum tube voltmeter of the heterodyne type. The intermediate frequency amplifier of this apparatus includes a highly selective quartz-crystal filter. The use of the heterodyne circuit renders the apparatus very useful for the recording of noise spectra, as it makes it possible to use a fixed frequency filter for the whole range of variable frequency. The narrow band-width of this instrument has a 4-cycle flat top and has a high rejection outside the passband. The wave analyzer's output is connected to a recorder which in turn drives the wave analyzer dial synchronously by means of a transmission link as illustrated in fig. 5.2.3.

The final element in the recording of the sound spectrum was a Bruel and Kjaer High Speed Level Recorder, Model BL-2304. This is a graphic recording peak indicating

a.c. voltmeter, designed for a frequency range of 20 to 250,000 c.p.s. The principle of the level recorder's operation is that of a balanced type of stylus positioning system made possible by a potentiometer-controlled moving-coil driving system. The negative feedback servo-arrangement provides a high degree of stability and damping. The output of the recorder, a rectilinear trace, is produced by a sapphire stylus on opaque waxed paper. The writing speed is 500 mm per second and the chart speed 1 mm per second.

During the recordings of the motor noise the output of Calibrator type 1552-A was also recorded for the determination of the absolute sound level.

Before presenting the records of the sound measurements a discussion on the accuracy of the measurement seems indicated. According to manufacturer's information the accuracy of the type 1551-A Sound Level Meter and associated microphone is within plus and minus 1 db, and that of type 1552-A Sound Level Calibrator also plus or minus 1 db. Careful experiments by R.J. Wells[1] seem to indicate that the tape recording may also introduce errors of 1 db in the frequency range between 1,200 and 2,500 c.p.s. The type BL 2304 Recorder has an accuracy of plus or minus

---

1 74

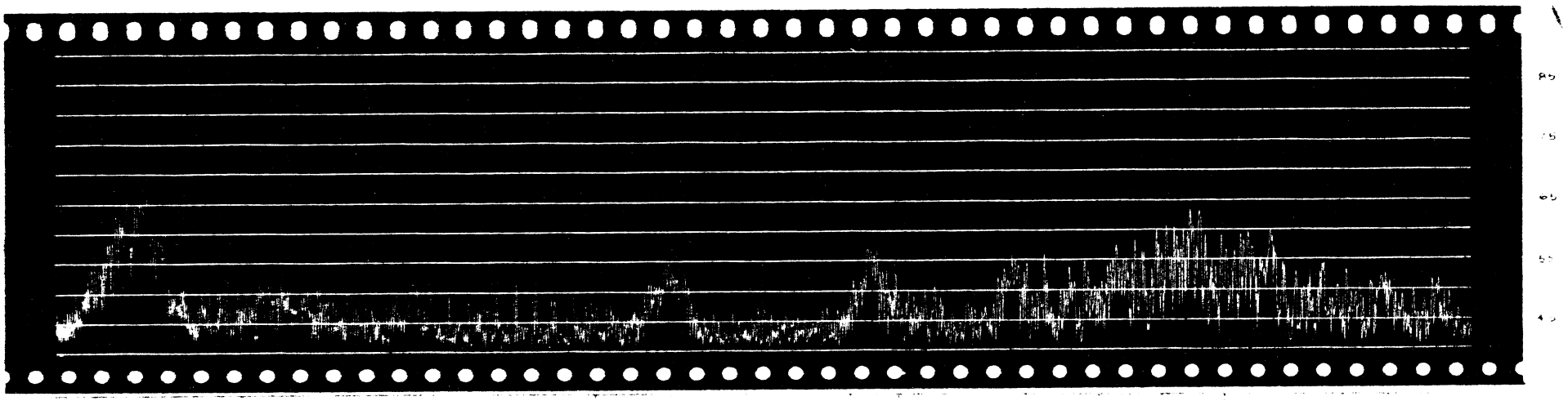

Fig. 5.2.4

Sound Spectrum of Experimental Motor at 4[illegible] Amp, 440 V, 60 cps, (Overall SPL 88 db)

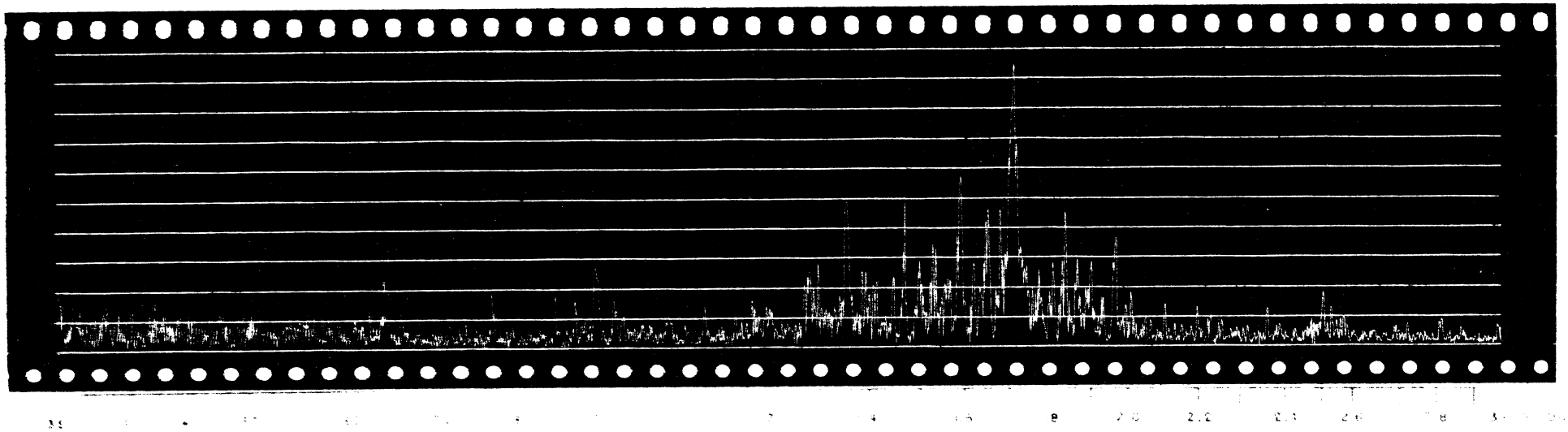

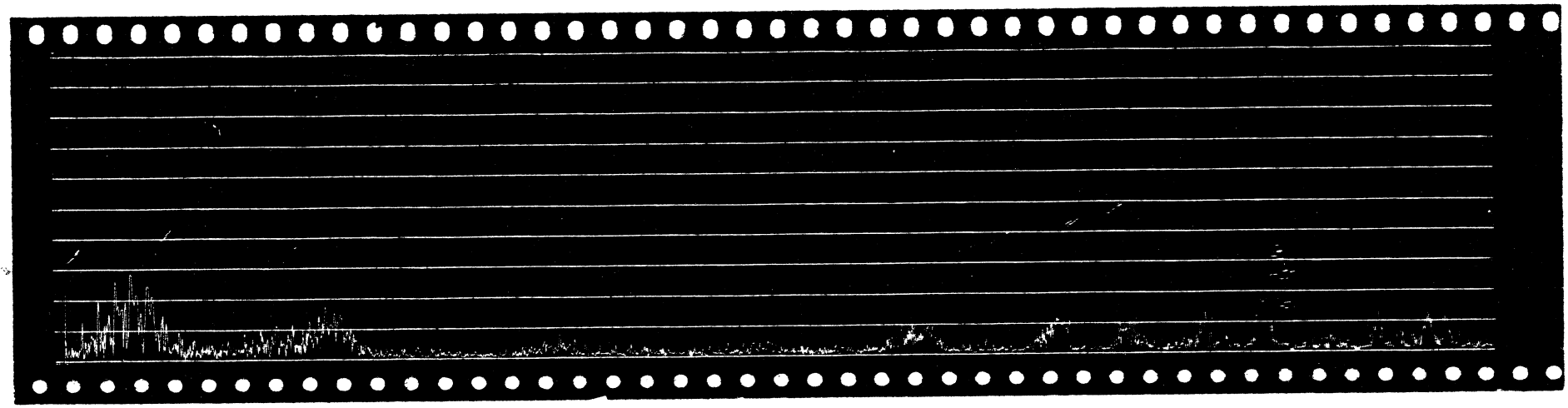

Fig. [illegible]

Sound Spectrum of Experimental Motor at [illegible] Amp, [illegible] V, 50 cps. (Overall SPL 91 db)

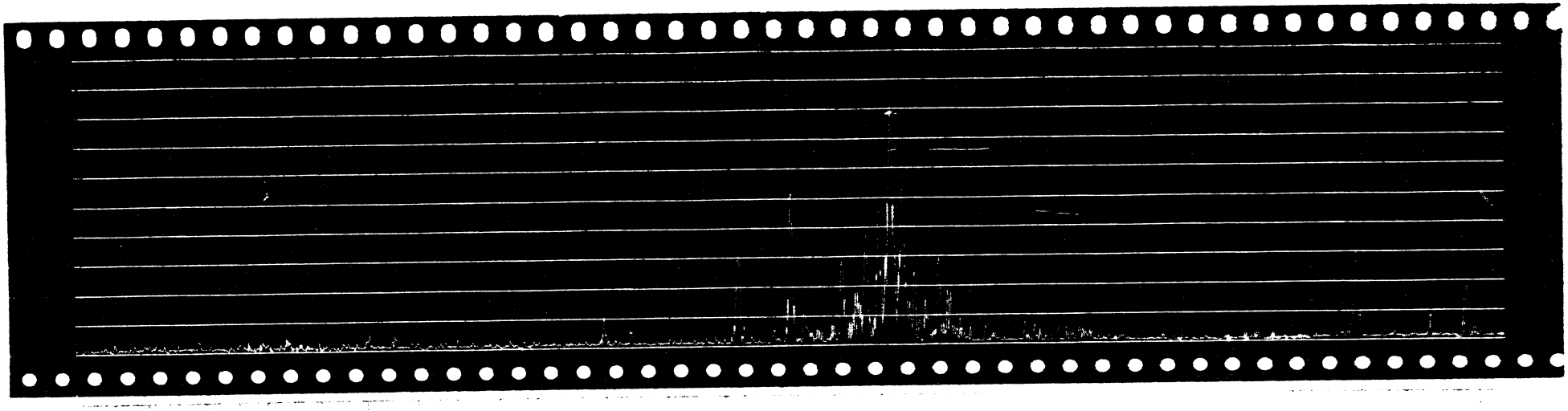

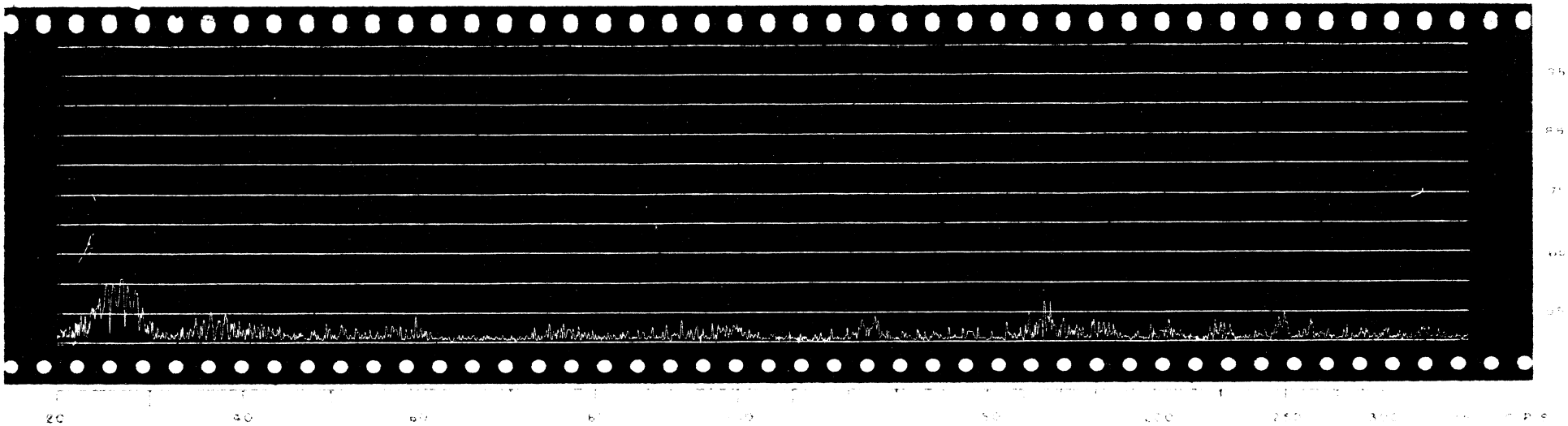

Fig. 5.2.5

Sound Spectrum of Experimental Motor at 40 Amp, 292 V, 40 cps. (Overall SPL 94 db)

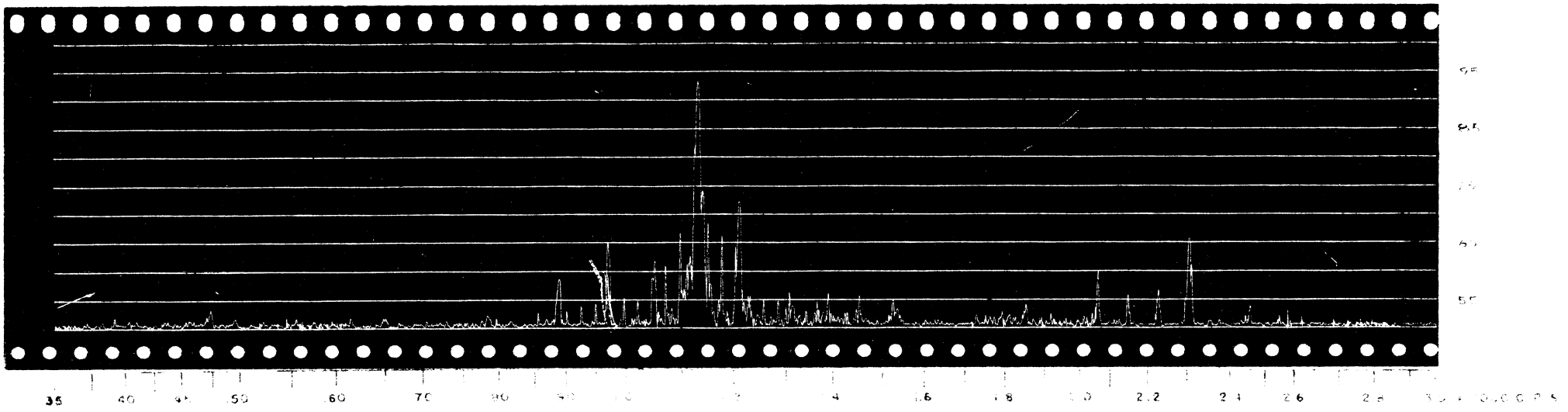

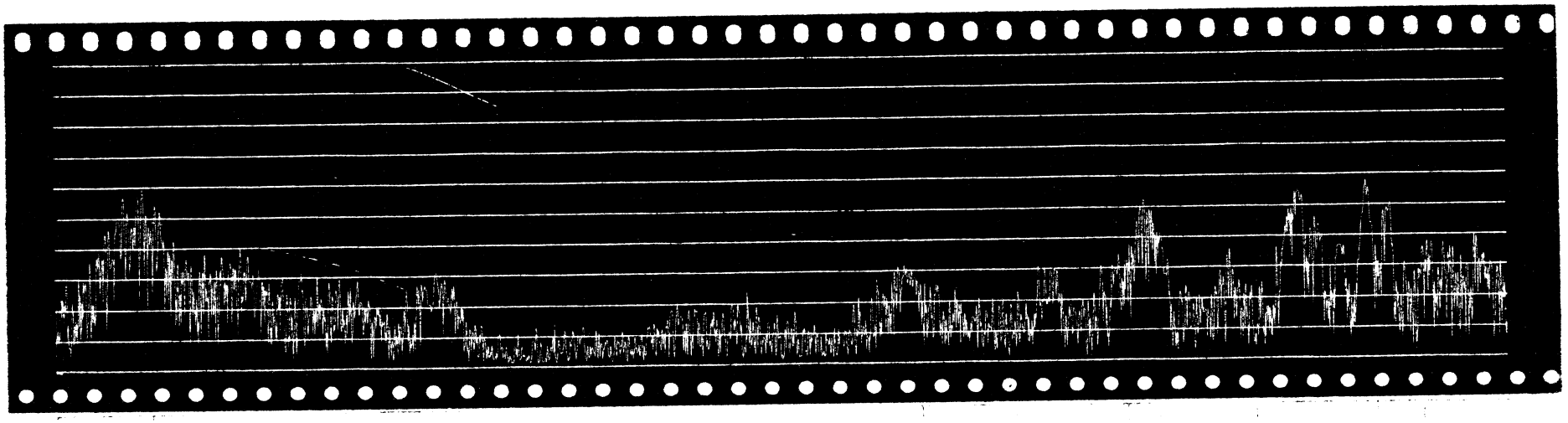

Fig. 5.2.7

Sound Spectrum of Experimental Motor at No Load, 440 V, 60 cps. (Overall SPL 75 db)

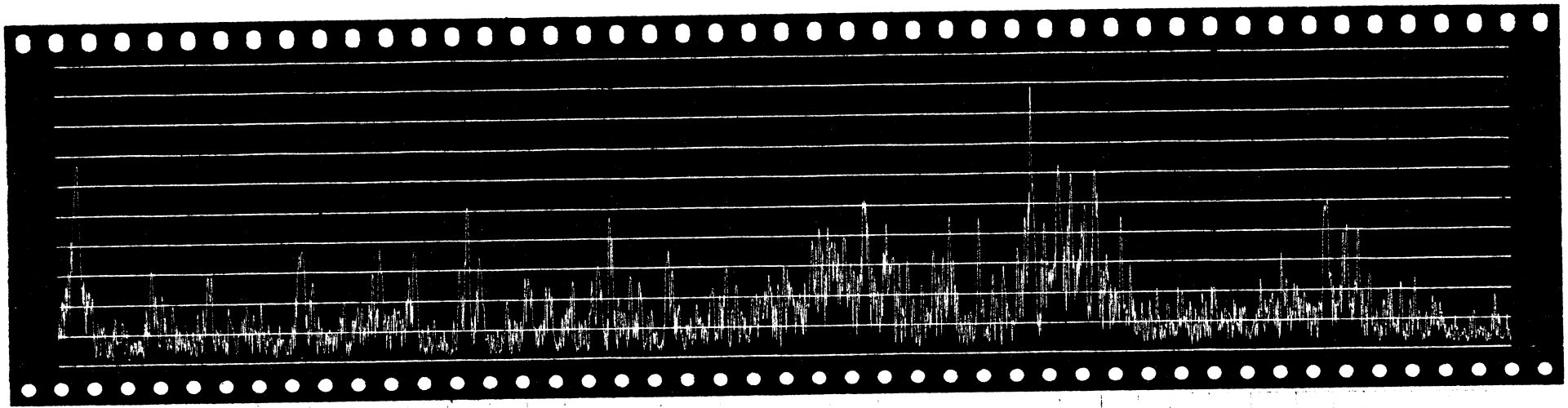

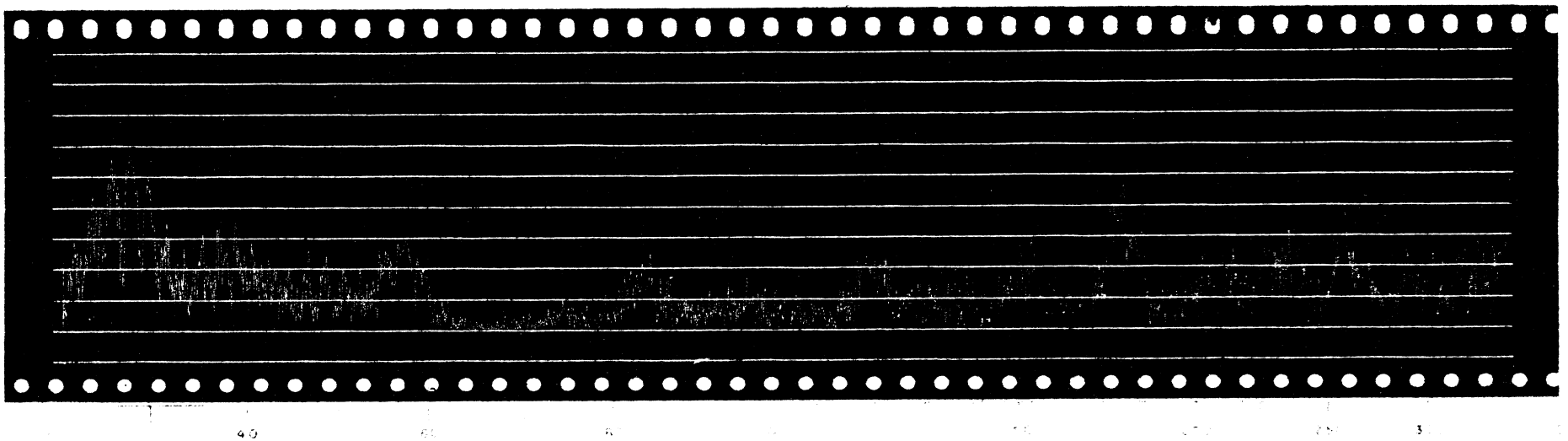

Fig. 5.2.9

Sound Spectrum of Experimental Motor at No Load, No Excitation

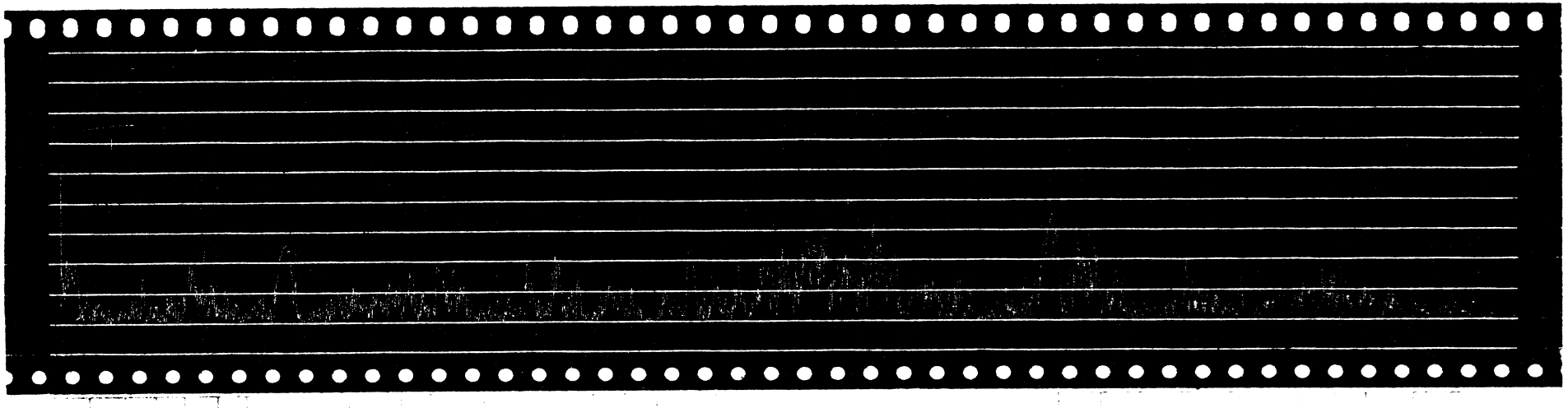

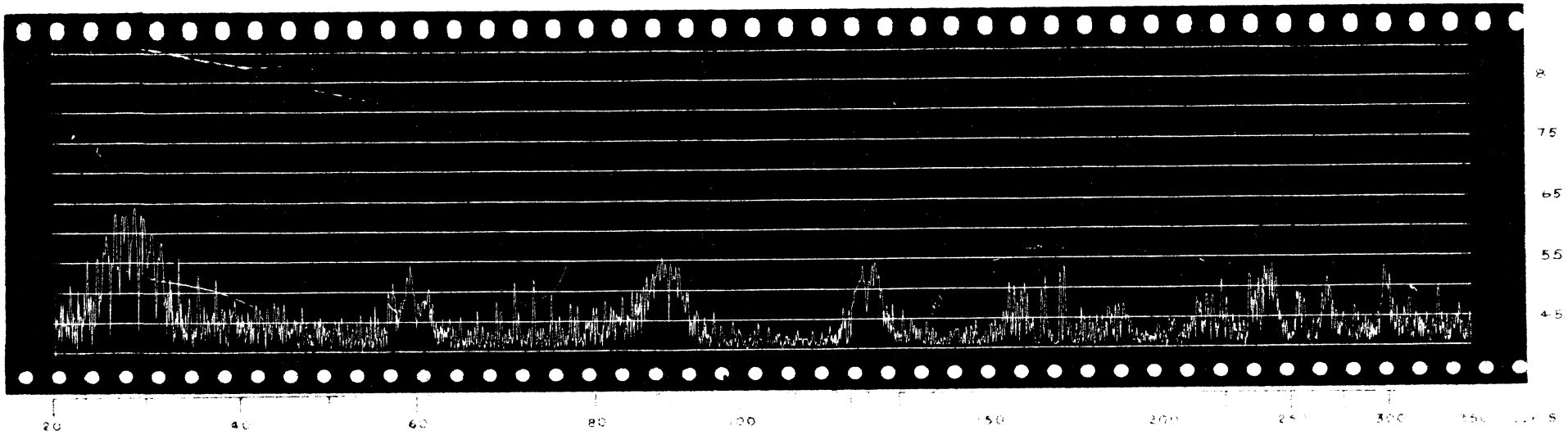

Fig. 5.2.9

Sound Spectrum of Experimental Motor at 40 Amp, 440 V, 60 cps. (Overall SPL 84 db)

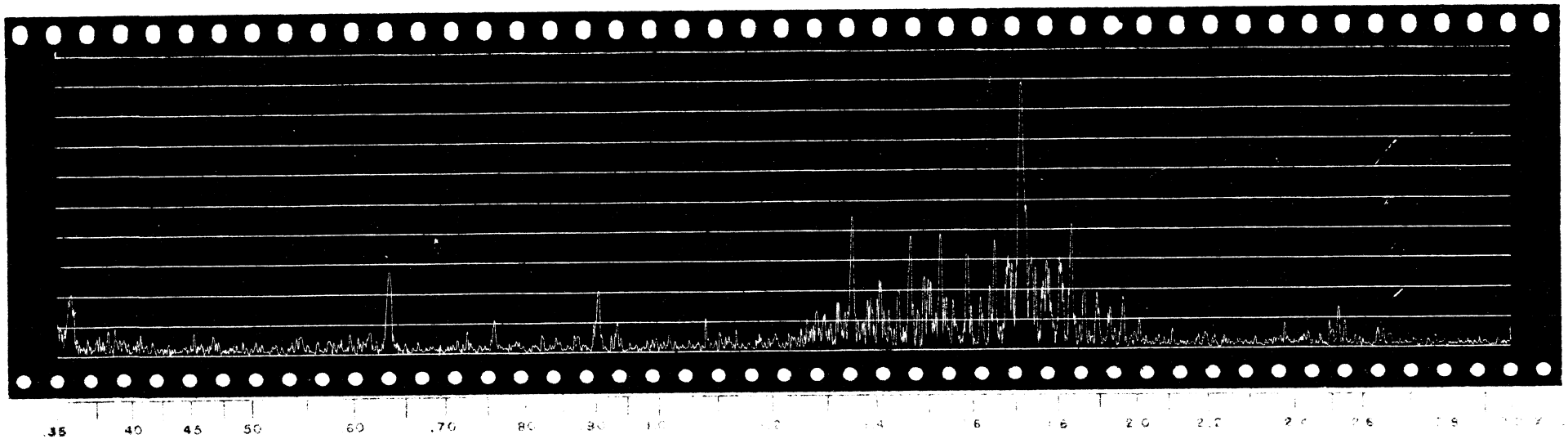

Note: The microphone at this recording was 2 feet from the motor.

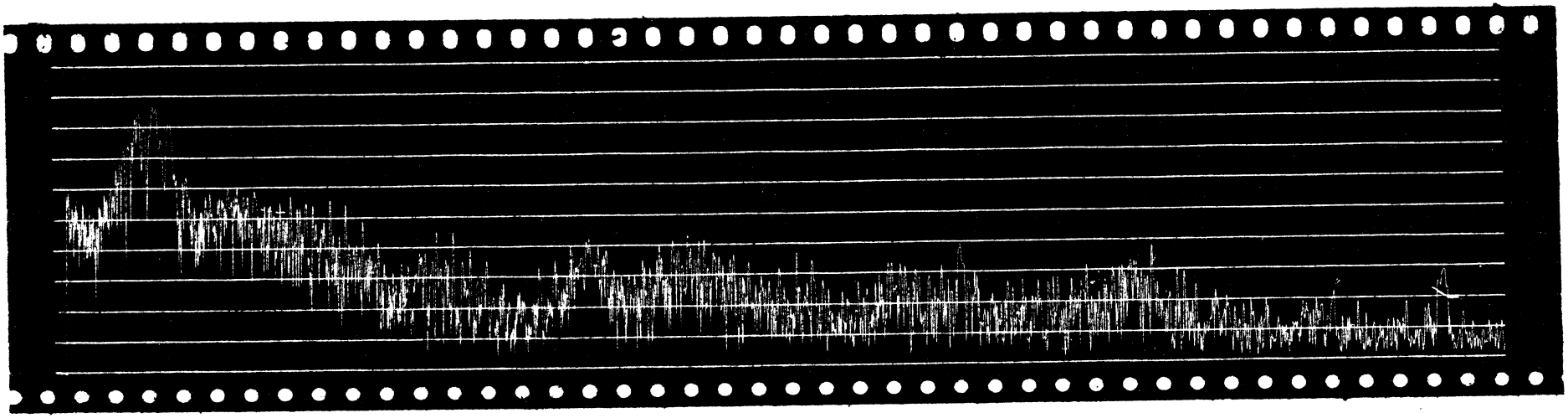

Fig. 5.2.10

Sound Spectrum of Ambient Noise in Anechoic Room (SPL 63 db)

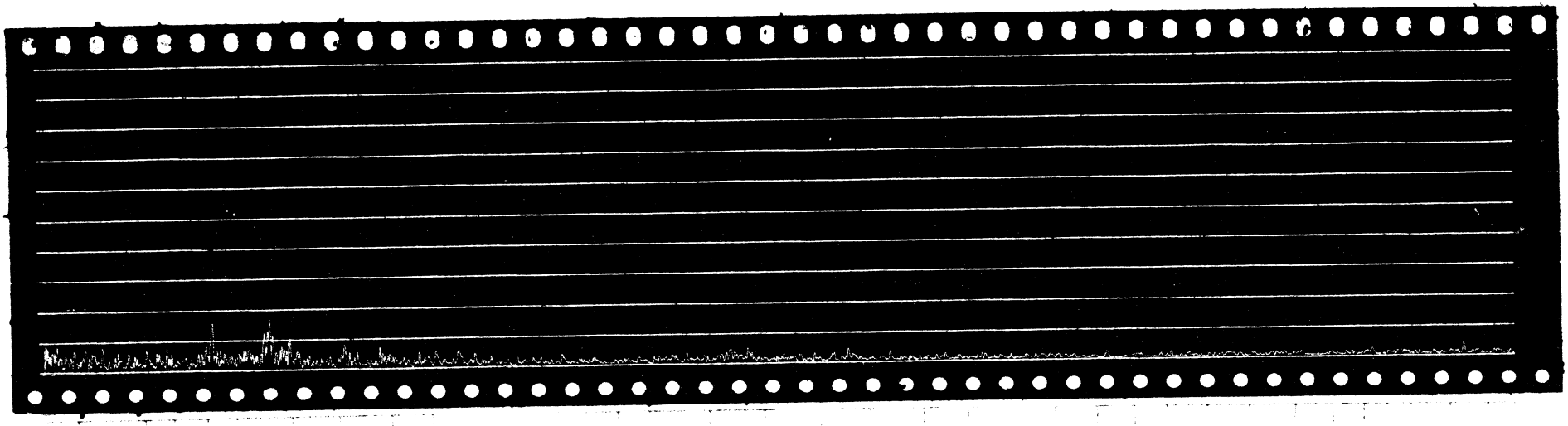

one per cent. As most of the recordings were at 90 db SPL it may safely be assumed that the overall accuracy of the recordings should be in the neighborhood of plus and minus 4 db.

Figures 5.2.4 and 5.2.10 are the records of sound spectra taken at different operating conditions of the motor. At all recordings, except the one illustrated in fig. 5.2.9, the microphone was at a distance of 12" from the stator in a radial line through the geometric center of the top rib. The position of the microphone for the recording in fig. 5.2.9 was in the same line at 24" from the stator.

5.3 Determination of Mode Shapes under Operating Conditions

This test is important for the determination of the predominant mode of vibration while the motor is operating. It serves as another check on the conclusions drawn from the theoretical analysis.

The vibrating operating motor is sensed simultaneously by two vibration pickups. The output of each pickup is connected to a General Radio Type 760-B Sound Analyzer. One of the sound analyzers is connected to X terminals, while the output of the other is coupled to the Y terminals of C.R.O.

The sound analyzer is a battery operated, continuous spectrum instrument. It includes a 3-stage, direct

coupled amplifier which is made selective by means of a tunable null circuit in a negative feedback loop. The frequency can be selected by a single dial and a set of five push-buttons. The band width is a constant percentage of the frequency to which the analyzer is tuned. This is very important as the speed of the motor under test is not absolutely constant.

During the test one of the pickups was fixed to a characteristic point (on the outer ring at the center of the top rib) of the motor with the aid of a magnet. The sound analyzer was tuned to the same frequency as the motor vibration whose shape was to be determined. A second vibration pickup was placed near the first one and its sound analyzer also tuned. The trace on the screen of the C.R.O. was the characteristic Lissajous figure of two vibrations of the same frequency in phase, that is a coinciding straight line.

After this adjustment the second pickup was gradually moved along a circle of the outer shell until the axes of the elliptical trace on the C.R.O. became horizontal and vertical, respectively. This point of the vibrating body is a quarter length from the fixed point of the first vibration pickup. By moving the second pickup farther away, a point was reached where the other diagonal of the rectangle enclosing the elliptical Lissajous figure appeared. This point was exactly one half wave length from the fixed

pickup.

The predominant mode shape of the 1,716 c.p.s. main noise and the 1,475 c.p.s. side noise had been investigated and both found to be second mode vibrations.

VI. CONCLUSIONS

The major objective of the present thesis is to establish, in a general manner, a method for the calculation of sound pressures caused by the magnetic noise of medium induction motors, at a characteristic point near the motor. This task has been performed in three steps:

1) the development of a theory for the calculation of the electromagnetic forces in the airgap of induction motors
2) a theoretical procedure for calculating the natural behavior and the forced response to electromagnetic force waves in medium induction motors
3) the development of a method to calculate the sound pressures resulting from the forced vibration of induction motor stators.

The results of the theoretical analysis are given at the end of chapter 5, and test results in chapter 6. These results are compared prior to the discussion of the merit of the method presented in this thesis.

6.1 Discussion of Results

Table 6.1.1 assembles the resonant frequencies of the experimental induction motor in different modes of vibration as calculated in section 3.5, and the experi-

Table 6.1.1

Comparison of Calculated and Measured

Resonant Frequencies of the Experimental Motor

Mode	Descrip. of Mode	Calculated		Measured		Error
		cps	in table	cps	Fig.	Per Cent
	Counter-tact sine	1,140	3.5.11	1,220	5.1.2d	-6.6
2nd	In-tact cosine	460	3.5.11	468	5.1.2a	-1.8
				482	5.1.2b	-4.4
	In-tact sine	490	3.5.11	473	5.1.2c	+3.6
	In-tact sine	1,225	3.5.12	1,240	5.1.3a	-1.25
3rd	In-tact cosine	1,170	3.5.12	1,080	5.1.3b	+8.5
				1,156	5.1.3c	+1.2
	Counter-tact sine	1,580	3.5.12	1,540	5.1.3d	+2.5

Table 6.1.2

Comparison of Calculated and Measured Sound Pressure Levels

of the Experimental Motor

1	2	3	4	5	6	7	8
Motor Operation A, V, cps	ft	Descr. of Noise	Noise f cps	Calc. SPL db	Meas. SPL db	Rec. on Fig.	Error Per cent
40, 440, 60	1	main	1,716	85.9	87.8	5.2.4	-2.2
40, 367, 50	1	main	1,419	87.7	90.0	5.2.5	-2.6
40, 294, 40	1	main	1,121	90.8	94.0	5.2.6	-3.4
NL, 440, 60	1	main	1,735	74.8	74.0	5.2.7	+1.1
40, 440, 60	1	side	1,475	62.0	64.0	5.2.4	-3.1
40, 440, 60	2	main	1,716	82.1	84.5	5.2.9	-2.9

Col. 2 denotes distance of microphone from stator

Data in Col. 5 are taken from Table 4.4.5 on page 232.

mental results provided in figures 5.1.2 and 5.1.3. In table 6.1.2 the sound pressure levels of the magnetic noise of the experimental induction motor, calculated from theoretical considerations (table 4.4.5), are compared with the test results given in figures 6.2.4 to 6.2.10.

A study of the results reveals a good agreement of calculated and measured values. Considering the complexity of the problem, the approximations and assumptions, together with the large number of numerical operations which had to be made, the agreement between theory and experiment is better than expected. This close agreement may be partly due to unknown fortuitous circumstances. It would, as a rule, be unreasonable to expect the theoretical results to approach sound measurements by such a close margin.

In view of the agreement between theoretical and test results it can be concluded that a method has been established to calculate:

1) the natural behavior and forced response of stators of medium induction motors, and
2) the sound pressure levels of the magnetic noise caused by electromagnetic radial forces in the airgap of induction motors.

The author again stresses the fact, that while the

analysis as presented here is of a general nature, solutions for specific designs of induction motors would have to be carried out separately for each class of design.

A full appreciation of the method herein developed would require a comparison with results obtained by other methods. Unfortunately, however, no such complete studies accompanied by test records appear to have been published. Hence such a comparison seems impossible. This lack of data is explained by the fact that the predetermination of magnetic noise is still at an early stage of development.

6.2 Application of the Method

The obvious question arises if this tedious and complex method involving the use of most advanced electronic digital computers is practicable, in view of a designer's busy everyday schedule. Whenever a new line of motors is under design, the advanced design staff usually has the facilities to carry out the calculations for every new frame size. Curves representing the deflections as a function of frequency and mode order for a constant amplitude force wave can be plotted in the manner illustrated in fig. 1.2. The solution of the integral necessary for the calculation of sound pressure levels can also be plotted as a function of noise frequency and mode order for a characteristic point of the induction motor. The

resonant frequencies and eigenvectors of each frame can be tabulated as shown in table 3.5.10. The only analytical work left to be performed by the designer would be the calculation of the force waves. The remaining task would then be the selection of the right information from prepared curves and the calculation of the sound pressure level by simple slide rule operations. Clearly the total study is a greater task than can be carried out by a single individual. However, once done, it can be used readily in design practice.

P. L. Alger, who has discussed in considerable detail favorable slot combinations and other electrical design precautions to be taken in the construction of low magnetic noise induction motors, has very appropriately coined the expression "sonance design". An extension of Alger's recommendation should be underlined. Designers should realize the importance of the number of resonant frequencies in each mode, as already mentioned in the introduction, discussed theoretically in Chapter 3, and shown by test results in Chapter 5. It does not suffice to avoid low order force waves caused by slot harmonics, as belt harmonics may also cause low order force waves. These latter are of much lower amplitudes than those of the slot harmonics, and may become troublesome if their frequencies coincide with the natural frequencies of the motor in the same mode.

A strong word of caution is necessary. Generalizations by applying the results of one design to another, as often observed in design practice, may prove precarious. A few instances of false generalizations may serve as examples:

1. One of the opinions often encountered is that the magnetic noise could be considerably reduced by increasing the radial lenght of the non-slotted portion of the stator core. Although it is true that the static deflection will decrease approximately as the third power of the increase of the radial depth, it is wrong to assume that the dynamic deflections will decrease to a negligible value. In fact, the low mode natural frequencies of the stator will increase and, consequently, the resonance factor will substabtially increase. A careful estimate would prove that by increasing the radial depth of the stator core of the experimental motor by one inch, the main noise sound pressure level could be reduced by 3 or 4 decibels only.

2. From the results of Appendix IV one would tend to conclude that by replacing all radial ribs by tangential ribs, the coupling between the two rings would loosen, and the outer ring vibration amplitudes would decrease. Although this conclusion is correct, it fails to consider other essential changes. Both fig. 1.2 and the results

of section 3.5 reveal that the lowest mode cosine and sine frequencies are very close to each other. The designer may avoid both by one slot combination. By loosening the coupling of the two rings the two frequencies which are normally close together will be spread out, so that the designer will have great difficulty to choose an electrical design in order to avoid several natural frequencies of the stator.

3. It appears that many designers, well aware of the danger of second mode force waves, believe that the second mode vibrations could be suppressed by the selection of a frame design with six ribs. The results of the present thesis prove the fallacy of such a concept.

The foregoing examples support the general view expressed in this thesis that every individual design must be separately analyzed and the sound levels of the magnetic noise separately calculated. Broad generalizations may lead to major inaccuracies.

APPENDIX I

Data of the Experimental Motor

Name Plate Data

30 HP, 4-pole, 440 volts, 3-phase, 1,780 r.p.m.

38 amp., Temperature rise 40°C., Frame K365

Electrical Design Data

Outer diameter of stator punchings	13.5"
Diameter of stator bore	9.00"
Outer diameter of rotor	8.952"
Inner diameter of rotor	2.625"
Airgap (design)	0.024"
Airgap measured, average	0.0225"
Length of stator	5.75"
Net iron length of stator	5.175"
Flux per pole	0.012 weber
Number of stator slots	60
Depth of stator slot	1.15"
Average width of stator slot	0.30"
Stator slot opening	0.125"
Average width of stator tooth	0.225"
Stator slot pitch on bore	0.470"
Number of conductors in stator slot	16
Total number of conductors	960
Double-layer stator winding circuits	1

Phases connected in	delta
Coilpitch	1 to 12
Number of cast aluminum straight rotor bars	54
Rotor slot shape	fig. A 1.1
Cross-sectional area of cast aluminum rotor end rings	1.50 sq.in.

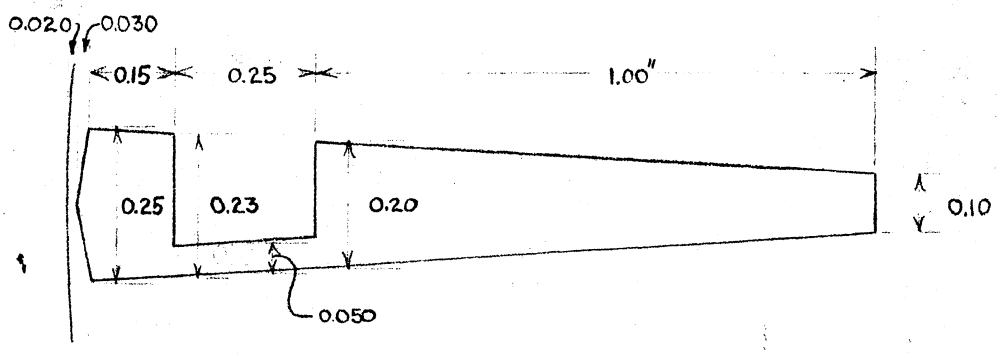

Fig. A 1.1

Rotor Slot of Experimental Motor

Evaluated Data for Section 2.10

Pitch factor, fundamental	0.914
Distribution factor, fundamental	0.956
Winding factor, fundamental	0.874
Airgap	5.7×10^{-4} meter
Carter coefficient	1.175.
Corrected airgap	6.7×10^{-4} meter
Pole pitch	0.18 meter
Net length of iron	0.13 meter
Length of stator	0.145 meter
Primary leakage reactance at normal operation	2.00 ohms

Primary effective resistance	0.75	ohm
Exciting susceptance	-1.54×10^{-2}	ohm
Iron loss conductance	2.2×10^{-3}	ohm
Secondary leakage reactance in primary terms	2.27	ohms
Secondary resistance (dc) in primary terms	0.3	ohm
Load resistance at 40 amp load in primary terms	19.7	ohms
High frequency leakage reactance of motor bar in secondary terms	1.01×10^{-4}	ohms

Test Conditions

Supply voltage at 60 c.p.s.	440	volt

(Note: The Supply voltage was reduced in ratio to the frequencies at tests as represented by figures 5.2.5 and 5.2.6)

Line current	40	amp
Phase current	23.2	amp
Power factor	0.895	
Slip	0.015	
Power output	32	HP
Efficiency	0.90	
No-load current	11.8	amp
No-load power factor	0.12	

Mechanical Design of the Stator

The details of the outer ring are illustrated in fig. A 1.2. A thorough inspection showed that not all of the dimensions of the actual casting were in agreement with the drawing. The correct measured dimensions are given in fig. A 1.3

Evaluation of Data for Sections 3.4 and 3.6

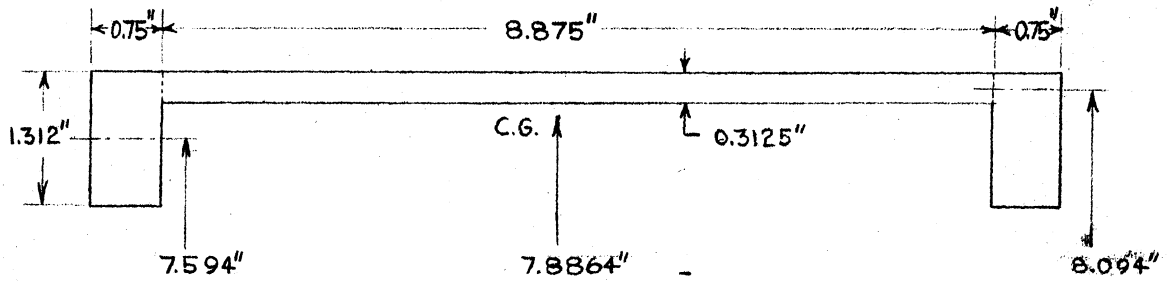

Fig. A 1.3

Outer Ring Cross-Section

Outer Ring Parameter

Inertia factor: The weight of the outer ring is 95 lb so that the inertia factor is

$$\pi\mu_o/2 = (\pi/2)(95/2\pi)(1/386) = 6.153 \times 10^{-2}$$

The centroid of the cross-section is at a radius of 7.89 inches; the moment of inertia is $I_0 = 0.5924$, and the flexural rigidity factor

$$(\pi D_D/2R^3) = (\pi/2)(16\times10^6/0.91)(0.5924/490.49) = 3.337\times10^4$$

Inner Ring

The weight of the inner ring is 120 lb and the inertia factor is

$$(\pi\mu_I/2) = (120/386)(1/2\pi)(\pi/2) = 7.778\times10^{-2}$$

The flexural rigidity factor of the inner ring is

$$(\pi D_I/2r^3) = (\pi/2)(30\times10^6/0.91)(5.175/12)(1.1/6.2)^3$$

$$= 1.24716\times10^6$$

Support Parameter

The length of the support is 9". The effective moment of inertia is 0.176 so that the bending rigidity factor is

$$D_s = 3.1\times10^6$$

Rib Constants

The rib is of a complicated shape. To simplify calculations it was replaced by an effective rib as shown crosshatched in fig. A 1.4

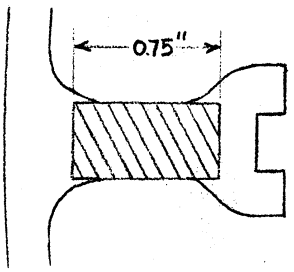

Fig. A 1.4

Detail of Rib Cross-section

The extensional rigidity factor will be

$$E_r A_r / l_r = (16 \times 10^6)(4/3)(3/8)(5.75) = 46 \times 10^6$$

and the bending rigidity factor will be

$$D_r = E_r I_r / (1-6^2) = (16 \times 10^6)(1/0.91)27/512)(1/12)(5.175)$$

$$= 3.8 \times 10^5$$

APPENDIX II

Energies of the Vibrating Rings
(Extensional Deformations Considered[1])

Preliminary calculations proved the influence of extensional deformations to be negligible for a low mode response of the experimental motor. However, 2-pole motors have generally very deep stator cores so that the ratio of the radial ring thickness to the median radius is larger than 0.15. In such cases the consideration of extensional deformation may provide more accurate results. The necessary formulae for the ring energies considering these deformations will be derived here for the inner ring only. The expression for the outer ring is analogous.

The radial displacement of the ring will be chosen according to equation 3.4.2, as

$$(A\ 2.1) \qquad u = \sum a_m \cos m\theta + b_m \sin m\theta$$

The tangential displacement is now expressed as

$$(A\ 2.2) \qquad w = \sum c_m \cos m\theta + d_m \sin m\theta$$

The Kinetic Energy can now be calculated by 3.2.17

$$T_I = (\mu_1/2) \int_0^{2\pi} (\dot{u}^2 + \dot{w}^2)\, d\theta$$

---

[1] 57

as

$$(A\ 2.3) \quad T_I = (\pi\mu_I/2) \sum (\dot{a}_m^2 + \dot{b}_m^2 + \dot{c}_m^2 + \dot{d}_m^2)$$

The Bending Energy of the ring can be calculated from equation 3.2.9 by introducing into this equation

$$-d^2u/d\theta^2 = m^2(a_m \cos m\theta + b_m \sin m\theta)$$

$$dw/d\theta = m\,(+d_m \cos m\theta - c_m \sin m\theta)$$

The resulting expression will be

$$(A\ 2.4) \quad V_{bI} = (D_I/2r^3) \int_0^{2\pi} [(ma_m+d_m)m \cos m\theta + (mb_m-c_m)m \sin m\theta]^2\, d\theta$$

which reduces to

$$(A\ 2.5) \quad V_{bI} = (\pi D_I/2r^3) \sum (m^2a_m+md_m)^2+(m^2b_m-mc_m)^2$$

The Extensional Energy can be calculated by introducing into

$$(3.2.12) \quad V_{tI} = (E_IA_I/2r) \int_0^{2\pi} [(dw/d\theta) + u]^2\, d\theta$$

the expansions of $dw/d\theta$ and u which will result in

$$(A\ 2.6) \quad V_{tI} = (\pi/2r)E_IA_I \sum (a_m + md_m)^2 + (b_m - mc_m)^2$$

Basically all the other expressions will remain unchanged.

APPENDIX III

Diagonalization of a Real Symmetric Matrix on the IBM 701 Electronic Data Processing Machine

The programing of the diagonalization of a real symmetric matrix is based on the theorem[1] that the eigenvalues of matrix $T^{-1}A\,T$ are identical with the eigenvalues of matrix A.

Given an arbitrary symmetric matrix, an orthogonal matrix S of the following form may be chosen

$$\begin{pmatrix} 1 & 0 & \cdots & 0 & \cdots & 0 \\ 0 & 1 & \cdots & 0 & \cdots & 0 \\ \vdots & & & & & \\ 0 & 0 & \cdots & r_{ii} & \cdots & r_{ij} \\ \vdots & & & & & \\ 0 & 0 & \cdots & r_{ji} & \cdots & r_{jj} \\ \vdots & & & & & \\ 0 & 0 & \cdots & 0 & \cdots & 1 \end{pmatrix}$$

where only the elements r_{ii}, r_{ij}, r_{ji}, r_{jj} are different from the corresponding element in the identity matrix (of the same order as matrix A), having the property that the element in the (i,j) position of the product S A S' is zero.

---

[1] 33;54

The first S_1 is so chosen that the first row, second column element in $S_1 A S_1'$ is zero. The S_2 is chosen so that the first row third column element vanishes in the $S_2 S_1 A S_1' S_2'$. This procedure is continued, sequentially annulling each element above and below the diagonal. Non-zero quantities may, however, reappear in off-diagonal positions at a later stage, and the matrix becomes non-diagonal when a cycle is completed, that is, when the n^{th} element in the $(n-1)^{st}$ row has been annulled. An orthogonal transformation though, leaves invariant the sum of the squares of the matrix elements. It has also been shown[1] that the sum of the squares of the diagonal elements increases monotonically throughout the process. It follows that the sum of the squares of the elements off the diagonal decreases monotonically.

After a cycle of operations is completed, the whole procedure is repeated, starting with the second element of the first row and continuing to the n^{th} element of the $(n-1)^{st}$ row, until the sum of the squares of the off-diagonal elements decreases monotonically so close to zero as to become negligible. Approximately 30 to 40 cycles will be necessary on the IBM 701 Electronic Data Processing Machine to render the sum of the squares of the off-diagonal elements negligible. The result will

---

[1] 40

now be a matrix

$$(S_m S_{m-1} \ldots S_1) A \, (S'_1 \ldots S'_{m-1} \, S'_m)$$

which is diagonal. This resultant matrix is of the form $T^{-1}A\,T$, and its diagonal elements are therefore the eigenvalues of matrix A. It has also been shown[1] that the columns of matrix $S'_1 \ldots S'_{m-1} \, S'_m$ are the elements of the eigenvectors of matrix A.

---

1 35;40

APPENDIX IV

Investigation of the Influence of the Tangential Ribs

The influence of the tangential ribs can be evaluated by adding the bending energy of the tangential ribs at $\theta = 60^\circ$, 120°, 240°, and 300°. As the effect is one of second order, a negligible error will be introduced in the final solution by supposing that the effect due to the tangential ribs is precisely the effect due to radial ribs of the same length. With this assumption, equation 3.2.29 applies for the tangential ribs. In the following discussion only the lowest modes will be considered.

The first term for the second mode can be calculated, using equation 3.2.29 and values of W_2, w_2, at $\theta = 60^\circ$, 120°, 240°, 300°, to be

$$V_{br1} = (D_r/l_r^3)(1/4)\Big(\big[(B_2-b_2)\cos 120+(A_2-a_2)\sin 120\big]^2 + \big[(B_2-b_2)\cos(-120)+(A_2-a_2)\sin(-120)\big]^2 + \big[(B_2-b_2)\cos 240+(A_2-a_2)\sin 240\big]^2 + \big[(B_2-b_2)\cos(-240)+(A_2-a_2)\sin(-240)\big]^2\Big) \tag{A4.1}$$

which can be simplified to read

$$V_{br1} = (3/2)(D_r/l_r^3)(B_2-b_2)^2-(9/2)(D_r/l_r^3)(A_2-a_2)^2 \tag{A4.2}$$

For the first bending term of the rib in the third mode, a

similar consideration will yield

$$(A4.3)\quad V_{br1} = (8/3)(D_r/l_r^3)(B_3-b_3)^2$$

The analogous evaluation of the second term in equation 3.2.29 for the second mode will be

$$(A4.4)\quad V_{br2} = 6(D_r/l_r^2R)(B_2^2-B_2b_2 + 3A_2^2-3A_2a_2) + \\ + 6(D_r/l_r^2r)(B_2b_2-b_2^2 + 3A_2a_2-3a_2^2)$$

For the third mode there results

$$(A4.5)\quad V_{br2} = 24(D_r^2/l_rR)(B_3^2-B_3b_3)+24(D_r^2/l_r^2r)(B_3b_3-b_3^2)$$

The third term of the bending energy as represented in equation 3.2.29, can be evaluated for the second mode, and is

$$(A4.6)\quad V_{br3} = 8(D_r/l_rR^2)(B_2+3A_2^2)+8(D_r/l_r^2r)(B_2^2+3a_2^2)+ \\ +8(D_r/l_rRr)(B_2b_2+3A_2a_2)$$

For the third mode, the contributing terms are

$$(A4.7)\quad V_{br3} = 72(D_r/l_rR^2)B_3^2+72(D_r/l_r^2r)b_3^2+72(D_r/l_rR_r)B_3b_3$$

The constants for the calculation of these terms, based on design data in Appendix I, are assembled in

Table A4.1

Constants of the Tangential Ribs

D_r/l_r^3	D_r/l_r^2R	D_r/l_r^2r	D_r/l_rR^2	D_r/l_rr^2	D_r/l_rR_2	
4.041	1.52	1.94	0.57	0.93	0.73	$x10^3$

The potential energies have been calculated, and added to the respective terms of tables 3.5.5, and 3.5.6.

The second mode determinant showing the effect of the tangential ribs is recorded in table A4.2 and for the third mode in table A4.3. The coefficients in the brackets give the corresponding terms of the same determinant, neglecting the bending energies of the tangential ribs. A close inspection reveals that the effect of the tangential rib on the behavior of the elastic system is negligible.

Table A4.2

Second Mode Determinant Showing Effect of Tangential Ribs

	A_2	B_2	a_2	b_2
A_2	92.79- (92.706)- $-.154\omega^2$	0.112 (0.112)	-92.01 (-92.00)	
B_2	0.112 (0.112)	8.225- (8.195)- $-.154\omega^2$		-5.022 (-5.012)
a_2	-92.01 (-92.00)		94.215- (94.245)- $-0.193\omega^2$	
b_2		-5.022 -5.013		5.56- (5.57)- $-0.1943\omega^2$

Table A4.3

Third Mode Determinant Showing Effect of Tangential Ribs

	A_3	B_3	a_3	b_3
A_3	$96.691-(96.691)-0.1367\omega^2$	-0.167 -0.167	(-92) (-92.00)	
B_3	0.167 (0.167)	$9.36-(9.1962)-0.1367\omega^2$		-1.93 (-1.953)
a_3	(-92.00) (-92.00)		$107.964-(107.964)-0.1727\omega^2$	
b_3		(-1.92) (-1.953)		$16.767-(16.706)-0.1727\omega^2$

BIBLIOGRAPHY

1. Alger, J. R. M., "Some Effect of Eccentric Airgaps in Induction Machines", M.S. Thesis, M.I.T., Cambridge, 1950.

2. Alger, P. L., The Nature of Polyphase Induction Machines, John Wiley & Sons, Inc., New York, 1951.

3. Alger, P.L., "The Magnetic Noise of Polyphase Induction Motors", A.I.E.E. Technical Paper No. 54-1 (1950).

4. Alger, P. L. and Oney, W.R., "Energy Flow in Induction Machines", General Electric Review, Vol. 56, (1953), No. 2, Page 56.

5. *Alger, P. L. and West, H. R., "The Airgap Reactance of Polyphase Machines", A.I.E.E. Proceedings, Vol. 66 (1947) Page 1.

6. Arnold, E., LaCour, J. L. and Fraenckel, A., Alternating Current Technology (in German) Vol. V, Part 1, Julius Springer, Berlin, 1909, Page 183.

7. Backhaus, H., "Vibrations of Continuous Media", (in German), Handbuch der Physik, Vol. VIII, Julius Springer, Berlin, 1927, Page 69.

8. *Bailey, B. F. and Gault, J. S., Alternating Current Machinery, McGraw-Hill Book Company, Inc., 1951.

9. Baker, B. B. and Copson, E. T., The Mathematical Theory of Huygen's Principle, Clarendon Press, Oxford, 1950, Page 25.

10. Baudry, R. A., Heller, P. A., and Curtis, L. P., "Magnetic Vibrations in Alternating Current Generator Stators", A.I.E.E. Technical Paper, No. 54-93. (1953).

The references marked with an asterisk are not quoted in the text but have contributed greatly to the author's background, and it is hoped that they will be of value to the reader.

11. Beranek, L. L., Acoustic Measurements, John Wiley & Sons, Inc., New York, 1949.

*12. Beranek, L. L., Acoustics, McGraw-Hill Book Company, Inc., New York, 1954.

13. Beranek, L. L., Sleeper Jr., H. P., "Design and Construction of Anechoic Sound Chambers", Journal Acoustic Society of America, Vol. 18 (1946), Page 140.

*14. Bickley, W. G., et alia, "Bessel Functions", Part I, British Association of the Advancement of Science Mathematical Tables, Vol. VI, University Press, Cambridge, 1937.

*15. Bickley, W. G., et alia, "Bessel Functions", Part II, British Association of Advancement of Science Mathematical Tables, Vol. X, University Press, Cambridge, 1952.

16. Bradford, C. E. and Rhudy, R. G., "Axial Magnetic Forces on Induction Motor Rotors", A.I.E.E. Power Apparatus & Systems, June 1953, Page 488.

17. Carter, F. W., "Flux Distribution in the Airgap of Electrical Machines", Electrical World and Engineering, Vol. 38 (1901), Page 884.

18. Chapman, F. H., "The Production of Noise and Vibration by Certain Squirrel Cage Induction Motors", Journal Inst. El. Engrs., Vol. 61, (1922), Page 39.

19. Churchill, R. V., Modern Operational Mathematics in Engineering, McGraw-Hill Book Company, Inc., New York, 1944.

20. Courant, R., "The Theory of Linear Partial Difference Equations", (in German) Nachrichten von der Gesellschaft der Wissenschaften zu Goettingen, 1925, Vol. 1, Page 98.

21. *Den Hartog, J. P., Mechanical Vibrations, McGraw-Hill Book Company, Inc., New York, 1947.

22. Doherty, R. E. and Nickle, C. A., "Synchronous Machines, Part I, an Extension of Blondel's Two-Reaction Theory", A.I.E.E. Transactions, Vol. 43, (1926),

23. Dreyfus, L., The Theory of Polyphase Induction Motors with Squirrel Cage, (in German) Ingeniorsvetenskapsakademiens Handlingar, Vol. 34, (1924)

24. * Firestone, F. A., Vibration and Sound, Edward Bros., Inc., Ann Arbor, Michigan, (1939).

25. Fluegge, W., Static and Dynamics of Shells, (in German) Edwards Brothers, In., Ann Arbor, Michigan, 1943, Page 49.

26. Frey, K., "The Application of Conformal Mapping to Practical Problems of Electrical Machine Design" (in German) Arbeiten Aus dem Elektrotechnischen Institute der Technischen Hochschule in Karlsruhe, Vol 4, Julius Springer, Berlin, 1925.

27. Fritze, H., "Noise Created by Electrical Machinery", (in German) Archiv fuer Elektrotechnik, Vol. 10, (1921), Page 73.

28. Gault, J. S., "Rotor Bar Currents in Squirrel Cage Induction Motors", A.I.E.E. Transactions, Vol. 60, (1941), Page 784.

29. Goldstein, H., Classical Mechanics, Addison-Wesley Press, Inc., Cambrdige, Mass., 1950, Page 14, Page 347.

30. Gross, E. E., "An Acoustic Calibrator for the Sound Level Meter", General Radio Experimenter, Vol. 24, (1949) No. 7.

31. Harrington, R. F., Advanced Field Theory (Mimeographed Edition of Lectures) Syracuse University, Syracuse 1952, Page 22.

32. Hartley, R. V. L., "Application of Vector Analysis to the Wave Equation", Letter to the Editor, Journal Acoustic Society of America, Vol. 22, (1950) Page 511.

33. Hildebrand, F. B., Methods of Applied Mathematics, Prentice-Hall, Inc., New York, 1952, Page 74.

34. Hildebrand, L. E., "Quiet Induction Motors", A.I.E.E. Transactions, Vol. 49 (1930) Page 848.

35. Horvay, G., Solution of Large Equation Systems and Eigenvalue Problems by Lanczos Matrix Iteration Method, General Electric Company, Schenectady, New York, 1953.

36. Jordan, H., The Low Noise Electric Motor (in German), W. Girrardet, Essen (1950).

37. Jordan, H., "Approximate Calculation of the Noise produced by Squrrel- Cage Motors", The Engineer's Digest, Vol. 10, (1949), Page 222

38. Kaplan, W., Advanced Calculus, Addison-Wesley Press, Inc., Cambridge, Mass., 1952, Page 616

39. Karman, von Th. and Biot, M. A., Mathematical Methods in Engineering, McGraw-Hill Book Company, Inc., New York, 1940, Page 162 , Page 186.

40. Kigbetliantz, E. G., "Diagonalization of a Real Symmetric Matrix", Private Communication to the Author, 1954

41. Kron, G., "Induction Motor Slot Combinations", A.I.E.E. Transactions, Vol. 50, (1931), Page 757

42. Krondl, M., "On the Differential Leakage of Induction Motors" (in French), Revue Générale de l'Electricité, Vol. 23, (1928), Page 440 and 479

43. Krondl, M., "The Parasitic Forces in Induction Motors", Bulletin Oerlikon, Vol. 24, (1931), Page 654 and Vol. 25, (1931) , Page 665.

44. Krondl, M., "Noise of Electrical Machinery" (in French) Conférence Internationale des Grands Réseaux Electriques à Haute Tension, Paris,(1933), Page 6

45. *Kuhlman, K., Theoretical Electrical Technology (in German) Vol. 3, Birkhaeuser Verlag, Basel, 1951

46. Knudson, V.O. and alia, The Acoustical Spectrum, (Sound wanted and unwanted), University of Michigan Press, Ann Arbor, Michigan, 1952.

47. *Langsdorf, A. S., Theory of Alternating Current Machinery, McGraw-Hill Book Company Inc., New York, 1935

48. *Liwschitz, M., A Treatise on Electrical Machinery, (in German), Vol.1-3, B. G. Teubner Verlag, Leipzig, 1931

49. *Love, A. E. H., A Treatise on the Mathematical Theory of Elasticity, Dover Publications, New York, 1944.

50. *McLachlan, N. W., Theory of Vibrations, Dover Publications, New York, 1951

51. *Milne, W. E., Numerical Calculus, Princeton University Press, Princeton, N. J., 1949.

52. Morrill, W. J., "Harmonic Theory of Noise in Induction Motors", A.I.E.E. Transactions, Vol. 59, (1940) Page 474.

53. *Morse, P. M., Vibration and Sound, McGraw-Hill Book Company, Inc., 1948.

54. Perlis, S., Theory of Matrices, Addison-Wesley Press, Inc., Cambridge, Mass., 1942, Page 169.

55. Peterson, A. P. G. and Beranek, L. L., Handbook of Noise Measurement, General Radio Company, Cambridge, Mass., 1953.

56. Plunkett, R., "Measurement of Mobility", Journal of Applied Mechanics, Vol. 21, (1954) Page 250.

57. Poritsky, H. and Horvay, G., "Stresses in Pipe Bundles", A.S.M.E., Applied Mechanics, Paper No. 50-A-80.

58. *Prescott, J., Applied Elasticity, Dover Publications, New York, 1946.

59. Rayleigh, Lord J. W., The Theory of Sound, Vol. I-II, Dover Publications, New York, 1945.

60. *Randall, R. H., An Introduction to Acoustics, Addison-Wesley Press, Inc., Cambridge, Mass., 1951.

61. *Richter, R., Electrical Machinery, (in German), Vol. I-V, Julius Springer, Berlin, 1924-1948.

62. Rossmaier, V., "Calculation of the Additional Losses Caused by Non-Insulated Rotor Bars.," Elektrotechnik und Maschinenbau, Vol. 57, (1939), Page 249.

63. Schuisky, W., "Additional Currents in Non-Insulated Squirrel-Cages" (in German) Bulletin des Schweitzer Elektrotechnischen Verbandes, Vol. 44, (1953) Page 330.

64. Sommerfeld, A. J. W., Partial Differential Equations in Physics, Academic Press Inc., New York, 1949, Page 189.

65. Stiel, W., "Experimental Investigation of Torques of Polyphase Induction Motors with different Number of Rotor Bars",(in German), Forschungsarbeiten auf dem Gebiete des Ingenieurwesens, V. D. I., Vol. 212, (1919), Page 2

66. Stratton, J. A., Electromagnetic Theory, McGraw- Hill Book Company, Inc., New York, 1941, Page 289, Page 349

67. Temple, G.F.J, and Bickley W. G., Rayleigh's Principle and its Application to Engineering, Oxford University Press, London, 1933

68. Trefftz, E., "Mathematical Theory of Elasticity" (in German), Handbuch der Physik, Vol. 6, Julius Springer, Berlin, 1928

69. Timoshenko, S. and Young, D. H. , Advanced Dynamics, McGraw-Hill Book Company Inc., 1948

70. Timoshenko, S. and Lessells, J. M. Applied Elasticity Westinghouse Press, East Pittsburgh, 1925, Page 119

71. Timoshenko, S., Theory of Plates and Shells, McGraw-Hill Book Company Inc., New York, 1940, Page 3

72. *Timoshenko, S., Vibration Problems in Engineering, D. Van Nostrand Company, Inc., New York, 1937

73. Weber, E., "The Slotting Factor in Electrical Machinery" (in German), Elektrotechnische Zeitschrift, Vol. 32, (1928), Page 858.

74. Wells, R. J., Noise Analysis Technique, Private Communication to the Author, 1954

75. *Whittaker, E. T., A Treatese on the Analytical Dynamics of Particles and Rigid Bodies, Dover Publications, New York, 1944

76. Report, "Inter-Society Co-operation urged to expedite Noise Study Agreement", Electrical Engineering, Vol. 50,(1931), Page 443.